Construction of Artificial Stem Cell Microniches

Sneha Agarwal

B.Sc., M.Sc.

Submitted for the degree of **Doctor of Philosophy**

Heriot-Watt University

School of Engineering and Physical Sciences

Department of Chemical Engineering

September 2011

ABSTRACT

Artificial embryonic stem cell niches were made from murine embryonic stem cells (ESCs) and SAOS-2 osteoblast-like cells (a human osteosarcoma cell line) by constructing aggregates with well-defined architectures with dielectrophoresis between the castellations of interdigitated oppositely castellated electrodes. This combination of the cells was chosen to mimic the bone marrow endosteal niche that harbours haematopoietic stem cells in a quiescent stage, with the aim of transforming the embryonic stem cells into hematopoietic precursor cells. Within aggregates made with dielectrophoresis cells are in very close contact, allowing strong cell-cell interactions to occur. Puramatrix gel was used to immobilize the cells; a concentration of 25% Puramatrix was found to be optimal. Aggregates consisting of only ESCs formed embryoid bodies upon aggregation with dielectrophoresis within 24 hours. The size of the electrodes determines the size of embryoid bodies. Embryonic bodies formed at electrodes with a characteristic size larger than 100 μm tended to split; electrodes smaller than 75 μm gave embryonic bodies which tended to merge. 75 to 100 μm was optimal. When aggregates were made containing both SAOS-2 and ESCs, the reorganization of the two cell types after their aggregation was found to be controlled by the different adhesive-cohesive properties of the two cell types and their initial position. Optimum cell-cell interaction was obtained in an aggregate with a layered architecture with the osteoblasts initially in bottom position, and the ESCs in top position. The study of differentiation in ESCs was made by conducting experiments with Bry ESCs, which mark the onset of differentiation along mesenchymal lineage with the production of GFP. The results indicated that aggregation with dielectrophoresis causes the ESCs to take the first steps towards differentiation along the mesenchymal lineage, and that the differentiation is stronger in aggregates formed at electrodes of 75 μm than at electrodes of 100 and 50 μm. Co-culture with SAOS-2 cells did not lead to differentiation along the mesenchymal lineage. Lastly it was shown that optical tweezers could be combined with dielectrophoresis to move individual cells between niches.

DEDICATION

This thesis is dedicated to my parents, Dr. R.L. Agarwal and Mrs. Saroj Agarwal my brother, Nikhil and sister, Snigdha, who have supported me throughout this period.

DECLARATION STATEMENT

ACADEMIC REGISTRY

Research Thesis Submission

Name*:*	Sneha Agarwal		
School/PGI:	School of Engineering and Physical Sciences		
Version: *(i.e. First, Resubmission, Final)*	First	Degree Sought (Award and Subject area)	PhD in Tissue Engineering

Declaration

In accordance with the appropriate regulations I hereby submit my thesis and I declare that:

1) The thesis embodies the results of my own work and has been composed by myself

2) Where appropriate, I have made acknowledgement of the work of others and have made reference to work carried out in collaboration with other persons

3) The thesis is the correct version of the thesis for submission and is the same version as any electronic versions submitted*.

4) my thesis for the award referred to, deposited in the Heriot-Watt University Library, should be made available for loan or photocopying and be available via the Institutional Repository, subject to such conditions as the Librarian may require

5) I understand that as a student of the University I am required to abide by the Regulations of the University and to conform to its discipline.

* *Please note that it is the responsibility of the candidate to ensure that the correct version of the thesis is submitted.*

Signature of Candidate*:*		Date:	14/09/11

Submission

Submitted By *(name in capitals):*	SNEHA AGARWAL
Signature of Individual Submitting:	
Date Submitted:	14/09/11

For Completion in the Student Service Centre (SSC)

Received in the SSC by *(name in capitals):*			
Method of Submission *(Handed in to SSC; posted through internal/external mail):*			
E-thesis Submitted ***(mandatory for final theses)***			
Signature:		Date:	

ACKNOWLEDGMENTS

This work has been conducted at the School of the Engineering and Physical Sciences, Heriot Watt University, from January 2008 to July 2011 under supervision of Dr. Gerard H. Markx, Professor of Bioprocessing and Dr. Lynn Paterson, lecturer in Physics.

I would like to thank my first supervisor, Prof. Gerard H. Markx for providing me the opportunity to work on such a scientifically interesting and challenging research project, and I would like to express my sincere gratitude for his help and guidance throughout this work. He has been truly supportive in offering advice and helping whenever I struggled. From tailoring my thesis to perfection, to allowing me to seek the answers to my own questions, Gerard has been very honest and I feel really fortunate to have had him as my supervisor. Special thanks to my second supervisor Dr. Lynn Paterson for all her help and support. I would also like to thank Dr. Lesley Forrester at University of Edinburgh, MRC centre for inflammation research, for her close collaboration and fruitful discussions. Dr. Forrester and her whole team have been very kind in providing cells and materials required in my project, also by giving me an opportunity to work in their lab and learn stem cell culturing and guiding me in the right direction. In particular, I would like to thank the lab manager Miss Helen Taylor at Edinburgh University, who has constantly helped me solve problems related to tissue culturing and I am grateful to her. Special thanks go to Dr. Stephen Euston, School of Life Sciences, Heriot Watt University for allowing me to work on his confocal microscope whenever required and more importantly trusting me with his equipment. In this regard, I would also like to thank Dr. Rory Duncan, who helped me with image analysis.

Additionally, I greatly appreciate the help from Dr. Anil Sebastian, postdoctorate researcher at Manchester University, for mentoring me at the early stages of my research. I am thankful that he taught me the fundamental basics and gave me motivation whenever I was lacking. I also had many useful conversations with research students including Allan Roy (MSc. Mathematics, Heriot Watt University), Dr. Rama Yusvana (Research associate at Glasgow University), Miss Ankita Singal (Researcher, The University of Manchester), Manuel Garcia-Albornoz (Researcher, Heriot Watt University), Mohammed El-Shaib (Researcher, Heriot Watt University) and William Ramsay (Researcher, Heriot Watt University).

I would like to give special thanks to the wonderful warden team as they made my made my stay at Heriot Watt University very pleasant. I would like to thank the director of student support and accommodation, Mrs. Christine Johnston for selecting me as a part of the brave warden team and Miss Dalila Capao (Researcher and senior warden at Heriot Watt University) and Robert James Colhoun (Deputy senior warden and student at Heriot Watt University) for being so supportive during my role as a warden. This was a huge opportunity to develop my leadership skills and enhanced my overall personality.

I would like to thank all my friends for pepping me with their talks and boosting my morale; Adnan, Shariq, Mariam, Bill, Mohammed, Tripti, and Adil for cheering me in tough times.

Last but not at the least, I am grateful to my parents. Words cannot express how much I thank them for their continuous support through my postgraduate research. It was not easy for my mother to send me far away from her for such a long time. Their patience was an inspiration for me.

With Deepest Gratitude,

Sneha Agarwal

TABLE OF CONTENTS

TOTAL NUMBER OF WORDS: 37, 080

LISTS OF TABLES AND FIGURES

LIST OF ABBREVIATIONS

2-D	Two-dimensional
3-D	Three-dimensional
ºC	Degree centigrade
µm	Micrometer
µl	Microliter
µm s^{-1}	Micrometer per second
µg ml^{-1}	Microgram per millilitre
AC	Alternating current
AGM	Aorta gonad mesonephros
BM	Bone marrow
bFGF	Basic fibroblast growth factor
BMECs	Bone marrow sinusoidal endothelial cells
BMP	Bone morphogenetic protein
Bry	Brachyury
$CaCl_2$	Calcium chloride
CCD	Charged-coupled device
cm^2	Centimeter square
CO_2	Carbon dioxide
DAH	Differential adhesion hypothesis
DC	Direct current
DEP	Dielectrophoresis
DNA	Deoxyriboneucleic acid
DP	Dermal papillae
EBs	Embryoid bodies
ECM	Extra cellular matrix
EDTA	Ethylenediaminetetraacetic acid
EGFR	Epidermal growth factor receptor
ESCs	Embryonic stem cells
FBS	Fetal bovine serum
FCS	Fetal calf serum
FGF	Fibroblast growth factor
GAGs	Glycosaminoglycans

GFP	Green fluorescent proteins
GJIC	Gap junction intercellular communication
GMEM	Glasgow minimal essential media
GSCs	Germline stem cells
HEPES	N-2-Hydroxyethylpiperazine-N'-2-Ethanesulfonic Acid
hMSCs	Human mesenchymal stem cells
HOT	Holographic optical tweezer
HSCs	Hematopoietic stem cells
Hz	Hertz
iPSC	Induced pluripotent stem cell
IRS	Inner root sheath
ITO	Indium tin oxide
kg	Kilogram
kHz	Kilo Hertz
LED	Light emiting diode
LIF	Leukemia inhibitory factor
LIFR	Leukemia inhibitory factor receptor
MEMS	Microelectromechanical systems
MHz	Mega Hertz
Mins	Minutes
mm	Millimeter
mM	Millimolar
mL	Millilitre
MRI	Magnetic resonance imaging
MSC	Mesenchymal stem cells
MPPs	Multi potent progenitors
PBS	Phosphate buffered saline
NSCs	Neural stem cells
NPCs	Neural progenitor cells
OT	Optical tweezer
Oct-4	Octamer-binding transcription factor 4
ORS	Outer root sheath
PEG	Polyethylene glycol
PGA	Polyglycolic acid

PGCs	Primordial germ line cells
PTH	Parathyroid hormone
RAs	Retinoic acid
RBC	Red blood cell
RNA	Ribonucleic acid
ROI	Region of interest
RPM	Revolutions per minutes
RPMI	Roswell park memorial institute
SAOS-2	Sarcoma osteogenic
SG	Sebaceous glands
SVZ	Subventricular zone
TE	Tissue engineering
TGF	Tumor growth factor
TVP	Textured vegetable protein
V_{pk-pk}	Voltage peak to peak
WBC	White blood cells
YS	Yolk sac

CHAPTER 1

Preface to the thesis

1.1 General introduction

Haematopoietic stem cells (HSCs) are cells that are capable of self-renewal and forming all types of blood cells that can be found in an adult (Spangrude *et al.*, 1988). The hematopoietic lineage is one of the earliest to arise in mammalian development, being specified from the first set of mesodermal precursors generated by gastrulation. Gastrulation is this process in the early phase in embryo formation during which a single layered blastula organizes itself into three germ layers namely ectoderm, mesoderm and endoderm, the structure collectively termed as gastrula. The tiny number of hematopoietic founder cells in the murine embryo makes molecular and cellular analysis difficult (Kyba and Daley, 2003). Conventional sources of HSCs are therefore bone marrow and umbilical cord blood, from which HSCs can be derived in relatively large numbers. Adult-derived HSC can be induced to form blood *in vitro*, but unfortunately they cannot be induced to self-renew. Embryonic stem cells (ESCs), however, can be grown in large numbers and differentiated synchronously. ESC can be induced to form hematopoietic stem cells, and the induction of mature blood cells ESC-derived HSCs could potentially provide an inexhaustible supply of blood cells. ESC-derived HSCs also have a number of other advantages over HSCs from conventional sources. ESC derived HSCs would be more immature compared to bone marrow derived HSCs, enabling more efficient production of specific blood types. ESC may eventually be derived by reprogramming of somatic cells, overcoming ethical issues, making the blood produced patient-specific, and giving less immunological response. The unlimited expansion of ESCs not only allows large absolute numbers of HSC to be generated but also enables the replenishment of banked samples (Sudo *et al*., 2000).

Unfortunately, although HSCs can be derived from ESCs, and different types of blood cells from HSCs, our ability to control the differentiation process is not yet very good. The problem is that many different factors can affect the fate of stem cells. These factors could be chemical signals including soluble factors (such as growth factors, chemokines, cytokines), direct cell-cell and cell-matrix interactions or physical forces like mechanical stresses and strains or even electric impulses (Underhill and Bhatia, 2007). Various studies are now being

done to investigate the behaviour of stem cells in response to these factors. Altering any factor could affect the behaviour of stem cells, but investigations are difficult because of the time-dependent and multi-factorial behaviour of many of the responses.

For stem cells to achieve their potential in regenerative medicine it is thus necessary for scientists to be able to not only isolate them efficiently, but also to propagate them in culture and then differentiate them efficiently and completely into many different cell types. In order to do so it is important to understand how stem cells interact with other cells, not only *in vivo* in their natural microenvironment, the so called stem cell niche, but also *in vitro* (Fuchs *et al*., 2004).

1.2 Aim of the project

The aim of the project is to create an artificial embryonic stem cell microniche for the in-vitro investigation of the factors that affect stem cell behavior, and study the long term behavior of the cells in it.

It has previously been shown that an AC technique dielectrophoresis can be used to make aggregates of cells which can act as artificial stem cell niches (Markx *et al.*, 2008). This technique will be used in this project to make artificial stem cell microniches for HSC production. Study of the fate of stem cells in these artificial micro niches could be extrapolated to assess in vivo situations. Manipulation of stem cells accordingly could have therapeutic significance for curing many diseases.

1.3 Objectives of the project

To achieve the aim of the project, the following objectives will have to be met:

1) Optimise conditions for niche construction.

How to construct artificial stem cell microniches using dielectrophoresis (DEP) is already known from previous work (Venkatesh & Markx, 2007; Sebastian *et al.*, 2007; Markx *et al.*, 2008). However, the long-term study of cell behaviour in artificial stem cell microniches has not been studied. Procedures for the formation of optimal aggregates and their immobilisation need to be established before their long term study can be explored.

2) Study long-term behaviour of ESC in aggregates formed by DEP.

Murine embryonic stem cells were chosen for this study because of their easy accessibility and the availability of many genetically modified (GM) markers cells and protocols. In absence of leukaemia inhibitory factor (LIF) murine ESCs form EBs. The effect of different factors on EB formation will need to be studied, including growth factors such as LIF, aggregate size and surface treatment.

3) Study long-term behavior of support cells in aggregates formed by DEP.

Support cells are cells that are not directly involved in blood production, but have still have a role in it. For this study osteoblasts were chosen as support cells in the artificial stem cell niches. The behavior of cells when co-cultured in 3D aggregates formed by DEP will need to be studied and depending upon the adhesive-cohesive properties of different cells in question, the niche construction would be determined. The diffusion co-efficient of the cells could give an idea of how quickly the cells would diffuse out from an aggregate.

4) Study the long-term behavior of cells in aggregates formed with DEP containing both ESC and support cells.

Using DEP aggregates can be made with different architectures. Changes in the position of the cells after the formation of the aggregates with DEP will need to be studied, and the architecture that gives the largest amount of cell-cell interaction determined.

5) Study of differentiation (whether cells differentiate, and along which lineage).

GM ESC marker cells (Brachyury ESCs) can be used to determine whether the cells differentiate along the HSC lineage.

6) Combining dielectrophoresis and optical tweezers for future investigation of stem cell commitment to their fate.

When a stem cell is placed in an artificial niche it receives signals from within its niche which may put it on a different developmental path; its fate may therefore change over time. Moving the stem cell from its niche to other niches could be used to determine whether the cell has committed to its new fate or whether it is just specified. Optical tweezers can be as a tool to move cells in between niches.

CHAPTER 2

Review of literature

2.1 Introduction to stem cells

The existence of stem cells was first postulated by the Russian histologist Alexander Maksimov in 1908 with their practical manifestation first demonstrated in bone marrow by McCulloch and Till at the University of Toronto in the 1960's (Becker *et al*., 1963; Siminovitch *et al*., 1963).

Stem cells are found in all multicellular organisms. They are unspecialised cells that have the capacity not only to produce other stem cells by way of mitosis but also to differentiate into specialised cells. Terminally differentiated cells, in contrast, cannot differentiate any further, are often unable to divide and may have short life spans. The unique abilities of stem cells, i.e. self-renewal and the formation of differentiated progeny, has led to strong interest in their exploration as regards the potential these cells harbour for medical applications.

Mammalian stem cells are often broadly divided into two types: embryonic stem cells and adult stem cells. The former are stem cells which have been isolated from very early embryos; often the term is used in reference to pluripotent stem cells isolated from the inner mass of blastocysts. Adult stem cells, on the other hand, are found in various tissues of more grown-up organisms (including children). A third type, fetal stem cells, is also sometimes mentioned and refers to stem cells which have been isolated from fetuses and associated tissues (e.g. placenta, umbilical cord and amniotic fluid). These cells have less developmental potential than embryonic stem cells.

2.2 Basic characteristics of stem cells

2.2.1 Stem cells are unspecialized

One of the fundamental properties of a stem cell is that it is devoid of any tissue-specific structures that allow it to perform specialized functions. Stem cells are divided into four categories based on the capacity of the cells to differentiate into other cell types.

Totipotent: Totipotent cells are capable of both forming completely new embryo and of developing into a new embryo. Such cells can create a complete viable organism (Scholer, 2007). A fertilized egg cell, and the cells formed from the fertilized egg cell after the first few divisions are examples of cells that are totipotent (Mitalipov, 2009).

Pluripotent: These are stem cells which can give rise to all the cell types found in the adult body (Scholer, 2007), i.e. the cells derived from any of the three germ layers of the embryo (Ulloa-Montoya *et al*., 2005), including heart muscle cells, blood cells or nerve cells. Embryonic stem cells isolated from the inner cell mass of blastocysts are pluripotent, but it is thought that some other cells (e.g. some cells isolated from bone marrow) may also be pluripotent. However, pluripotent stem cells lack the ability to develop into any of the extraembryonic tissues, such as the placenta.

Multipotent: Multipotent stem cells have the potential to develop into a number of somewhat closely related cell types (Scholer, 2007).

Oligopotent: Oligopotent stem cells can only differentiate into a very small number of different cell types (Scholer, 2007).

Unipotent: This variant of stem cells can produce only one type of cells (Scholer, 2007). They can be distinguished from non-stem cells through their capacity for self-renewal. An example is muscle stem cells which only produce muscles.

2.2.2 Stem cells are capable of renewing themselves and producing differentiated progeny

A stem cell is capable of renewing itself indefinitely whilst producing progeny that matures into more specialized organ-specific cells. Symmetric divisions give rise to identical stem cells which have equivalent properties to the original stem cell. Symmetric divisions lead to an expansion of the number of stem cells. However, if a division is asymmetric, one of the two daughter cells retains the stem cell characteristics whilst the other, the progenitor cell, takes the path of differentiation. The progenitor cell is destined to undergo a limited number of divisions which will produce more organ-specific cells. Said cells can undergo several cycles of cell division before terminally differentiating into mature cells (Beckman *et al*., 2007). A good example is blood formation. Cells found in blood include platelets,

erythrocytes, white blood cells and lymphocytes. These cells have limited life spans in the body. To replace them, the haematopoietic stem cell undergoes asymmetric division to produce a stem cell as well as a primitive progenitor cell (see Figure 2.1). The progenitor cell then divides rapidly and at the same time becomes increasingly specialized. This rapid division leads to an amplification of the number of cells which are produced from any given haematopoietic stem cell. The specialization, which occurs along specific lineages, ensures that cells of specific cell types are formed once the differentiation process has entered its final stages. What factors induce the haematopoietic stem cells to renew or differentiate along a specific lineage is currently the subject of intense investigation.

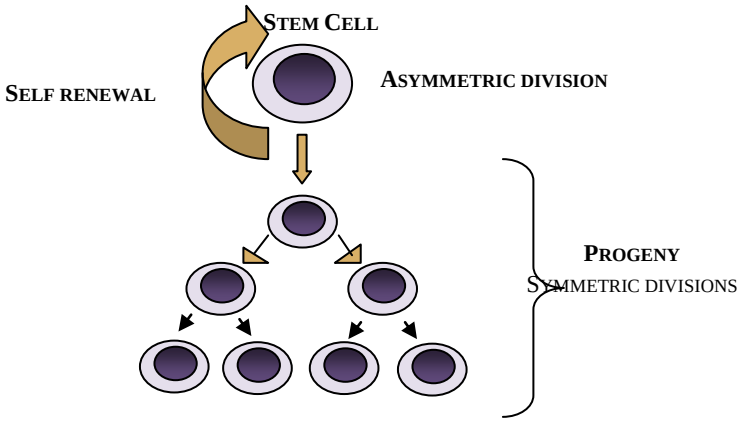

Figure 2.1: A model of stem cell division.

The stem cells divide asymmetrically, generating one cell that repeats the feature indefinitely and another that continues to divide symmetrically, dividing each time into two equal daughter cells.

Which cell type a stem cell differentiates into (i.e. its fate) is determined by a multitude of factors, both internal (intrinsic factors) and external (extrinsic cues). The asymmetric partitioning of cell fate determinants in the mother cell can produce daughter cells aligned to different cell fates, even though the two daughter cells reside in the same microenvironment (Watt and Hogan, 2000). External signals for cell differentiation include chemicals secreted in the medium by other cells, physical contact with neighboring cells, physical contact with surfaces and other factors. As many factors contribute to the fate of a cell, it can prove difficult to ascertain the effect of any individual factor.

2.3 The stem cell niche

The concept of a stem cell niche arose from the observation that many adult stem cells lose the potential to continue self-renewal when removed from their habitual cellular

environment, and that different signalling microenvironments can direct daughter cells to adopt different fates (Schofield, 1978; Morrison *et al*., 1997).

The precise spatial organisation of the stem cells with respect to the surrounding support cells plays an important role in the ability of the niche to adequately provide proliferative and anti-apoptotic signals and to exclude factors that promote differentiation. In either case, the stem cells are in intimate contact with surrounding support cells which serve as a source of critical signals controlling stem cell behaviour. Adhesion between stem cells and either an underlying basement membrane or the support cells themselves appears to play a significant role in harnessing the stem cells within the niche and close to self renewal signals. In addition, the niche could provide polarity cues to orient stem cells within its confines, so that, upon division, one cell is displaced outside the niche and into an alternative environment which encourages differentiation (Deng and Lin, 1997; Yamashita *et al*., 2003).

Some examples of stem cell niches that can be found within mammalian tissues

Specialised niches have been proposed to regulate the behaviour of stem cells in several mammalian tissues including the male germline, the epidermis, the intestinal epithelium and the hematopoietic system.

2.3.1 Mammalian testis

The seminiferous tubules of the mammalian testis are the site of spermatogenesis in the adult. Figure 2.2 shows the organisation of germ cells and somatic cells within a seminiferous tubule. In males, a Primordial Germ-line Cell (PGC) is known as a gonocyte. At the embryonic stage, the PGCs divide and migrate to the genital ridges. Gonocytes (spermatogonia) are found at the basement membrane of the seminiferous tubules where they differentiate into spermatogonial stem cells. Spermatogonia are presumptive stem cells which are found in the vicinity of supporting somatic cells known as the sertoli cells and the myoid cells. These cells may contribute to the stem cell niche (Brinster, 2002).

When spermatogonial stem cells were taken from a fertile mouse and transplanted into the seminiferous tubules of an immunodeficient mouse recipient they were able to migrate through layers of differentiating germ cells and sertoli cell tight junctions to find the stem cell

niche at the basement membrane and were also able to establish colonies of donor-derived spermatogenesis (Clouthier *et al*., 1996; Shinohara *et al*., 2001).

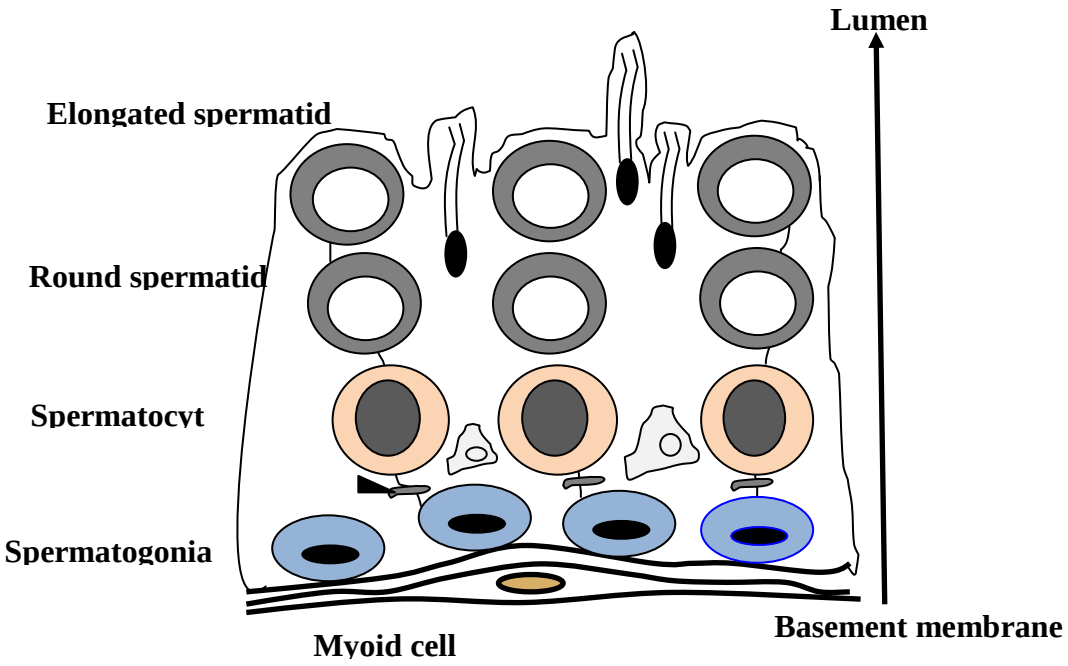

Figure 2.2: Organisation of germ cells and somatic cells within a seminiferous tubule (Caires et al. 2010)

2.3.1.2 Mammalian epidermis

Skin has a well-organised structure which provides an excellent platform from which to study the molecular mechanisms that regulate the stem cell self-renewal, proliferation, migration and lineage commitment (Fuchs and Serge, 2000). The mammalian epidermis is comprised primarily of keratinocytes, a subpopulation of which is the stem cells. The stem cells form a layer which is a single cell thick at the interface between the dermis and the epidermis. They are in continuous contact with a protein layer, the basal lamina, which provides signals that are thought to maintain stemcellness. Stem cells that divide either stay in contact with the basal lamina, or leave it. Stem cells that are no longer in contact with the basal lamina undergo terminal differentiation into keratinocytes. Skin is also home to various appendages, including hair follicles. Each hair follicle is composed of an area which includes sebaceous glands and the bulge area lying underneath (Figure 2.3). It undergoes developmental cycles consisting of an anagen phase (period of active growth), catagen phase (apoptosis-driven retraction), and telogen phase (a short period of rest) (Hardy, 1992). The bulge area functions as a stem cell niche (Niemann and Watt, 2000) where follicular epidermal

stem cells are maintained and harboured (Cotsarelis *et al*., 1990; Sun *et al*., 1991). These stem cells are multipotent. They produce progeny that can differentiate into interfollicular epidermis and sebocytes and contribute to all the differentiated cell types involved in the formation of the hair follicle, including the outer root sheath, inner root sheath and the hair shaft (Oshima *et al*., 2001; Ghazizadeh and Taichman, 2001).

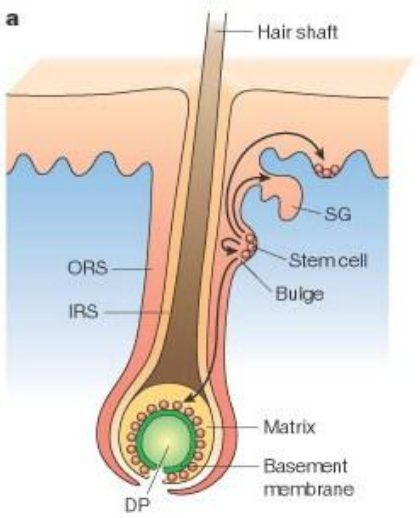

Dermal papilla (DP), Inner root sheath (IRS), Outer root sheath (ORS)

Figure 2.3: Mammalian epidermal stem cells.

A hair follicle and a segment of adjacent skin are illustrated. Approximately two-thirds of the way up an anagen follicle lies the bulge — an expanded region that contains long-term stem cells (red). These cells periodically replenish (arrows) the matrix cells, and also help maintain the Sebaceous Gland (SG) and the epidermal stem cells (red, top layer) which lie against the basement membrane (not shown) overlying the basal layer in interfollicular regions.

Source: http://www.nature.com/nature/journal/v414/n6859/fig_tab/414098a0_F5.html

2.3.1.3 Gut epithelium

Within the small intestine, the epithelial lining forms numerous crypts or finger like invaginations called villi. In the colon, there are many crypts which vary in size throughout the colon. Four main epithelial cell lineages exist in the colon, these being: columnar cells, mucin-secreting cells, endocrine cells and paneth cells (in the small intestine). Goblet cells containing mucin granules are found throughout the colonic epithelium, secreting mucus

throughout the lumen. It is hypothesised that all differentiated cells in the gastrointestinal epithelium originate from a common stem cell located in the intestine. Evidence suggests that the stem cells are situated at the base of the crypt of Lieberkuhn, in the small intestine, just above the paneth cells (Figure 2.5). In the large intestine however, they are located at the midcrypt of the ascending colon and the crypt base of the descending colon. The multipotent stem cells may reside at the base of the crypt to offer protection against toxins passing through the gut lumen. Crypts serve as a niche to support the stem cells, whilst also providing an environment to support the self-renewal of the intestinal stem cells. The cells lying close to the intestinal stem cells could be the source of the signals. As the stem cells differentiate into intestinal cells they migrate into the lumen of the gut. Around 200-300 cells leave the crypt into the ciliated villi of the lumen per day.

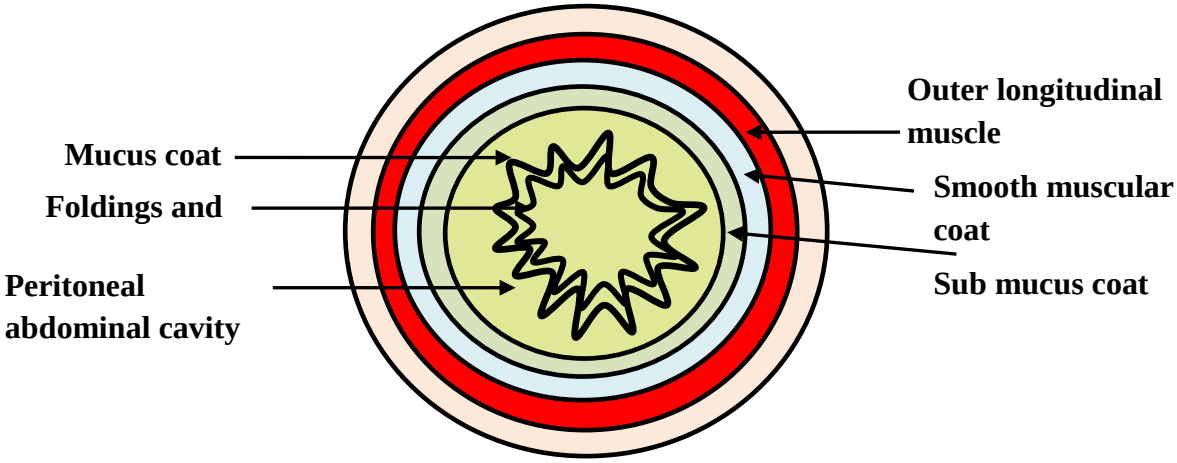

Figure 2.4: Transverse section of the gut.

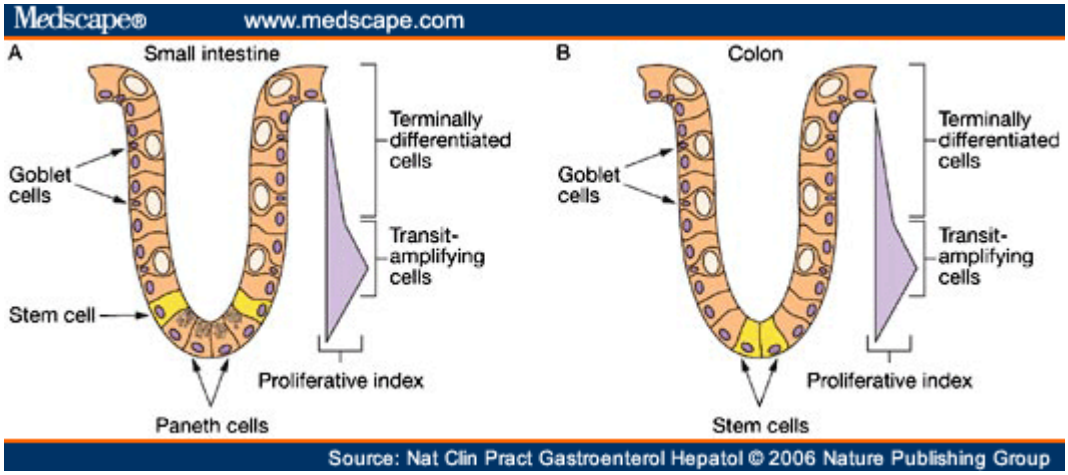

Figure 2.5: Schematic of the small intestinal and colonic crypts showing the location of the stem cells.(*A) In the small intestine, stem cells are thought to be located at position 4-5 distal to the Paneth cells. (B) In the colon, they are at the base of the crypt.*

Source: http://www.medscape.com/viewarticle/532504_3

2.3.1.4 Neural system

Neural stem cells have the capacity to self-renew and produce precursors which will differentiate into both neurons and glia. They have been isolated from the Sub-Ventricular Zone (SVZ) and hippocampus of the adult brain, but suggestions have been made that neural stem cells are not only located in the adult brain but also distributed throughout the adult central nervous system. When cultured *in vitro*, neural stem cells can generate free-floating spherical clusters called neurospheres, which contain mixed populations of stem cells and precursor cells. Growth factors such as FGF-2 and EGF have been found to support the growth of neurospheres (Penvy and Rao, 2003; Lois and Alvarez-Buylla, 1994), although it is not yet known whether these molecules also play a role *in vivo*.

2.3.1.5 The Hematopoietic system

The process of blood production is known as hematopoiesis. In adults, this process requires the replenishment of 7×10^9 blood cells per kg of body weight per day. All blood cells are ultimately derived from Haematopoietic Stem Cells (HSCs). It is thought that the whole body may contain no more than a few million HSC and, in some cases, as little as a few thousand (McCarthy, 2003). Blood contains a variety of different blood cells, including erythrocytes, platelets and a wide range of white blood cells of the lymphoid and myeloid lineages, which ultimately all derive from HSCs (Figure 2.6). The hematopoietic system achieves this remarkable feat by strongly regulating HSCs self-replication and differentiation, and amplification of the initial HSC differentiation by repeated division of progenitor cells. Haematopoiesis occurs in different anatomical sites during the different stages of development of an organism (Cumano and Godin, 2001; Mikkola and Orkin, 2006; Kaplan *et al*., 2007). The following sections will elaborate further on the hematopoietic stem cell niche.

.

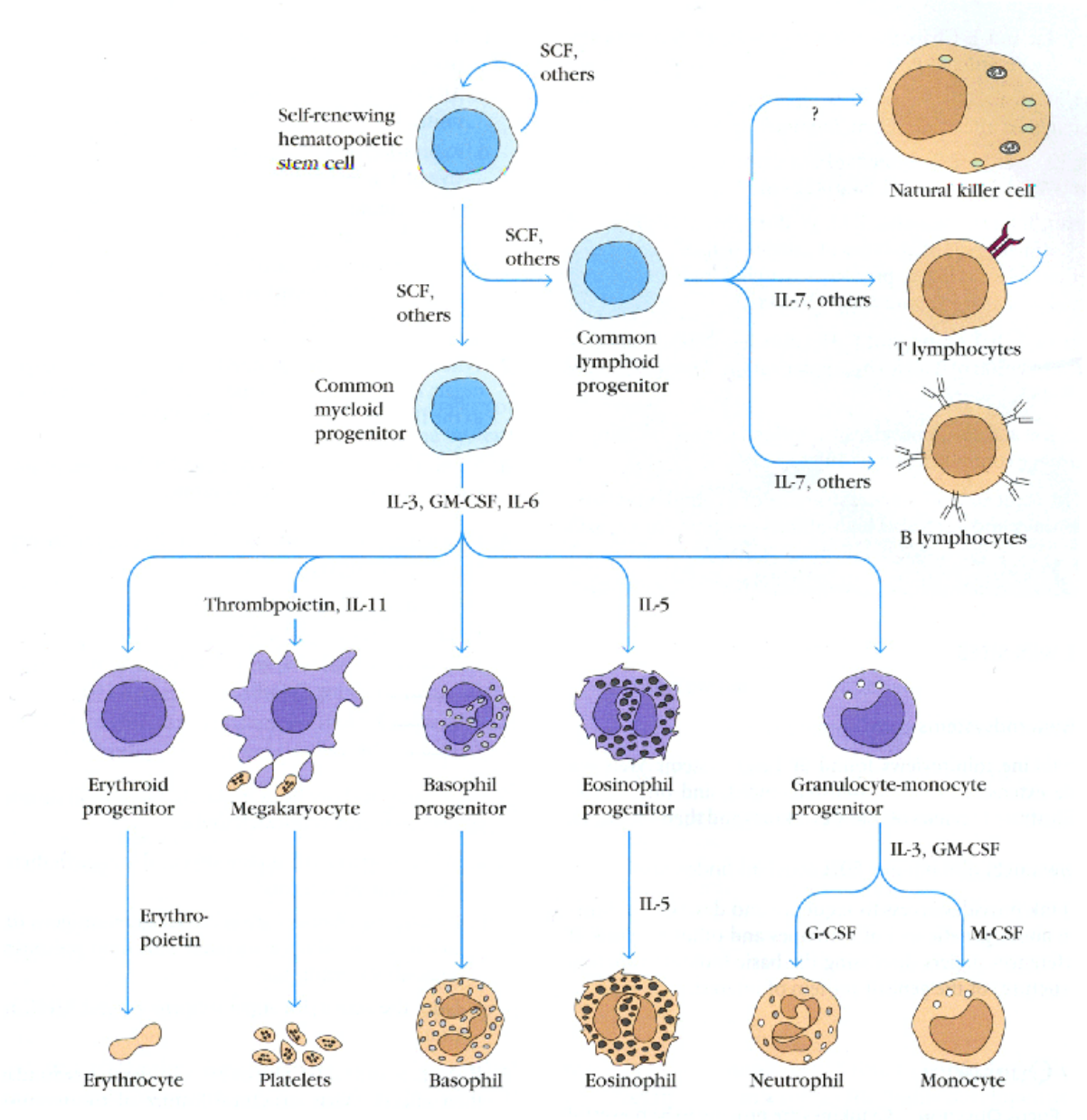

Figure 2.6: Hematopoiesis.

A hematopoietic stem cell is affected by various growth factors to initiate differentiation into different mature blood cell types.

Source:
http://www.d.umn.edu/~jfitzake/Lectures/DMED/CytAnt/Cytokines/HematopoieticAgents.html

2.4 Introduction to HSC niche

The hematopoietic stem cell niche is the anatomical location in which the HSCs both reside and self renew. Maintenance of these HSCs and regulation of their self renewal and differentiation *in vivo* is thought to depend on their specific microenvironment, which has been

historically referred to as the haematopoietic inductive microenvironment (Curry *et al*., 1967) or 'stem–cell niche' (Schofield, 1978). Once the HSCs are outside their niche they cease to self-renew, instead commencing the process of differentiation to produce mature blood cells. Little is known regarding the HSC niches in the liver and placenta. However, interest has been strong in the AGM niche (as it may give clues on how HSC may be derived from embryonic stem cells) and the HSC niches in bone marrow (because it may tell us how the various blood cell types are formed, and why things sometimes go wrong e.g. in leukemia, contributing to greater insight into how bone marrow transplants can be better performed).

During the lifetime of an organism, two separate hematopoietic systems exist. Both arise during embryonic development, although only one persists throughout the lifetime of an organism. The primitive system develops first. It emerges in the extraembryonic yolk sac and is characterized by the presence of nucleated erythroid cells which carry oxygen to the developing embryonic tissue. Primitive haematopoiesis leads to nucleated erythrocytes which express embryonic haemoglobin and do not require erythropoietin for differentiation (Cumano & Godin, 2001). The haematopoietic system in adults does not appear to be derived from the primitive haematopoietic system in the yolk sac. Instead, adult-type or definitive haematopoiesis appears to develop separately in the aorta-gonad-mesonephros (AGM) region (Ohneda *et al*., 1998; Takeuchi *et al*., 2009), where it can first be detected at day 10.5. It is characterised by the formation of enucleated erythrocytes and adult-type hemoglobin and cells of all the myeloid and lymphoid lineages; later differentiation and maturation stages are controlled by erythropoietin (Cumano & Godin, 2001). Definitive haematopoiesis first emerges in a region of the para-aortic splanchnopleural mesoderm containing the dorsal aorta, gonadal ridge and mesonephros, referred to as the Aorta-Gonad-Mesonephros or AGM region. During the latter stages of embryonic development, definitive haematopoiesis moves to the fetal liver (Takeuchi *et al*., 2009); and the fetal spleen, some haematopoiesis also occurs in the placenta (Rhodes *et al*., 2008; Gekas *et al*., 2010). Near birth the bone marrow (BM) becomes the main centre of haematopoiesis (Figure 2.7 and 2.8).

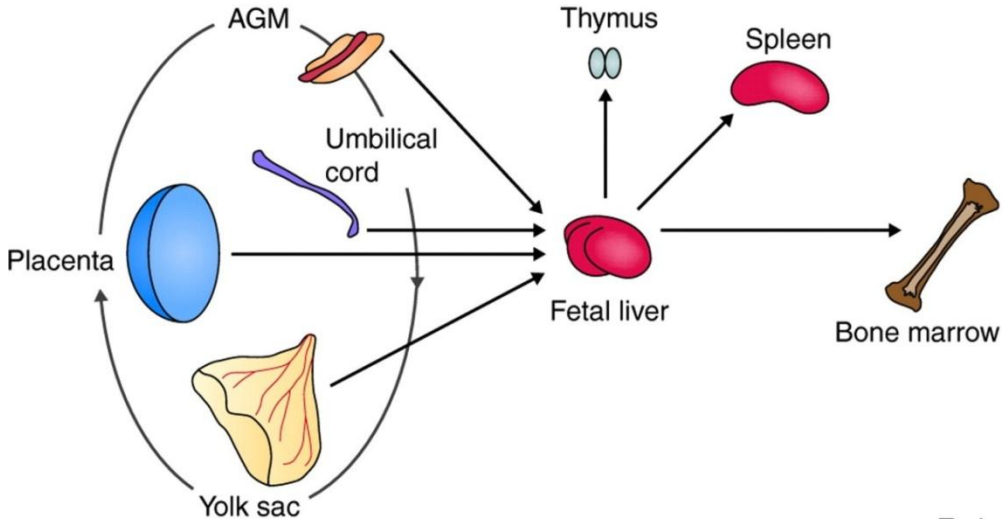

Figure 2.7: The route of definitive Hematopoietic Stem Cells (HSCs).

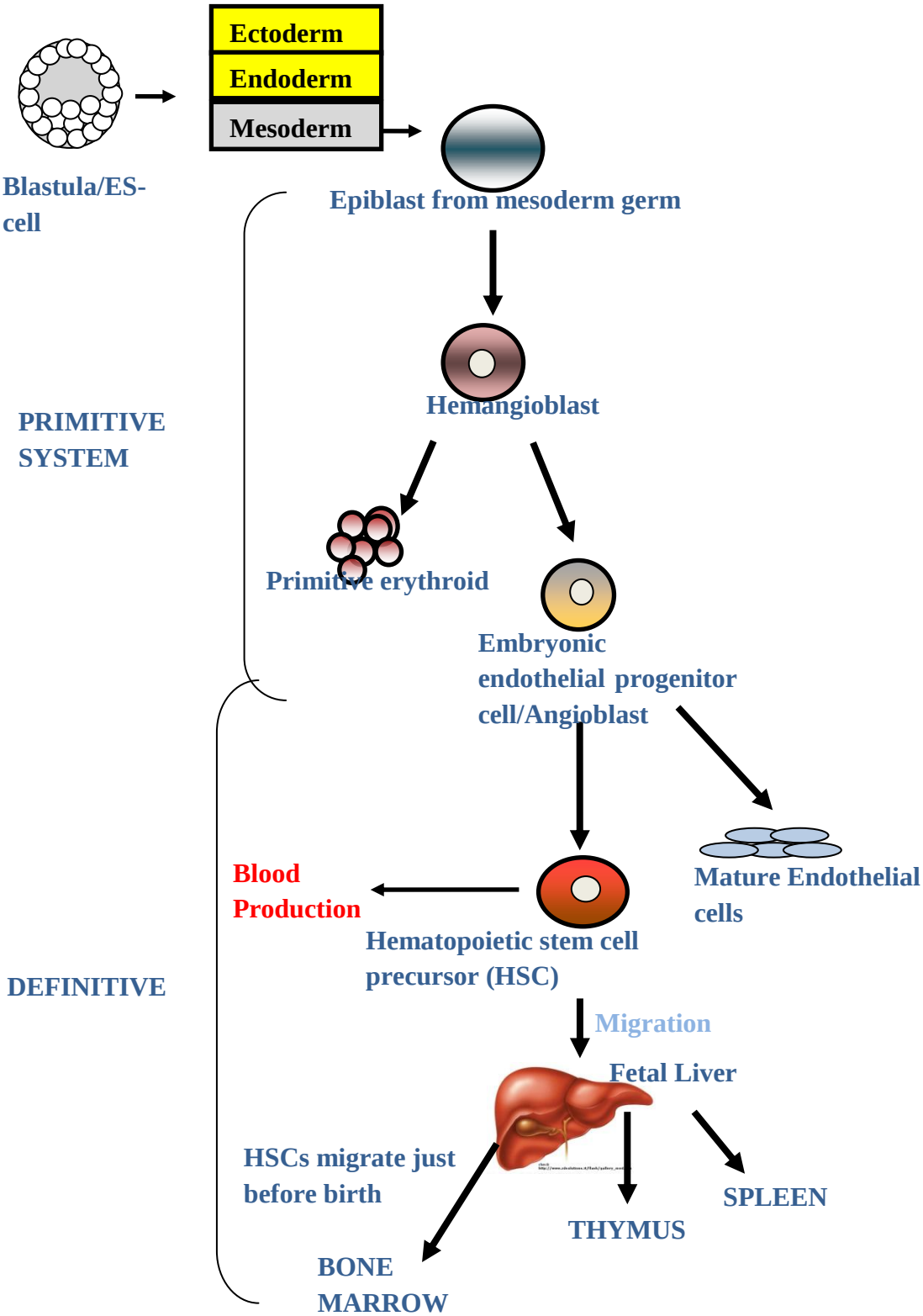

Figure 2.8: A pictorial presentation of an HSC migration from a primitive system to a definitive system.

2.4.1 Bone marrow architecture

BM tissue fills the cylindrical cavities of long bones and occupies the spaces of cancellous bones. The BM consists of the HSCs and their offspring, reticular cells, adipocytes, macrophages, fibroblasts and their fibrils and a network of blood vessels including the sinusoids (Wickramasinghe *et al*., 2003). The bone marrow can be subdivided into a hematopoietic cell compartment and the stroma, which is mainly composed of fibroblasts, adipocytes, nerves and the BM's vascular system (Fliender *et al*., 2002). The hematopoietic tissue is localized in the extravascular compartment (Figure 2.9). Early myeloid precursors lie close to the endosteal surface and the arterioles. Megakaryocytes and erythropoietic islands are seen to be associated with the marrow sinusoids in the central region of the marrow cavities (Thiele *et al*., 1993). The BM sinusoids are unique and cannot be compared to normal veins. The sinusoidal walls consist of a single layer of endothelial cells and are devoid of any supporting cells. This lack of a regular vessel wall makes the sinusoids highly permeable, facilitating the movement of the newly produced blood cells into the blood stream. Nerve fibers are associated with these blood vessels and are the source of various chemotactic factors which aid in the migration of mature cells from the marrow to the peripheral blood.

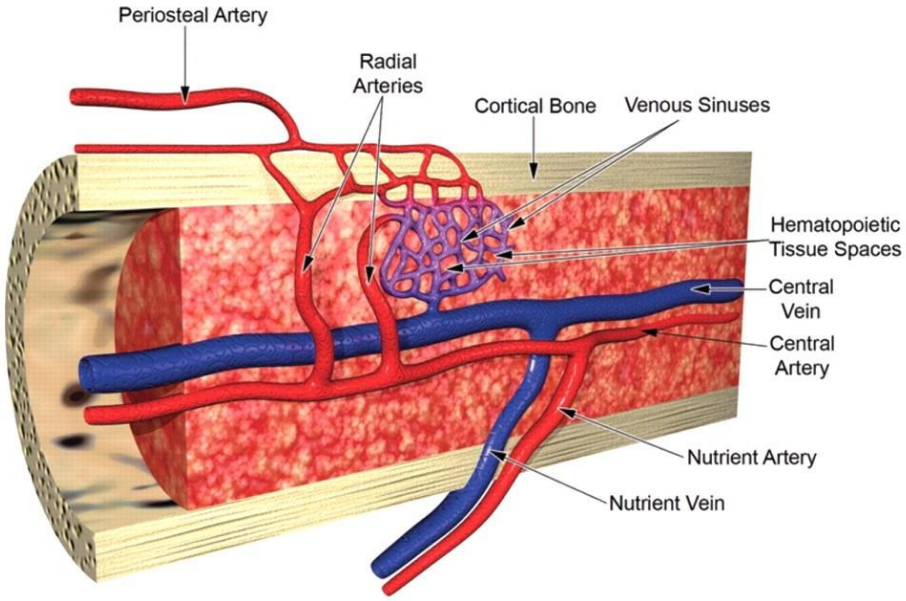

Figure 2.9: Vascular blood supply in the bone marrow (Travlos, 2006).

2.4.2 HSC niches in bone marrow

A large body of evidence suggests that HSCs are not randomly distributed in the BM. Rather, higher concentrations are found close to the endosteum of the bone (Calvi *et al*., 2003;

Fliedner *et al*., 2002; Lord *et al*., 1975) and in association with the vascular system (Kiel *et al*., 2005; Palmer *et al*., 2000; Shen *et al*., 2004). It has therefore been proposed that at least two niches exist in bone marrow (Li and Yin, 2006). One such niche is found close to the endosteum of the bone and is characterized by the presence of osteoblasts. Said niche is hence known as the endosteal or osteoblast niche. The other is found close to the sinusoids of the bone marrow's vascular system and is known as the vascular or the endothelial niche. How the HSCs migrate from the homing niche (endosteal niche) to the vascular niche is shown in Figure 2.10.

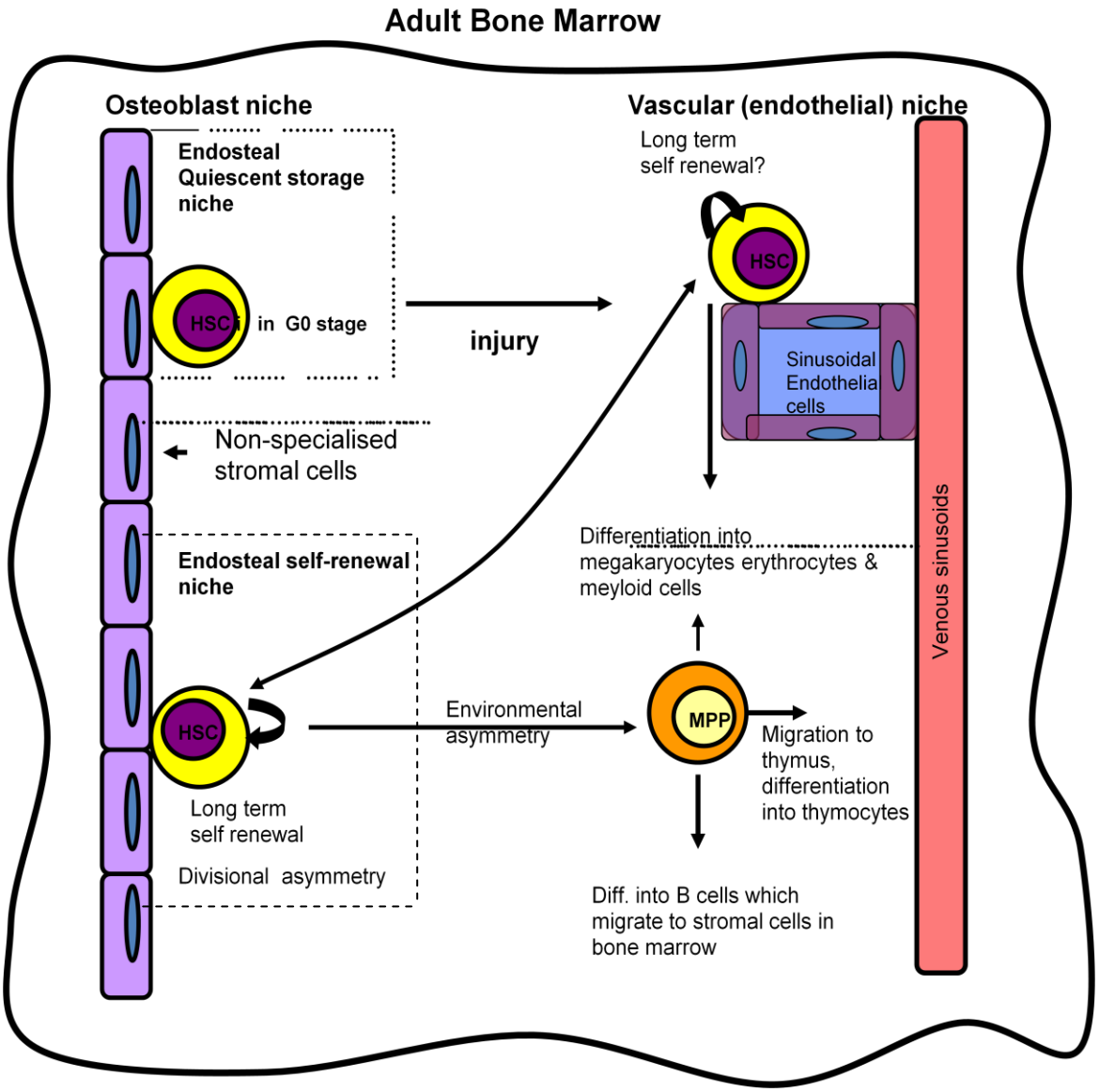

Figure 2.10: Model of bone marrow niches.

The endosteal bone surface is lined with stromal cells which serve niche HSC cells in maintaining quiescence and preventing differentiation of attached HSC cells. In response to injury, quiescent cells might be activated and recruited to the vascular niche. The endosteal

self renewal niche produces Multi-Potent Progenitors (MPPs) either by division or by environmental asymmetry. Symmetric division of HSCs produce further HSCs which can potentially provide the vascular niche with new HSCs. HSCs within the vascular niche promote differentiation and expansion along megakaryotic or myeloid lineages in response to injury. MPPs give rise to all hematopoietic lineages, including B-cell precursors. Unidentified T-cell precursors migrate to the thymus, thereby entering a new microenvironment where T-cell maturation takes place.

2.4.2.1 The endosteal or the osteoblastic bone-marrow HSC niche

The mammalian bone marrow architecture places the HSCs in close proximity to the endosteal surfaces, with more differentiated cells arranged loosely towards the central longitudinal axis of the bone (Emerson and Zhu, 2004). The weight of evidence suggests that HSCs are not randomly distributed in the BM but rather are localized close to the endosteum of the bone (Calvi *et al*., 2003; Fliedner *et al*., 2002; Lord *et al*., 1975). Two groups have verified the presence of this niche. Zhang *et al*. (2003) used a BMP receptor 1A conditional KO transgenic mouse to demonstrate that the down regulation of BMO signaling resulted in ectopic trabecular bone formation in the long bone and an increase in the HSC number. Calvi *et al*. (2003) investigated the endosteal niche using a transgenic mouse with constitutively expressed PTH and PTH-related receptors (PPRs) with a collagen-α1 promotor in osteoblastic cells. These PPR stimulated osteoblasts showed an increase in proliferation which correlated with an increase in the HSC number. Further verification of this niche was carried out by Arai *et al*. (2004) whose studies demonstrated that adhesion of HSCs to osteoblasts on the endosteal surface was essential in maintaining HSCs in a quiescent state. These works confirm that the osteoblastic niche provides signals for the maintenance of repopulating cells in an undifferentiated state (Calvi *et al*., 2003; Zhang *et al*., 2003; Arai *et al.*, 2004).

The osteoblasts lining the cancellous and trabecular endosteum serve as an essential location in the maintenance of HSCs. Although in practice multiple subsets of osteoblastic cells and mesenchymal progenitor cells constitute the endosteal niche (Nakamura *et al*., 2010), because of the prominence of osteoblastic cells in this niche the endosteal niche is also called the osteoblastic cells niche. The HSC and osteoblast relationship can be traced back to embryogenesis, where the HSC is derived from the mesodermal dorsal aorta with the bone precursors originating from the surrounding mesenchyme, therefore establishing a partnership

of the two tissues early in their development (Taichman, 2005). The osteoblastic niche provides the HSCs with a quiescent environment ideal for HSC maintenance.

2.4.2.2 The vascular niche

The vascular niche serves as a location which allows differentiation and ultimately mobilization to the peripheral circulation (Abkowitz *et al*., 2003). It is composed of at least two variants of cells: HSCs and the endothelial cells. During embryogenesis, both cell types follow a similar but distinct pattern in their development (Ueno and Weissman, 2006) as both lineages arise from the hemangioblast, a common embryonic precursor (Kiel *et al*., 2005). In adults, the endothelial cells contribute to the maintenance of HSCs *in vitro* (Li *et al*., 2004). *In vivo*, they are required for hematopoiesis (Avecilla *et al*., 2004). More recent work suggests that HSC niches are located around blood vessels (Kiel *et al*., 2005; Palmer *et al*., 2000; Shen *et al*., 2004). Ultra-structural studies suggest that mature rather than immature HSCs have close associations with the BM microvasculature (Shirota *et al*., 1991; Tavassoli *et al*., 1992). In contrast, vascular endothelial cells which are isolated from various adult non-haematopoietic organs have little or no ability to maintain HSCs *in vitro* (Li *et al*., 2004). Therefore, BM sinusoidal Endothelial Cells (BMECs) are functionally and phenotypically distinct from the microvasculature endothelial cells of other organs (Kopp *et al*., 2005). BMECs express cytokines such as CXC-chemokine Ligand 12 (CXCL12) and adhesion molecules such as endothelial cell selectin and Vascular Cell Adhesion Molecule 1 (VCAM1) which are important for HSC mobilization, homing and engraftment (Sipkins *et al*., 2005; Avecilla *et al*., 2004; Rafii *et al*., 1997).

The vascular niche thus represents an alternative niche for mobilized stem cells, promoting proliferation and further differentiation or maturation and their entry into the blood circulatory system. The sinusoids, which consist of single layered endothelial cells are designed for blood cell penetration, are also an ideal location for HSCs because they allow rapid response to hematopoietic stress or cytokine stimulation.

2.5 Introduction to stem cell fate

There are a range of different stem cell niches within the mammalian adult body. Each niche will have a different composition, will provide a different microenvironment for the stem cells, and has a different role to play in the maintenance of the organ wherein it is

present. The following sections will discuss the various factors within the microenvironment which could affect the fate of stem cells in their niches.

2.5.1 Factors determining the fate of stem cells

A complex set of signals from the cellular microenvironment determines stem cell fate. They include soluble factors present in the surrounding tissue or culture media, the composition of the Extra-Cellular Matrix (ECM), the biophysical environment and the presence of nearby cells which can elicit cell-to-cell signaling (Figure 2.11).

Cell signalling involves three steps: reception, transduction and response.

Reception of a signal involves a change in the receptor by the signal, for example the attachment or association of a chemical molecule to a protein in the plasma membrane.

Transduction is the conversion of the signal at the surface of the cell to a signal that mediates a specific intracellular signal that makes the cell respond. Signal transduction can involve many complicated steps.

Response varies according to the signals received by the cell. It involves turning on or off, one or many enzymatic activities. The response depends on a cell‘s particular collection of signal receptor proteins, relay proteins, and proteins needed to carry out the response (Campbell and Reece, 2002).

Together the factors act on the stem cells by both initiating and influencing a multitude of intracellular signaling pathways which ultimately govern whether a cell divides, differentiates, or dies (Metallo *et al*., 2007).

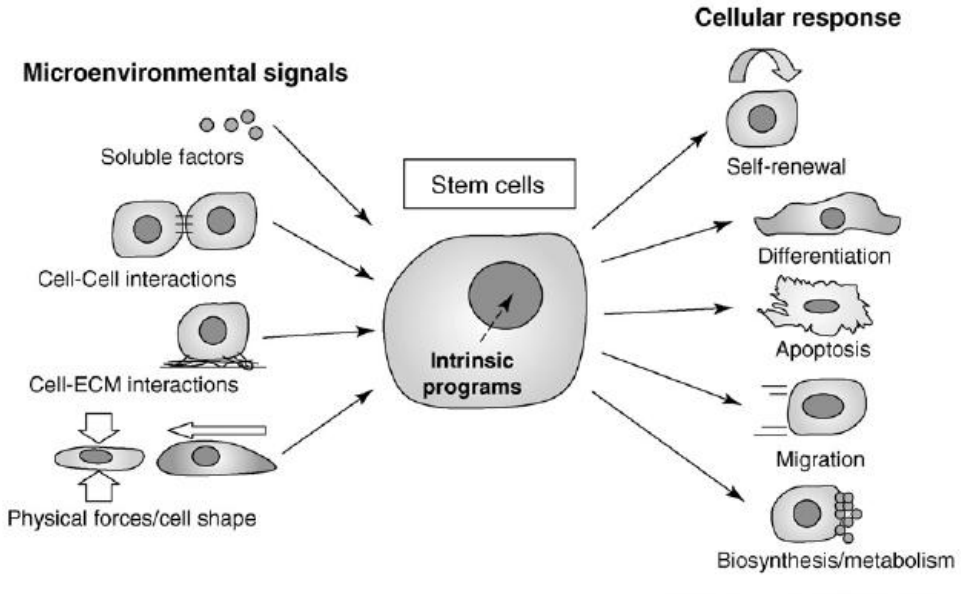

Figure 2.11: Interaction of the stem cells with different inputs from the microenvironment (Underhill and Bhatia, 2007).

2.5.1.1 Soluble chemical signaling molecules

Soluble factors play crucial roles in determining the fate of stem cells and are probably the best characterized environmental signals impacting stem cell behavior (Metallo *et al.*, 2007). They are easily isolated, produced and (re)introduced. Growth factors and morphogens can exert potent long term effects in the stem cell microenvironment. Their downstream signal transduction pathways are the best characterized determinants of stem cell fate and have been extensively used in *in vitro* stem cell culture systems.

Studies have shown that *in vivo* growth factors and morphogens are immobilised to the extracellular matrix by binding to specific hairpin–binding domains or directly to ECM molecules such as collagen or fibronectin. Also, they can be directly anchored to cell membranes (Rider *et al.*, 2006). These effects have been used to immobilise cytokines in high concentrations in the vicinity of the cell surface, and to reduce the levels of growth factor necessary to elicit a potent cellular response (Li *et al.*, 2006; Saha and Schaffer, 2006).

An example of a soluble signaling molecule which affects stem cells is the Leukemia Inhibitory Factor (LIF). LIF is a class six interleukin cytokine affecting cell growth and development. It is traditionally expressed in the trophectoderm of the developing murine embryo with its receptor (LIFR) expressed throughout the inner cell mass. As embryonic stem cells are derived from the inner cell mass at the blastocyst stage, their removal from the inner

cell mass also removes their source of LIF. The function of LIF is to maintain the stemness of murine embryonic stem cells. Removal of LIF thus pushes ESCs into differentiation. Therefore, LIF is used in maintaining mouse ESCs cell lines *in vitro* cultures.

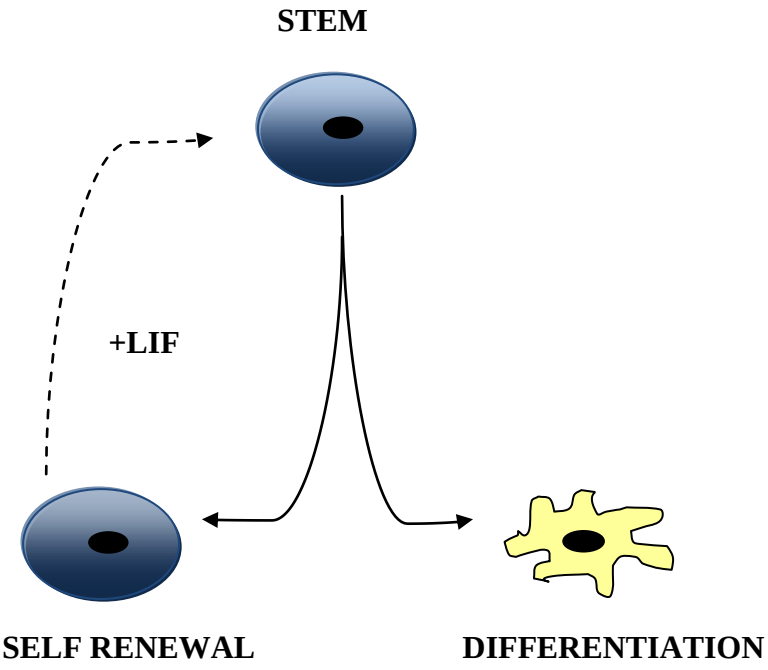

Figure 2.12: Characteristic role of Leukemia Inhibitory Factor (LIF) in embryonic stem cell self-renewal.

Some of the most important signalling molecules responsible for stem cell differentiation and the determination of the fate of cells are basic Fibroblast Growth Factor (bFGF or FGF2). bFGF is vital for the maintenance of neural stem cell population in the brain of the mouse (Zheng *et al.*, 2004). It can also enhance neural progenitor proliferation *in vitro* in several species (Ray *et al.*, 2006). bFGF was a key factor in the maintenance of human Embryonic Stem Cells (hESCs) in the undifferentiated state (Xu *et al.*, 2005). In the case of Mesenchymal Stem Cells (MSCs), bFGFs have been found to mediate the formation of various different phenotypes. The MSCs proliferate when bFGFs are added to the culture medium and they were also found to favour an osteogenic lineage (Sotiropoulou, 2006).

Transforming Growth Factor-β (TGF- β) is the growth factor molecule most frequently used by tissue engineers (Barry *et al.*, 2001). It induces a variety of responses in different stem cell lineages (Metallo *et al.*, 2007) and is used to stimulate stem cells in their transformation into chondrocytes.

All-trans Retinoic Acids (RAs) are strong differentiating agents involved in organogenesis and development (Niederreither, 2001; 2002). Fuchs (1981), during his work on human keratinocytes, discovered that these compounds prevented the terminal differentiation of epidermal stem cells. In 2005, Li *et al.* found that, *in vitro*, the RAs could direct neural stem cells to become neurons depending upon the concentration and the stage of development.

*In vitro s*oluble factors can be added independently or as a mixture. However, it has been found that a sequence of soluble factors can be used to program stem cell differentiation. The generation of functional motor neurons and pancreatic cells can be used as illustrative examples of how the sequential addition of soluble factors can be used to program stem cell differentiation. Differentiation of motor neurons from primitive ectoderm requires progression through two intermediate stages, each guided by a distinct set of soluble factors. Ectodermal cells first acquire an anterior neural fate through signalling by BMP, FGF and Wnt proteins (Munoz-Sanjuan and Brivanlou, 2002). The next transition involves the induction of a posterior fate in ectodermal cells by retinoic acid (Yamada, 1994). This is followed by progression to the formation of terminally differentiated motor neurons in the presence of Sonic hedgehog (Shh) (Briscoe and Ericson, 2001). In a landmark study, Jessell (2002) was able to guide mouse ESC down this pathway by applying the soluble factors involved in a step-by-step manner which emulates natural neural development, resulting in the *in vitro* generation of motorneurons that can survive and engraft *in vivo* (Wichterle *et al.*, 2002).

The development of the pancreas takes place as buds appear at two sites of the gut tube in the embryonic endoderm. To progress to the next stage of development, the embryonic mesoderm secretes Shh-antagonists (an inhibitor) (Hebrok *et al.*, 1998; Kim *et al.*, 1997). The pancreatic buds then grow and branch out; this is mediated by FGF10 (Bhushan *et al.*, 2001). This is followed by a formation of endocrine cells which is mediated by soluble signals from the surrounding endothelium which inhibit Notch signalling and initiate the expression of a cascade of transcription factors leading to the differentiation of insulin-producing cells (Gu *et al.*, 2004; Lammert *et al.*, 2001). When this sequence of signalling molecules was mimicked *in vitro,* scientists were able to generate functional insulin-producing cells from ESCs (D' Amour *et al.*, 2005; D' Amour *et al.*, 2006).

2.5.1.2 Cell and Extracellular Matrix (ECM) interactions

The Extra-Cellular Matrix (ECM) is the gel-like material which surrounds cells. The ECM not only serves to provide structural and organizational guides for tissue development but also defines and maintains cellular phenotypes and drives cell fate decisions. ECM also plays a critical role in defining cell shape, which in turn impacts upon cell survival (Huang *et al*., 1998), proliferation (Dike *et al*., 1999), and differentiation (McBeath *et al*., 2004).

ECM is composed of three major classes of molecules. These are:

- Structural proteins such as collagen and elastin;
- Specialized proteins such as fibronectin and laminin;
- Proteoglycans consisting of a protein core attached to long chains of repeating disaccharide units named glycosaminoglycans (GAGs) (Krause, 2002).

However, the actual composition of ECM varies within different tissues.

Adhesion of cells to the extracellular matrix is mediated by integrins. These are membrane proteins which span the cell membrane and act as receptors. The integrins bind not only with molecules in the extracellular matrix, but also associate with actin and intermediate filaments in the cell's cytoskeleton. They are thus able, not only to transmit information concerning the composition of the extracellular environment, but also, through their contact with the cytoskeleton, to impact upon cell shape, motility, metabolism and differentiation (Wolpert, 2007).

n example of a group of molecules in the ECM which influence cell differentiation, migration, adhesion and survival are the laminins. These are glycoproteins and can be found in almost every tissue of an organism. Laminins are major components of the basal lamina, a typical example being the protein layer between epidermis and dermis in skin. Signals from the basal lamina are necessary for the skin stem cells to maintain their stemness, while any loss of contact with the basal lamina will cause the skin stem cells to undergo a pathway of terminal differentiation into keratinocytes. Recombinant human laminin isoforms have been shown to support undifferentiated growth of human embryonic stem cells (Miyazaki *et al.*, 2008). Laminin has also been shown to play a role in the neural stem cell niche (Powell and Kleinman, 1997).

Array based methods have been employed in identifying the proteins (Soen *et al.*, 2006), peptides (Orner *et al.*, 2004), and polymers (Anderson *et al.*, 2004) in the ECM that are capable of directing stem cell fate. A common problem in stem cell work, however, is that stem cell substrates are often complex undefined mixtures. Therefore, recent work has focused on establishing synthetic matrices which will be capable of sustaining stem cell growth or differentiation (Metallo, 2007). Combining artificial protein engineering, molecular biology and recombinant deoxyribonucleic acid technology has made it possible to produce artificial proteins with functional domains derived from naturally occurring proteins. Because these matrices are synthetic, the exact composition is known and synthetic ECM can be formulated comprised of polymer backbones functionalised with adhesion motifs to dissect the mechanism by which ECM support stem cell fate decisions. Its future applications could include development of bioactive biomaterials, *in vitro* processing of stem cells before transplantation, and also supporting and programming the cells after transplantation.

The use of synthetic ECMs, has shown that the effect of a given growth factor can depend on the substrate background in which it is presented (Nakajima *et al.*, 2007). For example, in erythropoiesis, adhesion of primary erythroid progenitors to the niche ECM protein fibronectin is mediated by α4β1 integrin which is necessary for proliferation *in vitro* (Eshghi *et al.*, 2007). The signals from the ECM, therefore, cooperate with signals from the soluble factor erythropoietin to activate signaling pathways vital for terminal differentiation and proliferation.

Because of the direct link between the ECM and the cytoskeleton through membrane receptors such as the integrins, there is also a direct link between the mechanical properties of the matrix and stem cell fate (Ngalim *et al.*, 2010). Thus, differences in the mechanical properties of the substrate are known to influence the fate of a differentiated cell type (Discher *et al.*, 2005). For example, Engler (2006) studied the effect of matrix stiffness on MSC differentiation in non-inductive and tissue specific inductive media. Matrix stiffness by itself was shown to induce MSC differentiation when plated on matrices of different elasticities. Engler also showed that the soluble induction factors are less selective than the matrix stiffness in determining lineage specification. In tissue-specific inductive media, by matching the stiffness of the matrix to the cells, the level of various tissue specific protein marker levels could be raised to standards comparable to *in vivo* levels. Actin structures NMM IIA-C were likely to be involved in sensing matrix elasticity. It was not possible to reprogram MSCs that

were pre-committed for weeks on a given matrix. The overall result obtained was that, by controlling the thickness of the gel, one can establish how far stem cells can feel and their microenvironment could thus be defined (Engler *et al.*, 2006).

Straight and co-workers also showed that actin element NMM II was one of the other contributing factors in determining the fate of the cells. When the actin was inhibited by Blebbistatin it blocked differentiation of the cells (Straight *et al.*, 2003).

In vitro, the matrix elasticity can be mimicked with inert polyacrylamide gels. The elasticity of the gel is determined by a concentration of bis-acrylamide crosslinking (Pehlam and Wang, 1997). Mylona (2008) utilized substrates that were chemically identical but different in their physical parameter of rigidity. He showed that primary cells derived from human osteosarcoma responded to alterations in the mechanical properties of their substrate both morphologically and functionally.

2.5.1.3 Cell-cell interactions

In multicellular organisms cell-cell interaction plays an important role in the making of tissues, organs and the organism itself. Cell-cell interaction is one of the most important factors that affect the regulation of stem cell characteristics within the stem cell niche.
Cell-cell interactions can occur in three different ways.

1) Cell-cell interaction at a distance, in which the signals is transmitted through the extracellular space between cells. Typically these are chemical signals that can diffuse between cells.

2) Cell-cell interaction in which direct contact between the cells occurs, but there are no junctions between cells. Signals are transmitted by mediators on the cell surface.

3) Cell-cell communication via junctions directly linking adjacent cells. The signal passes directly from cell to cell.

Cell-cell interaction at a distance can occur at short range or at long range. At short range, soluble molecules, called local regulators, affect cells in the immediate vicinity only. Long range cell-cell communication is possible, however, via soluble molecules such as

hormones and growth factors. Soluble messengers are transported throughout the organism by the circulating blood but, only affect the cells that have the cognate receptors for that specific messenger molecule. The cell surface receptors bind to the messenger molecule and move it to the nucleus, where it affects the gene expression program of the cell. Within a local stem cell microenvironment, differentiated cells can express soluble proteins to exert negative feedback control over stem cell proliferation hence maintaining a balance of signals and cell type. For example a TGF-β family member was identified which inhibits neurogenesis in the olfactory epithelium, and it was subsequently shown that it was produced by differentiated neurons (Wu *et al*., 2003). Short range chemical signalling, also known as paracrine signalling, is also known to regulate human Embryonic Stem Cell (hESC) cultures. For example, when hESCs are grown in the absence of embryonic fibroblast or other feeder cells, they grow in heterogenous colonies which are composed of undifferentiated cells and hESC derived fibroblast-like cells which do not express ES cell markers (Stewart *et al*., 2006). Recent work has shown that fibroblast-like cells secrete factors necessary for hESC self-renewal (Bendall *et al*., 2007).

A typical example of cell-cell signalling in which signals are transmitted through direct contact between membranes is signalling through Delta-Notch interaction. Delta is a membrane-bound signalling molecule, whilst Notch is a membrane-bound receptor. Notch signalling is known to play a crucial role in the expansion of the hematopoietic stem cell compartment during bone development and participates in the commitment of mesenchymal cells to the osteoblastic lineage. Notch plays a leading role in hematopoietic stem cell maintenance and renewal (Nobta *et al*., 2005). Within the brain, there are locations where the Neural Stem Cells (NSCs) and the Neural Progenitor Cells (NPCs) are harboured. They are located in the sub-ventricular zone of the lateral ventricle and the dentate gurus of the hippocampus.

The Notch signalling pathway is known to maintain self-renewal and identity in NSCs within the brain and Epidermal Growth Factor Receptor (EGFR) affects the proliferation and migration of NPCs. Together, both signalling pathways help in maintaining the balance between NSC and NPC numbers. It is by the functional cell-to-cell interaction between NPCs and NSCs, via Notch signalling and EGFR that the balance between the two cell populations in the sub-ventricular zone within the brain is maintained (Aguirre *et al*., 2010). Whilst

essential for maintenance of the mammalian neural stem cells, they are not involved in their generation (Hitoshi *et al*., 2002).

Cell junctions occur in three variations, they are briefly discussed below.

Adherens junctions or desmosomes are defined as cell junctions whose cytoplasmic face is linked to the cytoskeleton. Adherens junctions comprise of cadherin and catenin proteins (Figure 2.13). They can appear as bands encircling the cells or as spots of attachment to the extracellular matrix. Adherens junctions provide a strong mechanical attachment between adjacent cells through homotypic binding between cadherin molecules on adjacent cells (Yeatman, 2004). For example, they hold cardiac muscle cells tightly together as the heart contracts and expands. Vasioukhin *et al.* (2001) and Huelsken *et al.* (2002) observed that epithelial cells formed adherens junctions with their closest neighbouring cells. This event caused a triggering of cell signalling pathways, resulting in changes to cell density, or loss of function mutations in adherens junctions which could also result in the initiation of cell divisions, mediating growth or tumour formation (Conacci-Sorrell *et al.*, 2003).

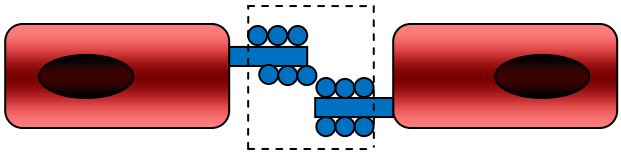

Figure 2.13: Cadherin molecule bonding between two adjacent cells (Yeatman, 2004).

Song *et al.* (2002) provided a working model to explain how Germline Stem Cells (GSCs) were recruited and anchored in their niche. They demonstrated that DE-cadherin-mediated cell adhesion was required for anchoring GSCs in the *Drosophila* ovary niche. Removal of these proteins from the GSCs thus resulted in stem cell loss.

Gap junctions are intercellular channels which permit free passage between cells to ions and small molecules (for example Calcium ions, Figure 2.14). They are 1.5-2 nm in diameter. Gap junctions in invertebrates are composed of proteins from the innexin family whereas vertebrate gap junctions consist of transmembrane proteins called pannexins and connexins (Levin *et al*., 2007). As gap junctions are capable of passing on ions, they allow cells to pass on membrane potentials, for example during rhythmic contractions of the heart muscles. A

prime example is the development of an embryo. From a single celled embryo as the cell starts to divide, short range cell-cell communication starts to emerge. In this case short range cell-cell interaction is aided by gap junctions which links cells to its neighbours through common transmembrane channels. The gap junctions then create a common intracellular environment between subcell population to ensure rapid cell-cell propagation of membrane permeability changes and intracellular messenger cell.

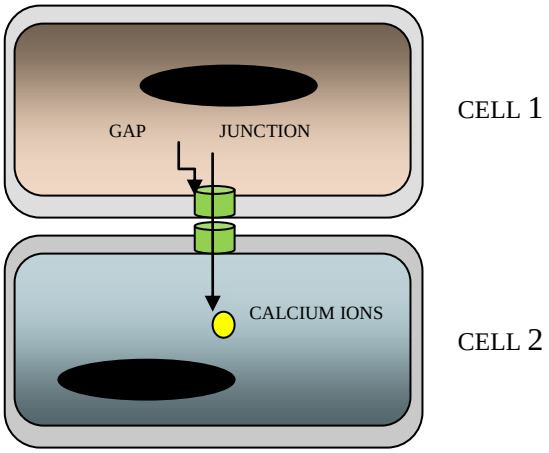

Figure 2.14: Transfer of calcium ions from one cell to another via gap junctions.

The role of Gap Junction Intercellular Communication (GJIC) in the regulation of stem cell proliferation, differentiation and apoptosis has been reviewed (Trosko *et al.*, 2002). Gap junction-permeable signals have been implicated in embryonic morphogenesis and neoplasm (Bruzzone *et al.*, 2003). New methods to study gap junctions in hESC, from the expression of gap junction proteins to the study of GJIC in hESC proliferation, apoptosis, colony growth and pluripotency has also recently been introduced (Wong and Pebay, 2010).

Tight junctions are the major regulators of permeability in simple epithelia where they play a major role in skin barrier integrity (Furuse *et al.*, 2002). They are composed of transmembrane and intracellular molecules that include occluding, junction adhesion molecules and claudins (Bazzoni and Dejana, 2001). Due to their capacity to control membrane permeability, tight junctions also have an important part to play in maintaining cell polarity. They act as a barrier to the diffusion of solutes through the intercellular space and create a boundary between the apical and basolateral plasma membrane domain (Tsukita *et al.*, 2001), whilst also displaying charge and size selectivity in their permeability. Ion exchange in tight junctions is cationic selective. Non-charged material such as water and sucrose moves readily across them.

Mammalian spermatogenesis is a prime example of a stem cell system in which tight junctions are important. The spematogonial stem cell niche is located at the basal lamina of the seminiferous tubules. They perpetually divide to self-renew and differentiate. The spermatogonia or the presumptive stem cells are found very close to several groups of supporting somatic cells (like the peritubular myoid and the sertoli cells) that may contribute to the stem cell niche (Kiger and Fuller, 2001). The sertoli cells lining the tubules are continuously joined to the germ stem cells by tight junctions that regulate the movement of cells and large molecules between the basal compartment and the lumen of the seminiferous tubules.

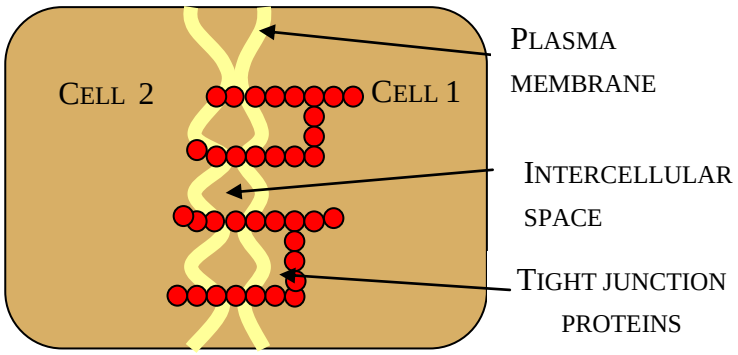

Figure 2.15: Junction proteins joining two cells very tightly (tight junctions).

Cell-cell interaction is one of the important factors that affect the regulation of stem cell characteristics within the stem cell niche. The interaction between stem cells, as well as interactions between stem cells and neighbouring differentiated cells could determine the fate of the stem cell. Bosnakovski *et al.* (2006) studied chondrogenic differentiation of bovine bone marrow Mesenchymal Stem Cells (MSCs) in different hydrogels. He and his coworkers showed that the strong cell-to-cell interactions established during pellet culture facilitated MSC differentiation towards chondrocytes, hence proving that cell-to-cell interaction is an important factor in fate determination.

2.5.2 Physical forces that affect stem cell fate

Physical effects which may influence stem cell behaviour include mechanical, magnetic, optical and electrical effects. The effects of mechanical forces and electrical fields are the factors that have been most frequently subjected to study.

2.5.2.1 Mechanical forces

It has long been recognised that different kinds of mechanical forces have an effect on cell differentiation. Mechanical signalling can control the gene transcription and differentiation programes. Mechanical signals are received by the cells and converted into biochemical signals (also known as mechano-signalling or mechano-transduction), that in turn switches on signalling cascades in response to the stimuli.

There are various ways by which cells respond to a mechanical stress (Figure 2.16). The mediators for cellular mechanotransduction include:

- Cell-cell adhesions, e.g. cadherins, gap junctions (Wang and Ingber, 1995; Yoshida *et al*., 1996; Potard *et al*., 1997; Ko *et al*., 2001);
- Cell-matrix adhesions, e.g. intergrins, focal adhesion (Balaban *et al*., 2001; Bershadskyt *et al.*, 2003);
- Surface processes, e.g. stereocilia, primary cilium (Kacahr *et al*., 1990; Wilson and Paul, 1990);
- Membranes, e.g. ion channels, surface receptors, caveolae (Anderson, 1998)
- ECM components, e.g. fibronectin, collagen, basement membrane (Traub and Berk, 1996);
- Cytoskeleton filaments, e.g. actin filaments (Beningo *et al*., 2001; Tamada *et al*., 2004), microtubules, intermediate filaments (Ingber, 2003).

Source:
http://www.learningmethods.com/downloads/pdf/ingber-cellular.mechanotransduction.pdf

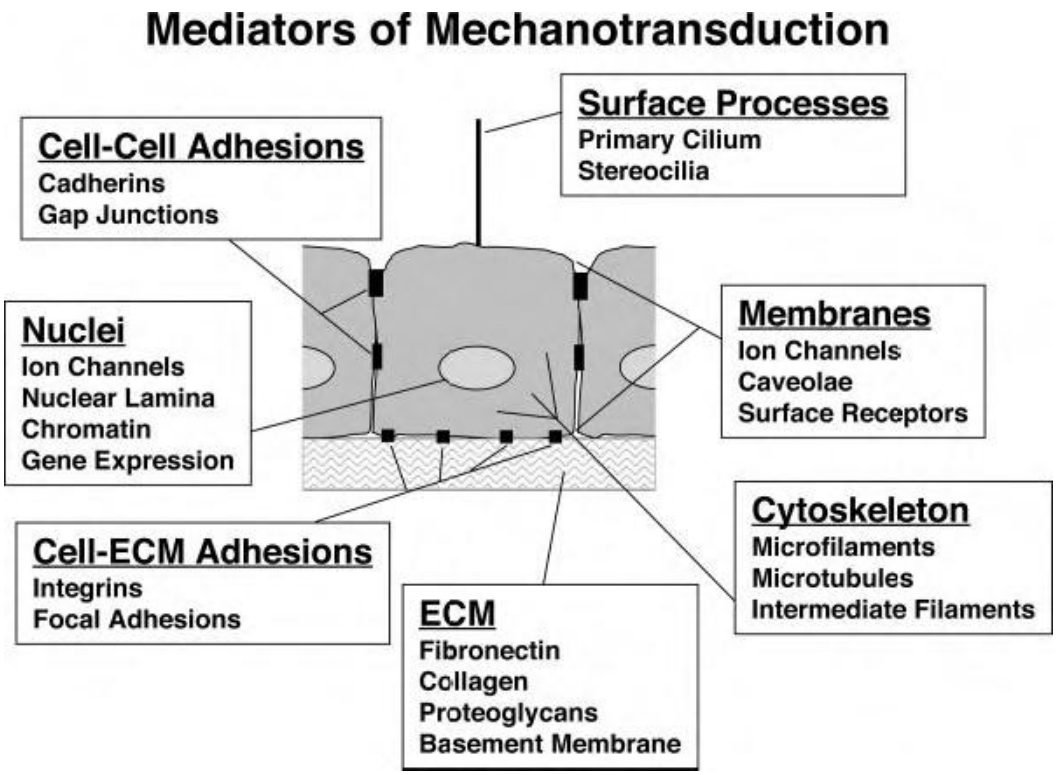

Figure 2.16: Mediators of mechanotransduction (Ingber, 2006).

Souce:

http://www.learningmethods.com/downloads/pdf/ingber--cellular.mechanotransduction.pdf

Much research on mechanotransduction in cells has been dedicated to exploring the effect of matrix stiffness. Studying how cells respond to varied matrix stiffness has enabled researchers to study the matrix stiffness-dependent changes in fibroblast, neural, bone cells and stem cells and their differentiation (Engler *et al.*, 2006). It has also been found that focal adhesion structures and the cytoskeleton are strongly affected by variations in the matrix stiffness (Bershadsky *et al.*, 2003; Cukierman *et al.*, 2001; Discher *et al.*, 2005; Engler *et al.*, 2004; Lo *et al.*, 2000; Pelham and Wang, 1997).

Mechanical forces can take different forms. Figure 2.17 shows the major types of mechanical forces that can act on a piece of tissue.

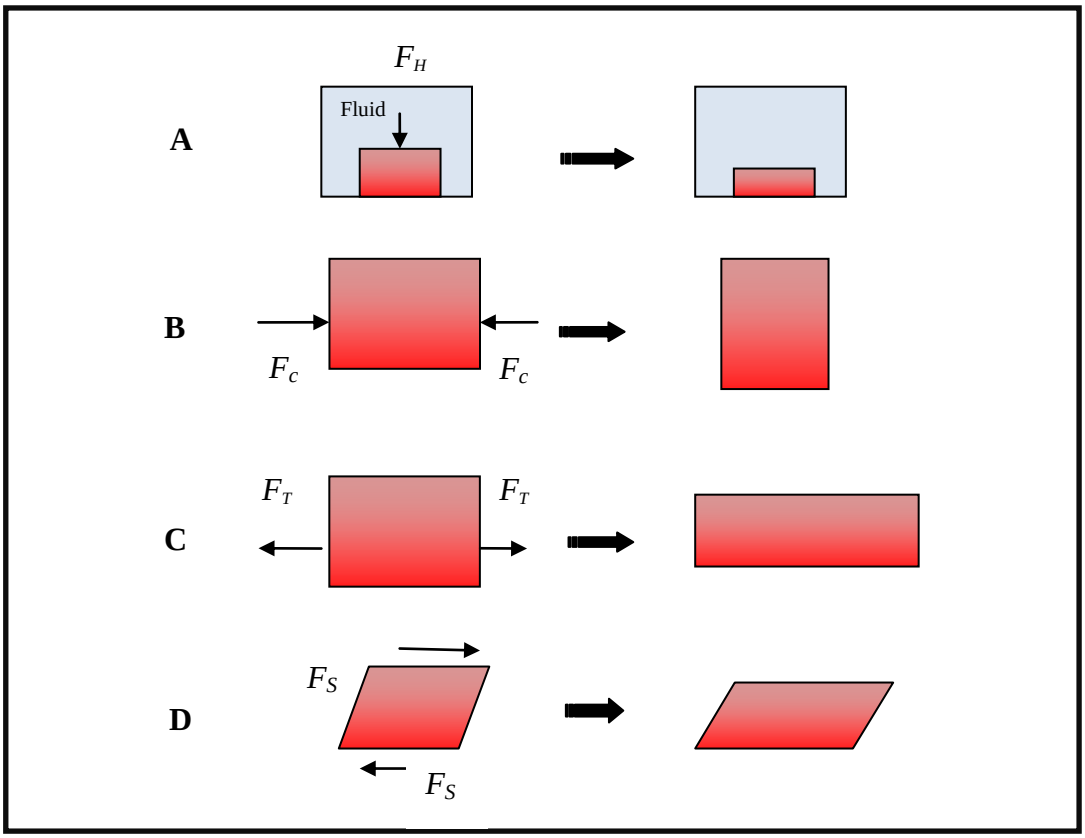

Figure 2.17: Mechanical forces on tissue.

A) *Hydrostatic force (F_h)* ***B)*** *Compressive force (F_c)* ***C)*** *Tensile force (F_t) and* ***D)*** *shear force (F_s) acting on a piece of tissue.*

Hydrostatic pressure is the pressure exerted or transmitted by a fluid at rest. Hydrostatic pressure increases directly with the density and the depth of the fluid. Changes in hydrostatic pressure could affect cells in different ways. For example, Tagil and Aspenberg in 1999 proved that when a mesenchymal tissue was subjected to controlled hydrostatic stress of 2 MPa and decreasing oxygen tension, a cartilage tissue would form. They also proved that in specimens without the mechanical load no cartilage was formed. They went on to hypothesise that persistent intermittent mechanical stimulation is required to maintain the differentiation of cartilage or else the cartilage would be replaced by bone (Tagil and Aspenberg, 1999). Hydrostatic pressure has been shown to enhance differentiation of MSCs in the presence of multipotent differentiation factors *in vitro* and it has been suggested that this particular loading regime may play a critical role during cartilage development and regeneration *in vivo* (Wanger *et al.*, 2008).

Tensile forces are the forces which, when applied to a substrate at both its ends, pull the ends of the substrate away from each other, causing elongation of the substrate. Tensional forces

are prominent in the skeletal system and usually arise due to the movement of articulated tissue for example, flexing of tendons or muscles contractions pulling on bones. Roux, in 1895 and 1912, hypothesized that mechanical stress was responsible for the differentiation of connective tissue. He proved that tensile stress resulted in fibrous tissue, whereas compressive stress resulted in bone formation, with the combination of the two resulting in cartilage formation. In instances where osteochondral progenitor cells or mesenchymal stem cells were subjected to tensile forces, they differentiated along the osteoblast lineage (Takahashi, 1996). When applied ectopically, tensional forces appeared to transform cartilaginous tissue into bone (Glucksmann, 1942; Takshashi, 1996; 2003).

Compressive stresses are the opposite of tensile stresses. Compressive stresses arise in tissues when cells proliferate or deposit large amounts of ECM in regions where expansion of the tissue is resisted by the presence of rigid external boundaries. These forces help to maintain the balance between cell growth and differentiation. Krompecher, in his work in 1937 and 1955, stated that hyaline cartilage formation was a result of compressive stress (Estes *et al*., 2004). Kobayashia *et al.* showed in 2004 that compressive stress was a more potent stimulant of stromal cell differentiation towards the smooth muscle cell lineage than shear stress, as indicated by the expression of smooth muscle cell-specific cytoskeletal proteins. Applying mechanical compression resulted in the reprogramming of MSC- like cells from an osteogenic to a chondrogenic fate (Saitoh *et al.*, 2000).

Shear stress In 1924, Benninghoff hypothesized that cartilage formation was a result of shear stress. High liquid shear stress is known to occur in developing myocardium (Hove *et al.*, 2003), fetal lung epithelium (Liu and Post, 2000) and the kidney (Serluca *et al.*, 2002). However, the most robust studies of the effects of shear stress have been carried out on the vascular endothelium (Orr *et al.*, 2006). Hove *et al.* (2003) found that altering the hydrodynamic forces of the flow into the heart of a zebrafish caused cardiac defects. Such defects included failure in valve formation, absence of heart looping and formation of a third chamber. Mechanical strain may be a key stimulus for the initiation of differentiation programs in stem cells (Sauer, 2006). Experimentally applied mechanical strain has been shown to stimulate cardiovascular differentiation of embryonic stem cells (Sauer, 2006).

2.5.2.2 Electric fields effects

The effect of electric fields on cells is complex, and the effects are also highly frequency dependent. In general, very high electric field strengths kill cells. Lower, sublethal field strengths can lead to various electrokinetic effects including cell movement (electrophoresis and dielectrophoresis), electro-orientation and cell elongation (electrostriction). Such effects are physical rather than biological. However, even quite small electric fields can lead to various long-term biological effects on cells including elongation, alignment, migration, adhesion, and other tissue responses including differentiation (Jhans *et al*., 2007; Rice *et al*., 2007; Dube *et al*., 2005). Disruption or alteration of ion gradients or cell surface charges by an applied electric field can lead to changes in cell signaling pathways and gene expression, resulting in differences in differentiation, proliferation, and mobility (Levin, 2003; Sun *et al*., 2006; 2007). Electric stimulation of stem and/or progenitor cells can initiate signaling pathways that enhance osteogenic differentiation (McCullen *et al*., 2010). hMSCs respond to electric field stimulation by osteogenic differentiation (Kim *et al*., 2009; Sun *et al*., 2007; Tsai *et al*., 2009; Hronik-Tupaj *et al*., 2011). The strength of an AC electric current at 60 kHz, 20 mV has been reported to increase osteogenic and chondrogenic differentiation markers, such as TGF-β1, type 2 collagen, proteoglycan, bone morphogenetic proteins, as well as hMSC proliferation (Xu *et al*., 2009; Wang *et al*., 2004; Zhuang *et al*., 1997; Lorich *et al*., 1998; Brighton *et al*., 2008). Exogenous electric fields have been implied in cardiac differentiation of mouse embryonic stem cells and the generation of reactive oxygen species (ROS) (Serena *et al*., 2009).

Another response of stem cells to electric field exposure could be expression of heat shock proteins. The presence of heat shock proteins can affect osteodifferentiation (Brown *et al*., 2007; Berge *et al*., 2008; Nogaard *et al*., 2006). Small heat shock proteins (molecular mass between 15 - 30 kDa), such as hsp27 are known to be expressed and regulated during differentiation and development in many organisms including humans, mice, and zebrafish (Brown *et al*., 2007).

2.6 Microfabrication in tissue engineering

Most cell culture is done in 2D. However, over the course of time the limitations of 2D culture have become obvious. Even when grown in monolayer (2D), cells are still 3D structures and, as such, are influenced by the complete spectrum of their environment (Lund *et*

al., 2009). Three-dimensional matrices *in vitro* and *in vivo* define the structural, mechanical and biochemical make-up of the cellular microenvironment and are crucial for allowing bidirectional interplay to exist between the cell and tissue during development (Griffith and Swartz, 2006). 2D systems allow precise control of (chemical) cues but are compromised by their inability to ask questions related to the complex spatial and temporal patterning of the cues that are seen *in vivo.*

Traditional tissue engineering strategies involve seeding cells on biodegradable polymeric scaffolds such as Poly-Glycolic Acid (PGA). In said approach, the cells would repopulate the scaffold and create the appropriate extra-cellular matrix (ECM) of a specific architecture with the help of growth factors, mechanical stimulation and perfusion. The drawback of this technique, however, is the difficulty in creating the intricate microstructural features of the tissue. With the aid of microfabrication techniques, however, engineers can now create more controlled environments, for example by making self-assembled aggregations in microwells or channels, creating cell sheets, or direct printing of tissue and microfabrication of cell-laden hydrogels by micro-moulding cells. Once the tissue is created it can be assembled by way of a number of methods such as random packing, stacking of layers or directed assembly.

2.6.1 Micromanipulation techniques

Micromanipulation involves performing delicate operations on and with cells under the high magnification of a microscope and through the co-ordinated movement of specialized tools. Micromanipulation techniques have found applications in cell biology, electrophysiology, clinical sciences and genetic engineering. Micromanipulation systems have been used in the production of chimeric animals through blastocyst injection with Embryonic Stem (ES) cells and the introduction of specific genes into the genomes of domestic and laboratory animals (Thuan, 2006). They have been used to isolate cells to obtain pure cultures, to elicit physical measurement of cells, to probe the shape or arrangement of organelles in living cells, to alter cell membrane permeability for drug design processes and much more.

There are several different methods of micromanipulating particles, of which some are direct while others are indirect. Direct micromanipulation of particles involves microchannels, inkjet printers and micropipettes etc whereas indirect micromanipulation techniques involve a

transducer placed at a distance from the particle and works by creating a force field. Some of the indirect techniques most widely used are as follows:

A. Ultrasound;
B. Dielectrophoresis;
C. Magnetophoresis;
D. Optical tweezers.

Each of the above mentioned micromanipulation techniques will be explained and discussed as to their suitability for this research.

2.6.1.1 Ultrasound

Ultrasound can be defined as "a sound with a frequency greater than 20000 Hz, approximately the upper limit of human hearing" (Neild *et al*., 2006). Ultrasound can be used for particle manipulation. An obvious advantage of this technique is that it is free from external contact, i.e. the particles are moved by the ultrasonic forces acting on them at a distance rather than through contact with an object. As the particles under consideration could be fragile (cells), any moisture in the atmosphere could mean they stick to any instruments being employed to move them directly (Haake and Dual 2002). A further advantage is the fact that the force can be applied to a large area and not just to small regions.

Ultrasonic forces have been successfully used to manipulate particles in suspension. For example, when compressional (ultrasound) waves are produced by a transducer and the sound waves constructively interfere with another wave (this can be the same wave reflected from a surface, or a wave generated by another transducer, ultrasonic standing waves are produced. When particles, such as cells, are suspended in a fluid in an ultrasonic standing wave they acquire a position dependant potential energy. The particles then tend to migrate to positions of minimum particle acoustic potential energy i.e. at half wavelength intervals (Coakley *et al.*, 2000). On the application of a standing wave ultrasound field to a suspension, a predictable heterogeneous distribution is created by the particles which are moved towards areas of minimal acoustic pressure (Gherardini *et al*., 2005). This effect has been used to effect in numerous biotechnological applications such as mammalian cell filtering and red blood cell sedimentation, but has also been used to create patterns of cells for the study of cell-cell interaction.

Researchers have focused their studies on the one dimensional movement of particles. For example, research conducted by Groschl in 1998 observed the formation of columns of particles separated at half-wavelength from which they can be extracted. In this type of manipulation, a resonator containing two parallel piezo disks placed at either end is used. Similarly, Haake and Dual (2002) studied the forces experienced by a spherical particle in a one-dimensional plane standing wave. As shown in figure 2.18, the particles to be manipulated are placed inside this resonator and the piezo disks create the planar standing waves (Haake and Dual, 2002).

It is not always necessary to generate compressional ultrasound waves. For example, studies by Haake and Dual (2005) have shown that, by applying an ultrasound field excited by a surface wave, small particles can be positioned in one or two dimensions.

Ultrasound has been used for patterning stem cells. Work carried by Haake and Bazou (Haake *et al*., 2005; Bazou *et al*., 2004) has successfully identified the ability of ultrasound to concentrate human cells using both standing waves and an ultrasonic pressure field. The results prove that the viability of the cells is neither affected nor modifies in vitro expression of surface receptor interactions on the application of ultrasonic pressure fields. Other works include Kim *et al.* (2004) working with HeLa cells and mesenchymal stem cells, aliquoted 50 µl of the cell solution into the milliscale chamber of the ultrasonic device. The applied frequency of the excitation signal was 1.2 MHz. Initially, randomly distributed HeLa cells and hMSCs aligned themselves into straight lines within a minute of being subjected to ultrasound standing waves. The lines were not equidistant as the sound field was not fully uniform in the chamber, though other disturbances such as convection from gravitationally, thermally, and acoustically generated hydrodynamic streaming currents as well as non-uniform properties of the medium could have contributory factors.

2.6.1.2 Dielectrophoresis

Electrical techniques have been used extensively for particle and cell manipulation. They have several advantages over optical tweezers and ultrasound techniques as they employ a much higher resolution than ultrasound and exemplify a much better ability to manipulate many cells simultaneously than optical tweezers (Markx, 2003). Moreover, different frequencies and variants of electric fields can be used, thus inducing different types of behaviour in the cells. The main disadvantage is that its application directly in growth media

is often difficult. Unlike ultrasound and optical tweezers, electrical techniques often work best in low conductivity media (Sebastian *et al.*, 2006).

The term dielectrophoresis encompasses a number of different AC electrokinetic techniques. DEP manipulation of particles includes normal dielectrophoresis (often simply called dielectrophoresis or DEP), rotating dielectrophoresis (electro-rotation), orienting dielectrophoresis (electro-orientation), and travelling wave dielectrophoresis (TWD).

Normal dielectrophoresis

Normal dielectrophoresis – also commonly referred to simply as dielectrophoresis or DEP - is the induced motion of a neutral or charged, but polarisable object (such as a cell) (Pohl and Crane, 1971) in a non-uniform electric field (AC or DC). The magnitude and polarity of the dipoles induced in a particle determines the dielectrophoretic motion.

In the presence of an electric field a charged particle faces a Coulomb force and moves. At the same time a dipole is induced in a polarisable body which may or may not induce motion in the particle. Coulomb's law states that: "The magnitude of the Electrostatics force of interaction between two point charges is directly proportional to the scalar multiplication of the magnitudes of charges and inversely proportional to the square of the distances between them."

The force exerted on a charge q by another charge Q is given by Coulombs Law:

$$F = K_e \frac{qQ}{r^2} \tag{2.1}$$

Where r is the distance between the two charges and K_e is the proportionality constant also called the Coulombs constant.

In a homogenous field, the polarisable body does not feel a net force since both the charges q and Q feel the same force acting in opposite direction. However in a non-homogenous field each charge experiences a different force creating a net force, called the dielectrophoretic force. When a neutral particle is placed in a non-homogenous electrostatic field $\bar{E}$, the particle gets polarised and a dipole is formed of equal and opposite charges $+q$

located at a distance $r+d$, and $-q$ at a distance r. the two values face a different field due to the vector field E. Therefore force experienced by $+q$ is given by the equation:

$$\bar{F} = q\bar{E}\left(\bar{r} + \bar{d}\right) \tag{2.2}$$

And theforce experienced by –q is given by the equation:

$$\bar{F} = -q\bar{E}(\bar{r}) \tag{2.3}$$

Combining the two equations:

$$\bar{F} = q\bar{E}\left(\bar{r} + \bar{d}\right) - q\bar{E}(\bar{r}) \tag{2.4}$$

By simplifying the first term in taylor series in equation (2.4) we get

$$\bar{E}\left(\bar{r} + \bar{d}\right) = \bar{E}(\bar{r}) + \bar{d} \cdot \nabla\bar{E}\,(\bar{r}) + higher\ order\ terms \tag{2.5}$$

The higher order terms have been neglected since |d| is very small compared to them. Now if we substitute equation 2.5 into 2.4, we get

$$\bar{F} = q\bar{E}(\bar{r}) + \bar{d} \cdot \nabla\bar{E}\,(\bar{r}) - q\bar{E}(\bar{r}) \tag{2.6}$$

$$\bar{F} = q\bar{d} \cdot \nabla\bar{E} \tag{2.7}$$

Since the dipole moment is given by the equation $\bar{P} = q\bar{d}$ the force acting on the dipole can be represented as

$$\bar{F}_{dipole} = \bar{P} \cdot \nabla\bar{E} \tag{2.8}$$

For neutral particles which are completely immersed in dielectric medium in a non-homogenous electric field $\bar{E}$, the particle gets polarised and experiences a net electric force given by

$$\bar{F} = (\bar{P}_{eff} \cdot \nabla)\bar{E} \tag{2.9}$$

Where $\bar{P}_{eff}$ is the effective dipole moment. In case of a spherical particle such as a cell the effective dipole moment is given by

$$\bar{P}_{eff} = 4\pi r^3 \varepsilon_m \left(\frac{\varepsilon_p^* - \varepsilon_m^*}{\varepsilon_p^* + 2\varepsilon_m^*}\right) \bar{E} \tag{2.10}$$

Where ε_m is the medium permittivity, r is the radius of the cell; ε_p^* is the complex permittivity of the particle and and ε_m^* is the complex permittivity of the medium .$\bar{E}$ is the strength of the electric field.

As the time averaged dielectrophoretic force is expressed in terms of the complex forms of the dipole moment and the electric field, written as

$$\bar{F}_{DEP} = \frac{1}{2} Re\left[\bar{P}_{eff} \cdot \bar{E}^*\right] \tag{2.11}$$

Therefore by substituting equation 2.10 in to 2.11 the dielectrophoretic force on a particle can be described by the following equation:

$$\bar{F}_{DEP} = 2\pi r^3 \varepsilon_m \left(\frac{\varepsilon_p^* - \varepsilon_m^*}{\varepsilon_p^* + 2\varepsilon_m^*}\right) \nabla E_{rms}^2 \tag{2.12}$$

And Clausius-Mossotti factor is given by,

$$\mathrm{Re}\left(K^*(\omega)\right) = \left(\frac{\varepsilon_p^* - \varepsilon_m^*}{\varepsilon_p^* + 2\varepsilon_m^*}\right) \tag{2.12}$$

$$\text{Therefore} \qquad \bar{F}_{DEP} = 2\pi r^3 \varepsilon_m \mathrm{Re}(K^*(\omega)) \nabla E_{rms}^2 \tag{2.13}$$

Where ε_m is the medium permittivity, r is the equivalent radius of the cell and *Re* is 'the real part of' the complex Clausius-Mossotti factor $K^*(\omega)$. The term '∇E^2_{rms}' defines the average local non-uniform field strength and the gradient, and is dependent on the applied voltage and the electrode geometry and size. In which:-

$$\varepsilon * = \varepsilon - j \frac{\sigma}{\omega}$$

$and\ j\ =\ \sqrt{-1}$ an imaginary number

ε is the permittivity of the particle, σ the conductivity of the particle and ω the radial frequency. The subscripts refer to the particle (p) and the medium (m) (Sebastian *et al.*, 2006). Equation (1) indicates that if Re $[K^*(\omega)] > 0$, the particle is attracted towards the strong electric fields. This phenomenon is referred to as positive dielectrophoresis or positive DEP where the particles move towards areas of high electric field indicated by a high density of electric flux lines. On the other hand, if Re $[K^*(\omega)] < 0$, the particle is pushed away from the strong electric field regions to regions of weak electric field. This phenomenon is known as negative dielectrophoresis or negative DEP. The particles move towards areas of low electric field strength, indicated by a low density of electric flux lines (Washizu and Kawabata, 2005).

Whether a material shows positive or negative DEP depends on three parameters (Washizu and Kawabata, 2005):

1) Frequency of the electric field applied;

2) Conductivity and permittivity or dielectric constant of medium;

3) Conductivity and permittivity or dielectric constant of substance.

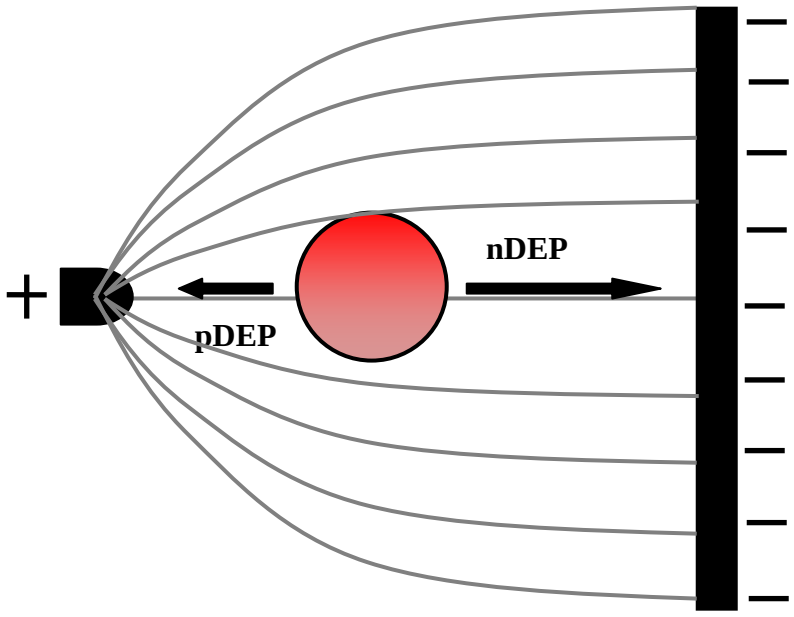

Figure 2.18: A polarisable particle in a non uniform electric field.

In the earlier work on dielectrophoresis metal sheets, wires, rods and pins were used as electrodes, whereas more recently microelectrodes have predominantly been used. There are several advantages to the downsizing of equipment. Firstly, a decrease in the electrode size by 100 fold will decrease the required operating voltage by roughly 1000 fold. Lower operating voltages are more easily generated, and also reduce electrical heating and electrochemical effects. A reduction in the surface area of the electrodes in contact with the fluid reduces any electrochemical processes that may occur (Pethig and Markx, 1997).

Applications of dielectrophoresis

DEP has found applications in many areas, although the primary interest resides in its use in biological applications. Due to the type of structure of biological cells, materials with very different electrical properties are found adjacent to one other. For example, the relative permittivity of the medium is around 80, whilst that of the cell membrane is approximately 5. The conductivity of cells can vary from 10^{-7} S m^{-1} at the membrane to 1 S m^{-1} at the interior (Pethig and Markx, 1997). At these boundaries, large interfacial polarizations are formed which are conducive to large induced-dipole moments. Moreover, these moments are highly dependent on the frequency of the applied field. Normal DEP of cells can be carried out in two ways, either with positive or with negative dielectrophoresis. Which one of them occurs depends on the physiology of cells - whether the cells are living or dead (Li *et al.*, 2002; Markx *et al.*, 1999), the frequency of the applied AC field and the relative complex permittivity of the cells and the suspending medium. Trapping by way of positive dielectrophoresis is more common and rapid than trapping through negative DEP (Albrecht *et al.*, 2004; Pohl *et al.*, 1978). Pohl explains for this can be attributed to the fact that the field distribution usually varies with the position in the field. Attractive forces tend to pull particles into a smaller region of higher attractiveness, whereas repulsive forces tend to repel the particles into large regions where the field rapidly becomes ineffective and the negative dielectrophoretic effect is readily dissipated.

Dielectrophoresis is now being applied for the selective spatial manipulation and separation of mixtures of bacteria, viable and unviable cells, cancerous and normal cells and red and white blood cells (Pethig and Markx, 1997; Doh and Cho, 2005; Hughes, 2002; 2003; Arnold, 2010). Recent studies have demonstrated the use of DEP in separating homogenous mixtures of neural stem cell populations. Neural Stem/Progenitor Cell (NSPC), neurons and

astrocytes can be separated owing to the fact that different electric phenotypes of cells respond differently to electric fields, allowing cell separation based on cell polarizability (Prieto *et al*., 2010; Valero *et al*., 2010).

In 1978, Pohl showed that AC micromanipulation techniques could be used to construct tissue-like materials from cell suspensions. This work was not built on until Pethig and co-workers took up this work again in the late 80s-early 90s. They showed that dielectrophoresis could be used to aggregate bacteria, blood cells and other cell types (Price *et al.*, 1988; Burt *et al.*, 1990; Markx *et al.*, 1994 a&b). Markx *et al*. (2006) used DEP to artificially construct bacterial biofilms. Multispecies biofilms could be constructed with well defined architectures. The first description of a tissue-like material with gel-immobilised animal cells was described by Matsue *et al*., in 1997.

Since then, dielectrophoresis has been used quite regularly in the creation of artificial mammalian tissues. Dielectrophoresis (DEP)-based cell patterning technique improves tissue engineering efficiency and quality by offering advantages such as ease of operation, low degree of cell damage, and precision, thus facilitating the exploration of 3-D cell-to-cell interaction (Lin, 2006). Dielectrophoresis–based techniques can be used to manipulate single cells (Gray *et al.*, 2004; Rosenthal and Voldman, 2005; Mittal *et al.*, 2007) as well as many cells simultaneously. For example, Gray *et al.* (2004) used very high fidelity micro fabrication techniques to create electrode arrays for trapping thousands of single individual cells between electrode castellations with a characteristic size of 3 μm. The dielectric force was capable of holding each cell against a destabilising fluid flow.

Recent work has shown that the application of positive DEP under conditions of high electric field strength and low medium conductivities can be used in the formation of multi-layered aggregates of mammalian cells (Sebastian *et al.*, 2006). In these experiments, microelectrodes with a size range of 50 to 250 μm were used and frequencies varying from 0 to 40 $V_{pk\text{-}pk.}$ Voltages above 30-40 V should be avoided as they lead to cell death. They also showed that by using a continuous flow of fresh sorbitol iso-osmotic buffer through the chamber, an increase in the medium conductivity by ion leakage from cells could be overcome and a high positive DEP force could be maintained throughout the formation of the aggregates. It was shown that, at low flow rates, the construction of aggregates of mammalian cells with heights over 150 μm was feasible using relatively low voltages (20 $V_{pk\text{-}pk}$, 1 MHz).

Ho *et al.* (2010) developed an integrated microfluidic platform for actively patterning mammalian cells. A system was developed with embedded arrays of PEG microwells fabricated on a planar ITO electrode. Due to their dielectric properties, PEG microwells define electrical energy landscapes thereby forming positive dielectrophoresis traps in a low conductivity environment. The group achieved efficient patterning of particles and cells like mouse embryonic stem cells in combination with external flow. With a seeding density of 10^7 cells/mL and a flow rate of 3 μL/min, trapping of cells in microwells was completed in tens of seconds after initiation of DEP. The viability of the cells was checked and was found to be positive as the cells formed homogeneous monolayer patterns. They suggested the approach could be used fabricating various cell microarrays for applications such as cell-based biosensors, drug discovery and cell microenvironment studies (Ho *et al.*, 2010).

Masato and co-workers (2010) showed that negative dielectrophoresis can be used to create versatile cell micropatterns without any pre-treatment of a culture slide for the study of cell-cell interactions. They constructed electrode arrays with four independent microelectrode subunits from indium-tin-oxide (ITO). A suspension of C2C12 cells was introduced into the patterning device and a negative DEP force was induced by applying a voltage (12 $V_{pk\text{-}pk}$ at 1 MHz) to interdigitated microelectrodes to direct cells to weaker electric field regions. The AC voltage was applied for five minutes to allow the cells to adsorb onto the culture slide. The voltage was then switched off and the device was flushed with pure medium to remove any non-adherent cells. A second cell type was then introduced, forming patterns parallel to the first lines and between the first lines by switching the way the voltage was applied. The two different cell types were patterned within 15 minutes (Masato *et al.*, 2010). Other work done by this group shows that when the adsorbed cell lines were cultured negative DEP had not significantly damaged the cells as the cell number increased readily (Masato *et al.*, 2010).

Albrecht *et al*. (2005) encapsulated living cells within PEG-based hydrogels to create a local 3-D microenvironment. This could be achieved using two techniques: first 'photopatterning' – selectively crosslinking hydrogels with photosensitive initiators by exposure through a mask; the gel contains living cells; and second, 'electropatterning' utilizing DEP forces to position cells within a prepolymer solution before crosslinking, forming cell patterns with micron resolution. Combination of these two methods enabled thm to achieve hierarchical control of cell positioning over lengths scales ranging from microns to centimetres. Using these techniques Albrecht *et al*. (2006) showed that changing cell-to-cell

interactions in 3D cell aggregates regulated bovine articular chondrocyte biosysnthesis. Albrecht *et al*. (2007) also formed a multiphase tissue consisting of micro-scale tissue sub-units in a 'local phase' biomaterial, which would in turn be organised by DEP forces in a separate, mechanically supportive 'bulk phase' material.

Other forces acting on particles during dielectrophoresis

For the description of the DEP forces in the previous sections it was tacitly assumed that the particles are far ways from each other. In practice this is often not the case. The interaction between the dipoles and the non-uniform electric fields created around the particles cause mutually attractive forces to occur between particles, causing pearl-chain formation. Pearl-chain formation has strong (mainly detrimental) effects on DEP separations (Markx *et al.*, 2004), but plays mainly a positive role in the formation of aggregates (Sebastian *et al.*, 2007b).

If a particle has a net charge then the particle may show electrophoresis. Electrophoresis can be prominent at lower radio frequencies, but becomes less important at higher radio frequencies (Price *et al*., 1988).

Apart from DEP and electrophoretic forces many other forces act upon particles when exposed to non-uniform electric (AC) fields. These forces include buoyancy and gravitational forces, viscous drag forces, and electro hydrodynamic forces such as electro-osmosis.

Buoyancy and gravitational forces are caused by gravitational field exerted by the Earth. The two forces always act in opposite directions, with the gravitational forces acting downward, and the buoyancy force upward. The two forces play important roles in the accumulation of particles in the electric fields generated near microelectrode arrays. For example, if the electrode array is placed at the bottom of the chamber, when particles are attracted to high field regions by positive DEP gravity aids the aggregation of particles whereas in negative DEP buoyancy helps the particles levitate (Flores-Rodrigues *et al.*, 2004).

When DEP forces induce a particle to move in an electric field, the fluid in which the particle is suspended exerts a viscous drag force on the particle. The viscous drag force on the particle moving through the medium is opposite but directly proportional to the velocity of

particle, causing the particle to reach its terminal velocity (which is directly proportional to the magnitude of the force propelling through the medium) in a few nanoseconds. Similarly, if the fluid in the chamber flows relative to the particle, viscous drag forces are exerted on the particle that will drag it along. Viscous drag forces play important roles during aggregate formation during DEP. Steric drag forces produced by a gentle fluid flow in the chamber can be used to separate cells by selectively lifting cells from potential energy wells produced by the electric field (Markx *et al.*, 2004). The fluid velocity is largest in the middle of the chamber and lowest at the walls; this effect has been used to advantage in DEP-Field Flow Fractionation, where particles lifted further away from the chamber wall move faster through the chamber than those closer to the wall (Hughes, 2002; 2003). Viscous drag forces also play important roles during aggregate formation when collecting particles from flow, as the viscous drag will remove any particle for which the viscous drag force is stronger than the sum of forces keeping it in the aggregate.

When an electric field is applied to sets of microelectrodes fluid movement is often induced by the electric field, which is described under the general term of electrohydrodynamics (EHD). Reviews of EHD forces generated near microelectrode structures have been given previously (Ramos *et al.*, 1998), but include electrothermal effects (fluid movement induced by density changes due to heating of the fluid in the electric field) and electro-osmotic effects (fluid movement induced by the movement of ions in the tangential electric field generated across the double layers at the electrodes). As a result of EHD forces on the liquid near microelectrodes a vortex of liquid is formed over the electrode edge that can often be seen to push particles onto the electrode surface (Gonzales *et al.*, 2000; Green *et al.*, 2002) at low frequencies. At the electrode edge the field gradient (and hence DEP force) is greatest, therefore the particle gets drawn by DEP force towards the electrode edge, whilst the EHD force pulls the particle inwards on top of the electrode edge (Hoettges *et al.*, 2003). Collection of particles on top of electrode pads is slower at higher frequencies where the influence of DEP may be stronger (Hughes, 2003). EHD motion of fluids is particularly significant in a relatively small electrode regions and volumes. EHD motion is dependent on the pH and temperature of the electrolyte and also the frequency.

2.6.1.3 Magnetophoresis

The magnetic analogue of dielectrophoresis is magnetophoresis – the manipulation of particles by the means of non-uniform magnetic fields.

The use of magnetic particles in numerous biological and medical applications has been established by the research carried by several researchers. Magnetite nanoparticles have been successfully used in the separation of biological materials using magnetically labelled beads. Moreover, the application of such particles in drug delivery and medicine or cell sorting has also been discovered (Honda, 2004).

Magnetophoresis has been used extensively in biological separations techniques such as the Magna-Sep separation system from Invitrogen. This is done by creating superparamagnetic nanometre-size particles of magnetite or maghemite which are treated with substances such as antibodies so they will adhere to a specific biological species (molecule or cell). With the help of strong magnetic fields created using a permanent magnet or an electromagnet these highly paramagnetic beads can be separated out of a solution along with the biological entity of interest. Biological materials are either diamagnetic or only weakly paramagnetic; this property aids the separation in being more specific. It is rather impractical to carry out magnetophoresis with permanent magnetic beads as they would attract one another and agglomerate so the experiments only work with superparamagnetic beads with no permanent magnetic dipole (Mikkelsen, 2005).

Magnetic forces have been used in the field of tissue engineering to construct multilayered keratinocyte sheets and harvest the sheets without enzymatic treatment (Ito *et al.*, 2004). In these experiments magnetite cationic liposomes were used to improve the absorption by cells as these liposomes have a positive surface charge which were then taken up by the target cells. A further study by Ito in 2004 involved the application of magnetic forces for the construction of a heterotypic and layered coculture system of rat hepatocytes and human aortic endothelial cells (HAECs) that was not limited by cell type. Ito *et al.* referred to the technique as “magnetic force-based tissue engineering (Mag-TE)”.

Studies have also proved that magnetic forces can be used, for preconditioning bone and stem cell seeded constructs and thus to produce a tissue engineered bone. El Haj and Cartmell (2002) employed magnetic beads to understand the mechanical stimulation of human osteoblasts and the influence on osteoblastic activity when magnetic particle technology was applied. Cartmell employed magnetic microparticles attached to primary bone cells via specific membrane receptors. On the application of an oscillating magnetic field, the

magnetite beads attached to the cells moved along the magnetic field and the cells experienced a force them as a result of the permanent magnet movement (Cartmell *et al*., 2003).

2.6.1.4 Optical tweezers

Optical tweezers are very sensitive instruments able to exert small but highly controllable forces on particles. The principle of an optical tweezers's mode of action can be explained in two ways. Like any electromagnetic radiation light has both particle and wave characteristics. The particle characteristics cause light to carry momentum that is proportional to its energy and in the direction of propagation. If there is a change in the direction of light either by reflection or refraction then there is a change in the momentum of light. When an object comes in the way of a light beam, it changes its momentum by bending it. Conservation of momentum requires that the object must undergo an equal and opposite momentum change. This gives rise to a force acting on the object. In a highly focused laser beam the net momentum force near a focal point is always in the direction of the focal point. A particle in the laser beam would therefore be directed to the focal point. An alternative explanation is that a focused light beam causes a very strong electric field gradient concentrated at the very tip of the focused beam, termed a beam waist. Dielectric particles are attracted towards the strongest electric field along the beam, in the same way as particles are attracted to high electric field regions by positive dielectrophoresis (Curtis *et al.*, 2002).

The optical tweezer is nowadays an established tool in many fields of science, particularly in the life sciences for the entrapment and movement of microscopic volumes of matter. A great level of control can be used on a range of particles with sizes ranging from tens of nanometres to tens of micrometers. Optical tweezer-based techniques play a vital role in biotechnology for the manipulation of biological particles such as single viruses, single living cells and even organelles within cells (Ashkin, 1997), and non-living materials such metal or plastic spheres. Optical tweezers have been used to study shape recovery of red blood cells (Bronkhorst *et al.*, 1995), and for measuring strectching forces on DNA (Bennink *et al*., 199l; Wang *et al*., 1997). Optical tweezers used for cell manipulation normally work in the near infrared (NIR) regions (0.75-1.4 micro meter wavelength) to avoid absorption that cause thermal and chemical deterioration that occurs at lower wavelengths. Pigmented skin however is comparatively absorbent in the NIR and cannot be used with this technique (Jacques and McAuliffe, 1991). Unlike dielectrophoresis, optical tweezers work well in high conductivity media but are typically only able to manipulate a single or very few particles at a given time.

However, techniques are under development which enable manipulation of many particles simultaneously. For example, Holographic Optical Tweezers (HOTs) have been developed with improved human-computer interfaces which can be used to manipulate many particles at the same time (Grieve *et al*., 2009).

CHAPTER 3

Materials and Methods

3.1 Introduction

This chapter provides information about materials and methods used throughout the work described in the thesis. More detailed information specific to individual experiments is given in each results chapter.

3.2 Culturing embryonic stem cells

Growth medium was made in aliquots of 500 mL of GMEM medium supplemented with 10% fetal calf serum (FCS), 1% of 1× non essential amino acids, 1 μg mL^{-1} β-mercaptoethanol and 10 μg ml^{-1} sodium pyruvate, and kept at -20^{o}C. Before the cells were passaged, all the cell culture solutions (growth medium, trypsin, serum, gelatine, PBS) were thawed in a 37˚C water bath. The culture flask was taken from the incubator and the cells were observed using an Olympus inverted microscope. If the confluency of the cells in the flask was more than 80% (a confluent T25 flask contained 5 to 7 million cells) or the medium had changed colour from pink to an orange hue, and there was no sign of infection, then the cells were passaged. First the growth medium was carefully aspirated off. The cells were given a wash with Phosphate Buffered Saline solution (PBS) 2 mL. 2 mL Trypsin buffer TVP (1% trypsin, 1% chick serum, 8.4×10^{-4} EDTA and 1× PBS (phosphate buffer saline) was added to the T25 flask. The flask was incubated for 2-5 minutes at 37^{o}C. The flask was then tapped on the bottom to suspend the cells. Later on, the clumps of cells after trypsin treatment are made into single cells by tituration with 8 mL fresh growth medium. The cells were then centrifuged at 1200 rpm for 5 mins. The pellet formed was dispersed with 10 mL growth medium and a cell count was performed with a hemocytometer. 1 million cells were added to T25 culture flasks, which were previously coated with 5 mL of 0.1% gelatine (Sigma) for 10-20 mins. Growth medium was added until to a total volume in the flask of 10 mL. 10 μl of LIF (Leukaemia Inhibitory Factor) was then added (1/1000 dilution). The cells were incubated in a 5% CO_2 incubator at 37°C for 40–48 hours until near 80% confluence was obtained.

To prepare cells for DEP, after trypsinizing and washing the cells in fresh growth medium, the cells were washed twice in 300 mM sorbitol solution. They were spun each time at 1200 rpm for 4 mins.

3.3 Culturing osteoblast-like cells (SAOS-2)

3.3.1 Growth medium

A cell line of adherent human osteoblast-like cells, SAOS-2, was grown in RPMI 1640 medium supplemented with 10% FBS, 2 mM L-glutamine, 10 units ml^{-1} penicillin and streptomycin solution (Sigma).

3.3.2 Trypsin EDTA

Before subculturing all the cell culture solutions (growth medium RPMI 1640, trypsin, serum, gelatine, PBS) were thawed in a 37˚C water bath. The culture flask was taken from the incubator and the cells were observed using an Olympus inverted microscope. If the confluency of the cells in the flask was more than 80% (a confluent T25 flask contained approximately 4 to 6 million cells or the medium had changed colour from pink to an orange hue, and there was no sign of infection, then the cells were passaged. First the growth medium was carefully aspirated off. The cells were given a wash with 2 mL Phosphate Buffered Saline solution (PBS). 2 mL trypsin EDTA (filter sterilised 0.5% trypsin and 0.5% ethylene diamine tetra acetic acid (EDTA) dissolved in 1 × PBS) was added to T25 flasks (3 mL trypsin EDTA was added to T75 flasks) for detachment of cells from the flask surface. The flask was incubated for 2-5 minutes. The flask was then tapped on the bottom surface to get cells into suspension. The clumps of cells after trypsin treatment are made into single cells by tituration with 8 mL fresh growth medium and cells are centrifuged at 1600 rpm for 5 mins. 2500 cells/cm^2 were seeded into a T25 flask and growth medium assed until the total volume was 10 ml. The flasks were incubated for 4 days in a humidified chamber with 95% air and 5% CO_2 at 37°C until near 90% confluence was obtained (3-4 days). Medium was exchanged every 2 days.

To prepare the cells for DEP, after the trypsinisation step the cells were washed in fresh medium and then washed twice with 300 mM D-sorbitol in order to lower the conductivity to allow patterning with positive dielectrophoresis.

3.4 Cell staining

SAOS-2 cells were stained with PKH26 (red cell membrane stain) obtained from Sigma. The concentrations of PKH26 stain was 8 x 10^{-6} M for 10 million cells. Cell staining was done using protocols from Sigma. After staining the cells were washed twice with 300 mM Sorbitol solution for patterning with positive DEP.

3.5 Microelectrodes

Microelectrodes (Figure 3.1) of the interdigitated oppositely castellated design with characteristic sizes between 50 and 250 μm were fabricated using photolithography from indium tin oxide (ITO) coated microscope slides (Delta Technologies Inc, Stillwater, USA) as described by Venkatesh *et al*. (2007). Photolithography was done as described previously (Flores-Rodriguez and Markx, 2004). A chamber was constructed on top of the slide from two strips of insulating tape and a microscopic slide coverslip. The chamber covered a single microelectrode region at a time. The height of the chamber was 560 μm, its length 20 mm and its width 5 mm.

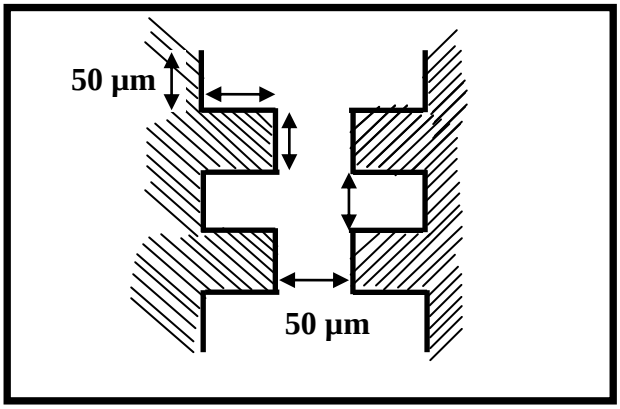

Figure 3.1: Sketch of a 50 μm electrode region (shaded region is ITO); all sides of the electrode measure the same.

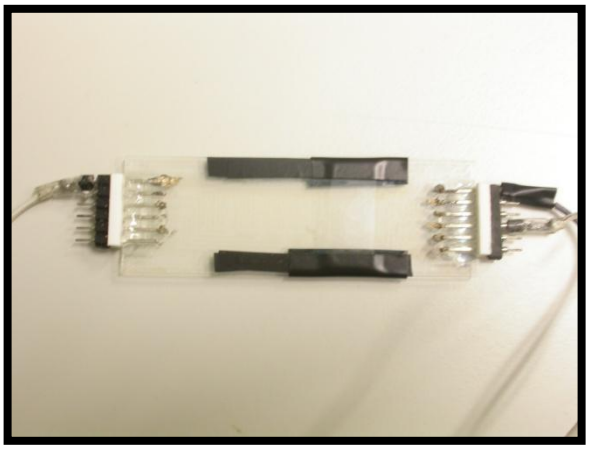

Figure 3.2: An ITO microelectrode slide with the connections made to supply voltage to the 75 µm regions only.

3.6 Dielectrophoretic formation of cell aggregates

A DEP set-up was used to form aggregates as described previously (Sebastian *et al*., 2007 a & b) (Figure 3.3 & 3.4). The chamber was autoclaved prior to use. The chamber was filled with the low conductivity 300 mM D-sorbitol solution, and following this electric fields were generated between the microelectrodes using signals of 1 MHz frequency and voltages of 10 $V_{pk\text{-}pk}$ for electrodes of 25-100 µm, and 20 $V_{pk\text{-}pk}$ for electrodes of 125-200 µm. Electric signals were generated using a Thurlby-Thandar TG120 function generator. Cells were introduced into the chamber and allowed to be attracted to the high field regions between the electrodes. Fresh sorbitol solution was passed through the chamber to redistribute the cells, remove non-attracted cells and maintain a low conductivity in the chamber. For aggregates containing a single cell type more cells were introduced until the height of the aggregate became constant. Methodology used for creating aggregates containing more than one cells type will be described in detail in the relevant chapters. It involved either introducing two cell types simultaneously, or stopping the aggregation of cells of one type before the final height was achieved, and then introducing the second type.

The total time needed to form the aggregates depended on the voltage and the electrode size, but was typically 5 min for aggregates of size 25 – 75 µm and 10 to 20 minutes for aggregates of size 100 – 200 µm.

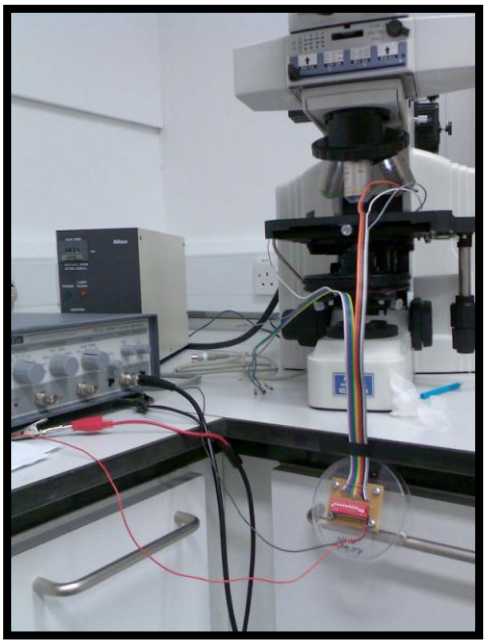

Figure 3.3: Overall set up for carrying out dielectrophoresis.

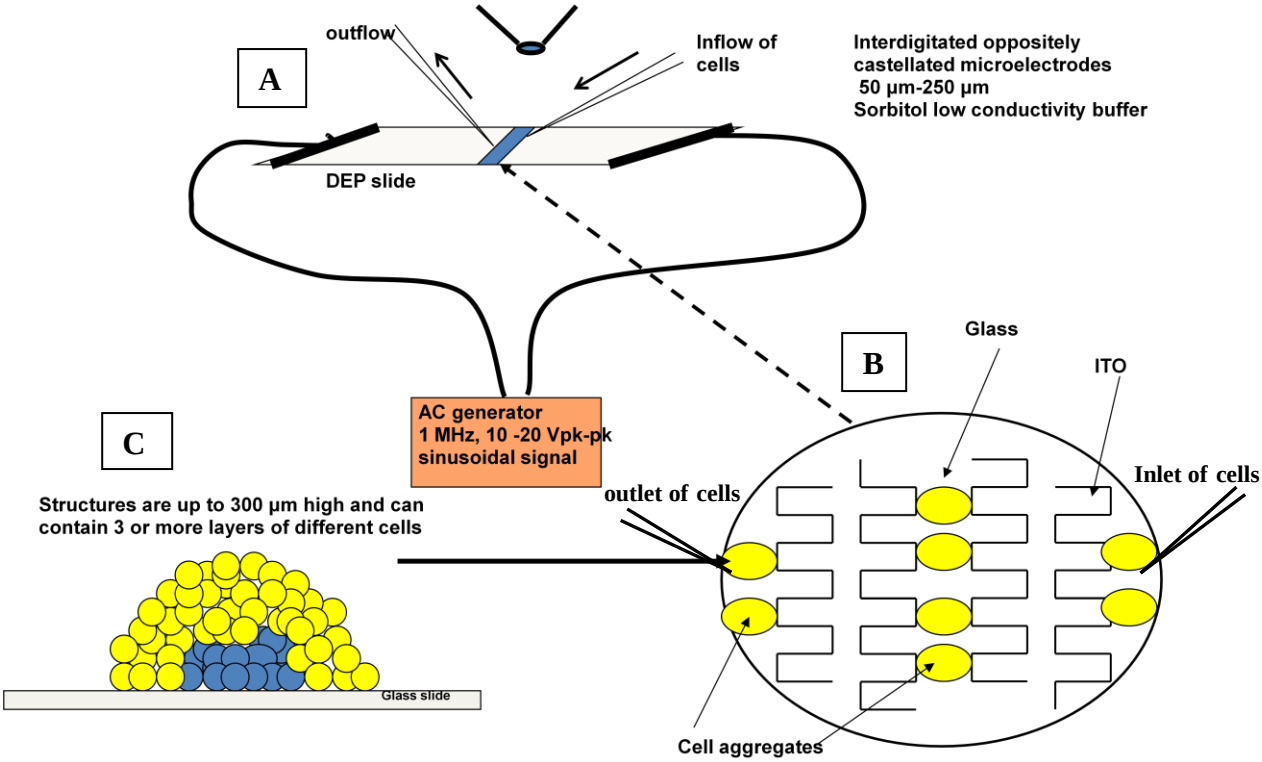

Figure 3.4: Pictorial representation of a dielectrophoresis setup.

A) *Chamber under the microscope, with two pipette tips at both end of the chamber for the inlet and outlet of fluids. The electrode is connected to the frequency generator.* ***B)*** *A magnified view of the electrodes and the cells in patterned aggregates.* ***C)*** *Longitudinal section of an aggregate composed of different cell types.*

3.7 Cell immobilization

After the stem cells and/or osteoblast-like cells had been aggregated with dielectrophoresis between the castellations of electrodes under a flow of 300 mM D-sorbitol the electric field was maintained for a further 10–15 min, in order to induce adhesion between the cells (Sebastian *et al*., 2007). Following this, the sorbitol solution was replaced by a Puramatrix solution. Puramatrix precursor solution was prepared at concentrations ranging from 20% to 50%, but typically 25%, by mixing pure Puramatrix as obtained from the supplier with 300 mM sorbitol solution. The Puramatrix precursor solution selected was brought into the chamber with a pipette tip, and at the same time sorbitol solution was withdrawn with a pipette from the other end of the chamber. The electric field was then removed and growth medium (GMEM for aggregates with only stem cells, RPMI 1640 for osteoblast-like and mixed cultures) was introduced at the edge of the chamber. Gel formation took 5 to 15 minutes (depending upon the concentration, less time for higher concentration and vice versa) from the introduction of the growth medium.

3.8 Aggregate culture

The chamber was placed in a sterile petri dish containing cell growth medium and incubated in mammalian cell culture incubator at 37^{o}C, 5 % CO_2. Over a period of 24-72 hours the petridish was regularly removed from the incubator and the aggregates were observed using a Nikon E600 fluorescence microscope fitted with a Nikon Coolpix 4500 digital camera or a Leica TCS2 confocal microscope.

CHAPTER 4

Optimisation of conditions for niche construction: Electrode size and Puramatrix™ concentration

4.1 Introduction

The induction of haematopoietic cells (HSCs) from embryonic (ESCs) or induced pluripotent stem cells (iPSCs) can give us information on how haematopoietic stem cells are formed during embryogenesis, and could potentially be used for the creation of production methods for blood-based products, including the different types of blood cells. The conventional method for the induction of HSCs from ESCs is a two step procedure in which the ES cells are differentiated as embryonic bodies (EBs) for 5-20 days, followed by dispersion of the cells into a single cell suspension and plating them in Macrophage conditioned medium (MCM) in the presence of appropriate cytokines for hematopoietic colony formation (Wiles & Keller, 1991; Keller *et al*., 1993). Previous studies have revealed that ES cells have been converted to primitive nucleated erythrocyte cells, followed by the formation of definitive erythroid, myeloid cells, neutrophils, mast cells and megakaryocyte cells (Wiles & Keller, 1991; Keller *et al*., 1993; Lieschke & Dunn, 1995). The literature suggests that the differentiated ES cells or the embryonic bodies can contribute to all the hematopoietic lineages (Potocnik *et al*. 1994; 1997; Bichet *et al*. 1999).

A recent review of the methods used for the formation of embryonic bodies from embryonic stem cells has been given by Bratt-Leal *et al*., (2009). The three basic methods for making embryoid bodies are liquid suspension culture in bacterial-grade dishes (Ramirez *et al*., 2007), culture in methylcellulose semisolid media, and culture in hanging drops (Dang *et al*., 2002; Dang *et al*., 2004). Unfortunately, these methods provide poor control over the (initial) cell distribution, and pose limitations to further manipulation of the suspending medium or cells. Physical micromanipulation of cells, on the other hand, potentially is able to allow the formation of aggregates containing stem cells with a high level of control over the initial distribution of the cells without limitations to further manipulation of the cells in the aggregates or to making changes in the composition of the suspending medium (Desai *et al*., 2007; Markx *et al*., 2005; Markx, 2008; Khademhosseini *et al*., 2006). This is particularly

important in attempts to induce the differentiation of haematopoietic cells from ESC or iPSC by coculture with other cells (Krassowska *et al*., 2006; Ledras *et al*., 2008).

The application of dielectrophoresis for the construction of three dimensional cell aggregates containing has previously been demonstrated (Venkatesh *et al*., 2007; Sebastian *et al*., 2007 a & b; Markx, 2009; Markx *et al*., 2009). Such aggregates can be used as artificial stem cell niches (Markx *et al*., 2009). Although it has been demonstrated in previous studies that the viability during the construction of the aggregates can be maintained (Sebastian *et al*., 2007), the long term behavior of the cells after the formation of the aggregates has not been explored. In this chapter we will describe study of the long term behavior of osteoblast-like cells and study of the use of positive dielectrophoresis for the formation of aggregates of embryonic stem cells at interdigitated oppositely castellated electrodes and the formation of EBs after the construction of the aggregates.

4.2 Materials and methods

4.2.1 Cells

ESCs used in the experiments were mouse embryonic stem cells of cell line 7a. Active 7a embryonic stem cells express green fluorescence protein (GFP) regardless of their differentiation state. The cells were grown as described previously (Chapter 3). For dielectrophoretic experiments the cells were washed with 300 mM D-sorbitol in deionised water twice to reduce the medium conductivity, and finally resuspended in 300 mM D-sorbitol solution ($\sigma = 4.7 \times 10^{-4}$ S m^{-1}) for patterning with positive dielectrophoresis.

4.2.2 Dielectrophoretic formation of cell aggregates

A dielectrophoresis setup was used as described previously in chapter three. The system was based around glass slides with ITO microelectrodes of the interdigitated oppositely castellated design with characteristic sizes between 50 and 250 μm. A chamber was constructed on top of the slide from two strips of insulating tape and a microscopic slide coverslip. The chamber covered a single microelectrode region at a time. The height of the chamber was 560 μm, its length 20mm and its width 5 mm. The chamber was autoclaved prior to use. The chamber was filled with the low conductivity 300 mM D-sorbitol solution, and following this electric fields were generated between the microelectrodes using signals of

1 MHz frequency and voltages of 10 Vpk-pk for electrodes with a characteristic size of 25-100 µm, and 20 Vpk-pk for electrodes of 125-200 µm. Electric signals were generated using a Thurlby-Thandar TG120 function generator. Cells were introduced into the chamber and allowed to be attracted to the high field regions between the electrodes. Fresh sorbitol solution was passed through the chamber to redistribute the cells, remove non-attracted cells and maintain a low conductivity in the chamber.

Puramatrix Concentration	**DEP voltage and frequency 1 MHz**	**Culture conditions for SAOS-2 cells**	**Electrode size**	**Repeats with SAOS-2 cells**	**Repeats with ESCs**
50 %	10 Vpk-pk	37º C, 5 % CO_2	100 µm	4	3
30 %	10 Vpk-pk	37º C, 5 % CO_2	100 µm	4	3
25 %	10 Vpk-pk	37º C, 5 % CO_2	75 µm	4	7
20 %	10 Vpk-pk	37º C, 5 % CO_2	100 µm	4	3

Table 4.1: Parameters for determining Puramatrix concentrations.

Electrode size for EB formation.	**DEP voltage and frequency 1 MHz**	**Culture conditions for SAOS-2 cells**	**Puramatrix Concentration**	**Repeats with ESCs**
200 µm	20 Vpk-pk	37º C, 5 % CO_2	25%	5
100 µm	10 Vpk-pk	37º C, 5 % CO_2	25%	5
75 µm	10 Vpk-pk	37º C, 5 % CO_2	25%	5
50 µm	10 Vpk-pk	37º C, 5 % CO_2	25%	5

Table 4.2: Parameters for determining correct electrode size for EB formation.

4.2.3 Surface treatment of sides

In some experiments, to minimize cell adhesion to the surface, glass slides with ITO microelectrodes were incubated for 48 hours in 1-hexadecanethiol (Sigma-Aldrich), washed thoroughly with deionised water, and wiped carefully with water soaked tissue paper. The slides were then checked for defects and the presence of any particles prior to use.

Electrode size for Thiolised slides.	DEP voltage and frequency 1 MHz	Cells	Puramatrix Concentration	Repeats with ESCs
250 µm	20 Vpk-pk	SAOS-2	25%	3
200 µm	20 Vpk-pk	SAOS-2 & ESCs	25%	3
75 µm	10 Vpk-pk	7a ESCs	25%	3

Table 4.3: Parameters for Thiol treated slides.
The Puramatrix concentration and the cell culture conditions were unchanged.

4.3 Results

4.3.1 Formation of aggregates of SAOS-2 osteoblast-like cells with DEP

Immobilization of the cells in the aggregates after the formation of the aggregates by DEP forms an essential step of any attempt to form stem cell microniches; without it, cells would soon disperse. Previous experiments involving the construction of stem cell microniches using DEP had primarily used fibrin gels as the hydrogel for cell immobilization (Sebastian *et al.*, 2007 a & b, Markx 2008; Markx *et al*., 2009). BD Puramatrix™ (3 DM Inc, Cambridge, USA) was chosen as the immobilization agent here because of the low viscosity of the precursor solution and because it is fully synthetic. Puramatrix is a peptide composed of 16 amino acids residues and contains no detectable growth factors or cytokines, allowing one to investigate the reproducibly investigate the effects of added growth factors or cytokines. It is supplied as a low ion solution. After addition of medium it forms a nano-fibrous scaffold resembling collagen in aqueous solution by hydrophobic and ionic bonding of the amino acids, causing the formation of the hydrogel.

To establish the most suitable concentration of Puramatrix, aggregates of osteoblast-like cells were made using DEP at the 75 and 100 µm electrode regions, and different concentrations of Puramatrix were used to immobilise the cells. The concentrations of Puramatrix tested were 50%, 30%, 25% and 20%. Figures 4.1-4.4 show the effects of different Puramatrix concentrations on the distribution of the osteoblast-like cells after 24 hour incubation in RPMI growth medium.

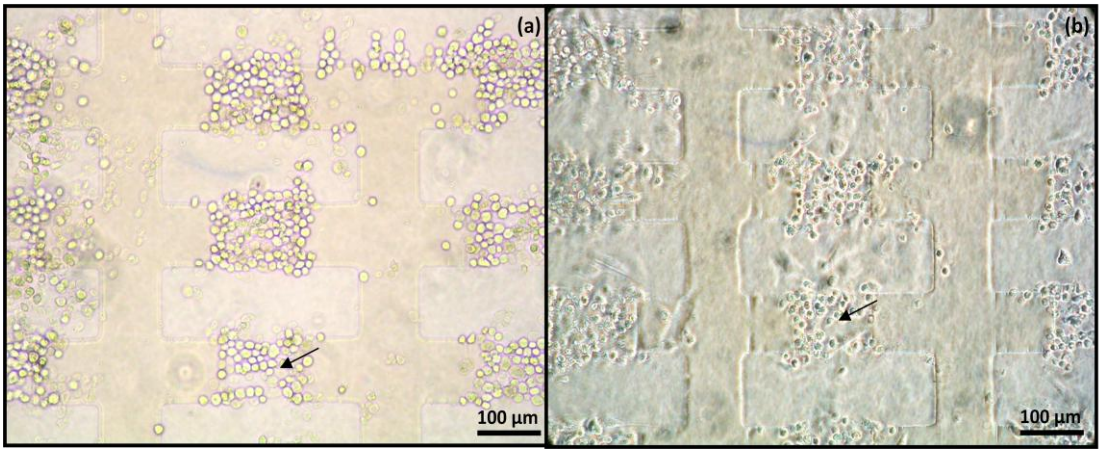

Figure 4.1: SAOS-2 cells immobilized with 50% Puramatrix.

Bright field images of aggregates of SAOS-2 cells formed with DEP between interdigitated oppositely castellated ITO microelectrodes on glass. The microelectrodes had a characteristic size of 100 µm. The electric field between the microelectrodes was induced by applying a 10 $V_{pk\text{-}pk}$, 1 MHz signal to the electrodes. ***A)*** *Aggregates of osteoblast-like cells at 0 hours.* ***B)*** *Aggregates after 24 hours. The Arrows point no movement of cells in the same aggregates.*

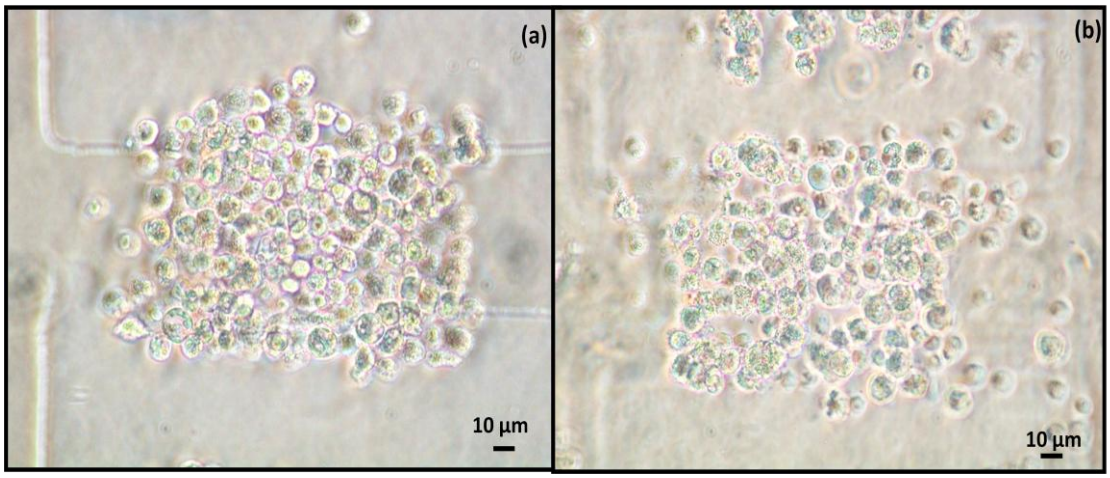

Figure 4.2: SAOS-2 cells immobilized with 30% Puramatrix.

Bright field images of aggregates of SAOS-2 cells formed with DEP between interdigitated oppositely castellated ITO microelectrodes on glass. The microelectrodes had a characteristic size of 100 µm. The electric field between the microelectrodes was induced by applying a 10 $V_{pk\text{-}pk}$, 1 MHz signal to the electrodes. ***A)*** *Aggregate at 0 hours.* ***B)*** *Aggregate after 24 hours.*

At 50% and 30% concentration the Puramatrix precursor solution is very viscous. This causes some cells to become dislodged from the aggregates DEP when the Puramatrix solution is introduced. After 24 hours of incubation the cells can be seen to remain rounded. SAOS-2 osteoblasts normally grow adherently; rounding is usually an indication that the cells are not

satisfied with the growing conditions. There is little evidence of cell movement or of cells adhering to the glass or ITO surface.

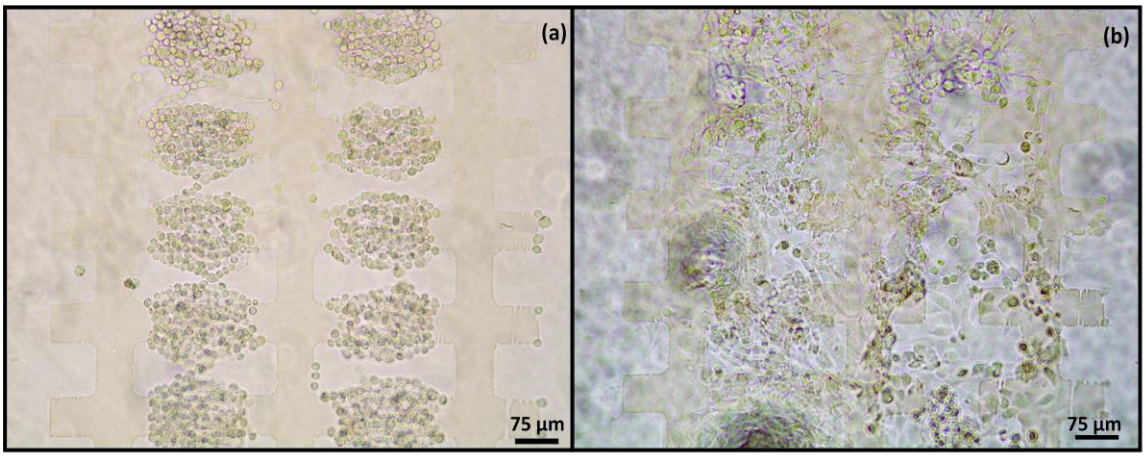

Figure 4.3: SAOS-2 cells immobilized with 25% Puramatrix.

Bright field images of aggregates of SAOS-2 cells formed with DEP between interdigitated oppositely castellated ITO microelectrodes on glass. The microelectrodes had a characteristic size of 75 µm. The electric field between the microelectrodes was induced by applying a 10 $V_{pk\text{-}pk}$, 1 MHz signal to the electrodes. ***A)*** *Aggregates at 0 hours.* ***B)*** *Aggregates after 24 hours.*

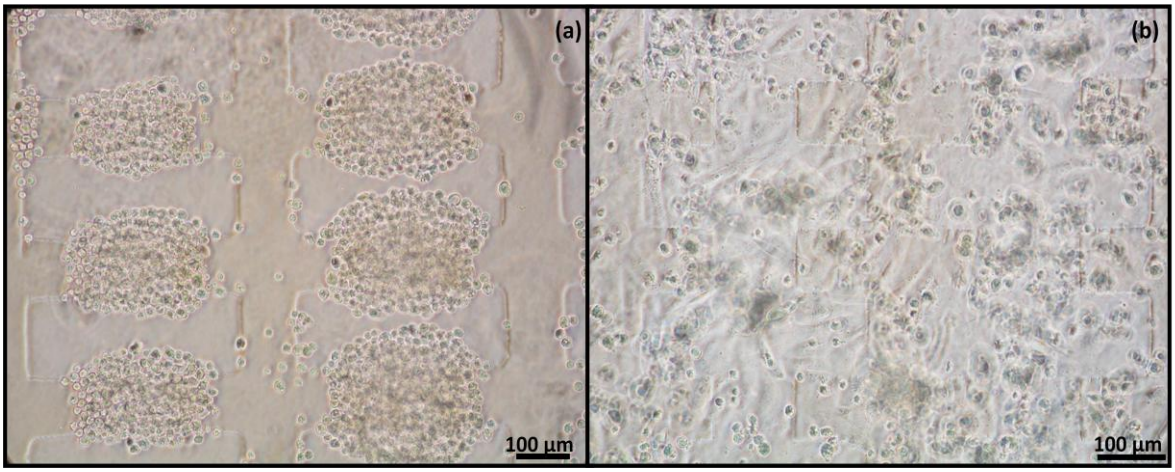

Figure 4.4: SAOS-2 cells immobilized with 20% Puramatrix.

Bright field images of aggregates of SAOS-2 cells formed with DEP between interdigitated oppositely castellated ITO microelectrodes on glass. The microelectrodes had a characteristic size of 100 µm. The electric field between the microelectrodes was induced by applying a 10 $V_{pk\text{-}pk}$, 1 MHz signal to the electrodes. ***A)*** *Aggregates at 0 hours.* ***B)*** *Aggregates after 24 hours.*

At Puramatrix concentrations of 25 and 20%, after 24 hours the cells close to the microelectrode surface had adhered to the electrode surface and had started spreading over the surface. There was no difference between the ITO and glass. Cells further away from the microelectrode surface could sometimes be seen to have started to adhere to each other forming dense aggregates; this was particularly prominent at the lower gel concentration (20%) and larger electrode size (100 μm). The gel formed at the lower Puramatrix concentration of 20% was mechanically weak and difficult to handle without disturbing the integrity of the gel or disturbing the aggregates.

The results indicate that the most suitable concentration of Puramatrix for the immobilization of osteoblast-like cells was 25%. At higher concentrations there were problems with cells becoming dislodged from the aggregates during the assembly process. Also the osteoblast-like cells remained rounded, indicating the cells are not satisfied with the growing conditions. Concentrations below 25% did not have sufficient mechanical strength. Therefore all further experiments were carried out at a concentration of 25%.

Figure 4.5 shows aggregates of SAOS-2 osteoblast-like cells in 25 % Puramatrix, at time zero immediate after their formation and after 24, 48 and 72 hours. At 24 hours the cell can be seen to have started to spread from the aggregates, but the initial location of the DEP aggregated can still be observed. This becomes increasing difficult at later times.

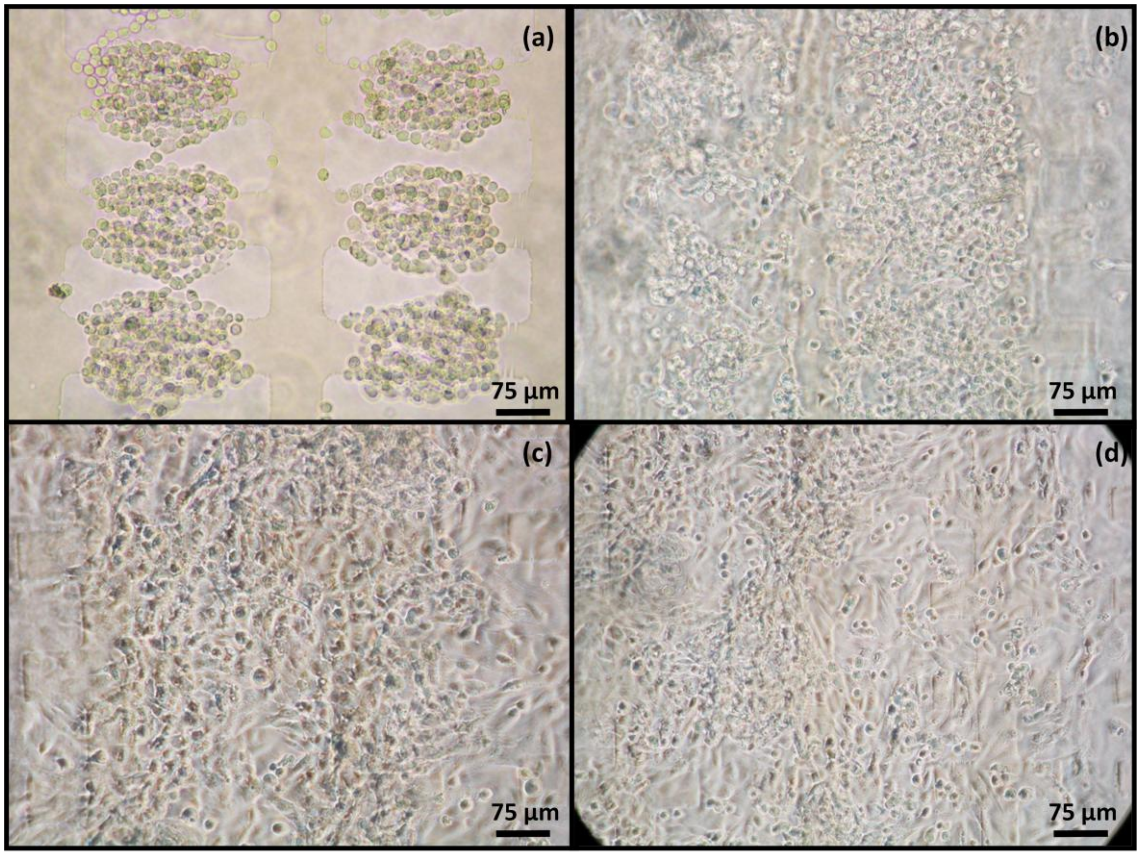

Figure 4.5: Bright field images of aggregates of SAOS-2 cells formed with DEP between interdigitated oppositely castellated ITO microelectrodes on glass.

The microelectrodes had a characteristic size of 75 µm. The electric field between the microelectrodes was induced by applying a 10 $V_{pk\text{-}pk}$, 1 MHz signal to the electrodes. The cells were immobilized with 25% Puramatrix. ***A)*** *Aggregates at 0 hours.* ***B)*** *24 hours.* ***C)*** *48 hours.* ***D)*** *72 hours.*

4.3.2 Formation of aggregates of 7a murine ES cells with DEP

Aggregates were made of murine ES cells at microelectrodes of different sizes ranging from 50 to 250 µm, and immobilised in 25% Puramatrix. Following this, the cells were incubated in GMEM growth medium with and without LIF. Also, control experiments were performed in which the cells were subjected to the same procedure as the DEP- immobilised cells, except that they were not aggregated.

Figure 4.6 shows green fluorescent images of ESC aggregates formed in regions of microelectrodes with a characteristic size of 50 µm. After 24 hours of incubation the cells within the aggregates seen to agglomerate with each other, with non-uniform embryoid body-like structures embedded in the cell agglomerates (Figure 4.5). This happened because the

space between the aggregates was less and the aggregates were closer to each other, making it possible for the single aggregates to merge and form larger aggregates.

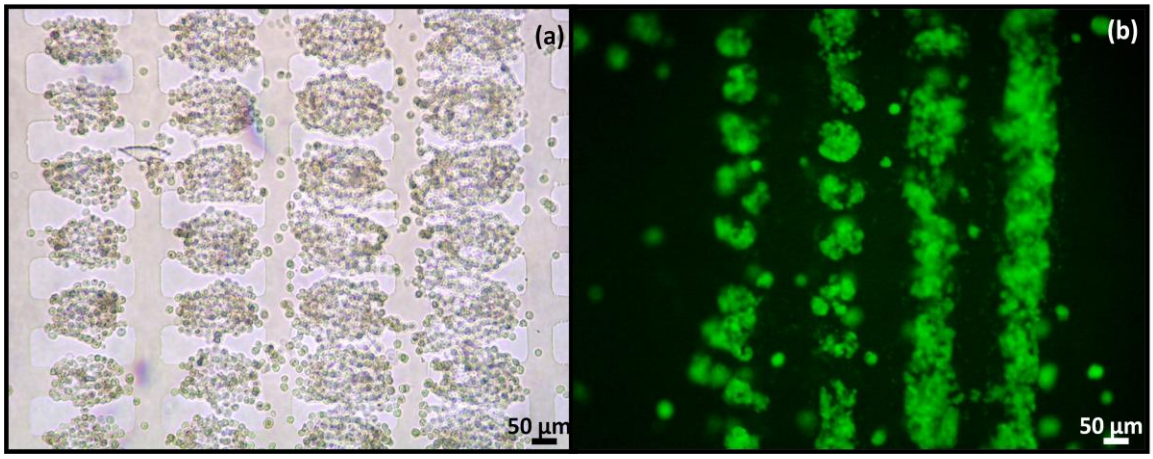

Figure 4.6: Aggregates of 7a ESCs formed by DEP at 10 $V_{pk\text{-}pk}$, 1 MHz in the 50 µm microelectrode regions.

The aggregates were immobilised in 25% Puramatrix, and provided with medium without LIF. ***A)*** *Bright field image of aggregates at 0 hours; cells were introduced from right to left, and more cells can be seen to have accumulated in the aggregates at the right hand side than on the left hand side.* ***B)*** *Green fluorescent image of aggregates after 24* hours *of incubation. Aggregates can be seen to have merged, especially in regions where more cells were in the aggregates at the start.*

When microelectrodes with characteristic sizes of 75 or 100 µm were used the initial distance between the ESC aggregates was slightly larger and the aggregates typically formed single EBs of regular shape and size (Figure 4.7 & 4.8). Since 75 and 100 µm regions showed similar EB formation only 75 µm results are displayed in this chapter.

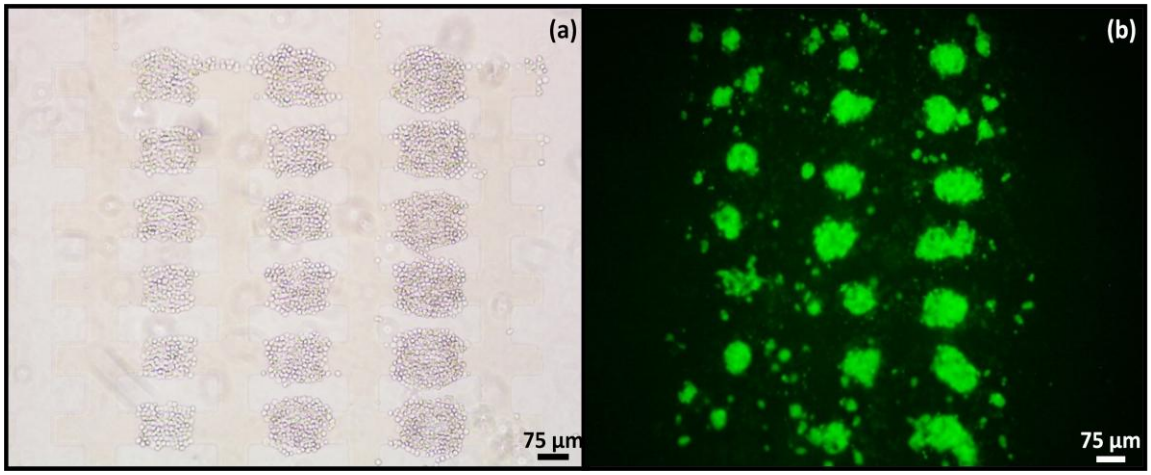

Figure 4.7: Aggregates of 7a ESCs formed by DEP at 10 $V_{pk\text{-}pk}$, 1 MHz in the 75 µm microelectrode regions.

The aggregates were immobilised in 25% Puramatrix, and provided with medium without LIF. ***A)*** *Aggregate at 0 hours.* ***B)*** *Aggregate after 24 hours of incubation.*

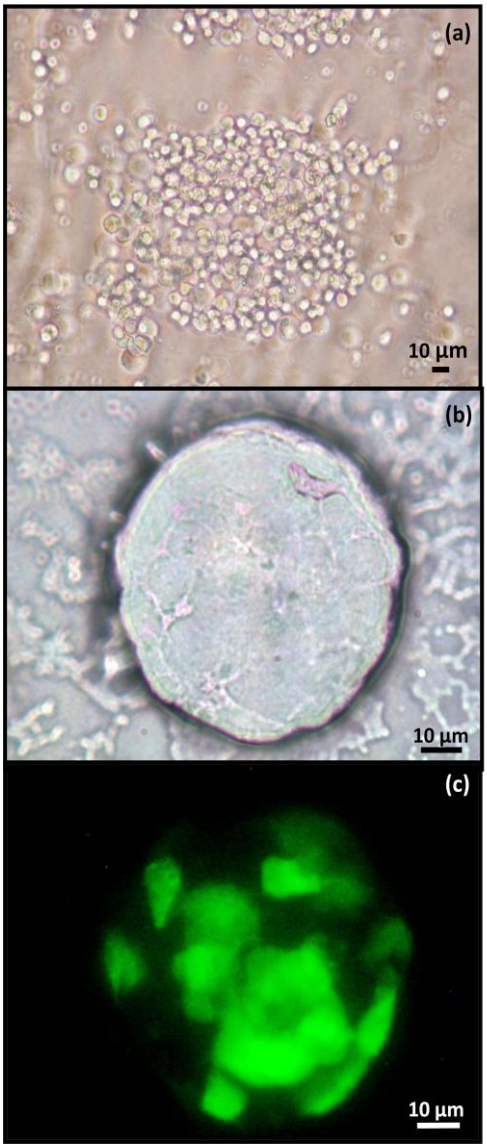

Figure 4.8: A closer look at the EB.

Aggregate of 7a embryonic stem cells formed by DEP at 10 $V_{pk\text{-}pk}$, 1 MHz in the 75 µm microelectrode regions. The aggregates were immobilised in 25% Puramatrix, and provided with medium without LIF. ***A)*** *Aggregate at 0 hours.* ***B)*** *Aggregate after 24* hours *of incubation. A single embryoid body can be seen.* ***C)*** *Green fluorescent image of the embryoid body.*

Figure 4.9 shows aggregates formed at microelectrodes with a characteristic size of 200 µm. At regions above 100 µm the cells within an individual aggregate condensed into several high density regions, causing the aggregates to split.

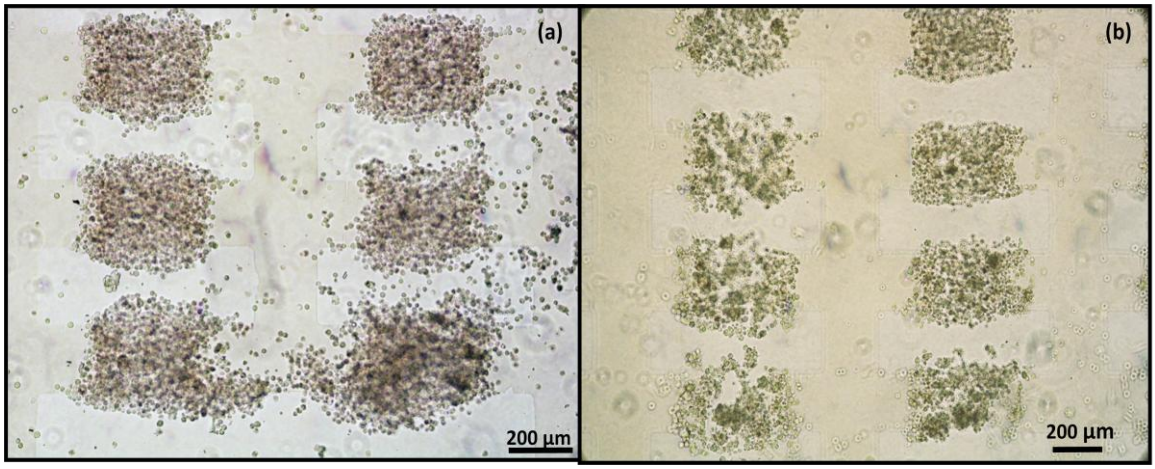

Figure 4.9: Aggregates of 7a ESCs formed by DEP at 20 $V_{pk\text{-}pk}$, 1 MHz in the 200 µm microelectrode regions.

The aggregates were immobilised in 25% Puramatrix, and provide with medium without LIF. ***A)*** *Aggregates at 0 hours.* ***B)*** *Aggregates after 24 hours of incubation. Within the aggrates many small cell clumps can be seen to have formed.*

The experiments were conducted both in medium containing LIF and without LIF. Aggregates cultured in medium without LIF showed rapid EB formation, typically within 24 hours. Aggregates cultured in medium containing LIF showed delayed formation of EB, however EB formation still occurred, typically within 48 hours. In control experiments cells were exposed to the same procedure as the cells which were aggregated with DEP, but electric field exposure was omitted, and no aggregation therefore occurred. When grown in medium with LIF the cells resumed undifferentiated growth as a monolayer, indicating that the handling of the cells, including their temporary suspension on a low conductivity sorbitol solution, did not change the characteristics of the stem cells.

Figure 4.10 shows aggregates of ESCs at 50 µm region at zero, 24, 48 and 72 hours. At 24 hours the aggregates start forming EBs and at 48 hours the EBs are seen to move towards closer EBs and agglomerate. At 48 hours the EBs still merge with nearby EBs and also grow in size.

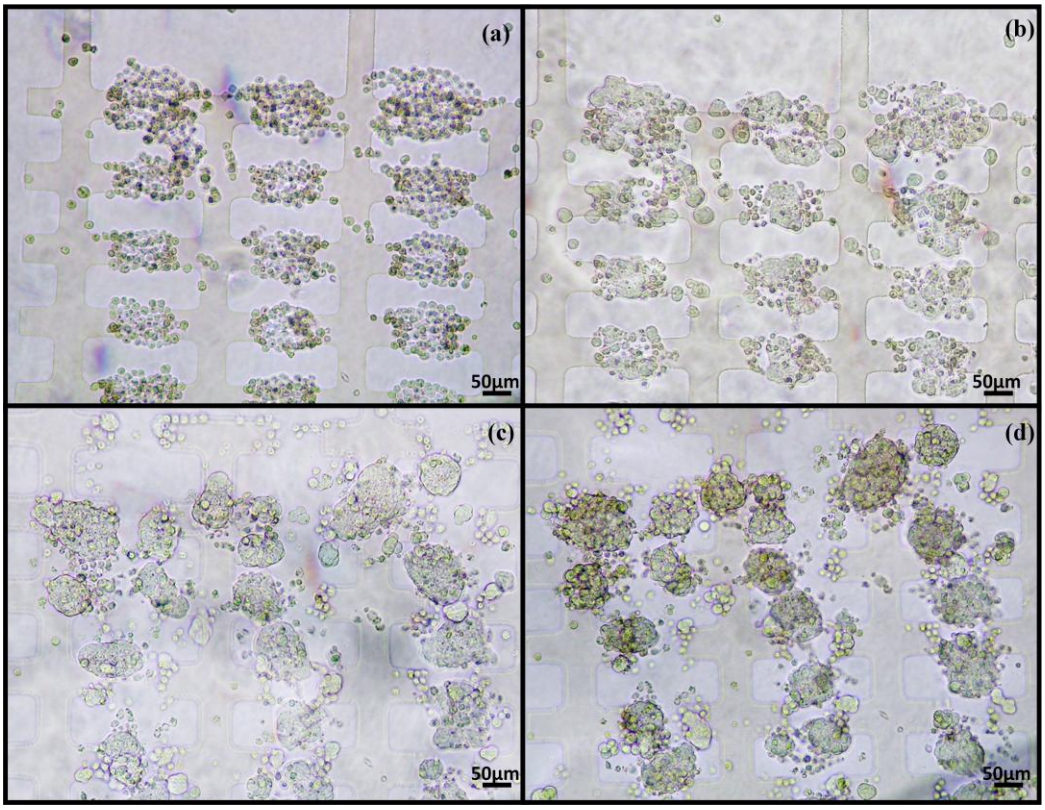

Figure 4.10: Agglomeration of EBs.

Aggregates of ESCs formed by DEP at 10 Vpk-pk, 1 MHz in the 50 µm microelectrode regions. The aggregates were immobilised in 25% Puramatrix. With time the aggregates form EBs and the EBs are move and agglomerate with other nearby EBs. ***A)*** *Aggregates at 0 hours.* ***B)*** *Aggregates after 24 hours of incubation.* ***C)*** *Aggregates after 48 hours.* ***D)*** *Aggregates after 72 hours.*

4.3.3 Influence of properties of the electrode surface on the merging of aggregates

The experiments with the 50 micron electrodes indicated that, when the aggregates are close, merging may occur between aggregates. The electrode surface might play a role in the movement of the EBs within the chamber. Therefore, to investigate the role of the electrode surface in the merging process, DEP slides were treated with 1-hexadecanethiol. Treatment with 1-hexadecanethiol would make the surface highly hydrophobic and could be expected to prevent cells from adhering to the surface and travelling between aggregates.

Figure 4.11 shows aggregates formed with DEP of SAOS-2 osteoblast-like cells on hexadecanethiol treated electrode surfaces. Treatment of the surface with 1-hexadecanethiol appears to make the electrode surface unsuitable for the attachment of SAOS-2 osteoblast-like cells. The cells were rounded, stayed mainly in their original position, and there was no

evidence of cells attachment or spreading over the surface. This behaviour was seen at all electrode sizes.

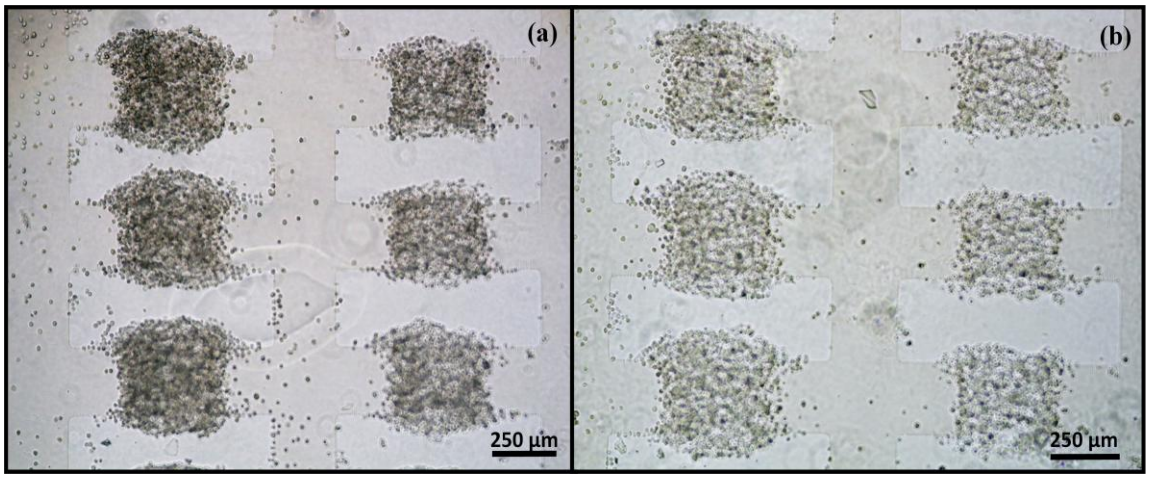

Figure 4.11: Aggregates of SAOS-2 cells formed by DEP at 10 $V_{pk\text{-}pk}$, 1 MHz in the 250 µm microelectrode thiolized regions.

The aggregates were immobilised in 25% Puramatrix. ***A)*** *Aggregates at 0* hours. ***B)*** *Aggregates after 24 hours of incubation. No cell adherence to the glass or the ITO surface can be seen.*

From Figure 4.12 it can be seen that after 24 hours on untreated surfaces embryonic bodies formation have been formed, but significant numbers of cells can also be seen between aggregates. After 72 hours there is evidence of significant cell growth; also merging of aggregates and movement of cells between aggregates has led to significant coarsening of the original pattern. Figure 4.13 and 4.14 shows the effects of microelectrode surface treatment on the behaviour of ES cells after the formation of cell aggregates with DEP. Figure 4.13 shows the effect of treating the surface with 1-hexadecanethiol. Unlike the previous experiment, although there is evidence of cell growth, there is no evidence of the exchange of cells between embryonic bodies, and merging of aggregates did not occur.

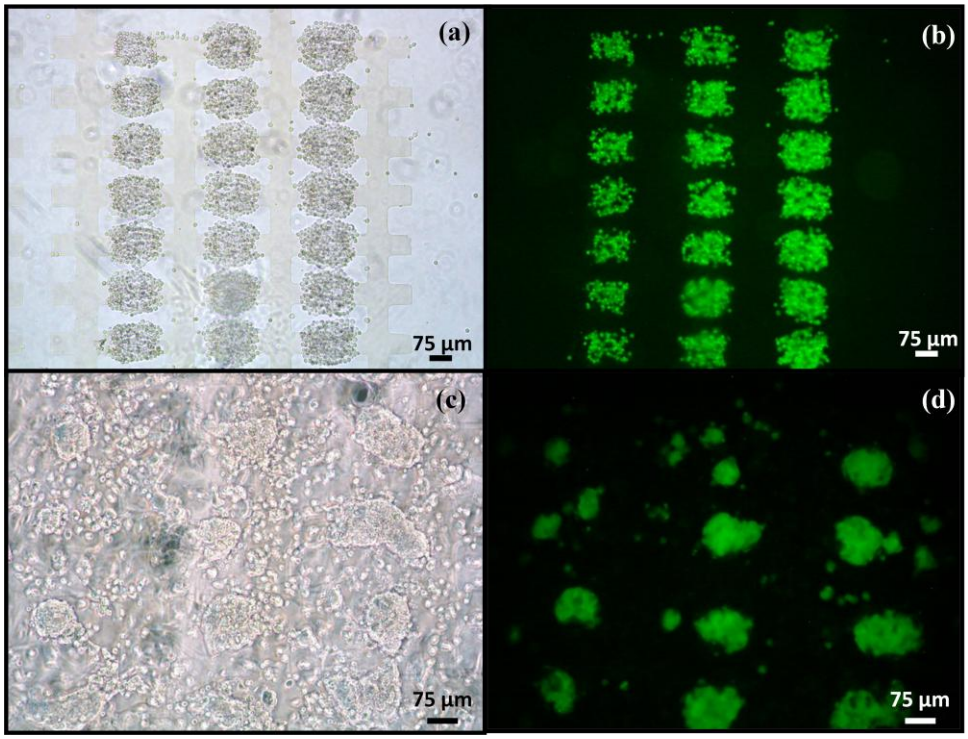

Figure 4.12: Aggregates of 7a murine ESCs and SAOS-2 cells formed by DEP at 10 $V_{pk\text{-}pk}$, 1 MHz in the 75 µm microelectrode regions (untreated slide).

The aggregates were immobilised in 25% Puramatrix, and provided with growth medium without LIF. ***A1 & A2)*** *0 hours bright field and fluorescent image respectively.* ***B1 & B2)*** *24 hours bright field and fluorescent image respectively, the top 3 rows of aggregates from image A1, are zoomed in on the image B1. The SAOS-2 cells are seen to spread on the substrate surface.*

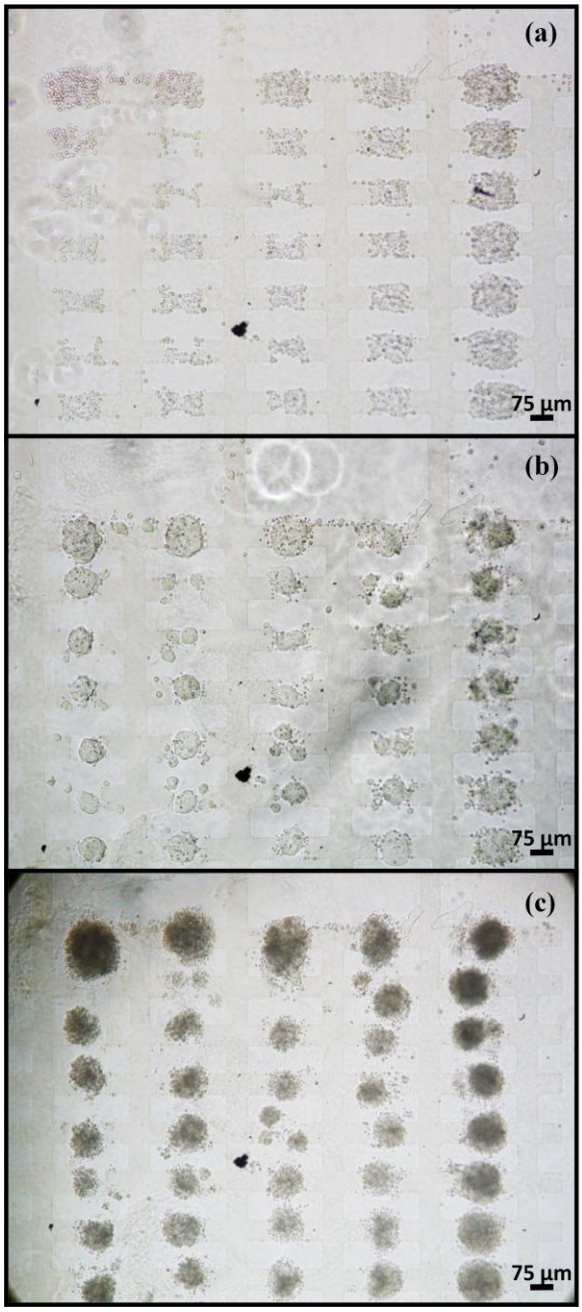

Figure 4.13: Aggregates of 7a murine ESCs formed by DEP at 10 $V_{pk\text{-}pk}$, 1 MHz in the 75 µm microelectrode regions, treated with 1-hexadecanethiol.

The aggregates were immobilised in 25% Puramatrix. ***A)*** *0* hours ***B)*** *24* hours ***C)*** *48* hours.

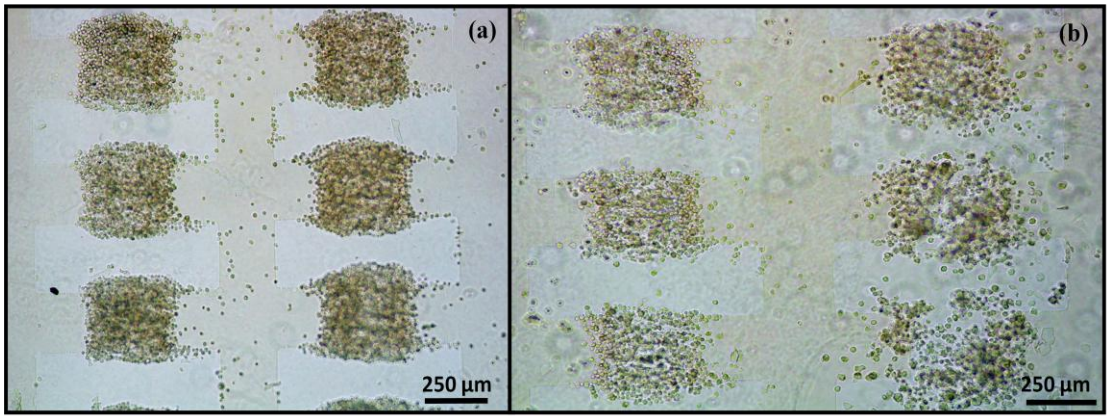

Figure 4.14: Aggregates of 7a ESCs and SAOS-2 cells formed by DEP at 20 $V_{pk\text{-}pk}$, 1 MHz in the 200 µm microelectrode regions on a thiolised slide.

The aggregates were immobilised in 25% Puramatrix, and provide with medium without LIF. ***A)*** *Aggregates at 0 hours.* ***B)*** *Aggregates after 24 hours of incubation. Within the aggrates many small EBs can be seen to have started to form.*

4.4 Discussion

The experiments showed that considerable cell rearrangement occurs after the formation of aggregates with DEP. Although some cell growth was also observed, adhesive forces appear to play the most dominant roles in the cell rearrangement process.

Adhesive forces can be divided into the cell-cell adhesion and adhesion between cells and the surrounding materials- in this case the Puramatrix gel and the microelectrode surface. The behaviour of the osteoblast-like cells can most simply be explained on the basis of their preference for (in this order) adherence to the microelectrode surface, each other, and the Puramatrix gel. The behavior of the stem cells is more complex. Upon aggregation the stem cells initiate the differentiation process and change the production of cell adhesion molecules, resulting in a loss of adhesion to the microelectrode surface, and an increase in cohesive forces, leading to the formation of embryonic bodies. Such behavior is similar to surface tension forces in mixed immiscible fluids (Steinberg *et al*., 2007).

After aggregation with DEP embryonic body formation occurs in medium with LIF as well as medium without LIF. The presence of LIF slows the onset of differentiation and embryoid body formation down, but does not prevent it. This indicates that aggregation by DEP initiates the differentiation process. It is well known that all human and murine ES cells need aggregation to initiate EB formation (Dang *et al*., 2002; Itskovitz-Eldor *et al*., 2000).

Engineered aggregation of stem cells has been shown to accelerate EB formation (Gothard *et al*., 2009), a finding which has been confirmed in our experiments. Established protocols for suspension culture technique, for producing EBs takes 3-5 days incubation of cells suspended in differentiation medium, where as hanging drop method requires 2 days incubation period (Kursad, 2006). However, with DEP the maximum required time depends upon the electrode size. For an average 100 -50 µm electrode size, the time required for ESCs to form EB without LIF is 24 hours, which is comparatively quicker than suspension culture and hanging drop method.

Although very low frequency (1 Hz) AC sinusoidal electric field have been shown to affect stem cell differentiation (McCullen *et al*., 2010), the AC fields used in this study were of a much higher frequency (1 MHz). It is not known from the experiments whether the electric field used to aggregate cells induces ESC differentiation, or the fact that the cells are aggregated.

The size of the aggregates plays an important role in the formation and survival of embryoid body-like structures and also determines the fate of the ES cells (Hwang *et al*., 2009). It is known that ES cell differentiation is affected by cues from the microenvironment, which directly or indirectly depend on the size of the EB (Watt *et al*., 2000; Falconnet *et al*., 2006; Ng *et al*., 2005). Because we did not investigate what cell type the cells differentiate into after the differentiation process has been started, it isn't known whether the formation of different sized aggregates with DEP affects cell fate.

Merging of EBs is known to hinder efficient cell growth and differentiation (Dang *et al*., 2002). Several ways have been introduced to prevent the agglomeration of EBs as they hinder the growth of the cells and the differentiation, including the use of hanging drops and encapsulation in various matrices (Magyar *et al*., 2001; Dang *et al*., 2004; Fernandes *et al*., 2007; Carpenedo *et al*., 2009; Nonaka *et al*., 2008; Levenberg *et al*., 2003). In the case of EBs formed with DEP, merging of the EBs can be prevented by making the surface of the substrate unsuitable for adhesion.

4.5 Conclusions

The work done concludes that dielectrophoresis can be used as a technique to make artificial aggregates of embryonic stem cells and induce them to not only to form embryoid

bodies, but also form at a faster speed when compared to the hanging drop method. This work has also looked into optimizing the factors essential for maintenance of EBs, like the concentration of the immobilizing agent being 25 % and the electrode sizes for embryonic body formation appearing to be around 75-100 micron. These parameters will be used in further experiments.

The existence of an embryonic stem cell niche in the presence of SAOS-2 cells showed different cell behavior. It is proposed that the behavior of the cells in the aggregates formed by DEP is mainly controlled by the adhesive properties of the cells to the different surfaces that are available to the cells, similar to the Differential Adhesion Hypothesis of Steinberg and co-workers (Steinberg, 1970; 1978; Foty and Steinberg, 2004). Cell rearrangement after their DEP patterning there appears to be controlled by their need to minimize their free adhesive energy. Therefore it becomes highly important to address this issue, to maintain maximum cell-cell interaction, the diffusion of cells from an aggregate need to be studied and initial rearrangement of cells would be experimented with, to maintain an embryonic stem cell niche, involving maximum cell-cell communication.

CHAPTER 5

Application of image analysis to the investigation of the movement of cells in artificial stem cell niches created with DEP

5.1 Introduction

Cell aggregates are important tools in the study of tissue development, permitting the correlation of cell-cell interactions with cell differentiation, viability, and migration, as well as subsequent tissue formation. Aggregate morphology permits re-establishment of cell-cell contacts normally present in tissues; therefore, cell function and survival are often enhanced in aggregate culture (Cirulli *et al*., 1993; Peshwa *et al*., 1994; Koide *et al*., 1989; Parsons-Wingerter and Saltzman, 1993; Falascaa *et al*., 2001). Because of this, cell aggregates may also be useful in tissue engineering, enhancing the function of cell-base hybrid artificial organs (Nyberg *et al*., 1993; Shimizu *et al*., 2003; Kelm and Fussenegger, 2004) or reconstituted tissue transplants (Langer, 1993).

Cell migration is the process by which cells translate from one location to another. Migration of individual cells from an aggregate or within a tissue is important in tissue engineering, and a critical element in the formation of the architecture of organs and organisms (Trinkhaus, 1984). Except for a small number of exceptions (e.g. sperm) mammalian cells cannot swim, and to migrate the cells need to attach to their surroundings. Cell-cell adhesion and cell-matrix adhesion is therefore important for cell motility. Cell migration involves a repetitive process of lamellipodial adhesions at new surface site, followed by detachment from an old site. Cell adhesion and traction helps the cell to pull itself forward. The rate of migration of cells is influenced by the presence of local signals in the form of diffusible factors and the composition of the extracellular matrix (Ablamunits *et al*., 1990; Geho *et al*., 2005).

Cell migration is often thought to be the result of a persistent random walk (Patlak, 1953). In the short term cell movement is persistent, i.e. continues in a specific direction. After a certain time the cell, however, reorients itself, and then continues in another direction. In a pure random walk the direction of the cell is purely random and the persistence time constant. This type of unbiased movement can be described like Brownian motion and can be

modeled using the standard diffusion equation. Random walks in which there is a bias in a preferred direction are termed biased random walks (BRWs). The bias may be due to different reasons. They include external physical fields, for example gravity (e.g. bottom heavy micro-organisms moving upwards under gyrotaxis (Hill & Hader, 1997); spatially varying factors, such as chemical gradients (Alt, 1980; Othmer *et al*., 1988), mean-reversion mechanisms, such as movement within a home range (Blackwell 1997), or a choice of direction by individuals at each step (Benhamou, 2003). Directed movement of mammalian cell is important in many phenomena, including metastasis (Poste and Fidler, 1980), embryogenesis (Trinkhaus, 1984), angiogenesis (Carmeliet and Jain, 2000), and immune response (Wilkinson and Lackie, 1979). The movement of cells which show BRW can be described by the drift–diffusion (Codling *et al*., 2008).

The physiological significance of cell migration has motivated numerous experimental studies (Bellairs *et al*., 1982; Lackie, 1986), beginning with seminal time-lapse studies of Comandon (Comandon, 1917). Imaging techniques have since permitted observation of movement of individual cells within living tissue *in vivo* and *in vitro*. Fluorescent dyes are often used to label cells. Immunological or genetic markers such as green fluorescent proteins (GFPs) can be introduced into specific cell populations by transfection (Misteli and Spector, 1997; Huang *et al*., 1998), to permit tracking of lineages during development and migration (Okada *et al*., 1999). Natural cell markers, example melanin, expressed by only a specific cell type are also used to track cells in vivo (Chambers *et al*., 1992; Luzzi *et al*., 1998). Tracking can be done by time-lapse microscopy (Okada *et al*., 1999; Kulsea *et al*., 1998; Kulsea *et al*., 2002) or conventional microscopy after sectioning (Sheen *et al*., 1995) or collecting tissue samples (Andrade *et al*., 1998). The time lapse technique permits quantitative analysis of movements of individual cells and can provide insights into the mechanisms of cell migration. Time lapse migration studies have been performed to evaluate cell migration in 2 dimensions (Cukierman *et al*., 2002) or 3 dimensions (Knapp *et al*., 2000; Schreiber *et al*., 2001; 2003). Techniques that have been used for cell tracking include laser scanning microscopes which enable visual analysis and measurement of submicron dynamic processes inside living cells and tissues. Non-linear laser microscopy based on two-photon imaging can be used to view DNA stains in developing embryos and cells (Denk *et al*., 1995; Williams *et al*., 1994). Automated image analysis systems have been used to record data to fit a persistent random walk model to cell migration experiments (Dunn and Brown, 1987). Dickinson and Tranquillo (1993) developed algorithms to estimate the migration and the traction of a population of cells

separately as time-invariant values, which made statistical comparisons among experiments easier. Barocas and Tranquillo (1997a) quantified cell migration by modeling cell movement as a persistent random walk analyzed with a generalized least squares regression (GLSR) algorithm. Knapp *et al*. (2000) developed an *in vitro* isometric cell traction assay that made it possible to collect the required data to calculate the random cell migration coefficient and the cell traction parameter for the same population of cells.

In previous work (this work, chapter 4) it was shown that aggregates could be made of mammalian cells using dielectrophoresis. It was also shown that dielectrophoresis can be used to create 3-dimensional artificial stem cell niches from osteoblast cells on a microelectrode surface. Cell movement occurred after the formation of aggregates. The adhesion of cells to the microelectrode surface and their spread from an aggregate, however, modifies the niche structure and affects cell-cell contacts. The cell movement in previous experiments was only observed intermittently, as aggregates could only be observed after prolonged intervals. In this chapter it is described how aggregates were formed of SAOS-2 cells with DEP, immobilized in Puramatrix gel, and then continuously monitored for 24 hours to study the the time-dependent movement of these cells from aggregates after the formation of the aggregates. Image analysis was used to analyse the movement of individual cell. It was attempted to interpret the movement of the cells in terms of a random walk. Such studies were expected to help in optimising the formation of cell aggregates for use as artificial stem cells niches.

5.2 Material and methods

5.2.1 Cells

SAOS-2 adherent osteoblast-like cells were grown in RPMI 1640 medium supplemented with 10% FCS, 12 mM glutamine, 100 units ml^{-1} penicillin and 100 µg ml^{-1} streptomycin in a humidified chamber with 5% CO_2 at 37°C until near 90% confluence was obtained (3-4 days). Medium was exchanged every 2 days. The cells were harvested using filter sterilized 0.5% trypsin and 0.5% EDTA dissolved in 1X PBS. Following this, the cells were washed twice with 300 mM D-sorbitol in order to lower the conductivity to allow patterning with positive dielectrophoresis.

5.2.2 Dielectrophoretic formation of cell aggregates

A DEP set-up was used to form aggregates as described previously (chapter 3; Sebastian *et al*., 2006). Microelectrodes were of the interdigitated oppositely castellated design; only microelectrodes with a characteristic size of 75 μm were used in the experiments. The chamber was autoclaved prior to use. The chamber was filled with the low conductivity D-sorbitol solution, and following this electric fields were generated between the microelectrodes using signals of 1 MHz frequency and voltages of 10 $V_{pk\text{-}pk}$ generated using a Thurlby-Thandar TG120 function generator. Cells were introduced into the chamber and allowed to be attracted to the high field regions between the electrodes. Fresh sorbitol solution was passed through the chamber to redistribute the cells, remove non-attracted cells and maintain a low conductivity in the chamber. More cells were introduced until the height of the aggregate became constant. The electric field was then maintained for a further 10 minutes to force the cells to adhere to each other and the glass surface. The electric fields could then be removed.

To immobilize the cells, 25% Puramatrix, mixed with 300 mM sorbitol solution was introduced into the chamber. RPMI 1640 medium was introduced at the edge of the chamber in order to initiate gel formation. Gel formation took 5 to 10 minutes from the introduction of the medium. The chamber was placed in a sterile petri dish on top of a microscope stage containing 60 mL RPMI1640 cell growth medium; HEPES buffer was added to the medium at a final concentration of 25 mM to maintain the pH level in the medium. The microscope had a heated stage and was covered by a transparent hood to keep temperature constant at 37^{o}C. A small vessel with water was placed inside the hood to maintain humidity inside the chamber.

5.2.3 Image analysis

A CCD video camera was used to take live video of the cells over a period of 24 hours**.** The video camera was connected to a laptop to simultaneously view and record images. The video would only run actively for one hour and then would automatically stop. Therefore every hour the video had to be reactivated; at this time a check was made whether the lens was accurately focused on the aggregate.

From the video the position of a given cell was traced onto graph paper (see Figure 5.1) and its position (x and y axis co-ordinates) at 15 minutes time intervals was extracted

from the trace. The data was then put into Matlab and plotted using the algorithm given in appendix II and III.

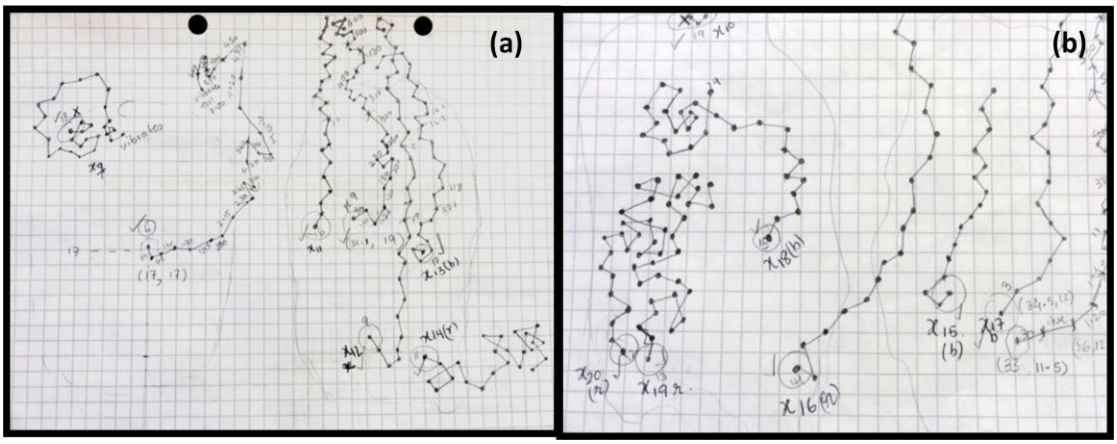

Figure 5.1: Trajectories of randomly selected cells plotted every 15 minutes on a graph sheet A & B show path of cells.

Each dot represents a 15 minutes time period.

It was assumed that the movement of the cells could be described by a random walk with short-term directional persistence. The movement of a given cell was therefore expected to persist in whatever direction a cell was migrating at short observation times, but at long observation times the migration would be random. The path chosen by the cell was therefore impossible to predict in the long term, however if a number of cells were tracked in the same lattice the average manner in which cells moved should be predicable. The mean squared displacement of the cells in the random walk would be expected to increase linearly with time (Denny, 1993).

In this study the cells were embedded in a 3D tissue construct which was observed from the top only. The average mean squared displacement was calculated from the cell position (x and y coordinate) by the equation

$$X_x(n)^2 + X_y(n)^2 = n\delta^2 \qquad (5.1)$$

Where $X_x(n)$ and $X_y(n)$ are the x and y coordinates, respectively, relative to the starting position at step n (see Appendix I for a derivation of the equation). δ is the distance travelled by a cell during a step. If it is assumed that a cell takes a constant step δ every τ seconds, and the number of steps taken is equal to t/τ, where t is the time since the particle started its walk, then inserting this expression for n in equation 7.1 gives:

$$< X_x(t)^2 + X_y(t)^2 > = \frac{\delta^2}{\tau} t \quad (5.2)$$

The mean squared distance travelled by the cell increases directly with time at a rate that is dependent on the ratio of δ^2 to τ. This ratio is equivalent to a diffusion coefficient (Denny, 1993).

$$\text{Diffusion coefficient } D = \frac{\delta^2}{\tau} \quad (5.3)$$

In a purely random walk, the average displacement should be zero. However, during the experiment it was observed that the average displacement was not zero. The most likely cause for this fact was most likely drift of the gel matrix during the experiment. The drift velocity could be estimated by dividing the total measured average displacement by the total time. The drift velocity (in direction $i = x, y$) was therefore:

$$V_i = \frac{average\ total\ displacement}{total\ time} \quad (5.4)$$

Assuming that the drift velocity was approximately constant during the experiment, the displacement due to drift ($x_{id} = V_i \times t$) was subtracted from the measured displacement to find the displacement due to the random walk only.

5.4 Results

After forming the aggregates the cells were monitored for 24 hours. Two randomly chosen aggregates were studied. Active cell movement was observed in the first 7 hours. The movement of the cells then slowed down. Cell lysis was observed near the end of the 24 hours period. This indicated that the conditions on the microscope and the medium composition were not optimal for the cells. Only data from the first 7 hours were analysed.

Figure 5.2 shows stills of the video of the cells obtained at different time intervals. It is clear from the stills that the cells at different regions of the electrode move differently within the immobilized gel over time.

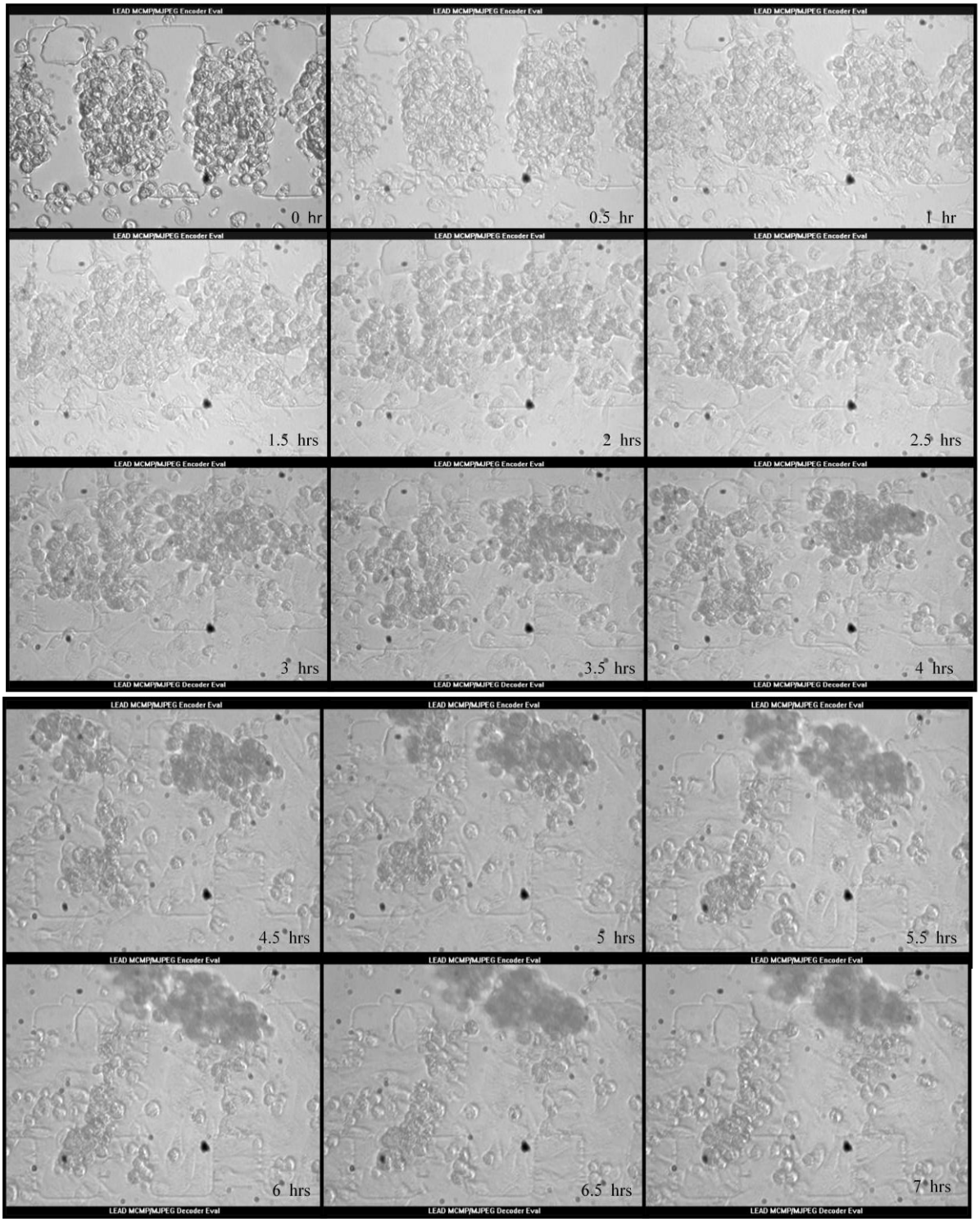

Figure 5.2: Real time imaging of SAOS-2 cell aggregates formed by DEP at 75 µm electrode region, 10 $V_{pk\text{-}pk}$ and 1 MHz.

The cells were observed under the Nikon E60 microscope for 24 hours but image up to 7 hours only are shown.

To investigate this further, the paths of a number of single cells within the aggregates were traced and plotted. Results are shown in Figure 5.3.

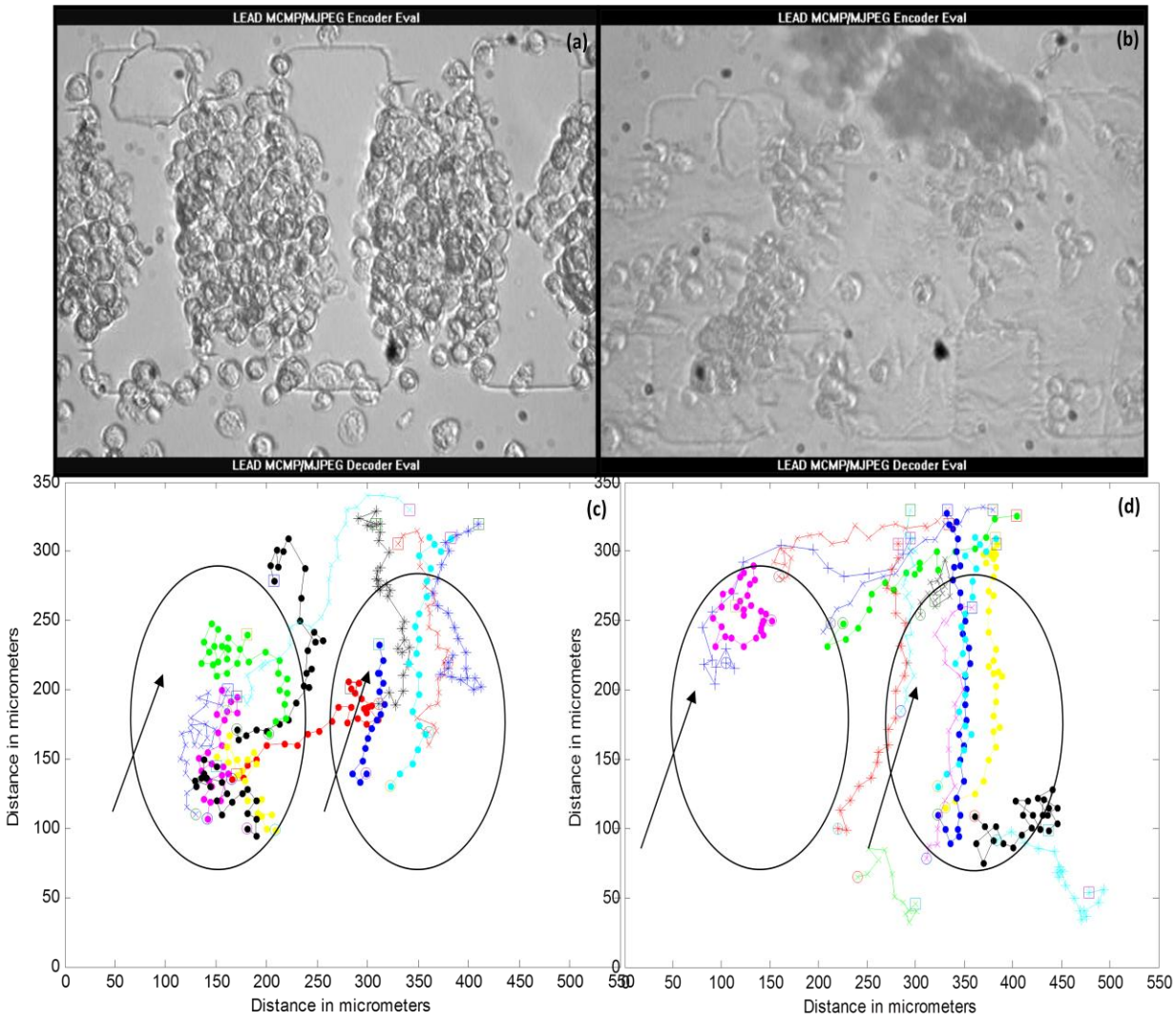

Figure 5.3: Migration trajectories of random SAOS-2 cells.

A) *Image of two aggregates at time zero in the 75 µm region, immobilized in 25% Puramatrix.* ***B)*** *Image of two aggregates after 7th hour.* ***C)*** *and* ***D)*** *Migration trajectories of cells from the centre (C) and the periphery (D) of the aggregates. All the cells are in different colors and have a different marking style. Each point on the line roughly indicates a 15 minute gap. The starting position of a given cell is indicated by a circle and the end point is indicated by a square. The arrows indicate the overall direction of migration/drift. In C) cells in the centre of the aggregate can be seen to either perform a random walk within the aggregate, or migrate towards the top right hand side of the image. In D) cells on the periphery can be seen to perform a random walk over the microscope slide surface, with a significant drift/migration towards the top right hand side of the image. The Oval structure represents the initial aggregates size and shape.*

B) From the video, and the analysis of the movement of single cells, the following picture now emerges:

- Most if not all cells made short term random movements during the observation period. These short term random movements were more prominent for the cells at the periphery (which had more space to move, and also could propel themselves easily over the electrode surface to which they adhered) than for the cells in the centre of the aggregates, which were inhibited in their movement by neighbouring cells, and often did not have direct access to an electrode surface to adhere to.

- Cells in the centre of the aggregate had a tendency to clump together. This was particularly prominent for cells at the top of the aggregate. The cells at the top in each aggregate had formed separate clumps by 4.5 hours after the start of the experiment, but near the end of the experiment the two clumps had come closer together and the two clumps had started to merge.

- Many cells appeared to drift during the experiment towards the top right hand corner of the image. This was particularly prominent for cells in the clumps formed at the top of the aggregates, but was also quite prominent for some cells on the periphery.

Equation 5.2 predicts that there should be a linear relation between the mean square displacement of the cells and time, and that the slope would represent an equivalent diffusion coefficient for the movement of the cells. A plot of the mean square displacement as a function of time, as shown in Figure 5.4 (with and without compensation for drift), shows that this indeed is the case, though a line is obtained with two gradients. The first part, up to 5000 seconds, has a smaller gradient, indicating that cell movement at first was slow. The second part (after 5000 seconds) has a larger gradient, indicating that the cells speeded up during the later part of the experiment.

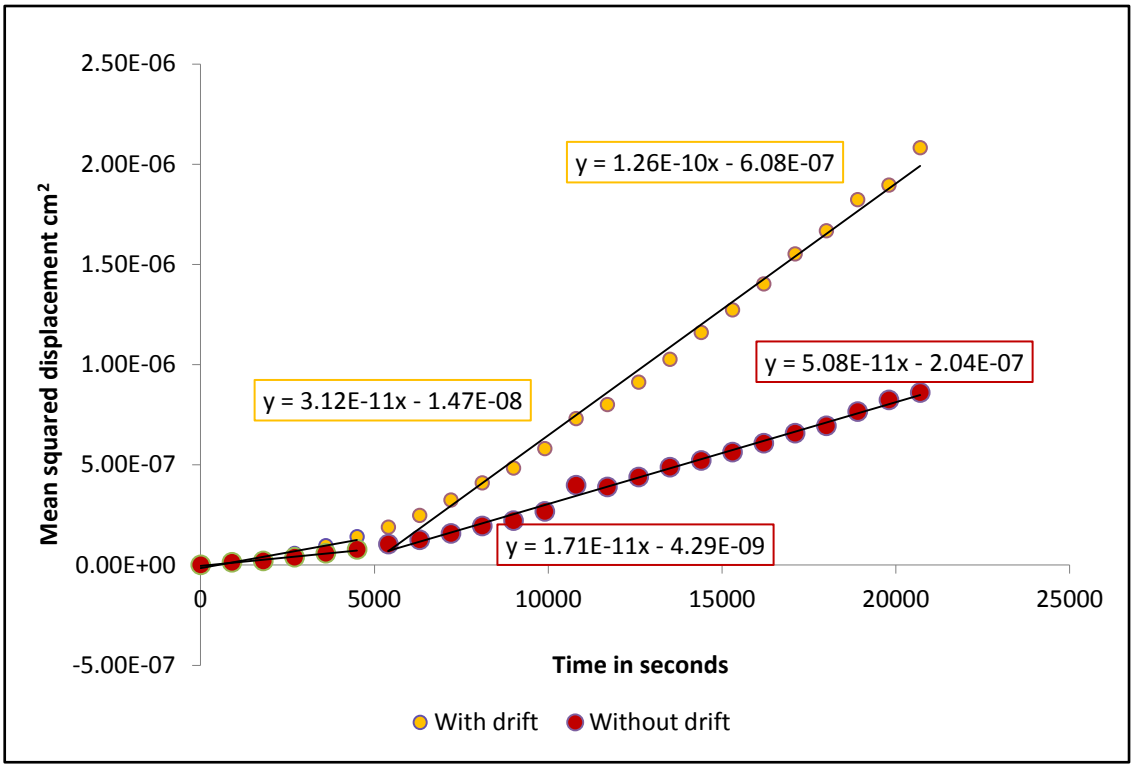

Figure 5.4: Mean square displacement of osteoblast cells from aggregates formed with DEP as a function of time.

Data are shown with and without compensation for drift. After compensation for drift the equivalent diffusion coefficient is found to be 1.71 ± 0.13 × 10^{-11} cm^2 s^{-1} for the period up to 5000 seconds, after which it increases to 5.08 ± 0.11 × 10^{-11} cm^2 s^{-1}.

5.5 Discussion

Cell movement in aggregates created with DEP has been proven to be quite complex, with different types of behavior occurring in different regions. A crucial factor appears to be access to a surface to adhere to. Cells in the periphery were close to and had direct access to the electrode surface, and therefore moved at greater speed. Cell at the top did not have direct access to the electrode surface (because it was too far away, and other cells were in the way). Puramatrix on the other hand is a quite soft gel and SAOS-2 osteoblastic cell cells did not adhere to it, as no stretching of the cells in the Puramatrix was observed. Instead the cells appeared to prefer to adhere to each other, as shown by their tendency to clump together.

A significant drift was observed in both the cells that had clumped together away from electrode surface and the cells in the periphery that had adhered to the electrode surface. It is unlikely that this drift is directed migration of the cells as there was no obvious migratory cue for cell movement. Instead, the drift is most likely caused by creep of the gel matrix.

After the drift velocity of the gel was deducted from the average mean square displacement of the cells, a value for the equivalent diffusion coefficient for the SOAS-2 osteblast-ike cells was obtained of $5.08 \pm 0.11 \times 10^{-11}$ cm^2 s^{-1}.

Surface	*NIH-3T3 Estimated Diffusion Coefficient ($cm^2 s^{-1}$)*	*Saos 2 Estimated Diffusion Coefficient ($cm^2 s^{-1}$)*
Untreated	$2.5 \pm 0.2 \times 10^{-9}$	$1.0 \pm 0.1 \times 10^{-9}$
BSA	$0.8 \pm 0.3 \times 10^{-9}$	$0.4 \pm 0.1 \times 10^{-9}$
Collagen I	$2.6 \pm 0.2 \times 10^{-9}$	$0.8 \pm 0.1 \times 10^{-9}$
Collagen I W/BSA	$0.5 \pm 0.01 \times 10^{-9}$	$0.3 \pm 0.7 \times 10^{-9}$
Collagen IV	$1.6 \pm 0.2 \times 10^{-9}$	$1.4 \pm 0.2 \times 10^{-9}$
Collagen IV W/BSA	$0.6 \pm 0.1 \times 10^{-9}$	$1.7 \pm 0.3 \times 10^{-9}$
FBS	$2.6 \pm 0.2 \times 10^{-9}$	$1.0 \pm 0.2 \times 10^{-9}$
FBS W/BSA	$2.5 \pm 0.4 \times 10^{-9}$	$0.8 \pm 0.2 \times 10^{-9}$

Table 5.1: Estimated diffusion coefficient of NIH-3T3 mouse embryonic fibroblast cells and SAOS-2 human epithelial-like osteosarcoma cells on various treated surfaces (from Cooper-White et al., 2010).

Table 5.1 compares diffusion coefficient values of mouse embryonic fibroblasts of cell line NIH-3T3 with human epithelial-like osteosarcoma cells of cell line SAOS-2, on different surfaces. Fibroblasts travel faster than SAOS-2 cells on untreated surfaces as the value of the diffusion coefficient *D* for fibroblast cells for untreated surfaces is $2.5 \pm 0.2 \times 10^{-9}$ cm^2 s^{-1} whereas for SAOS-2 cells it is $1.0 \pm 0.1 \times 10^{-9}$cm^2 s^{-1}. Lower values for *D* ranging between 1.22 and 2.23×10^{-9} cm^2 s^{-1} have been determined for rat osteoblasts on RGDS and RDGS-modified glass, respectively (Dee *et al*., 1999). Work done by Sengers *et al*. (2007) showed a value of *D* $4.9 \pm 0.7 \times 10^{-9}$ cm^2 s^{-1} for an MG-63 human osteosarcoma cell line. The value of the diffusion coefficient for SAOS-2 cells that was determined in our studies was $5.08 \pm 0.11 \times 10^{-11}$ cm^2 s^{-1}. This is lower than any value in the previously mentioned study, indicating that cell movement was slower compared to the data available in literature. It was noted that cell viability declined in the later part of the experiment, however at the start cell viability appeared strong, and loss of viability can therefore be discounted as a reason for the lower equivalent diffusion rate. The main reason for the slow movement compared to the literature data is likely to be due to the fact that the cells in this study were immobilized in a gel, and cells in the experiment described in the literature were not. The rigid nature of the gel is likely to pose a challenge to cell movement. No literature data was found on the diffusion coefficient of SAOS-2 cells in gels. However Barocas *et al*. (1994) showed that fibroblasts had a diffusion coefficient of 1.7×10^{-10} cm^2 s^{-1} in a collagen microsphere. Given a typical value of

D for fibroblast cells in Table 7.1 of $2.5 \pm 0.2 \times 10^{-9}$ cm^2 s^{-1} this suggests cells may move more slowly in a gel by a factor 10. Given a typical value of *D* for osteoblasts on a surface of $1.0 \pm 0.1 \times 10^{-9}$ cm^2 $s^{-1,}$ a value of *D* of $5.08 \pm 0.11 \times 10^{-11}$ cm s^{-1} for SAOS-2 cells in Puramatrix gel seems justified.

5.6 Conclusions

Digital time-lapse video microscopy was employed to monitor the migration of the SAOS-2 cells immobilized in Puramatrix. The trajectories of the cells were reconstructed with MATLAB. By constantly observing the cell movement it was clear that the cells near the top of the aggregate appeared to congragte into clumps which then drifted with the gel while the cells near the microelectrode surface appeared to first move slowly whilst they attempted to adhere to it and then move over it rapidly once they did. The cells were shown to move with an equivalent diffusion coefficient of 5.08×10^{-11} cm^2 s^{-1} over the glass surface once they had adhered to the surface. This value was lower than the literature values for the equivalent diffusion coefficient for SAOS-2 cells on surfaces, and is most likely due to the presence of the Puramatrix gel matrix, which slows the cells down.

CHAPTER 6

Optimization of architecture of artificial stem cell niches using dielectrophoresis

---

6.1 Introduction

Haematopoiesis during development shifts to different locations in the body indicating that many different tissues are capable of providing suitable environments for haematopoiesis. This raises important questions as to what factors are common or different in the different stem cell niches in the different tissues (Durand *et al*., 2007; Chan *et al*., 2009).

The fate of the HSCs within tissues is determined by interaction of stem cells with its specialised microenvironment or stem cell niche (Schofield, 1978). Major components of the haematopoietic stem cell microenvironment are the non-haematopoietic cells, which from part of the niche but do not directly partake in haematopoiesis (Wilson and Trumpp, 2006; Ohneda *et al*., 1998; Takeuchi *et al*., 2009). Each different niche is likely to have different cells involved. For example, AGM derived stromal and endothelial cells have been shown to play important roles in the maintenance and expansion of the earliest definitive HSCs (Harvey and Dzeirzak, 2004). Coculture of hESC cells with fetal liver derived stromal cells line has been shown to lead to an increase in the formation of blood cells and HSC precursors (Ledran *et al*., 2008). Support for this hypothesis has been given by the fact that purified osteoblastic cells support HSC survival and limit proliferation (Taichman *et al*., 1994; 1996; Calvi *et al*., 2003). Active HSC differentiation and migration in bone marrow, on the other hand, is thought to be associated with the vascular niche which is formed by the small arterioles and sinusoids that spread throughout the marrow. The sinusoid wall consists of single layer endothelial cells and does not have any supporting cells, and endothelial cells are thought to play major roles in the vascular niche (Butler *et al*., 2010).

Osteoblastic cells can be the source of signals that guide stem cells (Emerson and Zhu, 2004; Durand *et al*., 2007; Dzierzak *et al*., 2009; Nakamura *et al*., 2010). We will describe how we have made mixed aggregates of embryonic stem cells and osteoblastic cells, and

discuss the effects of aggregate architecture on the observed redistribution of cells after the formation of the aggregates.

6.2 Materials and methods

6.2.1 Cells

Oct-4 mouse embryonic stem (ES) cells were used in the experiments. Oct-4 embryonic stem cells express Green Fluorescent Protein (GFP); GFP production is linked with Octamer-4 production. The production of Octamer-4 is essential for the self-renewal of undifferentiated embryonic stem cells and its presence can therefore be used as a marker for undifferentiated cells. Loss of fluorescence marks the onset of differentiation in the cells (Niwa *et al*., 2000).

Murine embryonic stem (ES) cells and osteoblastic cells (SAOS-2) were grown in T25 flasks as described previously in chapter 3. The cells were washed twice with 300 mM D-sorbitol in order to lower the conductivity to allow patterning with positive dielectrophoresis. The osteoblastic cells were stained with PKH26 red fluorescent membrane stains according to the protocols provided by the distributor (Sigma-Aldrich). The concentration of PKH26 was 4×10^{-6} M, for 10 million cells per mL. After staining the cells were washed with 300 mM D-sorbitol twice and then transferred to 300 mM D-sorbitol for patterning with positive dielectrophoresis. Oct-4 Embryonic stem cells expressed GFP, and did not need staining.

6.2.2 Dielectrophoretic formation of cell aggregates

A DEP set-up was used to form aggregates as described previously (chapter 3; see also Sebastian *et al*., 2007 a & b). The chamber was autoclaved prior to use. The chamber was filled with the low conductivity 300 mM D-sorbitol solution and, following this, electric fields were generated between the microelectrodes using signals of 1 MHz frequency and voltages of 10 $V_{pk\text{-}pk}$ for electrodes of 50-100 µm, and 20 V pk-pk for electrodes of 125-200 µm. Electric signals were generated using a Thurlby-Thandar TG120 function generator. Cells were introduced into the chamber and allowed to be attracted to the high field regions between the electrodes. Fresh sorbitol solution was passed through the chamber to redistribute the cells, remove non-attracted cells and maintain a low conductivity in the chamber.

For constructing layered aggregates in which cells of one type were covered by cells of another cell type, the cells that were to be patterned as the bottom layer on the electrode surface were introduced first and attracted with positive dielectrophoresis at 1 MHz frequency and 10 V_{pk-pk} at 100 and 20 V_{pk-pk} at 200 μm electrode regions. When a small aggregate had formed in the high field regions between the electrodes the cells of the second type that were to form the top layer were introduced, and layered on top with DEP until the aggregate reached its maximum height. The aggregates were immobilized in 25% Puramatrix gel and the whole chamber was immersed in growth media and placed inside a humidified incubator. The Experiments for each niche architectural construct was repeated three times to confirm the results.

6.3 Results

6.3.1 Formation of aggregates containing both ES cells and osteoblastic cells

Aggregates with 3 different architectures (Figure 6.1) were formed of mouse embryonic stem cells and SAOS-2 osteoblastic cells with positive DEP at 1 MHz 10 V_{pk-pk} at microelectrodes with 75 μm castellations. The first architecture, shown in Figure 6.2, consisted of an inner core of embryonic stem cells surrounded by osteoblastic cells. The second architecture, Figure 6.3, consisted of osteoblastic cells surrounded by embryonic stem cells. The third type of aggregates Figure 6.4, was formed simply by introducing mixture of both cell types at the same time. The initial distribution of stem cells and osteoblastic cells within these aggregates was therefore random.

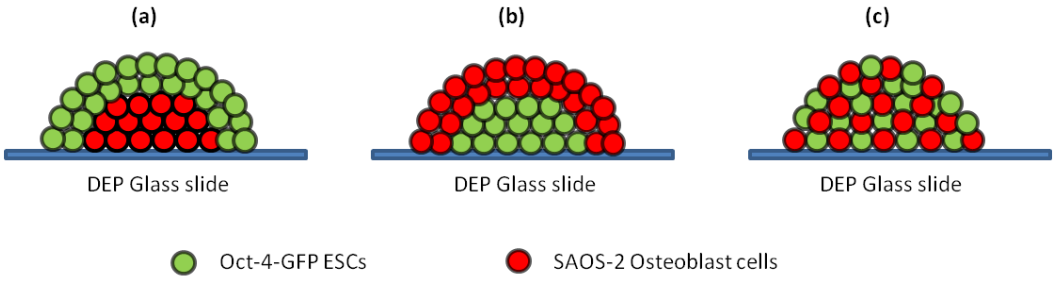

Figure 6.1: Pictorial presentation of the different architectural constructs of an artificial stem cell niche.

(a) *Layered aggregate with OCT-4-GFP cells surrounding osteoblasts.* ***(b)*** *Layered aggregate of Osteoblasts surrounding the OCT-4-GFP cells* ***(c)*** *Mixture of both the cell types.*

In all the aggregates, the stem cells condensed into embryoid body-like structures, and the osteoblastic cells spread out over the surface of the electrode. However, significant differences were observed in the behavior of cells in the different architectures. These differences related mainly to the ease by which the osteoblastic cells could reach and spread over the slide surface, and stem cells could find and adhere to each other without steric hindrance.

In a layered aggregate in which a core of stem cells was surrounded by osteoblastic cells (Figure 6.2), the stem cells were all close to each other in the centre of the aggregate at the start of the experiment. A single large embryonic body was therefore formed. The osteoblastic cells at the periphery of the aggregate near the electrode surface adhered to the surface and spread; osteoblastic cells near the top of the aggregate, however, were too far from the substrate surface and were also impeded from moving to the surface by the presence of the stem cells. The lack of a surface to adhere to, appears to cause the osteoblastic cells to round up and/or adhere to each other. There was little evidence of any adherence between osteoblastic cells and stem cells.

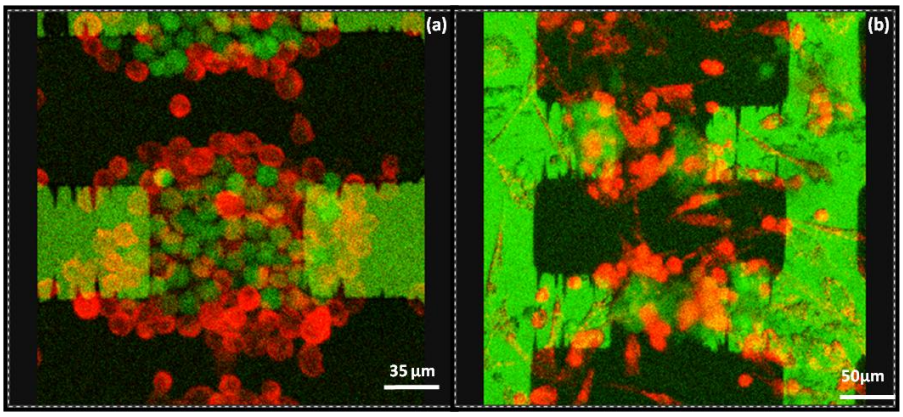

Figure 6.2: Aggregates of Oct-4 stem cells (green) surrounded by SAOS-2 osteoblastic cells (red). *Aggregates formed by DEP in a 75 micrometer electrode region using an applied signal of 1 MHz frequency and 10 $V_{pk\text{-}pk}$. The SAOS-2 osteoblastic cells were stained red with PKH26 membrane dye; the Oct-4 cells produced GFP, and therefore fluoresced green.* ***A)*** *Aggregate formed at time zero.* ***B)*** *Aggregate after 24 hours. The osteoblastic cells that were near the slide surface at the start have spread out over the slide surface; those further away from the surface have rounded up; some osteoblastic cells have adhered to each other. The stem cells have condensed into an embryonic body.*

In a layered aggregate in which the osteoblastic cells form the inner core, and the stem cells the outer layer, the observed behavior depended on the number of stem cells in the aggregate. When a relatively small number of stem cells were used, the stem cells were thinly spread over the aggregate surface at the start of the process. In this case many smaller embryonic bodies were often formed spread across the aggregate. When a larger number of embryonic stem cells were used, single embryonic bodies tended to be formed. In contrast to the previous architecture, the osteoblastic cells did not spread over the surface. Instead they tended to stay closely associated with the ES cells, presumably because steric hindrance and movement of the stem cells during the condensation process prevented them from spreading. The result was that after 24 hours most aggregates were round and consisted of both osteoblastic cells and ES cells.

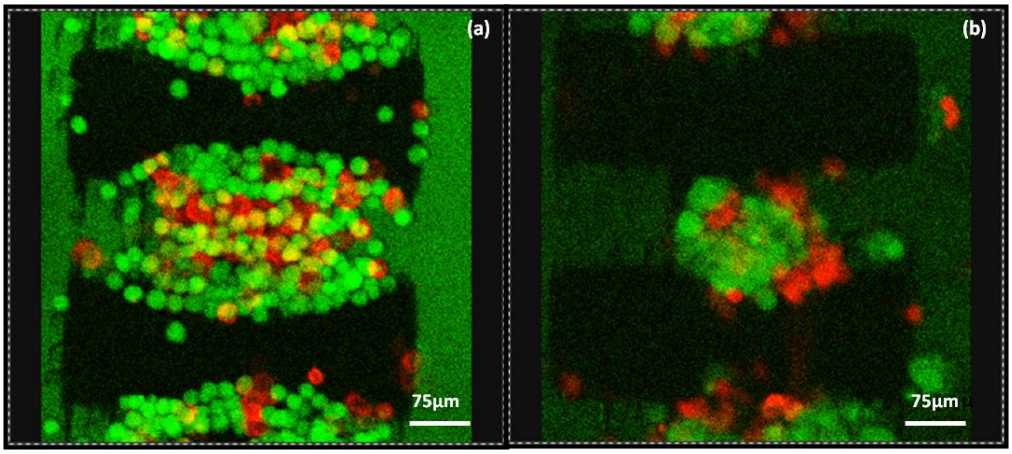

Figure 6.3: Aggregates of SAOS-2 osteoblastic cells surrounded by Oct-4 stem cells.
Aggregates formed by DEP in a 75 micrometer electrode region using an applied signal of 1 MHz frequency and 10 $V_{pk\text{-}pk}$. The SAOS-2 osteoblastic cells were stained red with PKH26 membrane dye; the Oct-4 cells produced GFP, and therefore fluoresced green. ***A)*** *Aggregate formed at time zero.* ***B)*** *Aggregate after 24 hours. The aggregate can be seen to have formed a ball shaped structure composed of both ES cells and osteoblastic cells. The osteoblastic cells did not spread out to a major extent over the slide surface.*

Mixed aggregates of ES cells and osteoblastic cells were also formed. Embryonic body formation in mixed aggregates was intermediate to the previous aggregates. Some of the osteoblastic cells (presumably those close to the surface at the start) tended to spread, whilst those further away from the substrate surface or hindered from reaching the surface tended to round up or adhere to each other. Condensation of the stem cells into embryonic bodies still occurred, but some steric hindrance of the condensation process occurred by the osteoblastic

cells. This often resulted in the formation of several small embryonic bodies within an individual aggregate rather than a single one.

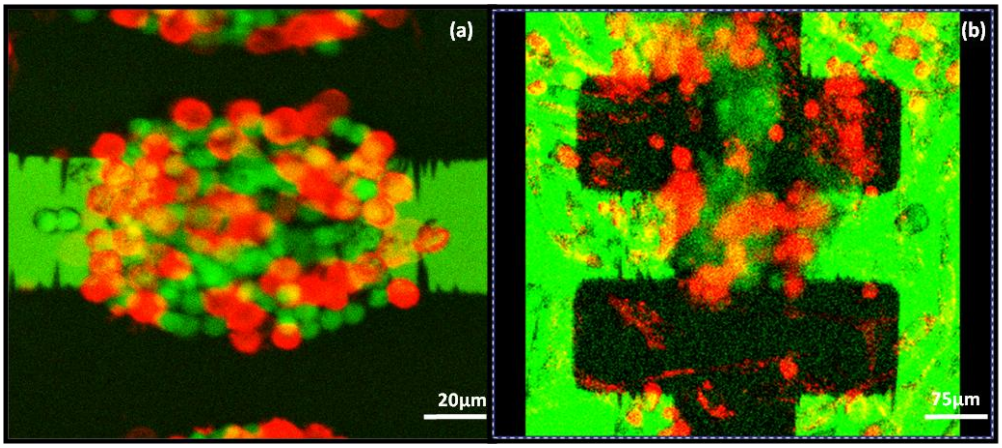

Figure 6.4: Aggregate consisting of a mixture of SAOS-2 and embryonic stem cells.
Aggerates formed by applying a 1 MHz, 10 $V_{pk\text{-}pk}$ signal to interdigitated oppositely castellated with a characteristic size of 75 micrometer. ***A)*** *Aggregate at zero hour* ***B)*** *After 24 hours the aggregate shows surface adherence and spreading of some of the osteoblastic cells and rounding/aggregation of others. The stem cells tended to form several embryonic bodies in this architecture.*

6.4 Discussion

The interaction between different cell types is an important factor in the determination of stem cell fate (Hwang *et al*., 2009). To construct microniches which are functionally efficient it is important to provide conditions that will enhance cell-cell communication. The construction of aggregates with DEP enhances cell-cell communication as the mutually attractive dielectrophoretic forces bring the cells together. After the formation of the aggregates by DEP and their immobilization in a gel, however, the cells will rearrange themselves. The two cell different cell types used in this study, i.e. osteoblastic cells and embryonic stem cells, have very different adhesive properties. Once the differentiation process has been initiated the stem cells appear to become strongly cohesive. They do no longer adhere to the glass surface, and condense into tight aggregates. With osteoblastic cells, on the other hand, under normal circumstances the adhesive forces between the cells and the substrate surface appear to dominate. Only when adhesion of the cells is not possible (because the surface does not allow cell adhesion, is too far away, or the osteoblastic cells are prevented from reaching the substrate surface by other cells) do cohesive forces dominate; osteoblastic

cells appear to prefer adhering to each other to adhering to the extracellular matrix formed by dilute Puramatrix. The reorganization of cells after the formation of aggregates with dielectrophoresis thus appears to be regulated by the initial distribution of the cells and the adhesive forces between the cells and their microenvironment, i.e. the substrate surface, the extracellular matrix, and each other.

The role of adhesive forces between cells has previously been explored in Steinberg's Differential Adhesion Hypothesis (DAH) (Foty *et al*., 1996, Steinberg, 1963; 2007). The DAH theory proposes that the cells of different kind adhere to each other with different strengths. Cells in mixed populations are thought to rearrange themselves to minimize their total adhesive free energy. In embryos the differential adhesion is thought to lead to the sorting of embryonic cells according to differences in the strengths of their intercellular adhesions, with less adhesive cells enveloping more adhesive cells (Steinberg, 1963; 1970; 1996; 2007). Extensions of the DAH theory have been proposed, and the theory has previously been used to explain cell rearrangement in other engineered tissues (Mironov *et al*., 2003; 2009). In our case an extension is needed to include the interaction between the cells and the surrounding materials, i.e. the microelectrode surface and the Puramatrix.

Surprisingly, the optimum aggregate for niche formation appears to be when the osteoblastic cells are at the microelectrode surface, and the stem cells in a thick layer on top. A simple explanation for this fact could be that in an aggregate with a thick layer of stem cells on top and osteoblastic cells at the bottom the osteoblastic cells are swept into the embryonic body as it is formed. In an architecture with osteoblastic cells on top and stem cells at the bottom, however, the osteoblastic cells at the top have too much for manoeuvre, which allows them to spread rather than be taken up in the embryonic body.

6.5 Conclusions

It was shown that aggregates could be made with dielectrophoresis with different architectures, for potential use as artificial stem cell niches. It is proposed that the optimal architecture for the formation of an artificial niche is an aggregate with osteoblastic cells at the bottom, and a relative large number of embryonic stem cells at the top as this leads to the formation of a single embryonic body with osteoblastic cells in close association with embryonic stem cells.

The reorganisation of the cells in the aggregates appears to be mainly determined by the adhesive forces between the cells and the surrounding materials, and can be adequately described by an extension of the differential adhesion hypothesis.

CHAPTER 7

Investigation of the differentiation of the embryonic stem cells in aggregates formed using DEP

7.1 Introduction

Recreation of stem cell niches *in vitro* could help to achieve a better understanding of the roles of support cells in stem cell differentiation, quiescence and expansion, and could be a powerful tool for developing therapies based on stem cells (Peerani and Zandstra, 2010; Lund *et al*., 2009; Bowman and Zon, 2009). The natural environment of stem cells is 3-dimensional, and although 2D co-cultures are often used for investigating the interaction between cells, they cannot be expected to be representative of the stem cells' natural environment. Indeed, a recent study directly comparing haematopoietic differentiation in a 2D and 3D system has shown that optimal haematopoietic cell differentiation occurs when a three-dimensional system is used (Zhang *et al*., 2005). Attempts at recreating the stem cell niche in vitro should therefore involve methods for creating 3D microenvironments.

When differentiating, embryonic stem cells often go through a stage in which they form spherical cell condensates called embryonic bodies. In order to make stem cell differentiation reproducible it is necessary to control EB formation. Amongst the methods used to reproducibly create EB, the hanging drop method is the most extensively used (Karmer *et al*., 2000; 2003; 2005; 2005b; Nieden *et al*., 2003). The hanging drop method involves plating drops of a cell suspension on the inside cover of a petridish. The cells in each droplet aggregate to form an EB. The final size of the EB is mainly determined by the number of cells initially put into the hanging droplet. The inclusion of other cell types in hanging drops is straightforward; however the hanging drop method does not give one control over the (initial) architecture of the EB.

EB size can affect fate decisions (Leahy *et al*., 1999; Koike *et al*., 2007), as can the composition and architecture of the initial aggregates. To obtain more direct control over stem cells fate in EB many microscale technologies have also been developed such as surface patterning, hydrogel microwells, and microfluidic systems (Khademhosseinni *et al.*, 2006;

Park *et al*., 2007; Peerani *et al*., 2007; Torisawa *et al*., 2007). Micropatterning has been used to evaluate the effect of EB size on ES cell differentiation. For example Park *et al*. (2007) microfabricated adhesive stencils used to pattern ES cells to control the initial ES cell aggregate size. Aggregate size was shown to influence the early differentiation of different germ layers (Park *et al*., 2007). In another study Hwang *et al*. (2009) regulated EB-size using non adhesive polyethylene glycol (PEG) hydrogel microwells of various diameters (150, 300 and 450 μm), forming homogenous EBs of different sizes. They found that ES cell differentiation into cardiac and endothelial lineage was a highly size dependent response (Hwang *et al*., 2009).

In the previous chapters it was shown that dielectrophoresis - the movement of particles in non-uniform electric fields – can also be used to form EBs. The method allows one to create aggregates of stem cells and non-stem cells on their own, and in various combinations in aggregates with well-defined architectures. However, in the experiments described only the redistribution of the ESC after the creation of the aggregates was investigated. The formation of EB by the ESC indicates that they have initiated their differentiation, but is does not tell one whether the ESC have differentiated along a specific lineage.

In this chapter we will use Brachyury marker ESCs to indicate if the cells are moving towards the mesenchymal lineage. This will be done by aggregating Bry ESCs using dielectrophoresis and then by using image analysis, production of the level of green fluorescence in the aggregates will give an indication of their mesenchymal fate determination. Also the Bry ESCs will be co-cultured with SAOS-2 cells, aggregated by DEP, to study the affect of support cells in fate determination of ESCs.

7.2 Materials and methods

7.2.1 Cells

Brachyury mouse embryonic stem cells (Bry ESC) and SAOS-2 osteoblast-like cells were used in the experiments. The Bry ESCs were genetically modified cells. Under normal circumstances the Bry ESCs do not fluoresce. However, when the cells commit to the mesenchymal lineage they express green fluorescence protein (GFP). The SOAS-2 osteoblast cells did not normally fluoresce. The murine Bry embryonic stem cells and osteoblasts cells were grown in T25 flasks as described previously in chapter 3. The cells were washed twice

with 300 mM D-sorbitol in order to lower the conductivity to allow patterning with positive dielectrophoresis. The osteoblast cells were stained with PKH26 red fluorescent membrane stains according to the protocols provided by the distributor (Sigma-Aldrich). The concentrations of PKH26 was 4×10^{-6} M, for 10 million cells per ml. After staining the cells were again washed with 300 mM D-sorbitol twice and then transferred to 300 mM D-sorbitol for patterning with positive dielectrophoresis. Embryonic stem cells were not stained.

7.2.2 Dielectrophoretic formation of cell aggregates

A DEP set-up was used to form aggregates as described previously (chapter 3, see also Sebastian *et al*., 2007 a & b). The chamber was autoclaved prior to use. The chamber was filled with the low conductivity 300 mM D-sorbitol solution. Electric signals (1 MHz, 10 $V_{pk\text{-}pk}$) were generated using a Thurlby-Thandar TG120 function generator and applied to interdigitated oppositely castellated microelectrodes made from ITO on glass. To form aggregates of ES cells of different sizes ESC were introduced into the chamber and attracted by dielectrophoresis to the high field regions between the castellations of micro electrodes with characteristic sizes of 50 µm, 75 µm, and 100 µm. Fresh sorbitol solution was passed through the chamber to redistribute the cells, remove non-attracted cells and maintain a low conductivity in the chamber. Once the cells reached the maximum height, the aggregates were immobilized in 25% Puramatrix gel and the whole chamber was immersed in GMEM growth medium and placed inside a humidified incubator.

To investigate the response of the Brachyury stem cells to the presence of osteoblasts, layered aggregates were constructed with SAOS-2 cells at the bottom/centre and Brachyury cells on top surrounding the SAOS-2. The protocol used for constructing these layered was previously described in chapter 5; see also Sebastian *et al*. (2007).

7.2.3 Image analysis

Images were taken with a Leica TCS2 confocal microscope. All settings of the confocal microscope were kept the same throughout all the experiments to ensure reproducibility of the results. Analysis of the images obtained with the confocal microscope was done with Fiji. Fiji is an open source image analysis programme based on ImageJ.

The protocol was as follows:

Three pictures were taken at zero hours and 24 hours for all three electrode region (50, 75 and 100 µm) were taken. All images were taken at the same magnification. The images were loaded into the Fiji software (the image was in TIFF format, JPEG images cannot be used by the software). A square block was placed in the picture in the centre of an aggregate in order to delineate the region of interest (ROI) where intensities values were to be measured. The ROI size was kept constant for every picture used in this set of data, simply by copying the block and pasting it on fresh image every time. Once the ROI was pasted onto the desired area, the analysis tool was selected within the software and; histogram and plot profiles of the areas were made. A histogram is a graph showing the number of pixels in an image at each different intensity value found in that image. For an 8-bit greyscale image there are 256 different possible intensities, and so the histogram will graphically display 256 numbers showing the distribution of pixels amongst those greyscale values. Figure 7.1 shows an example of what that histogram looked like. The mean and the standard deviation are also displayed. These data are very useful as the list of the values can be saved on Microsoft excel file and then the calculations for the data can be made.

Typically, there are 256 shades of gray ranging from black to white. These shades of gray are coded as unsigned one-byte integer values with 0 corresponding to black and 255 corresponding to white. The minimum intensity value is 0 and the maximum is 255. These pixel values can also be thought of as the intensity of the light where a greater intensity corresponds to a brighter pixel. The total number of pixels in the ROI is 9672. The frequency of number of pixels lying in the respective intensity is generated through the histogram. To get the true intensity, the frequency is multiplied with the respective intensity value. The sum of this value is divided by the total number of pixels in the ROI (9672) to get the average intensity value, which is plotted on the graph. The standard error is then calculated using the standard deviation equation.

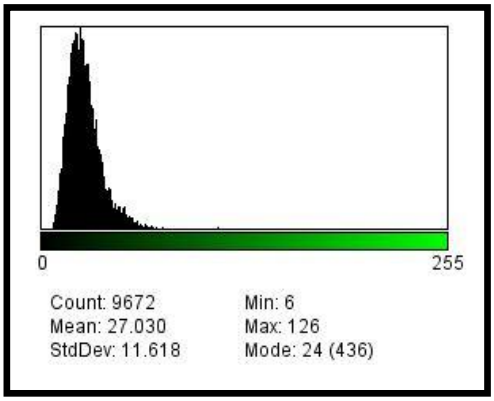

Figure 7.1: Example of the histogram.

Pixel and intensity values were plotted in excel graphs. The average was obtained from three images for each set of data, and the standard average standard deviation value was calculated. The average standard deviation from all the three set of intensity values represented the standard error. To obtain a 95% confidence level, the average standard deviation was multiplied with 1.96.

The Experiments were repeated three times at least to confirm the results.

7.3 Results

7.3.1 Formation of aggregates of different sizes containing Brachyury ES cells only

Aggregates were made with Brachyury stem cells in order to investigate whether differentiation along the mesenchymal lineage (as demonstrated by the production of GFP) is triggered by their aggregation by DEP, and whether EB size has any role to play in the onset of differentiation.

7.3.1.1 50 µm electrode size

The aggregates of Bry ESCs formed embryoid bodies when subjected to DEP. The embryoid bodies were formed over a period of 24 hours in the absence of LIF. The aggregates formed at the 50 µm electrode regions were seen to have negligible fluorescence 24 hours later (Figure 7.2 and 7.3), under the confocal microscope. On analysing the data with image analysis software, there was a slight increase in the green fluorescence (Figure 7.8). At zero hour the calculated average intensity value was 10 ± 4 (Figure 7.1 C), but after 24 hours it was 12 ± 7.5 (Figure 7.2 C).

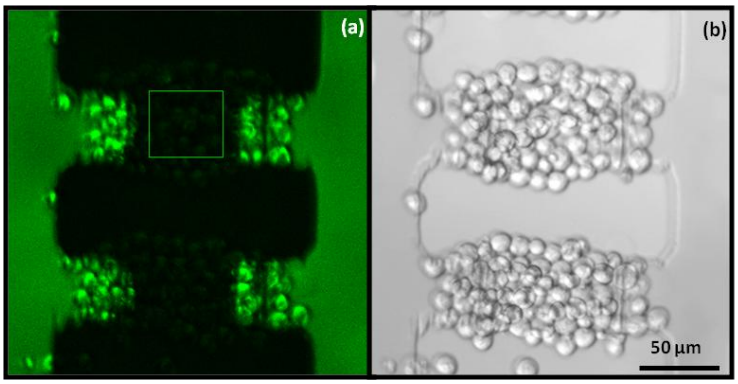

Figure 7.2: Aggregate of Brachyury embryonic stem cells at 50 µm electrode region at zero hours. *The aggregate was formed by applying a 1 MHz, 10 $V_{pk\text{-}pk}$ signal to interdigitated oppositely castellated electrodes.* ***A)*** *Green fluorescent image of an aggregate at zero hours, showing the ROI.* ***B)*** *Bright field image of an aggregate at zero hours.*

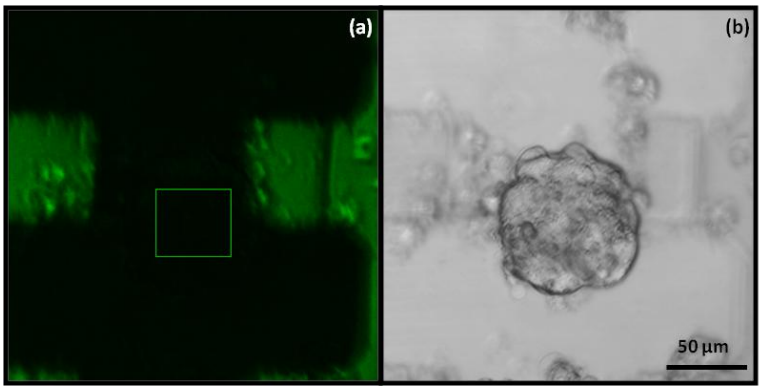

Figure 7.3: Aggregate of Brachyury embryonic stem cells at 50 µm electrode region at 24 hours. *The aggregate was formed by applying a 1 MHz, 10 $V_{pk\text{-}pk}$ signal to interdigitated oppositely castellated electrodes* ***A)*** *EB formation takes place, but after 24 hours there is observable green fluorescence.* ***B)*** *Bright field image showing EB formation in an aggregate at 24 hours.*

7.3.1.2 75 µm electrode size

Aggregates formed in the 75 µm region also formed embryoid bodies (Figure 7.5). On analysing the data with the Fiji image analysis software, there was found to be a significant increase in the average fluorescence intensity in embryoid body after 24 hours. At zero hour the average intensity value calculated was 9 ± 5 (Figure 7.8), but after 24 hours it was calculated to be 36 ± 17 (Figure 7.6 C) which shows an increase in the value. The increase was significantly higher than in the 50 µm region.

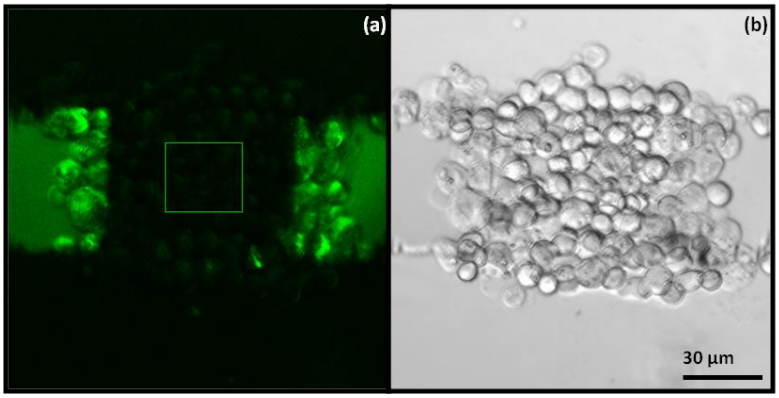

Figure 7.4: Aggregate of Brachyury embryonic stem cells at 75 µm electrode region at zero hours.
Formed by applying a 1 MHz, 10 $V_{pk\text{-}pk}$ signal to interdigitated oppositely castellated elctrodes. ***A)*** *Green fluorescence image of an aggregate at zero hours showing ROI.* ***B)*** *Bright field image of an aggregate at zero hours.*

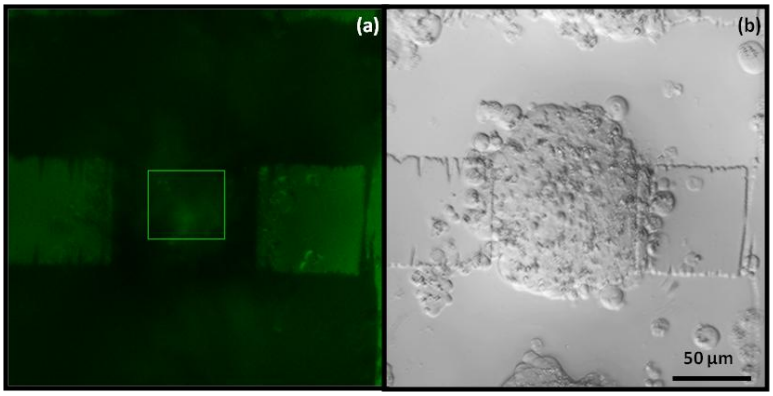

Figure 7.5: Aggregate of Brachyury embryonic stem cells formed at 75 µm electrode region after 24 hours.
The aggregate was formed by applying a 1 MHz, 10 $V_{pk\text{-}pk}$ signal to interdigitated oppositely castellated electrodes. ***A)*** *Green fluorescent image of an aggregate at 24 hours showing the ROI.* ***B)*** *Bright field image of an aggregate forming an EB after 24 hours.*

7.3.1.3 100 µm electrode size

Aggregates at 100 µm region also showed fluorescence in the centre of the embryoid body after 24 hours (Figure 7.7). An analysis of the data with the Fiji image analysis software and calculation of the average intensity at zero and 24 hours showed a negligible increase in the fluorescence (Figure 7.8). At zero hour the average intensity value calculated was 8.5 ± 5 and after 24 hours the average intensity calculated was 34 ± 18. The increase in the value was significantly larger than that in the 50 µm region but less than that in the 75 µm region.

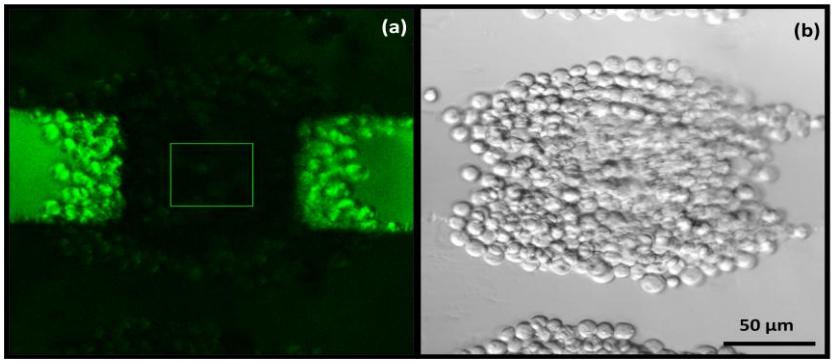

Figure 7.6: Aggregate of Brachyury embryonic stem cells at 100 µm electrode region at zero hours. *The aggregate was formed by applying a 1 MHz, 10 $V_{pk\text{-}pk}$ signal to interdigitated oppositely castellated electrodes.* ***A)*** *Green fluorescence image of an aggregate at zero hours with ROI.* ***B)*** *Bright field image of an aggregate.*

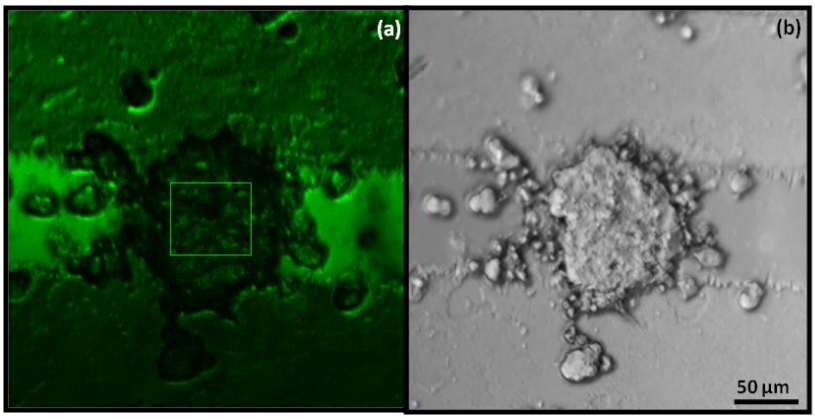

Figure 7.7: Aggregate of Brachyury embryonic stem cells at 100 µm electrode region at 24 hours. *Aggregates were formed by applying a 1 MHz, 10 $V_{pk\text{-}pk}$ signal to interdigitated oppositely castellated electrodes.* ***A)*** *Green fluorescent image of an aggregate at 24 hours. At this time the aggregates have formed embryonic bodies.* ***B)*** *Bright field image of an aggregate which had formed an EB at 24 hours.*

The average intensity values of the three electrode regions, at 0 and 24 hours were plotted on a graph, showing the standard error bars (Figure 7.8). The graph clearly shows the difference in the intensity values in each aggregate for the different electrode region over 24 hours time. The 50 µm region showed a negligible increase where as the 75 µm region showed a significant increase in intensity values and 100 µm showed slightly less increase in intensity values when compared to 75 µm electrode region. The increase in intensity values in the 100 µm region was also significantly higher than 50 µm region.

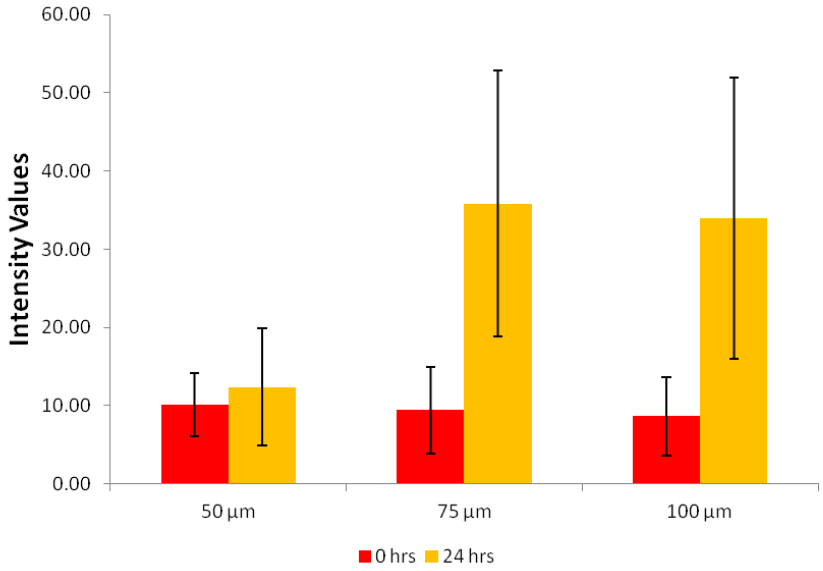

Figure 7.8: Comparative study of the average intensity values in Bry ESC aggregates.
Data were plotted at 0 and 24 hours for Brachyury ESC aggregates formed at different microelectrode regions. Also shown are 95% confidence values in the form of error bars.

7.3.2 Formation of layered aggregates containing Brachyury ES cells above the osteoblast cells (SAOS-2).

It has previously been found that the long-term bone marrow (BM) repopulating (LTR) HSCs are located in bone marrow trabecular bone surface, and that an osteoblastic (OB) cell is a critical component for sustaining HSCs. (Calvi *et al*., 2003; Zhang *et al*., 2003). In vitro coculture of HSCs with osteoblasts can expand the HSC population (Taichman and Emerson, 1998), and depletion of osteoblasts leads to loss of HSC tissue (Visnjic *et al*., 2004). The adhesion molecules osteoblasts express may facilitate adhesive interactions between osteoblasts and HSCs. These include VCAM-1 and ICAM-1, 10-15 CD44, CD164, and osteopontin 7, 16-18 In addition, Shh, N-cadherin, Wnt signaling pathways, Notch-1/Jagged-1 interactions, TGF-β/BMP pathways and Ang-1/Tie2–mediated events are believed to be crucial to establishing HSCs within a particular niche (Gomes *et al*., 2002; Ivanova *et al*., 2002; Park *et al*., 2002; Ramalho-Santoes *et al*., 2002; Akashi *et al*., 2003; Calvi *et al*., 2003; Zhang *et al*., 2003; Arai *et al*., 2004; Duncan *et al*., 2005). Cell- cell interaction between osteoblasts and HSCs are therefore important in the process of the anchoring and maintenance of the HSC population in the bone marrow. Given the role that osteoblasts play in HSC upkeep in bone marrow, a possible role of osteoblasts in ESC commitment to a HSC lineage could justifiably be proposed.

To investigate whether the ESCs differentiate quicker along the mesenchymal linage with osteoblast cells in proximity layered aggregates were made with DEP of Brachyury ESC with SAOS-2 osteoblasts in the 100 µm microelectrode region (Figure 7.9). In chapter 5 it was previously shown that the strongest interaction between ESC and SAOS-2 cells should occur in aggregates in which SAOS-2 cells were initially in the centre of the aggregates and ESCs at the top, and the aggregates were constructed accordingly. After 24 hours the ESCs can be seen to become EBs with a few SAOS-2 cells in the core and a few on the periphery (Figure 7.10). Histograms of the fluoresecence intensity in the ROI were obtained at 0 and 24 hours, and their intensity values were plotted against the average intensity values of 100 µm pure ESC aggregates (Figure 7.11).

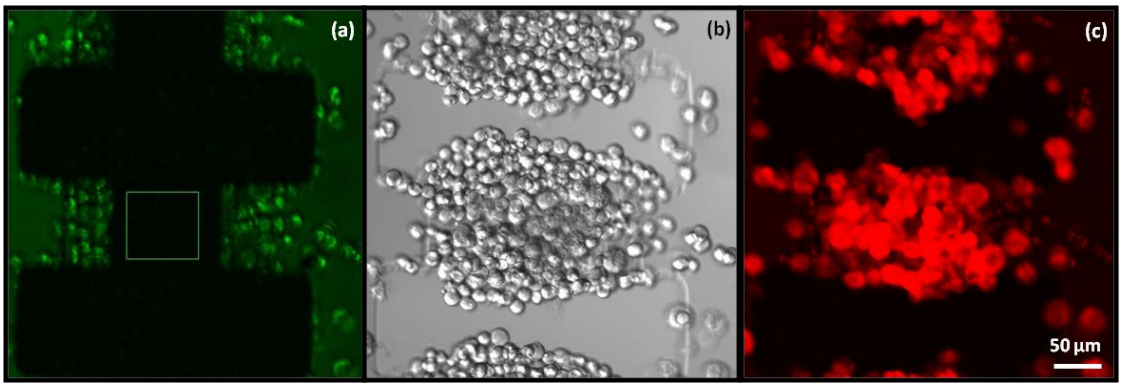

Figure 7.9: Aggregate of Brachyury ESCs and SAOS-2 cells, formed at 100 µm electrode region at 0 hours.

By applying a 1 MHz, 10 $V_{pk\text{-}pk}$ signal to interdigitated oppositely castellated. ***A)*** *Green fluorescent image of an aggregate with ROI.* ***B)*** *Bright field image of aggregate.* ***C)*** *Red stained SAOS-2 cells lie under the aggregate.*

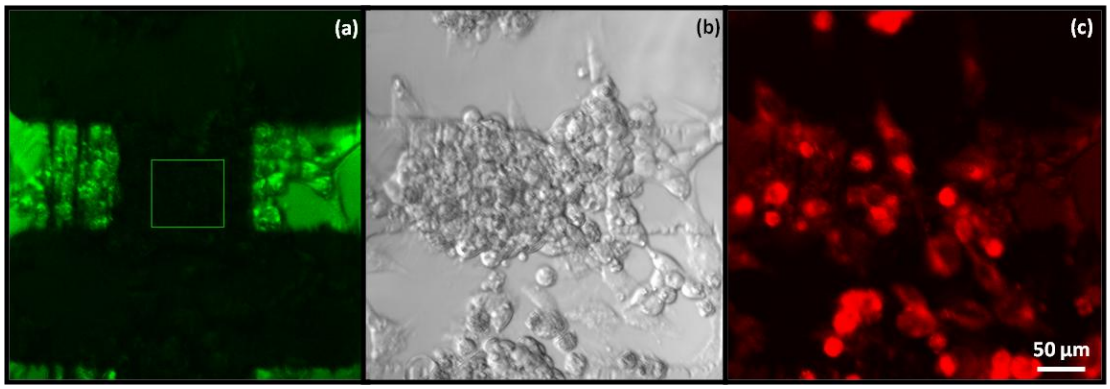

Figure 7.10: Aggregate of Brachyury ESCs and SAOS-2 cells after 24 hours.

The aggregate was formed at the 100 µm electrode region by applying a 1 MHz, 10 $V_{pk\text{-}pk}$ signal to interdigitated oppositely castellated electrodes. ***A)*** *Green fluorescence image*

showing EB formation with ROI. ***B)*** *Bright field image of an aggregate having formed an EB.* ***C)*** *Red stained SAOS-2 cells lying underneath the ESC cells.*

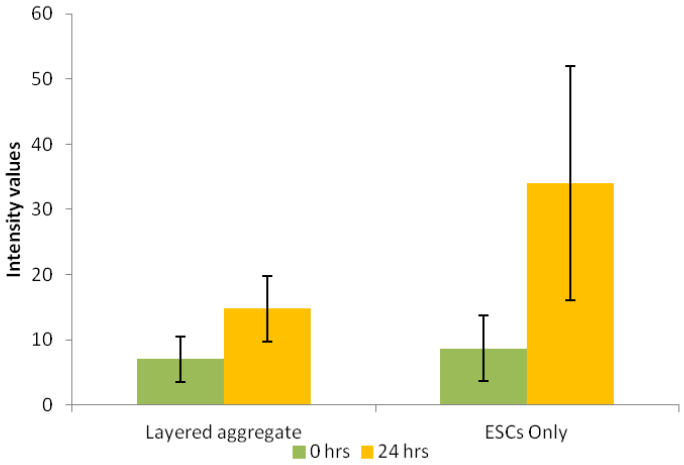

Figure 7.11: Comparative study of the average intensity values.
Data obtained at 0 and 24 hours *were plotted for aggregates containing only Brachyury ESC (right) and aggregates containing both SAOS-2 and ESCs. Aggregates were formed at 100 µm electrode regions.*

Figure 7.11 shows that the co-cultured aggregates of ESCs and SAOS-2 cells did not show the same intensity values as aggregates containing only ESC. At zero hours the intensity value for mixed aggregate was 7 ± 3.5 and at 24 hours the value was 14.75 ± 7. Reduction in intensity values could be a result of the reduction of ESCs in number, in order to accommodate SAOS-2 cells within the same aggregate region. The number of the cells could play an important role in fate determination, or the presence of SAOS-2 cells could have made the ESCs skip the early mesenchymal lineage fate and jumped to a fate down the mesenchymal lineage or it could also be too early to determine the fate and a long term study should be considered.

For long term study, the same combination of cells was used but was left for incubation for seven days. Because the aggregates were quite fragile data were only obtained 0 hours (figure 7.12) 76 hours (Figure 7.13) and 7 days (Figure 7.14) after the initial construction of the aggregate. No data was obtained at intermediate times. Like the previous experiments, histograms of the results at 0 hours, 76 hours and after 7 day were compared, and their intensity values were plotted (Figure 7.15). The results show a small increase in the intensity after 76 hours and then a drop on the 7^{th} day to an intensity value that is insignificant.

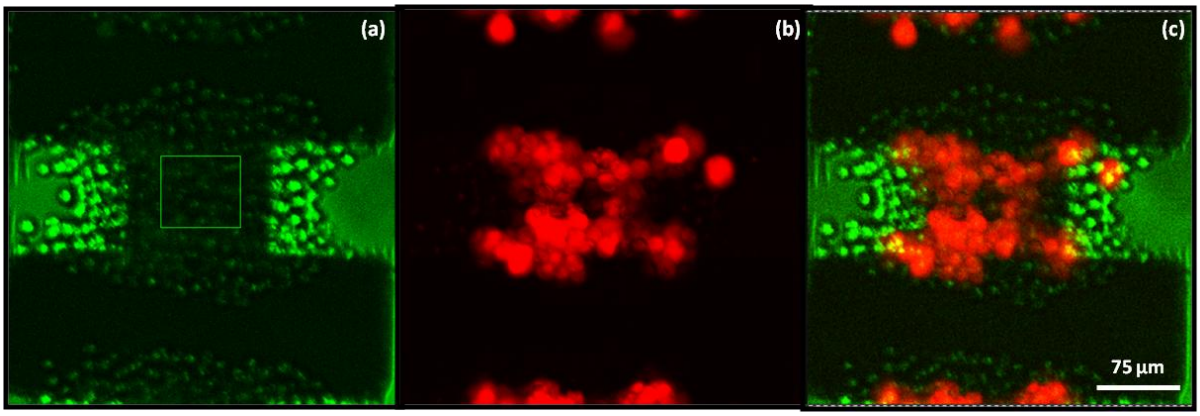

Figure 7.12: Aggregate of Brachyury embryonic stem cells and SAOS-2 osteoblast like cells at zero hours.

The aggregate was formed at 100 µm electrode region by applying a 1 MHz, 10 $V_{pk\text{-}pk}$ signal to interdigitated oppositely castellated electrodes. ***A)*** *Green florescent image of an aggregate at zero hours, showing the ROI on the image for image analysis.* ***B)*** *Red fluorescent image of SAOS-2 cells forming the core of the aggregate.* ***C)*** *Combined fluorescence image of A and B.*

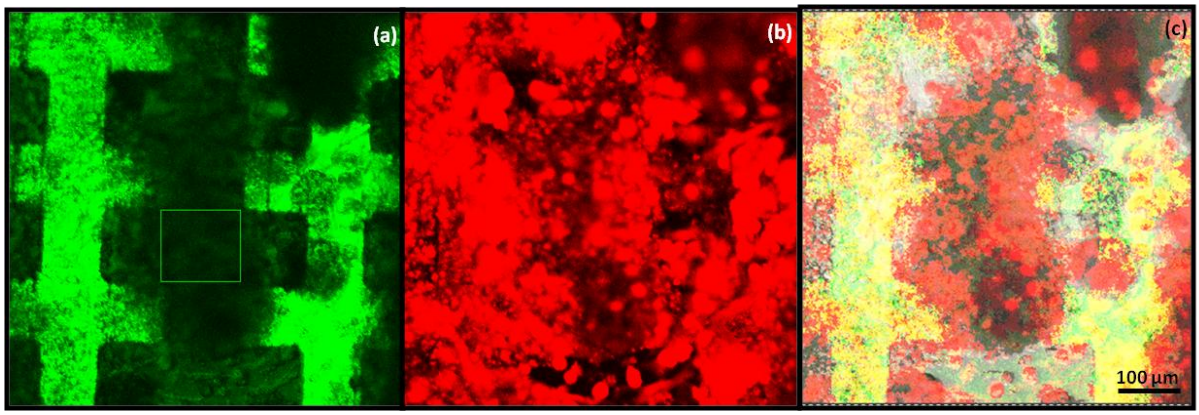

Figure 7.13: Aggregate of Brachyury embryonic stem cells and SAOS-2 osteoblast like cells, formed at 100 µm electrode region at 76 hours.

A) *Green fluorescent image of EB after 76 hour showing ROI.* ***B)*** *Red fluorescent in SAOS-2 cells forming the core of the aggregate seen to be in the middle of the aggregate and some on the outside.* ***C)*** *Combined image of the aggregate at 76 hours showing both red and green fluorescence.*

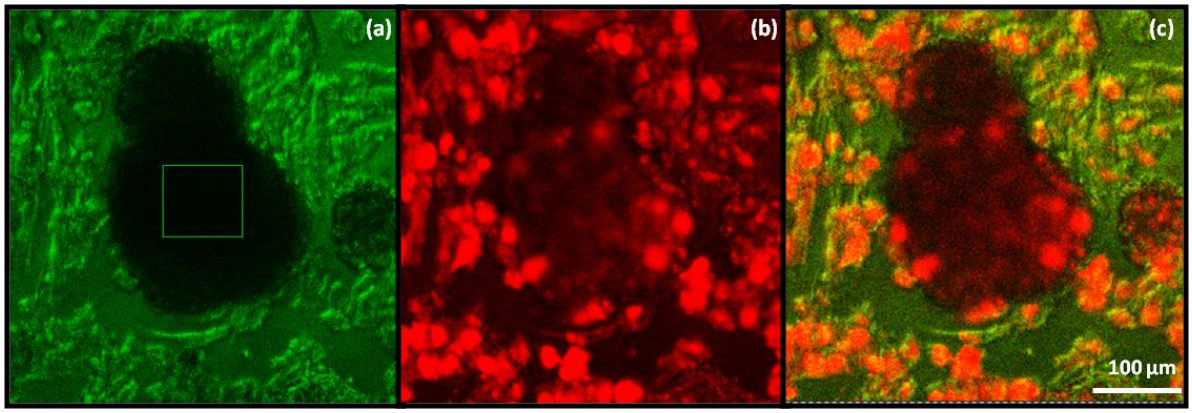

Figure 7.14: Aggregate of Brachyury embryonic stem cells and SAOS-2 osteoblast like cells, formed at 100 µm electrode region at day 7.

A) *Green fluorescent image with no green fluorescence seen in aggregate after 7 days in the ROI.* ***B)*** *Red fluorescent in SAOS-2 cells found in the periphery of the EB.* ***C)*** *Combined fluorescence image of A and B.*

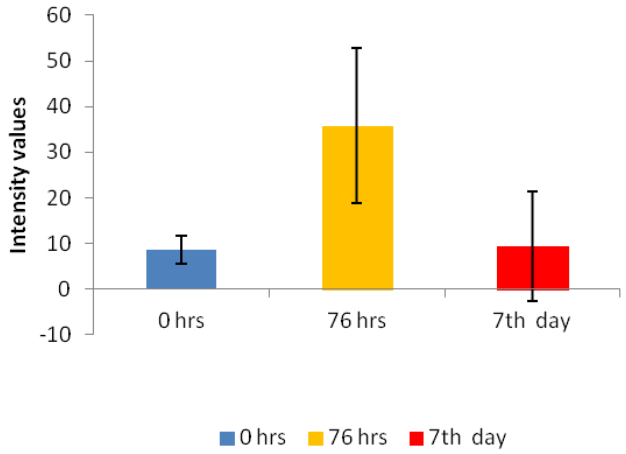

Figure 7.15: Comparative study of the intensity values of layered Bry ESCs and SAOS-2 aggregate. *Data were plotted for Brachyury ESC aggregates inside layered SAOS-2 and ESCs aggregates formed at 100 µm regions. Data are shown at 0 and 76 hours and after 7 days. The graph shows an increase of the intensity value after 76 hours, and then a drop to the background level on the 7th day.*

7.4 Discussion

The experiments indicate that Bry murine ESCs may be induced to commit to the mesenchymal lineage and show a quicker GFP response when aggregated with DEP than when

they are aggregated using the hanging droplet-method. The effect appears to be dependent on the aggregate size.

It is difficult to pin point a single factor that could have resulted in the earlier onset of GFP production in Brachyury marker ESCs. The cells have been subjected to a) low salt conditions in the osmotic buffer; b) mechanical stresses during centrifugation and DEP; c) high strengths electric fields during the DEP assembly process. The cells have also been d) aggregated, forcing the cells into close contact with each other.

Previous experiments (chapters 4 and 5) have shown that the preparation stages (i.e. centrifugation and temporary suspension in low salt buffers) do not affect stem cell differentiation, and that it was solely the aggregation (with DEP) that led to embryoid body formation. It is therefore unlikely that a) and b) are major factors. Cells are exposed to strong electric fields during the DEP assembly process. Electric fields have been shown to affect stem cell differentiation (Hronik-Tupaj *et al*., 2011), but in the main these are DC or low frequency AC fields, and not high-frequency AC fields. Given that electric field exposure during the DEP assembly process is also temporary, the most likely cause of the early onset of differentiation is d), i.e. the fact that the cells are brought into close contact with each other in the aggregate. This conclusion is given further credence by the observation that the fluorescence was seen to increase with the electrode size, indicating that the size of the embryonic body has a role to play in the differentiation of the cells (see also Hwang *et al*., 2009).

Murine hematopoietic stem cells (HSCs) originate from mesoderm and blood cell development during embryogenesis is initiated within the mesodermal germ layer. The Bry marker only marks the onset of mesoderm formation, but does not give any indication what type of mesodermal cell will ultimately be formed. Because the experiments were only conducted for 24 hours, it is not known whether there was a decrease or increase in the fluorescence after the first 24 hours. Therefore, even though the experiments show a positive result, i.e. GFP expression in cells, it was not possible to confirm that the cells were differentiating along the HSC lineage. Use of marker cells indicating HSC lineage would be required in future studies to establish this.

The experiment combining murine Bry ESCs and SOAS-2 osteoblasts was inconclusive. The architecture of the niche, designed in chapter 5, was shown to work well with Brachyury cells, and osteoblasts were seen to be in close contact with ESC cells. However, the change in the level of the green fluorescence from day 0 to 3 from 3 to 7 was insufficient to draw any definite conclusions. The reason for this lack of GFP response is unknown. A possible reason is that the number of ESC was quite small, and that there were simply insufficient numbers of Esc to elicit a response. However, the other possibility that cannot be excluded is that SAOS-2 cells to not express the right signals.

SAOS-2 cells do express bone morphogenetic proteins (BMPs)-1, 2, 3, 4 and 6 (Anderson *et al*., 1998). The bone morphogenetic protein (BMP) signal plays an essential role in inducing haematopoietic tissue during embryogenesis (Maeno *et al*., 1996; Davidson *et al*., 2000). Osteoblasts also produce haematopoietic growth factors (Taichman and Emerson, 1994; Taichman *et al*., 1996; 2001) and are activated by parathyroid hormone (PTH) or the locally produced PTH-related protein (PTHrP), through the PTH/PTHrP receptor (PPR) (Calvi *et al*., 2003). However, no PTH or PTHrP was added, and anyway Murray *et al*. (1987) showed that the SAOS-2 osteoblast-like cell line exhibited limited responsiveness to steroid hormones. A possible explanation is therefore simply that the SAOS-2 cells do not produce the right or sufficient amounts of the necessary signals. This hypothesis is further given credence by that fact that although osteoblasts (OBs) express many types of molecules that may facilitate adhesive interactions between OBs and HSCs (including VCAM-1 and ICAM-1, 10-15 CD44, CD164, and osteopontin (Nilsson *et al*., 2005; Stier *et al*., 2004; Balduino *et al*., 2005; Verfaillie, 1998), only N-cadherin-positive spindle-shaped osteoblastic cells (SNO cells) are HSC niche cells (Zhang *et al*., 2003). It may therefore be essential to use specific osteoblasts such as the SNO cells to elicit HSC differentiation of ESC rather than SAOS-2.

7.5 Conclusion

It has been shown that aggregation by DEP induces murine ESC to produce embryoid bodies more rapidly than the hanging droplet method, and that the cells were differentiate towards mesenchymal lineage. It is not known, however, whether the cells differentiate further along the HSC lineage, and further experiments are needed to determine this. The introduction of osteoblasts in the aggregates did not result in (faster) differentiation along the mesemchymal lineage, and it is not known whether this is due to the fact that the aggregate

contained too few ESC, or whether it was because the SOAS-2 osteoblast-like cells did not produce the right signals. Further experiments are needed to establish this.

CHAPTER 8

Combined use of DEP and optical tweezers to swap embryonic stem cells between niches

---

8.1 Introduction

Commitment of cells to their fate during embryonic development is commonly assessed by transplant experiments, in which cells are first marked and then transplanted from their normal tissue into another tissue. Depending on whether the fate of the cell has just been specified or has already been determined and the cues a cell receives from the new environment it finds itself in, the cell may maintain its current course of differentiation, or change it. What environmental factors provide the cues for changing cell fate is currently an area of strong research interest.

Stem cells normally reside in niches in the body which provide a microenvironment which controls the cell's path of differentiation. The same questions concerning commitment of the cell to their fate can also be asked of stem cells and other progenitor cells. Compared to mature cells, progenitor and stem cells may have even more rigid requirements for their niches (Fuchs *et al*., 2004; Jones and Wagers, 2008). Even mature stem cells often have a lot of plasticity, and changes in the environment can lead to changes in stem cell fate. For example, HSCs of bone marrow have been shown to become hepatic oval cells (Lasagge *et al*., 2000; Petersen *et al*., 1999; Alison *et al*., 2000). Mesenchymal stem cells from bone marrow have been shown to travel to and differentiate into skeletal muscle (Ferrari *et al*., 1998), differentiated into neuronal tissue (Azizi *et al*., 1998; Kopen *et al*., 1999) supplied mesangial cells during repair processes (Ito *et al*., 2001), and given rise to cardiomyocytes *in vitro* (Fukuda, 2002; Makino *et al*., 1999). Glial progenitors from the rat optic nerve normally have the ability to produce only oligodendrocytes and some astrocytes. However, under appropriate *in vitro* culture conditions, these progenitors can give rise to neurospheres capable of generating neurons, astrocytes and oligodendrocytes (Kondo and Raff, 2000). These observations strongly imply a critical influence of microenvironmental cues on cell fate.

Study of stem cells in their natural environment is often wrought with difficulties, but with the help of microfabrication and manipulation techniques artificial microniches can be created that could enable one to change and study the stem cell microenvironment in vitro. To study the commitment of cells to their fate in the artificial niche it will be necessary to transplant cells from one artificial niche into another. Preferentially this would be done one cell at a time.

We have previously shown that dielectrophoresis (DEP) can be used to create artificial microniches for stem cells (Markx *et al*., 2009; this thesis, chapters 6, 7). Optical tweezers (OTs) can be used for the manipulation of cells (Grier, 2003; Ashkin *et al*., 1987; Macdonald *et al*., 2003; Curtis *et al*., 2002; McGloin *et al*., 2003; Graces-Chaves *et al*., 2005; Paterson *et al*., 2007). Optical tweezers offer a high resolution tool for trapping single particles, but have a limited manipulation area is limited owing to tight focusing requirements; on the other hand, electrokinetic forces (DEP) provide high throughput manipulation, but lack the flexibility or the spatial resolution necessary for controlling individual cells easily. Whilst optical tweezers on their own could be used to create artificial stem cell niches (Zhou and Melton, 2008), the combination of DEP and OT setups may have advantages in terms of the size and number of aggregates that can be formed in a single step and the costs of the equipment (Markx, 2008). Hence, the aim of the study is to find out whether optical tweezers can be used in combination with dielectrophoresis to exchange of cells between niches for the study of the commitment of individual stem cells to their fate.

8.2 Materials and methods

8.2.1 Cells

7a stem cells were cultured as described in chapter 3; 7a stem cells emit GFP at all times, and can therefore be easily located by their green fluorescence. Simulated microenvironments were created using stained and unstained SAOS-2 osteoblastic cells. A red Sigma Aldrich PKH26 cell membrane stain was used for staining.

8.2.2 Dielectrophoresis

Microelectrodes were of the interdigitated oppositely castellated type as described previously (Venkatesh and Markx, 2007). In the experiments only microelectrodes in the 300

μm and 250 μm regions were used; the two microelectrode regions were adjacent to each other, with a gap of approximately 600 μm between the closest ends of the two electrode regions. Standard glass microscope slide cover slips were cut to a size that would cover the width of 250 μm region and another cover slip cut to the width of the 300 μm region. A small space was left between both the electrode regions and which would allow the introduction of stem cells into either of the regions.

The slide was autoclaved prior to use, and placed on the stage of a Nikon E2000 fluorescence microscope. The OT used did not have a fluorescence microscope attached to it; hence the DEP experiment was first carried out under a fluorescence microscope to make sure all the aggregates formed well at the desired location. The space between the microelectrodes and the cover slips was filled with the low conductivity 300 mM D-sorbitol solution. Electric fields were generated between the 250 μm microelectrodes using signals of 1 MHz frequency and voltages of 20 $V_{pk\text{-}pk}$ for electrodes, and unstained SAOS-2 cells were introduced and attracted to the high field regions between the electrodes. Fresh sorbitol was passed through the chamber to redistribute the cells, remove non-attracted cells and maintain a low conductivity in the chamber. The time required for aggregates to form and reach their maximum height was approximately 20 minutes. Following this and aggregate was made of stained SAOS-2 cells using the same methodology in the 300 μm region. The time required for the aggregates to reach their maximum height in the 300 μm region was approximately 25 minutes. A sketch of the final structure is shown in Figure 8.1.

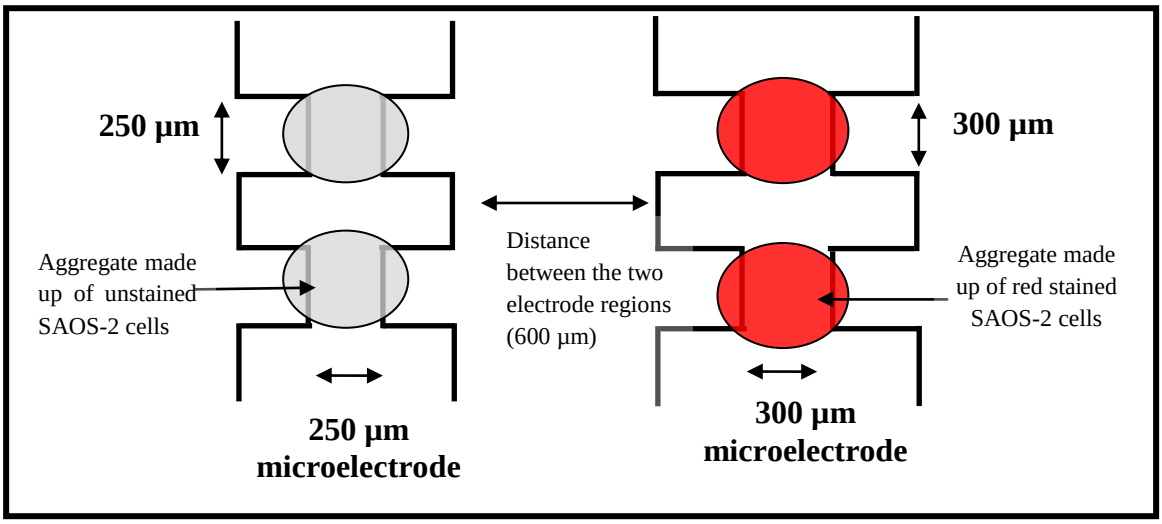

Figure 8.1: Slide.

Pictorial presentation of the experimental setup showing the microelectrodes with cell aggregates, before tweezing. Aggregates of stained (left) and unstained (right) osteoblastic cells were made with DEP at the 250 µm and 300 µm electrode regions, respectively, by applying a 20 $V_{pk\text{-}pk}$, 1 MHz signal to the electrodes.

8.2.3 Optical tweezer set up

Figure 8.2 shows a sketch of the combined set up of DEP and OT. Figure 8.3 shows the actual setup.

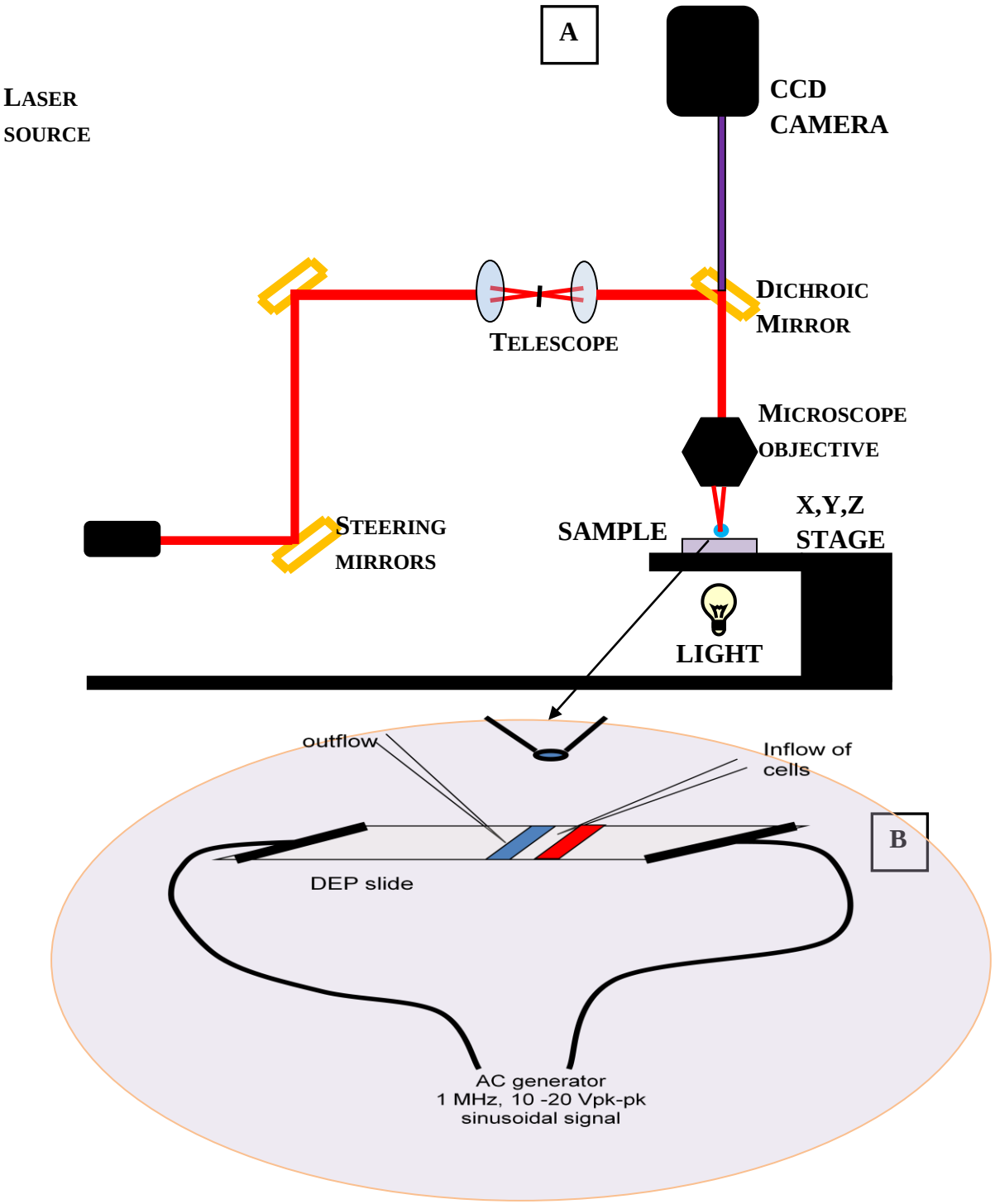

Figure 8.2: Optical tweezer setup with integrated dielectrophoresis chamber.

A) *Setup.* ***B)*** *Zoomed in pictorial presentation of DEP chamber showing the two electrode regions. Red indicates the 300 µm region for stained SAOS-2 cells and blue the 250 µm region for unstained SAOS-2 cells. Inflow and outflow of cells was done using a 10 µl Fine pipette.*

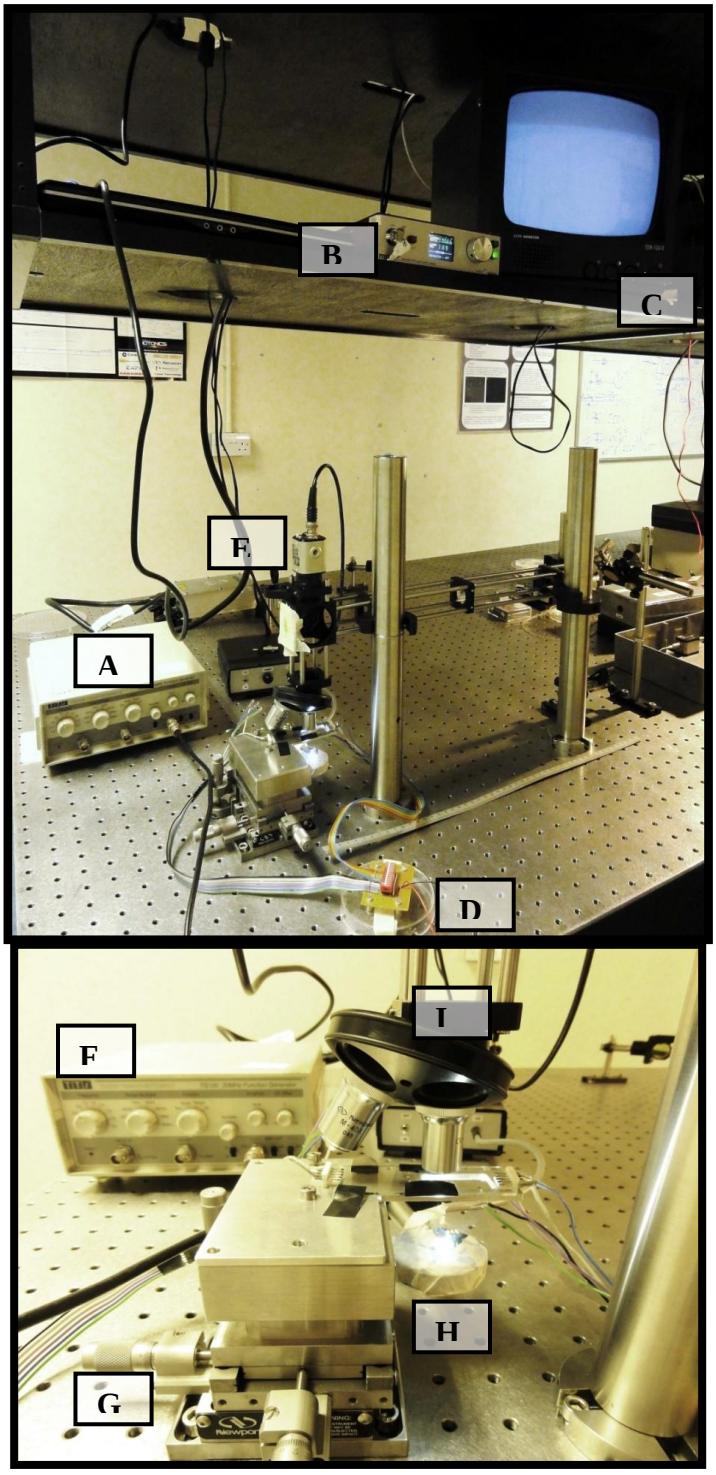

Figure 8.3: OT and DEP set up.

A) *Laser emitter.* ***B)*** *Device for controlling laser power.* ***C)*** *Video + TV .****D)*** *electrical switch/ controls and connections to microelectrode slide.* ***E)*** *CCD camera* ***F)*** *AC signal frequency generator.* ***G)*** *Sample stage, with X, Y and Z axis control knobs.* ***H)*** *LED light source.* ***I)*** *Turret with objective lens.*

After the formation of the aggregates with DEP the slide with aggregates was moved to the optical tweezer setup. For this it was necessary to disconnect the electrical supply from the DEP setup. In most cases there was little or no loss of cells from the aggregates during the move, but after reconnection of the frequency generator to the microelectrodes any cells that had come away from the aggregate were re-attracted to the aggregates with DEP.

Once both the aggregates had been formed 10 µl of a highly diluted suspension of 7a stem cells in sorbitol was introduced in the gap between the two electrode regions. The electric currents were still allowed to pass through the electrodes in order to keep the aggregates intact. The optical tweezer was then used to tweeze the stem cells into the SAOS-2 aggregate that was stained with a red fluorescent stain.

To do this a stem cell was trapped by the tweezer, pulled up on the z-axis, moved over the stained cell aggregate that had been formed at the 300 µm electrode region and then carefully dropped into one of the stained cell aggregates. During all this time the electric field remained switched on. Once the stem cell had been dropped into the selected aggregate, the AC electric current was switched off and electrical connections were removed. The slide was then moved to a Leica TCS2 confocal microscope to confirm a stem cell had been placed in an aggregate. Care was taken not to disturb the aggregates as they were moved. The chamber was then placed back in the OT setup and reconnected to the function generator. As the camera with the OT setup was black and white only, the aggregate concerned and the location of the stem cell in the aggregate was determined by locating the right electrode and counting the number of cells from one of the edges. Once spotted the stem cell was again trapped in the laser beam and lifted from the aggregate and moved towards the closest aggregate in the 250 µm region. The cell was dropped into this (unstained) aggregate and both the chambers were filled with 25% Puramatrix gel to keep the aggregates in position. The AC electric field was then switched off and 40 µl of fresh medium was added to the sides of each chamber to gelatinise the Puramatrix solution. Once again the chamber was disconnected from the wires and moved to the confocal microscope to confirm the location of the stem cell.

8.3 Results and discussion

Preliminary experiments with optical tweezers showed that it was relatively easy to move the cells with the laser in a sorbitol solution. In GMEM growth medium the cells tended to stick to the surface. It was difficult to move the cells around in Puramatrix gel due its high

viscosity. Therefore optical tweezing of cells was conducted while they were in the sorbitol solution.

Initial experiments indicated that the laser posed a threat to the ITO electrodes. When the NIR laser was focused on an ITO layer the electrode region tended to overheat, destroying the ITO layer. To avoid any contact of the focused beam with the electrodes the cells were first picked up on the z axis by the OT and then moved above the electrode region into the selected aggregates. For this reason aggregates were selected that were close to each other, and without much ITO surrounding them.

Following the construction of the aggregates of stained and unstained SAOS-2 osteoblasts, stem cells were introduced into the area in between the aggregates. A single stem cell was chosen randomly and tweezed into the stained aggregate of osteoblastic cells as shown in figure 8.4.

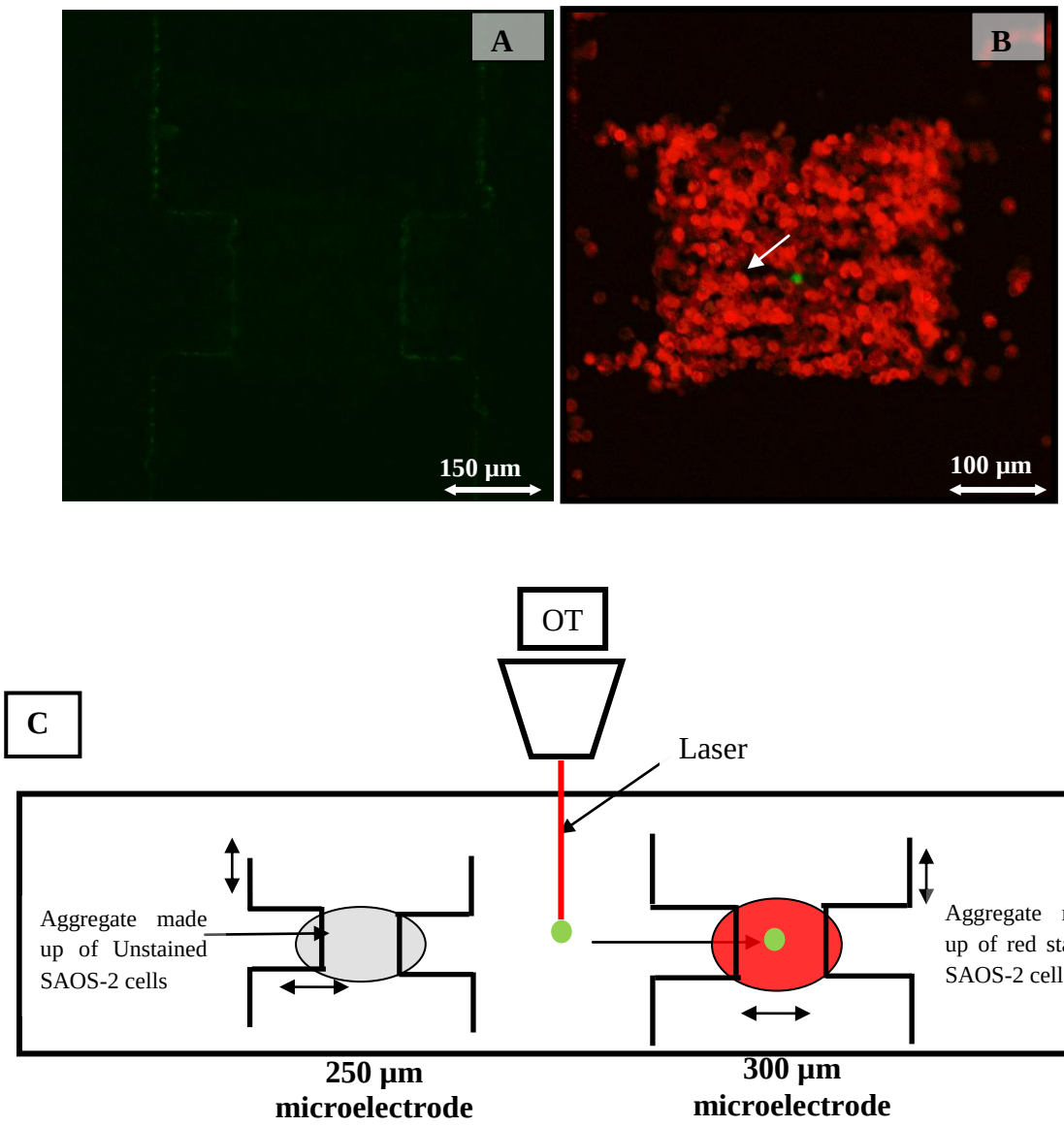

Figure 8.4: Introduction of a stem cell in niche 1.

A) *Aggregate of unstained osteoblastic cells formed with DEP by applying a 20 $V_{pk\text{-}pk}$, 1 MHz signal to the 250 µm region.* ***B)*** *Aggregate of osteoblastic cells stained with PKH26 cell membrane stain at 300 µm electrode region formed by DEP 20 $V_{pk\text{-}pk}$, 1 MHz; a green 7a stem cell incorporated by optical tweezer into the aggregate.* ***C)*** *Pictorial presentation of the optical tweezing of cells into a stained osteoblastic aggregate.*

Following confirmation with the confocal microscope, that a single stem cell had been moved into the first niche (formed by stained osteoblasts) the stem cell was lifted from the first niche with the tweezer and then moved into the aggregate of unstained osteoblastic cells (Figure 8.5).

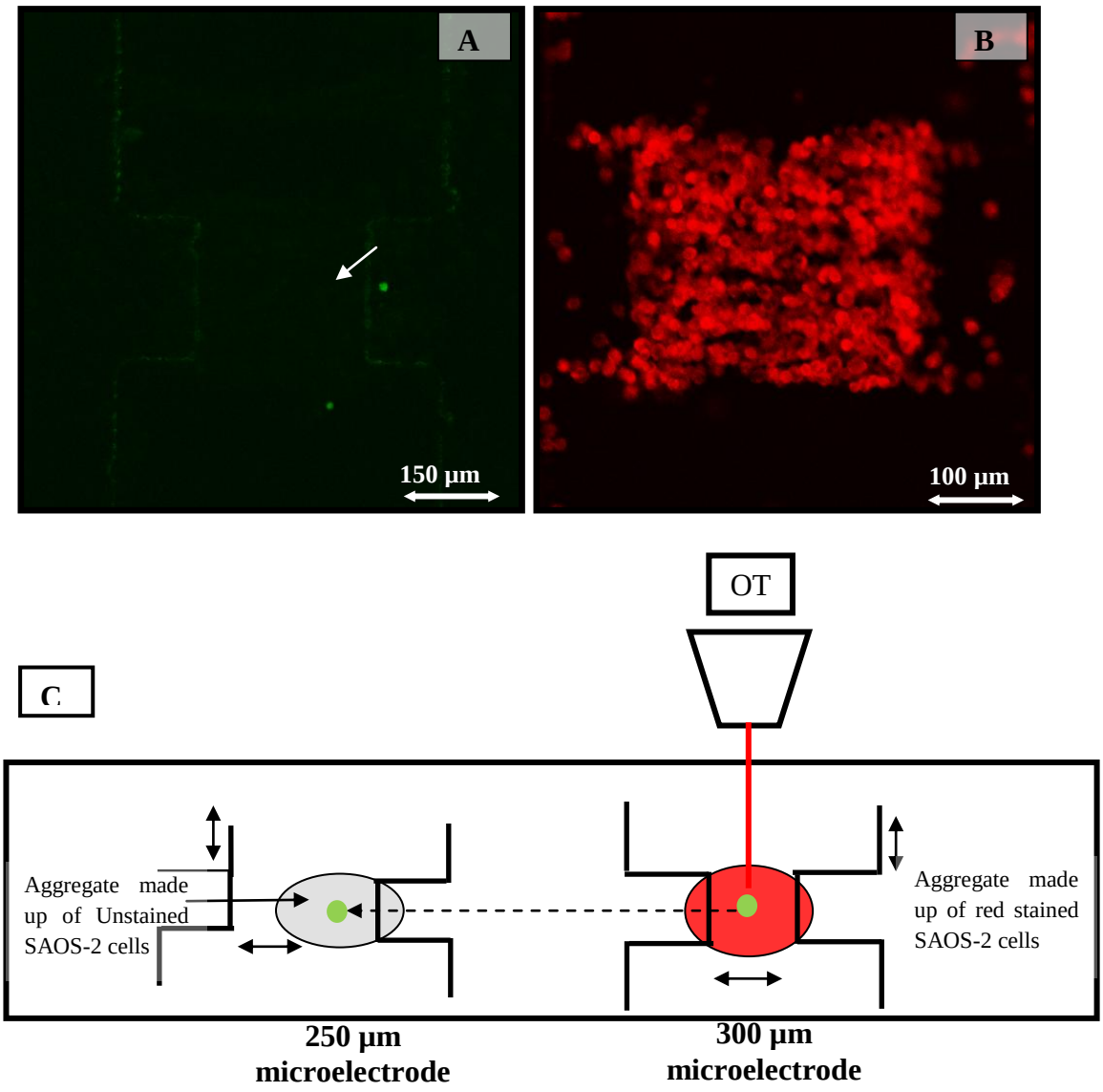

Figure 8.5: Movement of a stem cell between niches.

A) *Green fluorescent image of unstained osteoblastic cell aggregate formed by DEP at 250 µm region at 20 $V_{pk\text{-}pk}$, 1 MHz showing the transfer of the 7a stem cell from the stained osteoblastic aggregate into the unstained aggregate, by optical tweezer.* ***B)*** *Aggregate of osteoblastic cells stained with PKH26 cell membrane stain at 300 µm electrode region formed by DEP 20 $V_{pk\text{-}pk}$, 1 MHz; without any green 7a stem cell.* ***C)*** *Pictorial presentation of the optical tweezing of cell into unstained osteoblastic aggregate from stained osteoblastic aggregate.*

8.4 Conclusions and suggestions

The experiments conducted in this chapter were only a preliminary study of combining DEP and OT to construct artificial stem cell microniche. The study confirmed that OT can not only be used to control the insertion a particular number of stem cells into the micro niche, but also withdraw a given cell from the niche and transport it to another microniche. Although, the same cell type was used in this study in both niches (SAOS-2 with and without stain); in future work different cell types could be used to make an entirely different niches, e.g. osteoblasts and endothelial cell to create osteoblast and vascular niches. By using embryonic stem cell with marker genes as the switching on and off of genes could mark the lineage progression of the stem cell during this process. All experiments were performed in an unsterile atmosphere which means that long term culture of the cells was not possible. However, it is entirely possible to work sterile and perform long-term studies. Thus it is feasible to use a combination of DEP and OT to pursue long term studies of the commitment of stem cells to their fate.

CHAPTER 9

Conclusions and Suggestions for Future Work

9.1 Conclusions

In this study it has been shown that an artificial stem cell microniche can be created using the dielectrophoresis technique. The study showed that DEP could be used to create aggregates of cells of different sizes and offered more control in making different architectural constructs of aggregates comprising two different cell types. The construction of artificial niche could give an excellent opportunity to study the effect of chemical, physical or various environmental cues on the fate of stem cells, *in vitro.*

This study has focused on the optimization of conditions for the niche construction, giving a generalized view on how cells would behave in a compact 3D environment when assembled by DEP. It has also tried to study the long term behavior of cells in the niche, both ESCs and SAOS-2 cell individually and when co-cultured. By using ESC marker cells, the study of fate determination was also made possible.

One of the main findings of this research was the effect of DEP assembly on ESCs and the study of the effect of the electrode size on the EB formation. When the ESCs were assembled using DEP, they formed embryonic body (EB). The size of the electrode determines the size of the EBs. At electrode regions lower than 75 µm the aggregates merged or agglomerated with adjacent EBs to form larger EBs and at regions above 100 µm, the aggregates were seen to split into smaller EBs. At 100 and 75 µm regions of the electrode, the ES cells formed EBs which did not spilt and did not agglomerate easily with the neighboring EBs. They yielded good sized EBs, thus making these two electrode regions the ones most suitable for further study.

Secondly the study of the behavior of ESCs and SAOS-2 cells when co-cultured in 3D aggregates, gave an understanding of the interaction between the two cell types. The difference in their adhesive and cohesive properties made it difficult to form an aggregate that would keep both the cell types in close proximity and provide greater chances of close association, while the ESCs underwent the process of differentiation.

The findings suggested that the reorganisation of the cells in the aggregates was mainly determined by the adhesive forces between the different cells and between cells and the surrounding materials. To construct an artificial microniche, it appeared therefore vital to balance the adhesive and cohesive properties of both the cells and their surroundings and their initial position, to achieve maximum cell-cell contact. To achieve this study was conducted to determine the diffusion co-efficient of SAOS-2 cells and eventually led to the determination of the architecture of the stem cell niche constructs. Three main types of architectures were constructed. 1) Stem cells forming the core and SAOS-2 cells on the outside. 2) Stem cells on the outside and SAOS-2 cells forming the core and 3) a mixture of both cell types. Out of the three the second architecture worked the best, as SAOS-2 cells were swept into the EBs as they were formed.

Once the architecture was determined focus was made on stem cell fate determination. Previous experiments gave no indication of whether the stem cells were actually differentiating along the right path. The study was now taken a step further by using Brachyury ESCs. These cells could indicate, by producing GFP, when they were moving towards the early mesenchymal lineage. Differentiation along the mesenchymal lineage is the first step in the direction towards the hematopoietic stem cell lineage. Upon aggregation with DEP the ES cells formed EBs within 24 hours which showed GFP production (compared to 2-3 days in hanging droplets). GFP production started in the centre of the EB, and depended on the size of the EB. Maximum green fluorescence was seen in aggregates formed in the 75 µm and 100 µm electrode regions, with little or none seen at the 50 µm region.

In the next set of experiments, aggregates were made with SAOS-2 cells at the bottom of the aggregate covered by the Brachyury embryonic stem cells. An increase in the GFP level was seen on the 3rd day of incubation but on the 7th day the GFP level had started to decline. The reason for the delay in GFP production in mixed aggregates and the decline are unknown.

The combination of the optical tweezers and DEP is potentially quite powerful, as DEP allows aggregation of many cells at the same time, whilst OT on the other hand can be used to manipulate single cells with high precision. To demonstrate this, an optical tweezer was used to move cells from one niche created with DEP to another niche created with DEP. Two microniches were constructed next to each other, composed of stained and unstained SAOS-2 cells. Although it was shown that OT could be used to move a stem cell into one niche and

then, move the same cell into another niche the technique was not very straight forward and will require a lot of modification to be effectively used in future.

In general the research showed that the size of the aggregates and its composition along with the architecture had an important role to play in the ESC differentiation and niche maintenance. By manipulating these aspects variety of results could be achieved. The study would therefore serve as a base for future studies. With the basic parameters optimized, in future the affect of more complex factors such as chemical cues and physical forces could be measured/ studied on the niche constructs.

9.2 Limitations of current work and suggestions for future work

In this study only one type of microelectrodes (interdigitated oppositely castellated electrodes with a distance between electrodes and castellations equal to the castellation size) were used to generate DEP forces and form cell aggregates. Different kinds of DEP microelectrodes could be designed with varying electrode distance, sizes, shapes and patterns to see the effect of these factors on the formation of embryonic bodies/stem cell differentiation. The size of the embryoid bodies and their homogeneity are known to have an effect on the differentiation and fate determination.

Hwang *et al*. (2009) used microengineered hydrogel microwells to direct ES cell differentiation and also determined the role of WNT signaling pathway in directing the differentiation. The results elucidated that the EB size played a role in the differentiation and found that endothelial cell differentiation was increased in smaller EBs (150 μm in diameter) whereas cardiogenesis was enhanced in larger EBs (450 μm in diameter). Microwells could be fabricated onto slides to make aggregates of a well-defined structure and size; this could help in making homogenous EBs of accurately the same size and help prevent the agglomeration of EBs, as agglomeration has a negative effect on the proliferation and differentiation of ESCs (Dang *et al*., 2002).

In EBs, as they grow, the supply of nutrients and oxygen to the centre of the aggregate becomes limited. Due to the anoxic condition in the centre the cells start showing apoptosis followed by fluid filled cavitation, called “cystic EBs”. This is a part of the differentiation process and is normal. However for long term culture of EBs, it is vital that the cells get a fresh supply of nutrients. Therefore while designing electrodes, microchannels could be

incorporated between the adjacent aggregates, to make sure that the cells receive proper supply of oxygen, growth factors and nutrients.

Real time imaging could be a very useful tool to study the cells without disturbing the experimental setup. This could tell exactly how the cells are migrating from one niche to another or how the events involved in the agglomeration and splitting of EBS proceed. For this to be possible the microscope needs to be fitted with a closed chamber in which the temperature and atmosphere is much better controlled than in the current system. A microscope stage with XYZ control would help in keeping track of the cell, reproducibly move between areas, and have better focal control. Identification of stained cells under the OT would be very important in future studies. The OT used in the experiments did not allow coloured image viewing therefore it became very challenging to identify the different cell types.

To create an artificial microniche containing many types of cells, it is important to be able to identify the cells using different markers stains. Some simple modifications of the optical tweezer setup could significantly enhance its potential. Combining it with confocal imaging or even a standard epifluorescent microscope would make it much easier to spot cells with (fluorescent) markers. The camera that is currently attached to the OT setup only takes black and white images; its replacement with a colour camera would be beneficial.

In the studies shown in this thesis the OT is only used for manipulating one single cell at a time. However, OTs could be very useful in handling larger numbers of cells at a time. For example, recent studies have shown the utility of holographic optical tweezers (HOTs) for simultaneously manipulating many particles at the same time. The spatial light modulator employed for the generation of the holograms involves the use of a computer interface to control traps; this allows the control of the motion of the tweezers to be completely automated. New multitouch interface systems allow interactive real-time control of a HOT system and provide the user with the ability to interact with a computer in multiple locations simultaneously. This way several digital objects can be controlled independently (Grieve *et al*., 2009). Microfluidic system (MFS) when incorporated with HOTs, form a platform which can potentially be used to investigate chemo-mechanical processes, by using a reconfigurable force sensor array with piconewton resolution (Uhrig *et al*., 2009). This new technique may

provide a powerful tool for multi-cellular manipulation in the formation of cell arrangements and the creation of stimuli of engineered tissue (Zhang *et al*., 2008).

Microfluidic systems can be easily integrated with microphotonics such as optical traps to form micro-opto-fluidic system (MOFS) for single cell manipulation (Monat *et al*., 2008). Cultivating single cells in MOFS can produce daughter cells which are all the same - which is important for stem cell therapy. The method can potentially be applied to stem cell delivery or the creation of stem cell niches (Noort *et al*., 2009).

In order to understand lineage commitment it is important to use marker ES cells. In this study E14, 7a, Oct-4 and Brachyury ESCs were used. All these cells marked the onset of differentiation except for E14 ESCs. Brachyury cells were the ones that were most specific, marking the onset of mesenchymal lineage. Other more precise marker ESCs could be used that could directly show the onset of a HSC lineage.

Protein/DNA/RNA analysis of the differentiating cells should be used to prove the lineage commitment of cells. Similarly protein/DNA/RNA analysis could help in elucidating the role of various adhesion molecules in the stem cell niche. The effect of the addition of growth factors such as BMP4 could be also studied with respect to Brachyury cells, as these cells definitely progress towards mesenchymal fate in the presence of BMP4 growth factor.

Incorporating different cell types that are typical of the type of niche in consideration could be the next step to create a more functional and specific microniches. For example, stromal cells could be inserted to see whether the AGM niche can be recreated and endothelial cells for the vascular niche. Likewise architecture of the niches could also be modified by using three cell types or more instead of two.

The main limitation of this study was the limited availability of cells to experiment with. This study was conducted with embryonic stem cells which have different characteristics as compared to multipotent stem cells. ESCs tend to form embryoid bodies their interaction with other type of cells is very different than the multipotent stem cells which would not tend to form embryoid bodies. This means that basic adhesive-cohesive properties of different stem cells would change the whole niche construction. As embryonic stem cells were used in this study the niche construction depended on the adhesive-cohesive properties of ESCs and its

neighboring SAOS-2 cells. Hence, effort was made to try and increase cell-cell interaction, (an important factor in fate determination) as efficiently as possible. Further study would be required to establish the behavior of multipotent stem cells, for example HSCs in the niche constructs tested in this research.

REFERENCES

1. Abkowitz J.L., Robinson A.E., Kale S., Long M.W., Chen J. (2003). Mobilization of hematopoietic stem cells during homeostasis and after cytokine exposure. *Blood*; 102: 1249-1253

2. Ablamunits V.G., Bliumkin V.N., Mogilevskii G.M., Kirsanova L.A., Baranova F.S. (1990). Aggregates of islet cells, their structure and insulin-producing activity during cultivation in vitro. *Biull. Eksp. Biol. Med.*; 110(12): 650-653

3. Aguirre A., Rubio M.E., Gallo V. (2010). Notch and EGFR pathway interaction regulates neural stem cell number and self-renewal. *Nature*; 467(7313): 323-327

4. Akashi K., He X., Chen J., Iwasaki H., Niu C., Steenhard B., Zhang J., Haug J., Li L. (2003). Transcriptional accessibility for genes of multiple tissues and hematopoietic lineages is hierarchically controlled during early hematopoiesis. *Blood*; 101: 383-89

5. Albrecht D.R., Sah R.L., Bhatia S.N. (2004). Geometric and material determinants of patterning efficiency by dielectrophoresis. *Biophy. J.*; 87(4): 2131-2147

6. Albrecht D.R., Tsang V.L., Sah R.L., Bhatia S.N. (2005). Photo- and electropatterning of hydrogel-encapsulated living cell arrays. *Lab Chip*; 5:111-118

7. Albrecht D.R., Underhill G.H., Wassermann T.B., Sah R.L., Bhatia S.N. (2006). Probing the role of multicellular organization in three-dimensional microenvironments. *Nat. Methods*; 3: 369-375

8. Albrecht D.R., Underhill G.H., Mendelson A., Bhatia S.N. (2007). Multiphase electropatterning of cells and biomaterials. *Lab Chip*; 7: 702-709

9. Alison M.R., Poulsom R., Jeffery R., Dhillon A.P., Quaglia A., Jacob J., Novelli M., Prentice G., Williamson J., Wright N.A. (2000). Hepatocytes from non-hepatic adult stem cells. *Nature*; 406(6793): 257

10. Alt W. (1980). Biased random walk models for chemotaxis and related diffusion approximations. *J. Math. Biol.*; 9: 147-177

11. Anderson D.G., Levenberg S., Langer R. (2004). Nanoliter-scale synthesis of arrayed biomaterials and application to human embryonic stem cells. *Nat. Biotechnol.*; 22: 863-866

12. Anderson H.C., Hsu H.H.T., Raval P., Reynold P.R., Gurley D.J., Aguilera M.X., Davis L.S., Moylan P.E. (1998). The bone-inducing agent in SAOS-2 cell extracts and secretions. *Cells Mat.*; 8: 89-98

13. Anderson R.G. (1998). The caveolae membrane system. *Annu. Rev. Biochem.*; 67: 199-225

14. Andrade W.N., Johnston M.G., Hay J.B. (1998). The relationship of blood lymphocytes to the recirculating lymphocyte pool. *Blood*; 91(5): 1653-1661

15. Arai F., Hirao A., Ohmura M., Sato H., Matsuoka S., Takubo K., Ito K., Koh G.Y., Suda T. (2004).Tie2/angiopoietin-1 signaling regulates hematopoietic stem cell quiescence in the bone marrow niche. *Cell*; 118: 149-161

16. Arnold W.M. and Zimmermann U. (1988). Electro-rotation: development of a technique for dielectric measurements of individual cells and particles. *J. Electrostat.*; 21: 151-191

17. Arnold W.M. (2010). Dielectrophoretic Cell Separation: Some Hints and Kinks. Proc. ESA Annual Meeting on Electrostatics; 1-11

18. Ashkin A. (1997). Optical trapping and manipulation of neutral particles using lasers. *P.N.A.S.*; 94: 4853-4860

19. Ashkin A., Dziedzic J.M., Yamane T. (1987). Optical trapping and manipulation of single cells using infrared-laser beams. *Nature*; 330: 769-771

20. Avecilla S. T., Hattori K., Heissig B., Tejada R., Liao F., Shido K., Jin D.K., Dias S., Zhang F., Hartman T.E., Hackett N.R., Crystal R.G., Witte L., Hicklin D.J., Bohlen P.,

Eaton D., Lyden D., Sauvage F.D., Rafii S. (2004). Chemokine-mediated interaction of hematopoietic progenitors with the bone marrow vascular niche is required for thrombopoiesis. *Nature Med*.; 10: 64-71

21. Azizi S.A., Stokes D., Augelli B.J., DiGirolamo C., Prockop D.J. (1998). Engraftment and migration of human bone marrow stromal cells implanted in the brains of albino rats—similarities to astrocyte grafts. *P.N.A.S.*; 95: 3908- 3913

22. Balaban N.Q., Schwarz U.S., Riveline D., Goichberg P., Tzur G., Sabanay I., Mahalu D., Safran S., Bershadsky A., Addadi L., Geiger B. (2001). Force and focal adhesion assembly: a close relationship studied using elastic micropatterned substrates. *Nat. Cell Biol*.; 3: 466-472

22. Balduino A., Hurtado S.P., Frazao P., Takiya C.M., Alves L.M., Nasciutti L.E., El-Cheikh M.C., Borojevic R. (2005). Bone marrow subendosteal microenvironment harbours functionally distinct haemosupportive stromal cell populations. *Cell Tiss. Res*.; 319: 255-266

23. Barocas V.H. and Tranquillo R. (1994). Biphasic theory and in vitro assays of cell-fibril mechanical interactions in tissue-equivalent collagen gels. *In Cell Mechanics and Cellular Engineering.* Springer-Verlag, New York: pp 185–209

24. Barocas V.H. and Tranquillo R.T. (1997a). An anisotropic biphasic theory of tissue-equivalent mechanics: the interplay among cell traction, fibrillar network deformation, fibril alignment, and cell contact guidance. *J. Biomech. Eng.* 119: 137-145

25. Barry F., Boynton R.E., Liu B., Murphy J.M. (2001). Chondrogenic differentiation of mesenchymal stem cells from bone marrow: differentiation-dependent gene expression of matrix components. *Exp. Cell Res.*; 268: 189-200

26. Bazou D., Coakley W.T., Meek K.M, Yang M., Pham D.T. (2004). Characterisation of the morphology of 2-D particle aggregates indifferent electrolyte concentrations in an ultrasound trap. *Colloid Surf. A-Physicochem. Eng. Asp*.; 243: 97-104

27. Bazzoni G. and Dejana E. (2001). Pores in the sieve and channels in the wall: control of paracellular permeability by junctional proteins in endothelial cells. *Microcirculation*; 8: 143-152

28. Becker A.J., McCulloch E.A., Till J.E. (1963). Cytological demonstration of the clonal nature of spleen colonies derived from transplanted mouse marrow cells. *Nature*; 197: 452-454

29. Beckmann J., Scheitza S., Wernet P., Fischer J.C., Giebel B. (2007). Asymmetric cell division within the human hematopoietic stem and progenitor cell compartment: identification of asymmetrically segregating proteins. *Blood*; 109(12): 5494-501

30. Belliars R., Curtis A., Dunn G. (1982). *Cell behavior*. Cambridge, Cambridge University Press

31. Bendall S.C., Stewart M.H., Menendez P., George D., Vijayaragavan K., Werbowetski-Ogilvie T., Ramos-Mejia V., Rouleau A., Yang J., Bosse M., Lajoie G., Bhatia M. (2007). IGF and FGF cooperatively establish the regulatory stem cell niche of pluripotent human cells in vitro. *Nature*; 448: 1015-1021

32. Benhamou S. (2003). Bicoordinate navigation based on nonorthogonal gradient fields. *J. Theor. Biol.*; 225: 235-239

33. Beningo K.A., Dembo M., Kaverina I., Small J.V., Wang Y.L. (2001). Nascent focal adhesions are responsible for the generation of strong propulsive forces in migrating fibroblasts. *J. Cell Biol.*; 153: 881-888

34. Bennink M.L., Scharer O.D., Kanaar R., Sakata-Sogawa J.M., Schins J.S., Kander J.S., de Grooth B.G., Greve J. (1999). Single-molecule manipulation of double-stranded DNA using optical tweezers: interaction studies of DNA with RecA and YOYO-1. *Cytometry*; 36: 200-208

35. Berge U., Kristensen P., Rattan S. (2008). Hormetic modulation of differentiation of normal human epidermal keratinocytes undergoing replicative senescence in vitro. *Exp. Gerontology*; 43: 658-662

36. Bershadsky A.D., Balaban N.Q., Geiger B. (2003). Adhesion-dependent cell mechano-sensitivity. *Annu. Rev. Cell Dev. Biol.*; 19: 677-695

37. Bhushan A., Itoh N., Kato S., Thiery J.P., Czernichow P., Bellusci S., Scharfmann R. (2001). Fgf10 is essential for maintaining the proliferative capacity of epithelial progenitor cells during early pancreatic organogenesis. *Development*; 128(24): 5109-5117

38. Bianco P. and Robey P.G., (2001). Stem cells in tissue engineering. *Nature*; 414: 118-121

39. Bichet S., Wenger R.H., Camenisch G., Rolfs A., Ehleben W., Porwol T., Acker H., Fandrey J., Bauer C. and Gassmann M. (1999). Oxygen tension modulates beta-globin switching in embryoid bodies. *FASEB J.*; 13, 285-295

40. Birkbeck A.L., Flynn R.A., Ozkan M., Song D.Q., Gross M., Esener S.C. (2003). VCSEL Arrays as micromanipulators in chip-based biosystems. *Biomed. Microdev.*; 5: 47-54

41. Blackwell P.G. (1997). Random diffusion models for animal movement. *Ecol. Mod.*; 100: 87-102

42. Bonney E.A. and Matzinger P. (1997). The maternal immune system's interaction with circulating fetal cells. *J. Immunol*.; 158(1): 40-47

42. Bosnakovski D., Mizuno M., Kim G., Takagi S., Okumura M., Fujinaga T. (2006). Chondrogenic differentiation of bovine bone marrow mesenchymal stem cells (MSCs) in different hydrogels: influence of collagen type II extracellular matrix on MSC chondrogenesis. *Biotechnol. Bioeng.*; 93: 1152-1163

43. Bowman T.V. and Zon L.I. (2009). Lessons from the niche for generation and expansion of hematopoietic stem cells. *Drug Disc. Tod: Therap. Strat.* doi:10.1016/j.ddstr.2009.06.003

44. Bratt-Leal A.M., Carpenedo R.L., McDevitt T.C. (2009). Engineering the embryoid body microenvironment to direct embryonic stem cell differentiation. *Biotechnol. Prog.*; 25: 43-51

45. Brighton C., Wang W., Clark C. (2008). The Effect of Electrical Fields on Gene and Protein Expression in Human Osteoarthritic Cartilage Explants. *J. Bone Joint Surg. Am.*; 90: 833–848

46. Brinster R.L. (2002). Germ line stem cell transplantation and transgenesis. *Science*; 296: 2174-2176

47. Briscoe J. and Ericson J. (2001). Specification of neuronal fates in the ventral neural tube. *Curr. Opin. Neurobiol*.; 11: 43-49

48. Bronkhorst P.J., Streekstra G.J., Grimbergen J., Nijhof E.J., Sixma J.J., Brakenhoff G.J. (1995). A new method to study shape recovery of red blood cells using multiple optical trapping. *Biophys. J.*; 69: 1666-1673

49. Brown D., Christine K., Showell C., Conlon F. (2007). Small heat shock protein Hsp27 is required for proper heart tube formation. *Genesis*; 45: 667-678

50. Bruzzone R., Hormuzdi S.G., Brabe M.T., Herb A., Monyer H. (2003). Pannexins, a family of gap junction proteins expressed in brain. *P.N.A.S.*; 100: 13644-13649

51. Burt J.P.H., Pethig R., Gascoyne P.R.C., Becker F.F. (1990). Dielectrophoretic characterisation of friend murine erythroleukaemic cells as a measure of induced differentiation. *Biochim. Biophys. Acta*.; 1034: 93-101

52. Butler J.M., Nolan D.J., Vertes E.L., Varnum-Finney B., Kobayashi H., Hooper A.T., Seandel M., Shido K., White I.A., Kobayashi M., Witte L., May C., Shawber C., Kimura Y., Kitajewski J., Rosenwaks Z., Bernstein I.D., Rafii S. (2010). Endothelial cells are essential for the self-renewal and repopulation of Notch-dependent hematopoietic stem cells. *Cell Stem Cell*; 6: 251-264

53. Calvi L.M., Adams G.B., Weibrecht K.W., Weber J.M., Olson D.P., Knight M.C., Martin R.P., Schipani E., Divieti P., Bringhurst F.R., Milner L.A., Kronenberg, H.M., Scadden D.T. (2003). Osteoblastic cells regulate the haematopoietic stem cell niche. *Nature*; 425: 841-846

54. Cao T., Heng B.C., Ye C.P., Liu H., Toh W.H., Robson P., Li P., Hong Y.H., Stanton L.W. (2005). Osteogenic differentiation within intact human embryoid bodies result in a marked increase in osteocalcin secretion after 12 days of in vitro culture, and formation of morphologically distinct nodule-like structures. *Tiss. Cell*; 37(4): 325-334

55. Campbell N.A. and Reece J.B. (2002). *Biology*; 6th ed. San Francisco; Benjamin Cummings: pp 113

56. Carmeliet P. and Jain R.K. (2000). Angiogenesis in cancer and other diseases. *Nature*; 407(6801): 249-257

57. Carpenedo R.L., Bratt-Leal A.M., Marklein R.A., Seaman S.A., Bowen N.J., McDonald J.F., McDevitt T.C. (2009). Homogeneous and organized differentiation within embryoid bodies induced by microsphere-mediated delivery of small molecules. *Biomaterials*; 30: 2507-2515

58. Cartmell S.H., Dobson J., Verschueren S.B., El Haj A.J. (2002). Development of magnetic particle techniques for long-term culture of bone cells with intermittent mechanical activation. *IEEE Transact. Nanobiosci.*; 1(2): 92-97

59. Chambers A.F., Schmidt E.E., Macdonald I.C., Morris V.L., Groom A.C. (1992). Early steps in hematogenous metastasis of B16F1 melanoma cells in chick embryos studied by high-resolution intravital videomicroscopy. *J. Natl. Cancer Inst.*; 84: 797-803

60. Chan C.K.F., Chen C.C., Luppen C.A., Kim J.B., DeBoer A.T., Wei K., Helms J.A., Kuo C.J., Kraft D.L., Weissman I.L. (2009). Endochondral ossification is required for haematopoietic stem-cell niche formation. *Nature*; 457: 490-494

61. Choquet D., Felsenfeld D.P., Sheetz M.P. (1997). Extracellular matrix rigidity causes strengthening of integrin-cytoskeleton linkages. *Cell*; 88: 39-48

62. Cirulli V., Halban P.A., Rouiller D.G. (1993). Tumor necrosis factor-alpha modifies adhesion properties of rat islet B cells. *J. Clin. Invest.*; 91(5): 1868-1876

63. Caires K., Broady J. and McLean D. (2010). Maintaining the male germline: regulation of spermatogonial stem cells. *J. Endocrinol.*; **205**: 133-145

64. Clouthier D.E., Avarbock M.R., Brinster R.L. (2001). Rat spermatogenesis in mouse testis. *Nature*; 381: 418-421

65. Coakley W.T., Bazou D., Morgan J., Foster G.A., Archer C.W.K., Brothwick K.A.J., Twomey C., Bishop J. (2004). Cell-cell contact and membrane spreading in an ultrasound trap. *Colloid. Surf. B: Biointerf.*; 34: 221-230

66. Codling E.A., Plank M.J., Benhamou S. (2008). Random walk models in biology. *J. Royal Soc. Interf.*; 5: 813-834

67. Cooper-White J., Doran M.R., Mills R. (2010). Cell migration. World Intellectual Property Organisation; international publication number: WO2010/078623A1

68. Comandon J. (1917). Phagocytose in vitro des hematozoaires du calfat (enregistrement cinematographique). *Compt. Rend. Soc. Biol. (Paris)*; 80: 314-316

69. Conacci-Sorrell M., Simcha I., Ben-Yedidia T., Blechman J., Savagner P., Ben-Ze'ev A. (2003). Autoregulation of E-cadherin expression by cadherin-cadherin interactions: the roles of beta-catenin signaling, Slug, and MAPK. *J. Cell Biol.*; 163: 847-857

70. Cotsarelis G., Sun T.T, Lavker R.M. (1990). Label-retaining cells reside in the bulge area of pilosebaceous unit: implications for follicular stem cells, hair cycle, and skin carcinogenesis. *Cell*; 61: 1329-1337

71. Coucouvanis E. and Martin G.R. (1995) Signals for death and survival: a two step mechanism for cavitation in the vertebrate embryo. *Cell*; 83(2): 279-87

72. Cukierman E., Pankov R., Stevens D.R., Yamada K.M. (2001). Taking cell-matrix adhesions to the third dimension. *Science*; 294: 1708-1712

73. Cumano A. and Godin I. (2001). Pluripotent hematopoietic stem cell development during embryogenesis. *Curr. Opini. Immunol.*; 13: 166-171

74. Curry J.L., Trentin J.J., Wolf N. (1967). Hemopoietic spleen colony studies. II. Erythropoiesis. *J. Exp. Med.*; 125: 703-720

75. Curtis J.E., Koss B.A., Grier D.G. (2002). Dynamic holographic optical tweezers. *Optic. Comm.*; 207: 169-175

76. D'Amour K.A., Agulnick A.D., Eliazer S., Kelly O.G., Kroon E., Baetge E.E. (2005). Efficient differentiation of human embryonic stem cells to definitive endoderm. *Nat. Biotechnol.*; 23: 1534-1541

77. D'Amour K.A., Bang A.G., Eliazer S., Kelly O.G., Agulnick A.D., Smart N.G., Moorman M.A., Kroon E., Carpenter M.K., Baetge E.E. (2006). Production of pancreatic hormone-expressing endocrine cells from human embryonic stem cells. *Nat. Biotechnol.*; 24: 1392-1401

78. Dang S.M., Kyba M., Perlingeiro R., Daley G.Q., Zandstra P.W. (2002). Efficiency of embryoid body formation and hematopoietic development from embryonic stem cells in different culture systems. *Biotechnol. Bioeng.*; 78: 442-453

79. Dang S.M., Gerecht-Nir S., Chen J., Itskovitz-Eldor J., Zandstra P.W. (2004). Controlled, scalable embryonic stem cell differentiation culture. *Stem Cells*; 22: 275-282

80. Davidson A.J. and Zon L.I. (2000). Turning mesoderm into blood: the formation of hematopoietic stem cells during embryogenesis. *Curr. Top. Dev. Biol.*; 50: 45-60

81. Dee K.C, Andersen T.T, Bizios R. (1999). Osteoblast population migration characteristics on substrates modified with immobilized adhesive peptides. *Biomaterials*; 20: 221-227

82. Deng W. and Lin H. (1997). Spectrosomes and fusomes anchor mitotic spindles during asymmetric germ cell divisions and facilitate the formation of a polarized microtubule array for oocyte specification in *Drosophila*. *Dev. Biol.*; 189: 79-94

83. Denk W., Piston D.W., Webb W.W. (1995). Two-photon molocular excitation in laser-scanning microscopy, in J.B. Pawley, ed., *Handbook of Biological Confocal Microscopy*. New York: Plenum Press: pp 445-458

84. Desai J.P., Pillarisetti A., Brooks A.D. (2007). Engineering approaches to biomanipulation. *Ann. Rev. Biomed. Eng*.; 9: 35-53

85. Dickinson R.B. and Tranquillo R.T. (1993). Optimal estimation of cell movement indices from the statistical analysis of cell tracking data. *Am. Inst. Chem. Eng. J*.; 39:1995-2010

86. Dike L.E., Chen C.S., Mrksich M., Tien J., Whitesides G.M., Ingber D.E. (1999). Geometric control of switching between growth, apoptosis, and differentiation during angiogenesis using micropatterned substrates. *In Vitro Cell Dev. Biol. Anim*.; 35(8): 441-448

87. Discher D.E., Janmey P.A., Wang Y.-L. (2005). Tissue cells feel and respond to the stiffness of their substrate. *Science*; 310: 1139-1143

88. Doh I. and Cho Y-H. (2005). A continuous cell separation chip using hydrodynamic dielectrophoresis (DEP) process. *Sens. Actuat. A: Phys.*; 121(1): 59-65

89. Dube J., Methot S., Moulin V., Goulet D., Bourdage M., Auger F., Germain L. (2005). External electric fields induce morphological changes on human skin cells cultured in vitro. *Proc. USRI 2005 Meeting*, New Delhi

90. Duncan A.W., Rattis F.M., DiMascio L.N., Congdon K.L., Pazianos G., Zhao C., Yoon K., Cook J.M., Willert K., Gaiano N., Reya T. (2005). Integration of Notch and Wnt signaling in hematopoietic stem cell maintenance. *Nat. Immunol*.; 6: 314-322

91. Dunn G.A. and Brown A.F. (1986). Alignment of fibroblasts on grooved surfaces described by a simple geometric transformation. *J. Cell Sci*.; 83: 313-340

92. Dunn G.A. and Brown A.F. (1987). A unified approach to analysing cell motility. *J. Cell Sci. Suppl.*; 8: 81-102

93. Durand C., Robin C., Bollerot K., Baron M.H., Ottersbach K., Dzierzak E. (2007). Embryonic stromal clones reveal developmental regulators of definitive hematopoietic stem cells. *P.N.A.S.*; 104: 20838-20843

94. Dzierzak E., Medvinsky A., Bruijn de M. (2009). Qualitative and quantitative aspects of haematopoietic cell development in the mammalian embryo. *Drug Discovery Today: Theraputic Strategies*. Article in Press doi:10.1016/j.ddstr.2009.06.003

95. Emerson G.S. and Zhu J. (2004). A new bone to pick: osteoblasts and the haematopoietic stem-cell niche. *BioEssays*; 26: 595-599

96. Engler A.J., Griffin M.A., Sen S., Bonnemann C.G., Sweeney H.L., Discher D.E. (2004). Myotubes differentiate optimally on substrates with tissue-like stiffness: pathological implications for soft or stiff microenvironments. *J. Cell Biol.*; 166: 877-887

97. Engler A.J., Sen S., Sweeney H.L., Discher D.E., (2006). Matrix elasticity directs stem cell lineage specification. *Cell*; 126: 677-689

98. Eshghi S. and Schaffer D. (2008). Engineering microenvironments to control stem cell fate and function. Stembook, doi/10.3824/stembook, http://www.stembook.org

99. Estes B.T, Gimble J.M., Guilak F. (2004). Mechanical signals as regulators of stem cell fate. *Curr. Topics Dev. Biol.*; 60: 91-126

100. Ezekiel U.R. (2007). Single embryoid body formation in a multiwell plate. *Electron J. Biotechnol.*; 10: 328-335

101. Falascaa L., Micchelib A., Sartorib E., Tomassinib A., Devirgiliisc L.C. (2001). Hepatocytes entrapped in alginate gel beads and cultured in bioreactor: rapid repolarization and reconstitution of adhesion areas. *Cells Tiss. Org.*; 168: 126-136

102. Falconnet D., Csucs G., Grandin H.M., Textor M. (2006). Surface engineering approaches to micropattern surfaces for cell-based assays. *Biomaterials*; 27 (16): 3044-3063

103. Fernandes A.M., Fernandes T.G., Diogo M.M., da Silva C.L., Henrique D., Cabral J.M. (2007). Mouse embryonic stem cell expansion in a microcarrier-based stirred culture system. *J. Biotechnol.*; 132: 227-236

104. Ferrari G., Cusella-De Angelis G., Coletta M., Paolucci E., Stornaiuolo A., Cossu G., Mavilio F. (1998). Muscle regeneration by bone marrow-derived myogenic progenitors. *Science*; 279: 1528-1530

105. Flanagan L.A., Lu J., Wang L., Marchenko S.A., Jeon N.L., Lee A.P., Monuki E.S. (2008). Unique dielectric properties distinguish stem cells and their differentiated progeny. *Stem Cells*; 26(3): 656-665

106. Fliedner T.M., Graessle D., Paulsen C., Reimers K. (2002). Structure and function of bone marrow hemopoiesis: mechanisms of response to ionizing radiation exposure. *Cancer Biother. Radiopharm.*; 17: 405-426

107. Flores-Rodriguez N. and Markx G.H. (2004). Improved levitation and trapping of particles by negative dielectrophoresis by the addition of amphoteric molecules. *J. Phys. D.: Appl. Phys.*; 37: 353-361

108. Foty R.A., Pfleger C.M., Forgacs G., Steinberg M.S. (1996). Surface tensions of embryonic tissues predict their mutual envelopment behavior. *Development*; 122: 1611-1620

109. Foty R.A. and Steinberg M.S. (2004). Cadherin-mediated cell–cell adhesion and tissue segregation in relation to malignancy. *Int. J. Dev. Biol.*; 48: 397-409

110. Franze K., Gerdelmann J., Weick M., Betz T., Pawlizak S., Lakadamyali M., Bayer J., Rillich K., Gogler M., Lu Y-B., Reichenbach A., Janmey P., Kas J. (2009). Neurite branch retraction is caused by a threshold-dependent mechanical impact. *Biophys. J.*; 97: 1883-1890

111. Fuchs E. and Green H. (1981). Regulation of terminal differentiation of cultured human keratinocytes by vitamin A. *Cell*; 25: 617-625

112. Fuchs J.R., Nasseri B.A., Vacanti J.P. (2001). Tissue engineering: A 21st century solution to surgical reconstruction. *Ann. Thorac. Surg.*; 72: 577-591

113. Fuchs E. and Serge J.A. (2000). Stem cells: A new lease on life. *Cell*; 100: 143-155

114. Fuchs E., Tumbar T., Guasch G. (2004). Socializing with the neighbours: stem cells and their niche. *Cell*; 116: 769-778

115. Fuhr G. and P. Kuzmin. (1986). Behavior of cells in rotating electric fields with account to surface charges and cell structures. *Biophys. J.*; 50: 789-795

116. Fukuda K. (2002). Molecular characterization of regenerated cardiomyocytes derived from adult mesenchymal stem cells. *Congenit. Anomal*.; 42(1): 1-9

117. Furuse M., Hata M., Furuse K., Yoshida Y., Haratake A., Suigitani Y., Noda T., Kubo A.,Tsukita S. (2002). Claudin-based tight junctions are crucial for the mammalian epidermal barrier: a lesson from claudin-1-deficient mice. *J. Cell Biol*.; 156(6): 1099-1111

118. Garces-Chavez V., Dholakia K., Spalding G.C. (2005). Extended-area optically induced organization of microparticles on a surface. *Appl. Phys. Lett*.; 86: 031106, doi:10.1063/1.1843283

119. Geho D.H., Bandle R.W., Clair T., Liotta L.A. (2005). Physiological Mechanisms of Tumor-Cell Invasion and Migration. *Physiology*; 20(3): 194-200

120. Gekas C., Rhodes K.E., Van Handel B., Chhabra A., Ueno M., Mikkola H.K.A. (2010). Hematopoietic stem cell development in the placenta. *Int. J. Dev. Biol*.; 54: 1089-1098

121. Gerisch A. and Painter K.J. (2010). Mathematical modelling of cell adhesion and its applications to developmental biology and cancer invasion. *In: Cell mechanics: from single scale-based models to multiscale modeling*. A. Chauviere and L. Preziosi. Chapter 12: 319-350

122. Ghazizadeh S. and Taichman L.B. (2001). Multiple classes of stem cells in cutaneous epithelium: a lineage analysis of adult mouse skin. *EMBO J.*; 20: 1215-1222

123. Gherardini L., Cousins C.M., Hawkes J.J., Spengler J., Radel S., Lawler H., Devcic-kuhar B., Gröschl M., Coakley W.T., Mcloughlin A.J. (2005). A new immobilisation method to arrange particles in a gel matrix by ultrasound standing waves. *Ultrasound Med. Biol.*; 31: 261-272

124. Gimsa J., Schnelle T., Zechel G., Glaser R. (1993). Dielectric spectroscopy of human erythrocytes: investigations under the influence of nystatin. *Biophys. J.*; 66: 1244-1253

125. Gimsa J. (2001). A comprehensive approach to electro-orientation, electrodeformation, dielectrophoresis, and electrorotation of ellipsoidal particles and biological cells. *Bioelectrochem.*; 54(1): 23-31

126. Glucksmann A. (1942). The role of mechanical stresses in bone formation in vitro. *J. Anat*.; 76; 231-239

127. Gothard D., Roberts S.J., Shakesheff K.M., Butery L.D. (2009). Controlled embryoid body formation via surface modification and avidin-biotin cross-linking. *Cytechnology*; 61: 135-144

128. Goater A.D., Burt J.P.H., Pethig R. (1997). A combined electrorotation and travelling wave device: applied to the concentration and viability of Cryptosporidium. *J. Phys. D: App. Phys.*; 33: L65-L70

129. Gomes I., Sharma T.T., Edassery S., Fulton N., Mar B.G., Westbrook C.A. (2002). Novel transcription factors in human CD34 antigen-positive hematopoietic cells. *Blood*; 100: 107-119

130. Gonzales A., Ramos A., Green N.G., Castellanos A., Morgan H. (2000). Fluid flow induced by nonuniform AC fields in electrolytes on microlectrodes. II. A linear double-layer analysis. *Phys. Rev. E.*; 61: 4019-4028

131. Garces-Chavez V., Dholakia K., Spalding G.C. (2005). Extended-area optically induced organization of microparticles on a surface. *Appl. Phys. Lett*.; 86: 031106, doi:10.1063/1.1843283

132. Gray S.D., Tan J.L., Voldman J., Chen C.S., (2004). Dielectrophoretic registration of living cells to a microelectrode array. *J. Biosens. Bioelectron*.; 19: 771-780

133. Green N.G., Ramos A., Gonzales A., Morgan H., and Castellanos A. (2002). Fluid flow induced by nonuniform AC electric fields in electrolytes on microelectrodes. III. Observation of streamlines and numerical simulation. *Phys. Rev. E.*; 66: 026305-1-11

134. Grier D.G. (2003). A revolution in optical manipulation. *Nature*; 424: 810-816

135. Grieve J.A., Ulcinas A., Subramanian S., Gibson G.M., Padgett M.J., Carberry M., Miles M.J. (2009). Hands-on with optical tweezers: a multitouch interface for holographic optical trapping. *Opt. Exp.*; 17(5): 3595-3602

136. Griffith L.G., Swartz M.A. (2006). Capturing complex 3D tissue physiology in vitro. *Nat. Rev. Mol. Cell Biol.*; 7(3): 211-24

137. Groschl M., Burger W., Handl B., Doblhoff-dier O., Gaida T., Schmatz C. (1998). Ultrasonic separation of suspended particles. Part I: Fundamentals. *Acustica*; 84(3): 432-447

138. Gu G., Wells J.M., Dombkowski D., Preffer F., Aronow B., Melton D.A. (2004). Global expression analysis of gene regulatory pathways during endocrine pancreatic development. *Development*; 131: 165-179

139. Haake A. and Dual J. (2002). Micro-manipulation of small particles is node position control of an ultrasonic standing wave. *Ultrasonics*; 40: 317-322

140. Haake A. and Dual J. (2004). Positioning of small particles by an ultrasound field excited by surface waves. *Ultrasonics*; 42: 75-80

141. Haake A., Neild A., Kin D.H., Ihm J.E., Sun Y., Dual J., Ju B-K. (2005). Manipulation of cells using an ultrasonic pressure field. *Ultrasound Med. Biol.*; 31: 857-864

142. Hagedorn R., Fuhr G., Müller T., Gimsa J. (1992). Traveling-wave dielectrophoresis of microparticles. *Electrophoresis*; 13(1-2): 49-54

143. Halliday N.L. and Tomasek J.J. (1995). Mechanical properties of the extracellular matrix influence fibronectin fibril assembly in vitro. *Exp. Cell Res.*; 217: 109-117

144. Haibo L. and Bashir R. (2002). Dielectrophoretic separation and manipulation of live and heat-treated cells of Listeria on microfabricated devices with interdigitated electrodes. *Sens. Act. B: Chem.*; 86(2-3): 215-221

145. Harris A.K., Stopak D., Wild P. (1981). Fibroblast traction as a mechanism for morphogenesis. *Nature*; 290: 249-251

146. Hardy M.H. (1992). The secret life of the hair follicle. *Trends Genet.*;8: 55-61

147. Hamazaki T., Oka M., Yamanaka S., Terada N. (2004). Aggregation of embryonic stem cells induces Nanog repression and primitive endoderm differentiation. *J. Cell Sci.*; 117: 5681-5686

148. Harvey K. and Dzierzak E. (2004). Cell-cell contact and anatomical compatibility in stromal cell-mediated HSC support during development. *Stem Cells*; 22: 253-258

149. Hebrok M., Kim S.K., Melton D.A. (1998). Notochord repression of endodermal Sonic hedgehog permits pancreas development. *Genes Dev*.; 12: 1705-1713

150. Hill N.A. and Hader D.-P. (1997). A biased random walk model for the trajectories of swimming micro-organisms. *J. Theor. Biol*.; 186: 503-526

151. Hitoshi S. Alexson T., Tropepe V., Donoviel D., Elia A.J., Nye J.S., Conlon R.A., Mak T.W., Bernstein A., Van der Kooy D. (2002). Notch pathway molecules are essential for the maintenance, but not the generation, of mammalian neural stem cells. *Genes Dev*.; 16 (7): 846-858

152. Hoettges K.F, McDonnell M.B., Cotton A., Hopkins N.A.E., Hughes M.P. (2003). Optimizing particle collection for enhanced surface-based biosensors. *IEEE Eng. Med. Biol. Mag.*; 22(6): 0739-5175

153. Honda H., Shinkai M., Kubo T., Matsuoka F., Sugita T., Kobayashi T. (2004). Hyperthermia using magnetite cationic liposomes for hamster osteosarcoma. *Biomag. Res. Technol.*; 2: 1-6

154. Holzel R. (1997). Electrorotation of single yeast cells at frequencies between 100 Hz and 1.6 GHz. *Biophys. J.*; 73(2): 1103-1109

155. Hove J.R., Koster R.W., Forouhar A.S., Bolton G.A., Fraser S.E., Gharib M. (2003). Intracardiac fluid forces are an essential epigenetic factor for embryonic cardiogenesis. *Nature*; 421: 172-177

156. Hronik-Tupaj M., Rice W.L., Cronin-Golomb M., David L., Kaplan D.L., Georgakoudi I. (2011). Osteoblastic differentiation and stress response of human mesenchymal stem cells exposed to alternating current electric fields. *BioMed. Eng. OnLine*; 10(1): 1-9

157. Huang G.Y., Cooper E.S., Waldo K., Kirby M.L., Gilula N.B., Lo C.W. (1998). Gap junction–mediated cell–cell communication modulates mouse neural crest migration. *J. Cell Biol*.; 143: 1725-1734

158. Huang S., Chen C.S., Ingber D.E. (1998). Control of cyclin D1, p27 (Kip1), and cell cycle progression in human capillary endothelial cells by cell shape and cytoskeletal tension. *Mol. Biol. Cell*.; 9(11): 3179-3193

159. Huelsken J. and Behrens J. (2002). The Wnt signalling pathway. *J. Cell Sci.*; 115: 3977-3978

160. Hughes M.P. (2002). Strategies for dielectrophoretic separation in laboratory-on-a chip systems. *Electrophoresis*; 23: 2569-2582

161. Hughes M.P. (2003). *Nanoelectromechanics in Engineering and Biology*. Boca Raton, Florida. CRC press: pp 322

162. Hwang Y.S., Cho J., Tay F., Heng J.Y., Ho R., Kazarian S.G., Williams D.R., Boccaccini A.R., Polak J.M., Mantalaris A. (2009). The use of murine embryonic stem cells, alginate encapsulation, and rotary microgravity bioreactor in bone tissue engineering. *Biomaterials*; 30: 499-507

163. Hwang Y-S., Chung B.G., Ortmann D., Hattori N., Moeller H-C., Khademhosseini A. (2009). Microwell-mediated control of embryoid body size regulates embryonic stem cell fate via differential expression of WNT5a and WNT11. *PNAS.*; 106(40): 16978-16983

164. Ingber D.E. and Tensegrity I. (2003). Cell structure and hierarchical systems biology. *J. Cell Sci*.; 116: 1157-1173

165. Ino K., Ito A., Honda H. (2007). Cell micropatterning using magnetite nanoparticles and magnetic force. *Biotechnol. Bioeng.*; 97: 1309-1317

166. Ito T., Suzuki A., Okabe M., Imai E., Hori M. (2001). Application of bone marrow-derived stem cells in experimental nephrology. *Exp. Nephrol.*; 9: 444-450

167. Ito A., Hayashida M., Honda H., Hata K-I., Kagami H., Ueda M., Kayashi T. (2004). Harvest of multilayered keratinocyte sheets using magnetite nanoparticles and magnetic force. *Tiss. Eng.*; 10: 873-880

168. Itskovitz-Eldor J., Schuldiner M., Karsenti D., Eden A., Yanuka O., Amit M., Soreq H., Benvenisty N. (2000). Differentiation of human embryonic stem cells into embryoid bodies compromising the three embryonic germ layers. *Mol. Med.*; 6: 88-95

169. Ivanova N.B., Dimos J.T., Schaniel C., Hackney J.A., Moore K.A., Lemischka I.R. (2002). A stem cell molecular signature. *Science*; 298: 601-604

170. Javier L. Prieto J.L., Nourse J., Lu J., Flanagan L., Lee A.P. (2010). Dielectrophoretic separation of heterogenous stem cell populations. 890-892, 978-0-9798064-3-8/μTAS 2010/$20©2010 CBMS

171. Jacques S.L. and McAuliffe D.J. (1991). The melanosome: threshold temperature for explosive vaporization and internal absorption coefficient during pulsed laser irradiation. *Photochem. Photobiol*.; 53(6): 769-775

172. Jessell T.M. (2000). Neuronal specification in the spinal cord: Inductive signals and transcriptional codes. *Nat. Rev. Genet*.; 1: 20-29

173. Jahns M., Lou E., Durdle N., Bagnall K., Raso J., Cinats D., Barley R., Cinats J., Jomha N. (2007). The effect of pulsed electromagnetic fields on chondrocyte morphology. *Med. Biol. Eng. Comp*.; 45: 917-925

174. Jiang Z. and Emerson S.G. (2004). A new bone to pick: osteoblasts and the haematopoietic stem-cell niche. *BioEssays*.; 26(6): 595-599

175. Jones D.L. and Wagers A.J. (2008). No place like home: Anatomy and function of the stem cell niche. *Nat. Rev. Mol. Cell Biol*.; 9: 11-21

176. Kacahr B., Parakkal P., Fex J. (1990). Structural basis for mechanical transduction on the frog sensory apparatus*:* I. The otolithic membrane. *Heart Res*.; 45: 179-190

177. Kaplan R.S., Psaila B., Lyden D. (2007). Niche-to-niche migration of bone-marrow-derived cells. *Trends Mol. Med*.; 13: 72-81

178. Karp J.M., Yeh J., Eng G., Fukuda J., Blumling J., Suh K. Y., Cheng J., Mahdavi A., Borenstein J., Langer R., Khademhosseini A. (2007). Controlling size, shape and homogeneity of embryoid bodies using poly (ethylene glycol) microwells. *Lab Chip*; 7: 786-794

179. Kehoe D.E., Lock L.T., Parikh A., Tzanakakis E.S. (2008). Propagation of embryonic stem cells in stirred suspension without serum. *Biotechnol. Prog*.; 24: 1342-1352

180. Kehoe D.E., Jing D., Lock L.T., Tzanakakis E.M. (2009). Scalable stirred-suspension bioreactor culture of human pluripotent stem cells. *Tissue Eng. Part A*; 16(2): 405-421

181. Keller G., Kennedy M., Papayannopoulou T. and Wiles M.V. (1993). Hematopoietic commitment during embryonic stem cell differentiation in culture. *Mol. Cell. Biol*.; 13: 473-486

182. Kelm J.M. and Fussenegger M. (2004). Microscale tissue engineering using gravity-enforced cell assembly. *Trends Biotechnol*.; 22: 195-202

183. Khademhosseini A., Ferreira L., Blumling J., Yeh J., Karp J.M., Fukuda J., Langer R. (2006). Co-culture of human embryonic stem cells with murine embryonic fibroblasts on microwell-patterned substrates. *Biomaterials*; 27: 5968-5977

184. Khademhosseini A., Langer R., Borenstein J., Vacanti J.P. (2006). Microscale technologies for tissue engineering and biology. *P.N.A.S.*; 103: 2480-2487

185. Kiger A.A. and Fuller M.T. (2001). Male germ-line stem cells. *Stem Cell Biol*.; 149-187

186. Kiel M.J., Yilmaz O.H., Iwashita T., Terhorst C., Morrison S.J. (2005). SLAM family receptors distinguish hematopoietic stem and progenitor cells and reveal endothelial niches for stem cells. *Cell*; 121: 1109-1121

187. Kim S.K., Hebrok M., Melton D.A. (1997a). Notochord to endoderm signaling is required for pancreas development. *Development*; 124: 4243-4252

188. Kim K.Y., Kovacs M., Kawamoto S., Sellers J.R., Adelstein R.S. (2005). Disease-associated mutations and alternative splicing alter the enzymatic and motile activity of nonmuscle myosins II-B and II-C. *J. Biol. Chem*.; 280: 22769-22775

189. Kim I., Song J., Song Y., Cho T., Lee T., Lim S., Kim S., Hwang S. (2009). Novel effect of biphasic electric current on in vitro osteogenesis and cytokine production in human mesenchymal stem cells. *Tissue Eng. Part A*; 15: 2411-2422

190. Knapp D.M., Tower T.T., Tranquillo R.T., Barocas V.H. (2000). Estimation of cell traction and migration in an isometric cell traction assay. *AIChE J.*; 45(12): 2628-2640

191. Ko K.S., Arora P.D., McCulloch C.A. (2001). Cadherins mediate intercellular mechanical signaling in fibroblasts by activation of stretch-sensitive calcium-permeable channels. *J. Biol. Chem*.; 276: 35967-35977

192. Kobayashia N., Yasuc T., Uebaa H., Satad M., Hashimotoc S., Kurokia M., Saitoc M., Kawakamia M. (2004). Mechanical stress promotes the expression of smooth muscle-like properties in marrow stromal cells. *Exp. Hematol*.; 32: 1238-1245

193. Koide N., Shinji T., Tanabe T., Asano K., Kawaguchi M., Sakaguchi M., Koide Y., Mori M., Tsuji T. (1989). Continued high albumin production by multicellular spheroids of adult rat hepatocytes formed in the presence of liver-derived proteoglycans. *Biochem. Biophys. Res. Commu.*; 161(1): 385-391

194. Koike M., Kurosawa H., Amano Y. (2005). A round-bottom 96-well polystyrene plate coated with 2-methacryloyloxyethyl phosphorylcholine as an effective tool for embryoid body formation. *Cytotechnology*; 47: 3-10

195. Koike M., Sakaki S., Amano Y., Kurosawa H. (2007). Characterization of embryoid bodies of mouse embryonic stem cells formed under various culture conditions and estimat ion of differentiation status of such bodies. *J. Biosci. Bioeng*.; 104: 294-299

196. Konberg L., Earp H.S., Parsons J.T., Schaller M., Juliano R.L. (1992). Cell adhesion or integrin clustering increases phosphorylation of a focal adhesion-associated tyrosine kinase. *J .Biol. Chem*.; 267: 23439-23442

197. Kondo T. and Raff M. (2000). Oligodendrocyte precursor cells reprogrammed to become multipotential CNS stem cells. *Science*; 289: 1754-1757

198. Konno T., Akita K., Kurita K., Ito Y. (2005). Formation of embryoid bodies by mouse embryonic stem cells on plastic surfaces. *J. Biosci. Bioeng*.; 100: 88-93

199. Konuma N. and Wakabayashi K. (2008). Mouse embryonic stem cells give rise to gut like morphogenesis including intestinal stem cells in the embryoid body model. *Stem Cells Dev.*; 18(1): 113-126

200. Kopen G.C., Prockop D.J., Phinney D.G. (1999). Marrow stromal cells migrate throughout forebrain and cerebellum, and they differentiate into astrocytes after injection into neonatal mouse brains. *P.N.A.S.*; 96: 10711-10716

201. Kopp H.G., Avecilla S.T., Hooper A.T., Rafii S. (2005). The bone marrow vascular niche: home of HSC differentiation and mobilization. *Physiology.*; 20: 349-356

202. Korineck V., Barker N., Morin P.J., Van Wichen D., De Weger R., Kinzler K.W., Vogelstein B., Clevers H. (1997). Constitutive transcriptional activation by a beta-catenin-tef complex in APC colon carcinoma. *Science*; 275: 1784-1787

203. Kramer J.; Hegert C.; Guan K.; Wobus A.M.; Mueller P.K., Rohwedel J. (2000). Embryonic stem cell-derived chondrogenic differentiation in vitro: activation by BMP-2 and BMP-4. *Mech. Dev.*; 92(2): 193-205

204. Kramer J., Hegert C., Rohwedel J. (2003). In vitro differentiation of mouse ES cells: Bone and cartilage. *Meth. Enzym.*; 365: 251-268

205. Kramer J., Hegert C., Hargus G., Rohwedel J. (2005a). Mouse ES cell lines show a variable degree of chondrogenic differentiation in vitro. *Cell Biol. Int.*; 29(2): 139-146

206. Kramer J., Klinger M., Kruse C., Faza M., Hargus G., Rohwedel J. (2005b). Ultrastructural analysis of mouse embryonic stem cell-derived chondrocytes. *Anat. Embryol.*; 210(3): 175-185

207. Krassowska A., Gordon-Keylock S., Samuel K., Gilchrist D., Dzierzak E., Oostendorp R., Forrester L.M., Ansell J.D. (2006). Promotion of haematopoietic activity in embryonic stem cells by the aorta–gonad–mesonephros microenvironment. *Exp. Cell Res.*; 312: 3595-3603

208. Krause D.S. (2002). Regulation of hematopoietic stem cell fate. *Oncogene*; 21: 3262-3269

209. Kulesa P.M. and Fraser S.E. (1998). Neural crest cell dynamics revealed by time-lapse video microscopy of whole embryo chick explant cultures. *Dev. Biol.*; 204(2): 327-344

210. Kulesa P.M. and Fraser S.E. (1998). Cell dynamics during somite boundary formation revealed by time-lapse analysis. *Science*; 298: 991-995

211. Kursad T. (2006). Embryonic stem cell protocols. *Methods Mol. Biol*., 330(2): 48-49

212. Kyba M. and Daley G.Q. (2003). Hematopoiesis from embryonic stem cells: Lessons from and for ontogeny. *Exp. Hemat.*; 31: 994-1006

213. Lackie J.M. (1986). *Cell Movement and Cell Behaviour*. London: Allen & Unwin

214. Lagasse E., Connors H., Al-Dhalimy M., Reitsma M., Dohse M., Osborne L., Wang X., Finegold M., Weissman I.L., Grompe M. (2000). Purified hematopoietic stem cells can differentiate into hepatocytes in vivo. *Nature Med.*; 6:1229-1234

215. Lammert E., Cleaver O., Melton D. (2001). Induction of pancreatic differentiation by signals from blood vessels. *Science*; 294: 564-567

216. Langer R., Khademhosseini A., Yeh J., Eng G., Karp J., Kaji H., Borenstein J., Farokhzad O.C. (2005). Cell docking inside microwells within reversibly sealed microfluidic channels for fabricating multiphenotype cell arrays. *Lab Chip*; 5: 1380-1386

217. Lavrik N.V., Sepaniak M.J., Datskos P.G. (2004). Cantilever transducers as a platform for chemical and biological sensors. *Rev. Sci. Instrum.*, 75(7): 2229-2253

218. Leahy A., Xiong J.W., Kuhnert F., Stuhlmann H. (1999). Use of developmental marker genes to define temporal and spatial patterns of differentiation during embryoid body formation. *J. Exp. Zool*.; 284: 67-81

219. Ledran M.H., Krassowska A, Armstrong L., Dimmick I., Renstro J., Lang R., Yung S., Santibanez-Coref M., Dzierzak E., Stojkovic M., Ostendorp R.A.J., Forrester L., Lako M. (2008). Efficient hematopoietic differentiation of human embryonic stem cells derived from hematopoietic niches. *Cell Stem Cell*; 3: 85-98

220. Lee J., Ishihara A., Oxford G., Johnson B., Jacobson K. (1999). Regulation of cell movement is mediated by stretch-activated calcium channels. *Nature*; 400: 382-386

221. Levenberg S., Huang N.F., Lavik E., Rogers A.B., Itskovitz- Eldor J., Langer R. (2003). Differentiation of human embryonic stem cells on three-dimensional polymer scaffolds. *P.N.A.S.*; 100: 12741-12746

222. Levin M. (2003). Bioelectromagnetics in morphogenesis. *Bioelectromagnetics*; 24(5): 295-315

223. Levin M. and Oviedo N.J. (2007). Smedinx-11 is a planarian stem cell gap junction gene required for regeneration and homeostasis. *Development*; 134: 3121-3131

224. Li M., Tang H.X., Roukes M.L. (2007). Ultra-sensitive NEMS-based cantilevers for sensing, scanned probe and very high-frequency applications. *Nature Nanotechnol*.; 2(2): 114-120

225. Li W., Johnson S.A., Shelley W.C., Yoder M.C. (2004). Hematopoietic stem cell repopulating ability can be maintained in vitro by some primary endothelial cells. *Exp. Hematol*.; 32: 1226-1237

226. Li Y.J., Chung E.H., Rodriguez, R.T., Firpo M.T., Healy K.E. (2006). Hydrogels as artificial matrices for human embryonic stem cell self-renewal. *J. Biomed. Mater. Res. A.*; 79: 1-5

227. Li X.J., Du Z.W., Zarnowska E.D., Pankratz M., Hansen L.O., Pearce R.A., Zhang S.C. (2005). Specification of motoneurons from human embryonic stem cells. *Nat. Biotechnol*.; 23: 215-22

228. Lian M., Islam N., Wu J. (2006). Particle line assembly/patterning by microfluidic AC electroosmosis. *J. Phys.: Confer. Ser.*; 34: 589-594

229. Lieschke G.J. and Dunn A.R. (1995). Development of functional macrophages from embryonal stem cells in vitro. *Experimental Hematol*.; 23: 328-334

230. Lin R-Z., Ho C-T., Liu C-H., Chang H-Y. (2006). Dielectrophoresis based-cell patterning for tissue engineering. *Biotechnol. J.*; 1: 949-957

231. Liu M. and Post M. (2000). Invited review: mechanochemical signal transduction in the fetal lung. *J. Appl. Physiol*.; 89: 2078-2084

232. Liu C.Y., Apuzzo M.L.J., Tirrell D.A. (2003). Engineering of the extracellular matrix: working toward neural stem cell programming and neurorestoration- concept and progress report. *Neurosurgery*; 52(5): 1154-1167

233. Lo C.M., Wang H.B., Dembo M., Wang Y.L. (2000). Cell movement is guided by the rigidity of the substrate. *Biophys. J.*; 79: 144-152

234. Lois C. and Alverez – B.A. (1994). Long distance neuronal migration in the adult mammalian brain. *Science*; 264: 1145-1148

235. Lord B.I, Testa N.G., Hendry J.H. (1975). The relative spatial distributions of CFUs and CFUc in the normal mouse femur. *Blood*; 46: 65-72

236. Lorich D., Brighton C., Gupta R., Corsetti J., Levine S., Gelb I., Seldes R., Pollack S. (1998). Biochemical pathway mediating the response of bone cells to capacitive coupling. *Clin. Orth. Rel. Res.*; 350: 246-256

237. Lund A.W., Yener B., Stegemann J.P., Plopper G.E. (2009).The natural and engineered 3D microenvironment as a regulatory cue during stem cell fate determination. *Tiss. Eng. Part B Rev*.; 15(3): 371-380

238. Luzzi K.J., Macdonald I.C., Schmidt E.E., Kerkvliet N., Morris V.L., Chambers A.F., Groom A.C. (1998). Multistep nature of metastatic inefficiency: Dormancy of solitary cells after successful extravasation and limited survival of early micrometastases. *Am. J. Pathol*.; 153: 865-873

239. Maeno M., Mead P.E., Kelley C., Xu R.H., Kung H.F, Suzuki A., Ueno N., and Zon L.I. (1996). The role of BMP-4 and GATA-2 in the induction and differentiation of hematopoietic mesoderm in *Xenopus laevis*. *Blood*; 88: 1965-1972

240. Maguire T., Novik E., Schloss R., Yarmush M. (2006). Alginate-PLL microencapsulation: effect on the differentiation of embryonic stem cells into hepatocytes. *Biotechnol. Bioeng.*; 93: 581-591

241. Magyar J.P., Nemir M., Ehler E., Suter N., Perriard J.C., Eppenberger H.M. (2001). Mass production of embryoid bodies in microbeads. *Ann. N. Y. Acad. Sci.*; 944: 135-143

242. Makino S., Fukuda K., Miyoshi S., Konishi F., Kodama H., Pan J., Sano M., Takahashi T., Hori S., Abe H., Hata J., Umezawa A., Ogawa S. (1999). Cardiomyocytes can be generated from marrow stromal cells in vitro. *J. Clin. Invest.*; 103: 697-705

243. Markx G.H., Alp B., McGilchrist A. (1992). Electro-orientation of Schizosaccharomyces pombe in high conductivity media. *J. Microbiol. Meth.*; 50(1): 55-62

244. Markx G.H., Huang Y., Zhou X.F., Pethig R. (1994a). Dielectrophoretic characterisation and separation of micro-organisms. *Microbiol.*; 140: 585-591

245. Markx G.H, Talary M.S., Pethig R. (1994b). Separation of viable and non viable yeast using dielectrophoresis. *J. Biotechnol*.; 32: 29-37

246. Markx G.H. and Davey C.L. (1999). The dielectric properties of biological cells at radiofrequencies: applications in biotechnology. *Enzyme Microb. Technol.*; 25(3-5): 161-171

247. Markx G.H., Alp Andrews A.S., Mason V.P., Thompson I.P., Wolowacz R. (2003). Building structured biomaterials using ac electrokinetics. *IEE Eng. Med. Biol. Mag.*; 6: 91-97

248. Markx G.H., Andrews J.S., Mason V.P. (2004). Towards microbial tissue engineering? *Trends Biotechnol*.; 22: 417-422

249. Markx G.H. and Buckle A.M. (2005). Tissue engineering: AC electrokinetics. In: Wnek G, Bowlin G, editors. *Encyclopedia of Biomaterials and Biomedical Engineering.* New York: Taylor and Francis. DOI: 10.1081/E-EBBE-120041779

250. Markx G.H. (2008). The use of electric fields in tissue engineering. *Organogenesis*; 4: 11-17

251. Markx G.H., Carney L., Littlefair M., Sebastian A., Buckle A-M. (2009). Recreating the hematon: microfabrication of artificial haematopoietic stem cell microniches in vitro using dielectrophoresis. *Biomed. Microdev.*; 11(1): 143-150

252. Masato A., Tomoyuki Y., Hitoshi S., Tomokazu M. (2010). Negative dielectrophoretic patterning with different cell types. *Ann. Biomed. Eng.*; 38(12): 3777-3788

253. Matsue T., Matsumoto N., Uchida I. (1997). Rapid micrpatterning of living cells by repulsive dielectrophoretic force. *Electrochim. Acta*.; 42: 3251-3256

254. Maye P., Becker S., Kasameyer E., Byrd N., Grabel L. (2000). Indian hedgehog signaling in extraembryonic endoderm and ectoderm differentiation in ES embryoid bodies. *Mech. Dev.*; 94(1–2): 117-32

255. Metallo C.M., Mohr J.C., Detzel C.J., Pablo J.J.de. (2007). Engineering the stem cell microenvironment. *Biotech. Prog.*; 23: 18-23

256. Meyvantsson I. and Beebe D.J. (2008). Cell culture models in microfluidic systems. *Annu. Rev. Anal. Chem.*; 1: 423-449

257. Mikkelsen C.I. (2005). Magnetic separation and hydrodynamic interactions in microfluidic systems. *J. Mag. Mag. Mat.*; 293: 578-583

258. Mikkola H.K. and Orkin S.H. (2006). The journey of developing hematopoietic stem cells. *Dev.*; 133: 3733-3744

259. Miller R.D. and Jones T.B. (1993). Electro-orientation of ellipsoidal erythrocytes. *Biophys. J.*; 64: 1588-1595

260. Mironov V., Boland T., Trusk T., Forgacs G., Markwald R.R. (2003). Organ printing: computer-aided jet-based 3D tissue engineering. *Trends Biotechnol.*; 21: 157-161

261. Mironov V., Visconti R.P., Kasyanov V., Forgacs G., Drake C.J., Markwald R.R. (2009). Organ printing: Tissue spheroids as building blocks. *Biomat.*; 30: 2164-2174

262. Misteli T., Ca´ceres J.F., Spector D.L. (1997). The dynamics of a pre-mRNA splicing factor in living cells. *Nature*; 387: 523-527

263. Mitalipov S. and Wolf D. (2009). Totipotency, pluripotency and nuclear reprogramming. *Adv. Biochem. Eng. Biotechnol*.; 114: 185-99

264. Mittal N., Rosenthal A., Voldman J. (2007). nDEP microwells for single-cell patterning in physiological media. *Lab Chip*; 7(9): 1146-115

265. Miyazaki T., Futaki S., Hasegawa K., Kawasaki M., Sanzen N., Hayashi M., Kawase E., Sekiguchi K., Nakatsuji N., Suemori H. (2008). Recombinant human laminin isoforms can support the undifferentiated growth of human embryonic stem cells. *Biochem. Biophys. Res. Commun*.; 175(1): 27-32

266. Mohr J.C., de Pablo J.J., Palecek S.P. (2006). 3-D microwell culture of human embryonic stem cells. *Biomat.*; 27: 6032-6042

267. Morgan H., Green N.G., Hughes M.P., Monaghan W., Tan T.C. (1997). Large-area travelling-wave dielectrophoresis particle separator. *J. Micromech. Microeng.*; 7(2): 65

268. Morgan H. and Green N.G. (2003). *AC electrokinetics: colloids and nanoparticles*. Herts: Research Studies Press

269. Monat C., Domachuk P., Grillet C., Collins M., Eggleton B.J., Cronin-Golomb M., Mutzenich S., Mahmud T., Rosengarten G., Mitchell A. (2008). Optofluidics: a novel generation of reconfigurable and adaptive compact architectures. *Microfluid. Nanofluid*.; 4: 81-95

270. Morales P.-D. M., Grabulosa M., Alcaraz J., Mullol J., Maksym G.N., Fredberg J.J., Navajas D. (2001). Measurement of cell microrheology by magnetic twisting cytometry with frequency domain demodulation. *J. Appl. Physiol*.; 91: 1152-1159

271. Morrison S.J., Shah N.M., Anderson D.J. (1997). Regulatory mechanisms in stem cell biology. *Cell*; 88: 287-298

272. Munoz-Sanjuan I. and Brivanlou A.H. (2002). Neural induction, the default model and embryonic stem cells. *Nat. Rev. Neurosci.*; 3: 271-280

273. Murray E., Provvedini D., Curran D., Catherwood B., Sussman H., Manolagas S. (1987). Characterization of a human osteoblastic osteosarcoma cell line (SAOS-2) with high bone alkaline phosphatase activity. *J. Bone Mineral Res.*; 2(3): 231-238

274. Mylona E. (2008). Cancer cell migration: substrate mechanics and intracellular mechanisms. *Proceedings of the American Society of Cell Biology Annual Meeting*

275. MacDonald M.P., Spalding G.C., Dholakia K. (2003). Microfluidic sorting in an optical lattice. *Nature*; 426: 421-424

276. McBeath R., Pirone D.M., Nelson C.M., Bhadriraju K., Chen C.S. (2004). Cell shape, cytoskeletal tension, and RhoA regulate stem cell lineage commitment. *Dev. Cell*.; 6(4): 483-95

277. McCarthy K.F. (2003). Marrow frequency of rat long-term repopulating cells: evidence that marrow hematopoietic stem cell concentration may be inversely proportional to species body weight. *Blood*; 101: 3431-3435

278. McCullen S.D., McQuilling J.P., Grossfeld R.M., Lubischer J.L., Clarke L.I., Loboa E.G. (2010). Application of low-frequency alternating current fields via interdigitated electrodes: effects on cellular viability, cytoplasmic calcium, and osteogenic differentiation of human adipose-derived stem cells. *Tiss. Eng. Part C-Meth.*; 16: 1377-1386

279. McGloin D., Spalding G.C., Melville H., Sibbett W., Dholakia K. (2003). Three dimensional arrays of optical bottle beams. *Opt. Commun.*; 225: 215-222

280. Nakagawa S., Pawelek P., Grinnell F. (1989). Extracellular matrix organization modulates fibroblast growth and growth factor responsiveness. *Exp. Cell Res*.; 182: 572-582

281. Nakajima M., Ishimuro T., Kato K., Ko I.K., Harita I., Arima Y., Iwata H. (2007). Combinatorial protein display for the cell-based screening of biomaterials that direct neural stem cell differentiation. *Biomat.*; 28: 1048-1060

282. Nakamura Y., Arai F., Iwasaki H., Hosokawa K., Kobayashi I., Gomei Y., Matsumoto Y., Yoshihara H., Suda T. (2010). Isolation and characterization of endosteal niche cell populations that regulate hematopoietic stem cells. *Blood*; 116: 1422-1432

283. Neagu A., Jakab K., Jamison R., Forgacs G. (2005). Role of physical mechanisms in biological self-organization. *Phys. Rev. Lett.*; 95(17): 178104

284. Neild A., Oberti S., Haake A., Dual J. (2006). Finite element modelling of a microparticle manipulator. *Ultrasonics*; 44: 455-460

285. Ng E.S., Davis R.P., Azzola L., Stanley E.G., Elefanty A.G. (2005) Forced aggregation of defined numbers of human embryonic stem cells into embryoid bodies fosters robust, reproducible hematopoietic differentiation. *Blood*; 106(5): 1601-1603

286. Ngalim S.H., Magenau A., Le S.G., Gooding J.J., Gaus K. (2010). How do cells make decisions: engineering micro- and nanoenvironments for cell migration. *J. Oncol.*; DOI: 10.1155/2010/363106

287. Niebruegge S., Bauwens C.L., Peerani R., Thavandiran N., Masse S., Sevaptisidis E., Nanthakumar K., Woodhouse K., Husain M., Kumacheva E., Zandstra P.W. (2009). Generation of human embryonic stem cell-derived mesoderm and cardiac cells using size-specified aggregates in an oxygen-controlled bioreactor. *Biotechnol. Bioeng.*; 102: 493-507

288. Nieden N.I., Kempka G., Ahr H.J. (2003). In vitro differentiation of embryonic stem cells into mineralized osteoblasts. *Differentiation*; 71: 18-27

289. Niederreither K., Vermot J., Messaddeq N., Schuhbaur B., Chambon P., Dolle P. (2001). Embryonic retinoic acid synthesis is essential for heart morphogenesis in the mouse. *Development*; 128: 1019-1031

290. Niederreither K., Vermot J., Schuhbaur B., Chambon P., Dolle P. (2002). Embryonic retinoic acid synthesis is required for forelimb growth and anteroposterior patterning in the mouse. *Dev.*; 129: 3563-3574

291. Niemann C. and Watt F.M. (2002). Designer skin: Lineage commitment in postnatal epidermis. *Trends Cell. Biol.*; 12: 185-192

292. Nilsson S.K., Johnston H.M., Whitty G.A., Williams B., Webb R.J., Denhardt D.T., Bertoncello I., Bendall L.J., Simmons P.J., Haylock D.N. (2005). Osteopontin, a key component of the hematopoietic stem cell niche and regulator of primitive hematopoietic progenitor cells. *Blood*; 106: 2004-2011

293. Niwa H., Miyazaki J., Smith A.G. (2000). Quantitative expression of Oct-3/4 defines differentiation, dedifferentiation or self-renewal of ES cells. *Nat. Genet*.; 24(4): 372-376

294. Nonaka J., Yoshikawa M., Ouji Y., Matsuda R., Nishimura F., Yamada S., Nakase H., Moriya K., Nishiofuku M., Ishizaka S., Sakaki T. (2008). CoCl(2) inhibits neural differentiation of retinoic acid-treated embryoid bodies. *J. Biosci. Bioeng.*; 106: 141-147

295. Nobta M., Tsukazaki T., Shibata Y., Xin C., Moriishi T., Sakano S., Shindo H., Yamaguchi A. (2005). Critical regulation of bone morphogenetic protein-induced osteoblastic differentiation by Delta1/Jagged1-activated notch1 signaling. *J. Biol. Chem.*; 280(16): 15842-15848

296. Noort D.V., Ong S.M., Zhang C., Zhang S., Arooz S., Yu H. (2009). Stem cell in microfluidics. *Biotechnol. Prog*.; 25: 52-60

297. Norgaard R., Kassem M., Rattan S. (2006). Heat Shock-Induced Enhancement of Osteoblastic Differentiation of hTERT-Immortalized Mesenchymal Stem Cells. *Ann. N. Y. Acad. Sci*.; 1067: 443-447

298. Nyberg S.L., Shatford R.A., Peshwa M.V., White J.G., Cerra F.B., Hu W.S. (1993). Evaluation of a hepatocyte-entrapment hollow fiber bioreactor: a potential bioartificial liver. *Biotechnol. Bioeng.*; 41(2): 194-203

299. Odde D.J. and Renn M.J. (2000). Laser-guided direct writing of living cells. *Biotechnol. Bioeng.*; 67: 312-318

300. Ohneda O., Fennie C., Zheng Z., Donahue C., La H., Villacorta R., Cairns B., Lasky L.A. (1998). Hematopoietic stem cell maintenance and differentiation are supported by embryonic aorta-gonad-mesonephros region-derived endothelium. *Blood*; 92: 908-919

301. Okada A., Lansford R., Weimann J.M., Fraser S.E., McConnell S.K. (1999). Imaging cells in the developing nervous system with retrovirus expressing modified green fluorescent protein. *Exp. Neurol.*; 156: 394-406

302. Orner B.P., Derda R., Lewis R.L., Thomson J.A., Kiessling L.L. (2004). Arrays for the combinatorial exploration of cell adhesion. *J. Am. Chem. Soc*.; 126: 10808-10809

303. Orr A.W., Helmke B.P., Blackman B.R., Schwartz M.A. (2006). Mechanisms of mechanotransduction. *Dev. Cell*; 10(1): 11-20

304. Oshima H., Rochat A., Kedzia C., Kobayashi K., Barrandon Y. (2001). Morphogenesis and renewal of hair follicles from adult multipotent stem cells. *Cell*; 104: 233-245

305. Othmer H.G., Dunbar S.R., Alt. W. (1988). Models of dispersal in biological systems. *J. Mathem. Biol.*; 26: 263-298

306. Palmer T.D., Willhoite A.R., Gage F.H. (2000). Vascular niche for adult hippocampal neurogenesis. *J. Comp. Neurol. I.*; 425: 479-494

307. Park I.K., He Y., Lin F., Laerum O.D., Tian Q. (2002). Differential gene expression profiling of adult murine hematopoietic stem cells. *Blood*; 99: 488-498

308. Park J., Cho C.H., Parashurama N., Li Y., Berthiaume F., Toner M., Tilles A.W., Yarmush M.L. (2007). Microfabrication-based modulation of embryonic stem cell differentiation. *Lab Chip*; 7: 1018-1028

309. Parsons-Wingerter P. and Saltzman W.M. (1993). Growth versus function in the three-dimensional culture of single and aggregated hepatocytes within collagen gels. *Biotechnol. Prog.*; 9(6): 600-607

310. Paterson L., Briscoe T., Riches A.C. (2007). Passive optical separation within a 'nondiffracting' light beam. *J. Biomed. Opt.*; 12: 054017

311. Patlak C.S. (1953). Random walk with persistence and external bias. *Bull. Math. Biol.*; 15(3): 311-338

312. Peerani R., Rao B.M., Bauwens C., Yin T., Wood G.A., Nagy A., Kumacheva E., Zandstra P.W. (2007). Niche-mediated control of human embryonic stem cell self-renewal and differentiation. *EMBO J.*; 26: 4744-4755

313. Peerani R. and Zandstra P.W. (2010). Enabling stem cell therapies through synthetic stem-cell niche engineering. *J. Clin. Invest.*; 120: 60-70

314. Pelham R.J. and Wang Y.-L. (1997). Cell locomotion and focal adhesions are regulated by substrate flexibility. *P.N.A.S.*; 94: 13661-13665

315. Penvy L. and Rao M.S. (2003). The stem cell managerie. *Trends Neurosci*.; 26: 351-359

316. Perez-Pomares J.M. and Foty R.A. (2006). Tissue fusion and cell sorting in embryonic development and disease: biomedical implications. *Bioessays*; 28: 809-821

317. Peshwa M.V., Wu F.J., Follstad B.D., Cerra F.B, Hu W-S. (1994). Kinetics of Hepatocyte Spheroid Formation. *Biotechnol. Prog.*; 10(5): 460-466

318. Petersen B.E., Bowen W.C., Patrene K.D., Mars W.M., Sullivan A.K., Murase N., Boggs S.S., Greenberger J.S., Goff J.P. (1999). Bone marrow as a potential source of hepatic oval cells. *Science*; 284: 1168-1170

319. Pethig R. and Markx G.H. (1997). Applications of dielectrophoresis in biotechnology. *Trends Biotechnol*.; 15: 426-432

320. Pethig R., Huang Y., Wang X.B., Burt J.P.H. (1992). Positive and negative dielectrophoretic collection of colloidal particles using interdigitated castellated microelectrodes. *J. Phys. D.: Appl. Phys.*; 24: 881-998

321. Pohl H. A., Kaler K., Pollock. K. (1981). The continuous positive and negative dielectrophoresis of microorganisms. *J. Biol. Phys*.; 9: 67-86

322. Pohl H.A. and Crane J.S. (1971). Dielectrophoretic force. *J. Theor. Biol*.; 37: 1-13

323. Pohl H.A. (1978). *Dielectrophoresis*. Cambridge: Cambridge University Press.

324. Poste G. and Fidler I. (1980). The pathogenesis of cancer metastasis. *Nature*; 283: 139-146

325. Potard U.S., Butler J.P., Wang N. (1997). Cytoskeletal mechanics inconfluent epithelial cells probed through integrins and E-cadherins. *Am. J. Physiol*.; 272: 654-663

326. Potocnik A.J., Kohler H., Eichmann K. (1997). Hematolymphoid in vivo reconstitution potential of subpopulations derived from in vitro differentiated embryonic stem cells. *P.N.A.S USA*; 94: 10295-10300

327. Potocnik A.J., Nielsen P.J., Eichmann K. (1994). In vitro generation of lymphoid precursors from embryonic stem cells. *EMBO J*.; 13: 5274-5283

328. Powell S.K. and Kleinmann H.K. (1997). Neuronal laminins and their cellular receptors. *Int. J. Biochem. Cell Biol*.; 29: 401-414

329. Prakash S., Khan A., Paul A. (2010). Nanoscaffold based stem cell regeneration therapy: recent advancement and future potential. *Expert Opin. Biol. Therapy*; 10: 1649-1661

330. Price J.A.R., Burt J.P.H., Pethig R. (1988). Application of a new optical technique for measuring the dielectrophoretic behaviour of microorganisms. *Biochim. Biophys. Acta*.; 964: 221-230

331. Purpura K.A., Morin J., Zandstra P.W. (2008). Analysis of the temporal and concentration-dependent effects of BMP-4, VEGF, and TPO on development of embryonic stem cell–derived mesoderm and blood progenitors in a defined, serum-free media. *Exp. Hematol*.; 36: 1186-1198

332. Rafii S., Mohle R., Shapiro F., Frey B.M., Moore M.A. (1997). Regulation of hematopoiesis by microvascular endothelium. *Leuk. Lymphoma*; 27: 375-386

333. Ramalho-Santos M., Yoon S., Matsuzaki Y., Mulligan R.C., Melton D.A. (2002). "Stemness": transcriptional profiling of embryonic and adult stem cells. *Science*; 298: 597-600

334. Ramirez M.A, Pericuesta E., Fernandez-Gonzalez R., Pintado B., Gutierrez-Adan A. (2007). Inadvertent presence of pluripotent cells in monolayers derived from differentiated embryoid bodies. *Int. J. Dev. Biol*.; 51: 397-407

335. Ramos A., Margon H., Green N.G., Castellanos A. (1998). AC electrokinetics: a review of forces in microelectrode structures. *J. Phys. D: Appl. Phys*.; 31(18): 2338-2353

336. Ray J. and Gage F.H. (2006). Differential properties of adult rat and mouse brain-derived neural stem/progenitor cells. *Mol. Cell. Neurosci*.; 31: 560-573

337. Rice W., Kaplan D., Georgakoudi I. (2007). Quantitative biomarkers of stem cell differentiation based on intrinsic two-photon excited fluorescence. *J. Biomed. Opt.*; 12: 060504

338. Rider C.C. (2006). Heparin/heparin sulphate binding in the TGF-beta cytokine superfamily. *Biochem. Soc. Trans*.; 34: 458-460

339. Rhodes K.E., Gekas C., Wang Y., Lux C.T., Francis C.S., Chan D.N., Conway S., Orkin S.H., Yoder M.C., Mikkola H.K. (2008). The emergence of hematopoietic stem cells is

initiated in the placental vasculature in the absence of circulation. *Cell Stem Cell*; 2: 252-263

340. Rosenthal A. and Voldman J. (2005). Dielectrophoretic traps for single-particle patterning. *Biophys. J.*; 88: 2193-2205

341. Saha K. and Schaffer D.V. (2006). Signal dynamics in Sonic hedgehog tissue patterning. *Development*; 133: 889-900

342. Saitoh S., Takahashi I., Mizoguchi I., Sasano Y., Kagayama M., Mitani H. (2000). Compressive force promotes chondrogenic differentiation and hypertrophy in midplatal suture cartilage in growing rats. *The Anatom. Rec.*; 260: 392-401

343. Sauer H., Schmelter M., Ateghang B., Helmig S., Wartenberg M. (2006). Embryonic stem cells utilize reactive oxygen species as transducers of mechanical strain-induced cardiovascular differentiation. *FASEB J.*; 20: 1182-1184

344. Schofield R. (1978) .The relationship between the spleen colony-forming cell and the haematopoietic stem cells. A hypothesis. *Blood Cells*; 4: 7-25

345. Schöler H.R. (2007). The potential of stem cells: An inventory. In Knoepffler, Schipanski, and Sorgner. *Human Biotechnology as Social Challenge*. Ashgate Publishing Ltd.: pp 28

346. Shreiber D.I, Barocas V.H, Tranquillo R.T. (2003). Temporal variations in cell migration and traction during fibroblast-mediated gel compaction. *Biophys. J.*; 84(6): 4102-4114

347. Shreiber D.I., Enever P.A.J., Tranquillo R.T. (2001). Effects of PDGF-BB on rat dermal fibroblast behavior in mechanically stressed and unstressed collagen and fibrin gels. *Exp. Cell Res.*; 266: 155-166

348. Sebastian A., Buckle A-M., Markx G.H. (2006). Formation of multilayer aggregates of mammalian cells by dielectrophoresis. *J. Micromech. Microeng.*; 16: 1769-1777

349. Sebastian A., Buckle A.M., Markx G.H. (2007a). Tissue engineering with electric fields: immobilisation of mammalian cells in multilayer aggregates using dielectrophoresis. *Biotechnol. Bioeng.*; 98: 694-700

350. Sebastian A., Venkatesh A.G., Markx G.H. (2007b). Tissue engineering with electric fields: Investigation of the shape of mammalian cell aggregates formed at interdigitated oppositely castellated electrodes. *Electrophoresis*; 28: 3821-3828

351. Sengers B.G., Please C.P., Oreffo R.O.C. (2007). Experimental characterization and computational modelling of two-dimensional cell spreading for skeletal regeneration. *J. R. Soc. Interface*; 4(17): 1107-1117

352. Serena E., Figallo E., Tandon N., Cannizzaro C., Gerecht S., Elvassore N., Vunjak-Novakovic G. (2009). Electrical stimulation of human embryonic stem cells: cardiac differentiation and the generation of reactive oxygen species. *Exp. Cell Res.*; 315(20): 3611-3619

353. Serluca F.C., Drummond I.A. Fishman M.C. (2002). Endothelial signaling in kidney morphogenesis: a role for hemodynamic force. *Curr. Biol.*; 12: 492-497

354. Sheetz M.P., Felsenfeld D.P., Galbraith C.G. (1998). Cell migration: regulation of force on extracellular matrix-integrin complexes. *Trends Cell Biol*.; 8: 51-54

355. Sheen V.L. and Macklis J.D. (1995). Targeted neocortical cell death in adult mice guides migration and differentiation of transplanted embryonic neurons. *J. Neurosci.*; 15(12): 8378-8392

356. Shekhawat G., Tark S.H., Dravid V.P. (2006). MOSFET-embedded microcantilevers for measuring deflection in biomolecular sensors. *Science*; 311 (5767): 1592-1595

357. Shen Q., Goderie S.K., Jin L., Karanth N., Sun Y., Abramova N., Vincent P., Pumiglia K., Temple S. (2004). Endothelial cells stimulate self-renewal and expand neurogenesis of neural stem cells. *Science*; 304: 1338-1340

358. Shimizu T., Yamato M., Kikuchi A., Okano T. (2003). Cell sheet engineering for myocardial tissue reconstruction. *Biomaterials*; 24: 2309-2316

359. Shinohara T., Orwig K.E., Avarbock M.R., Brinster R.L. (2001). Remodeling of the postnatal mouse testis is accompanied by dramatic changes in stem cell number and niche accessibility. *P.N.A.S.*; 98: 6186-6191

360. Shirota T. and Tavassoli M. (1991). Cyclophosphamide-induced alterations of bone marrow endothelium: implications in homing of marrow cells after transplantation. *Exp. Hematol.*; 19(5): 369-73

361. Shreiber D.I., Barocas V.H., Tranquillo R.T. (2003). Temporal variations in cell migration and traction during fibroblast-mediated gel compaction. *Biophys. J.*; 84(6): 4102-4114

362. Shreiber, D.I., Enever P.A., Tranquillo, R.T. (2001). Effects of pdgf-bb on rat dermal fibroblast behavior in mechanically stressed and unstressed collagen and fibrin gels. *Exp. Cell Res.*; 266(1): 155-166

363. Siminovitch L., McCulloch E.A., Till J.E. (1963). The distribution of colony-forming cells among spleen colonies. *J. Cellul. Compar. Physiol.*; 62(3): 327–336

364. Sipkins D.A., Wei X., Wu J.W., Runnels J.M., Côté D., Means T.K., Luster A.D., Scadden D.T., Lin C.P. (2005). In vivo imaging of specialized bone marrow endothelial microdomains for tumour engraftment. *Nature*; 435: 969-973

365. Soen Y., Mori A., Palmer T.D., Brown P.O. (2006) Exploring the regulation of human neural precursor cell differentiation using arrays of signaling microenvironments. *Mol. Syst. Biol.*; 37: 1-14

366. Song X., Zhu C.-H., Doan C., Xie T. (2002). Germline stem cells anchored by adherens junctions in the Drosophila ovary niches. *Science*; 296: 1855-1857

367. Sotiropoulou P.A., Perez S.A., Salagianni M., Baxevanis C.N., Papamichail M. (2006). Characterization of the optimal culture conditions for clinical scale production of human mesenchymal stem cells. *Stem Cells*; 24: 462-471

368. Steinberg M.S. (1963). Reconstruction of tissues by dissociated cells: some morphogenetic tissue movements and the sorting out of embryonic cells may have a common explanation. *Science*; 141: 401-408

369. Steinberg M.S. (1970). Does differential adhesion govern self-assembly processes in histogenesis? Equilibrium configurations and the emergence of a hierarchy among populations of embryonic cells. *J. Exp. Zool*.; 173: 395-434

370. Steinberg M.S. (1978). Cell–cell recognition in multicellular assembly: levels of specificity. *Symp. Soc. Exp. Biol*.; 32: 25-49

371. Steinberg M.S. (1996). Adhesion in development: an historical overview. *Dev. Biol*.; 180: 377-388

372. Steinberg M.S. (2007). Differential adhesion in morphogenesis: a modern view. *Curr. Opin. Genet. Dev.*; 17: 281-286

373. Spangrude G.J., Heimfeld S., Weissman I.L. (1988). Purification and characterization of mouse hematopoietic stem cells. *Science*; 241: 58-62

374. Stephens M., Talary M.S., Pethig R., Burnett A.K., Mills K.I. (1996). The dielectrophoresis enrichment of CD34+ cells from peripheral stem cell harvests. *Bone Marrow Transplan.*; 18: 777-782

375. Stewart M.H., Bosse M., Chadwick K., Menendez P., Bendall S.C., Bhatia M. (2006). Clonal isolation of hESCs reveals heterogeneity within the pluripotent stem cell compartment. *Nat. Meth.*; 3: 807-815

376. Stier S., Ko Y., Forkert R., Lutz C., Neuhaus T., Grünewald E., Cheng T., Dombkowski D., Calvi L.M., Rittling S.R., Scadden D.T. (2004). Matrix glycoprotein osteopontin is a

stem cell niche constituent that constrains the hematopoietic stem cell pool size. *Blood*; 104: 191A

377. Straight A.F., Cheung A., Limouze J., Chen I., Westwood N.J., Sellers J.R., Mitchison T.J. (2003). Dissecting temporal and spatial control of cytokinesis with a myosin II Inhibitor. *Science*; 299: 1743-1747

378. Sun T.T., Cotsarelis G., Lavker R.M. (1991). Hair follicular stem cells: The bulge-activation hypothesis. *J. Invest. Dermatol*.; 98: 77s-78s

379. Sun S., Titushkin I., Cho M. (2006). Regulation of mesenchymal stem cell adhesion and orientation in 3D collagen scaffold by electrical stimulus. *Bioelectrochem.*; 69: 133-141

380. Sun S., Liu Y., Lipsky S., Cho M. (2007). Physical manipulation of calcium oscillations facilitates osteodifferentiation of human mesenchymal stem cells. *FASEB J.*; 21: 1472-1480

381. Sudo K., Ema H., Morita Y., Nakauchi H. (2000). Age-associated characteristics of murine hematopoietic stem cells. *J. Exp. Med*.; 192: 1273-1280

382. Tagil M., Aspenberg P., de Rooij P.P., Siebrecht M.A.N. (2001). The fate of mechanically induced cartilage in an unloaded environment. *J. Biomech*.; 34: 961-966

383. Taichman R.S. and Emerson S.G. (1998). The role of osteoblasts in the hematopoietic microenvironment. *Stem Cells*; 16(1): 7-15

384. Taichman R.S. and Emerson S.G. (1994). Human osteoblasts support haematopoiesis process through the production of granulocyte colony-stimulating factor. *J. Exp. Med.*; 179: 1677-1682

385. Taichman R.S., Reilly M.J., Emerson S.G. (1996). Human osteoblasts support human haematopoietic progenitor cells in vitro bone marrow cultures. *Blood*; 87: 518-524

386. Taichman R., Reilly M., Verma R., Ehrenman K., Emerson S. (2001). Hepatocyte growth factor is secreted by osteoblasts and cooperatively permits the survival of haematopoietic progenitors. *Br. J. Haematol*.; 112: 438-448

387. Taichmann R.S. (2005). Blood and bone: two tissues whose fates are intertwined to create the hematopoietic stem cell niche. *Blood;* 105(7): 2631-2639

388. Takeuchi M., Sekiguchi T., Hara T., Kinoshita T., Miyajima A. (2009). Cultivation of aorta-gonad-mesonephros-derived hematopoietic stem cells in the fetal liver microenvironment amplifies long-term repopulating activity and enhances engraftment to the bone marrow. *Blood*; 99: 1190-1195

389. Taichman R.S. and Emerson S.G. (1994). Human osteoblastic cells support haematopoiesis process through the production of granulocyte colony-stimulating factor. *J. Exp. Med*.; 179: 1677-1682

390. Taichman R.S., Reilly M.J., Emerson S.G. (1996). Human osteoblastic cells support human haematopoietic progenitor cells in vitro bone marrow cultures. *Blood*; 87: 518-524

391. Takahashi I., Mizoguchi I., Nakamura M., Sasano Y., Saitoh S., Kagayama M., Mitani H. (1996). Effects of expansive force on the differentiation of mid palatal suture cartilage in rats. *Bone*; 18: 341-348

392. Takahashi I., Onodera K., Sasano Y., Mizoguchi I., Bae J.W., Mitani H., Kagayama M., Mitani H. (2003). Effect of stretching on gene expression of beta1 integrin and focal adhesion kinase and on chondrogenesis through cell-extracellular matrix interactions. *Eur. J. Cell Biol*.; 82: 182-192

393. Takeuchi M., Sekiguchi T., Hara T., Kinoshita T., Miyajima A. (2002). Cultivation of arota-gonad-mesonephros-derived hematopoietic stem cells in the fetal liver microenvironment amplifies long-term repopulating activity and enhance engraftment to bone marrow. *Blood*; 99: 1190-1196

394. Talary M.S, Mills K.I., Hoy T., Burnett A.K., Pethig R. (1995). Dielectrophoretic separation and enrichment of CD34+ cell subpopulation from bone marrow and peripheral blood stem cells. *Med. Biol. Eng. Comp.*; 33: 235-237

395. Tamada M., Sheetz M.P., Sawada Y. (2004). Activation of a signalling cascade by cytoskeleton stretch. *Dev. Cell*; 7: 709-718

396. Tan W. and Desai T.A. (2004). Layer-by-layer microfluidics for biomimetic three-dimensional structures. *Biomaterials*; 25: 1355-1364

397. Tanase M., Felton E.J., Gray D.S., Hultgren A., Chen C.S., Reich D.H. (2005). Assembly of multicellular constructs and microarrays of cells using magnetic nanowires. *Lab Chip*; 5: 598-605

398. Tavassoli M. (1981). Structure and function of sinusoidal endothelium of bone marrow. *Prog. Clin. Biol. Res.*; 59B: 249-256

399. Tavassoli M. (1992). Hemopoietic endothelium, incognito. *Exp. Hematol.*; 20: 386-387

400. Thuan N.V. (2006). Micromanipulation technology: Intracytoplasmic sperm injection and somatic cell nuclear transfer. *Proceedings of International Workshop on Biotechnology in Agriculture*; Ho Chi Minh City: pp 25-28

401. Thiele J., Meuter R.B., Titius R.B., Zankovich R., Fischer R. (1993). Proliferating cell nuclear antigen expression by erythroid precursors in normal bone marrow, in reactive lesions and in polycythaemia rubra vera. *Histopathology*; 22(5): 429-435

402. Tomasek J.J., Gabbiani G., Hinz B., Chaponnier C., Brown R.A. (2002). Myofibroblasts and mechano-regulation of connective tissue remodelling. *Nat. Rev. Mol. Cell Biol.*; 3: 349-363

403. Torisawa Y., Chueh B.-H., Huh D., Ramamurthy P., Roth T.M., Barald K.F., Takayama S. (2007). Efficient formation of uniform-sized embryoid bodies using a compartmentalized microchannel device. *Lab Chip*; 7: 770-776

404. Traub O. and Berk B.C. (1996). Laminar Shear Stress: Mechanisms by which endothelial cells transduce an atheroprotective force. *Arterioscl. Thromb. Vasc. Biol.*; 18: 677-685

405. Travlos G.S. (2006). Normal Structure, Function, and Histology of the Bone Marrow. *Toxicol Pathol.*; 34(5): 548-565

406. Trinkhaus J.P. (1984). *Cells into organs. The forces that shape the embryo*, 2nd ed. Englewood cliffs, NJ: Prentice-Hall

407. Trosko J.E., Chang C-C., Wilson M.R., Upham B., Hayashi T., Wade M. (2000). Gap junctions and the regulations of cellular functions of stem cells during development and differentiation. *Methods*; 20(2): 245-264

408. Tsai M., Li W., Tuan R., Chang W. (2009). Modulation of osteogenesis in human mesenchymal stem cells by a pulsed electromagnetic field stimulation. *J. Ortho. Res.*; 27(9): 1169-1174

409. Tuskita S., Furuse M., Itoh M. (2001). Multifunctional strands in tight junctions. *Nature Rev. Mol. Cell Biol.*; 2: 285-293

410. Ueno H. and Weissman I.L. (2006). Clonal analysis of mouse development reveals a polyclonal origin for yolk sac blood islands. *Dev. Cell*; 11: 519-533

411. Uhrig K., Kurre R., Schmitz C., Curtis J.E., Haraszti T., Clemen A.E., Spatz J.P. (2009). Optical force sensor array in a microfluidic device based on holographic optical tweezers. *Lab Chip*; 9: 661-668

412. Ulloa-Montoya F., Verfaillie C.M., Hu W.S. (2005). Culture systems for pluripotent stem cells. *J. Biosci. Bioeng.*; 100(1): 12-27

413. Underhill G.H. and Bhatia S.N. (2007). High-throughput analysis of signals regulating stem cell fate and function. *Curr. Opin. Chem. Biol.*; 11: 357-366

414. Valero A., Braschler T., Demierre N., Renaud P. (2010). A miniaturized continuous dielectrophoretic cell sorter and its applications. *Biomicrofluidics*; 4: 022807; doi:10.1063/1.3430542

415. Vasioukhin V., Bauer C., Degenstein L., Wise B., Fuchs E. (2001). Hyperproliferation and defects in epithelial polarity upon conditional ablation of alpha-catenin in skin. *Cell*; 104: 605-617

416. Venkatesh A.G. and Markx G.H. (2007). On the height of cell aggregates formed with positive dielectrophoresis. *J. Phys. D: Appl. Phys*.; 40: 106-113

417. Verfaillie C.M. (1998). Adhesion receptors as regulators of the hematopoietic process. *Blood*; 92: 2609- 2612

418. Visnjic D., Kalajzic Z., Rowe D.W., Katavic V., Lorenzo J., Aguila H.L. (2004). Hematopoiesis is severely altered in mice with an induced osteoblast deficiency. *Blood*; 103: 3258-3264

419. Vykoukal J., Vykoukal D.M., Freyberg S., Alt E.U., Gascoyne P.R.C. (2008). Enrichment of putative stem cells from adipose tissue using dielectrophoretic field-flow fractionation. *Lab Chip*; 8(8): 1386-1393

420. Wang M.D., Yin H., Landick R., Gelles J., Block S.M. (1997). Stretching DNA with optical tweezers. *Biophys. J.*; 72: 1335-1346

421. Wang N. and Ingber D.E. (1995). Probing transmembrane mechanicalcoupling and cytomechanics using magnetic twisting cyto-metry. *Biochem. Cell Biol*.; 73: 327-335

422. Wang X.B., Huang Y., Burt J.P.H., Markx G.H., Pethig R. (1993). Selective dielectrophoretic confinement of bioparticles in potential energy wells. *J. Phys. D.: Appl. Phys.*; 26: 1278-1285

423. Wang W., Wang Z., Zhang G., Clark C., Brighton C. (2004). Up-regulation of chondrocyte matrix genes and products by electric fields. *Clinic. Orth. Rel. Res.*; 427: s163-s173

424. Wang X., Wang W., Ma J., Guo X., Yu X., Ma X. (2006). Proliferation and differentiation of mouse embryonic stem cells in APA microcapsule: A model for studying the interaction between stem cells and their niche. *Biotechnol. Prog.*; 22: 791-800

425. Wanger D.R., Lindsey D.P., Li K.W., Tummala P., Chandran S.E., Smith R.L., Longaker M.T., Carter D.R., Beaupre G.S. (2008). Hydrostatic pressure enhances chondrogenic differentiation of human bone marrow stromal cells in osteochondrogenic medium. *Annals. Biomed. Eng.*; 36: 813-820

426. Watt F.M. and Hogan B.L. (2000). Out of Eden: stem cells and their niches. *Science*; 287: 1427-1430

427. Wichterle H., Lieberam I., Porter J.A., Jessell T.M. (2002). Directed differentiation of embryonic stem cells into motor neurons. *Cell*; 110: 385-397

428. Wickramasinghe S.N. and Mccullough J. (2003). *Bone and Bone Marrow Pathology*. Edinburgh: Churchill Livingstone publications. Pp 74-78

429. Wiles M.V. and Keller G. (1991). Multiple hematopoietic lineages develop from embryonic stem (ES) cells in culture. *Development*; 111: 259-267

430. Wilkinson P.C. and Lackie J.M. (1979). The adhesion, migration, and chemotaxis of leukocytes in inflammation, in H.Z. Movat. ed., *Inflammatory Reactions.* Berlin: Springer-Verlag: pp 47-88

431. Williams R.M., Piston D.W., Webb W.W. (1994). Two-photon molecular excitation provides intrinsic 3-dimensional resolution for laser-based microscopy and microphotochemistry. *FASEB. J.*; 8(11): 804-813

432. Wilson L.J. and Paul D.H. (1990). Functional morphology of the telson- uropod stretch receptor in the sand crab *Emerita analoga*. *J. Comp. Neurol*.; 296: 343-358

433. Wilson A. and Trumpp A. (2006). Bone-marrow haematopoietic-stem-cell niches. *Immunology*; 6: 93-106

434. Wolpert L., Beddington R., Jessell T., Lawrence P., Meyerowitz E., Smith J. (2007). *Principles of development* (3rd ed.). Oxford: Oxford University Press

435. Wong R.C. and Peblay A. (2010). Study of gap junctions in human embryonic stem cells. *Methods Mol. Biol*.; 584: 211-228

436. Wu H.H., Ivkovic S., Murray R.C., Jaramillo S., Lyons K.M., Calof A.L. (2003). Autoregulation of neurogenesis by GDF11. *Neuron*; 37: 197-207

437. Xu C., Rosler E., Jiang J., Lebkowski J. S., Gold J.D., O'Sullivan C., Delavan-Boorsma K., Mok M., Bronstein A., Carpenter M.K. (2005). Basic fibroblast growth factor supports undifferentiated human embryonic stem cell growth without conditioned medium. *Stem Cells*; 23: 315-323

438. Xu J., Wang W., Clark C., Brighton C. (2009). Signal transduction in electrically stimulated articular chondrocytes Involves translocation of extracellular calcium through voltage-gated channels. *Osteoarth. Cart.*; 17: 397-405

439. Yamada T. (1994). Caudalization by the amphibian organizer: Brachyury, convergent extension and retinoic acid. *Dev.*; 120: 3051-3062

440. Yamashita Y., Jones D.L., Fuller M.T. (2003). Orientation of asymmetric stem cell division by the APC tumor suppressor and centrosome. *Science*; 301: 1547-155

441. Yang M., Zhang X., Vafai K., Ozkan C.S. (2003). High sensitivity iezoresistive cantilever design and optimization for analyte-receptor binding. *J. Micromech. Microeng*.; 13(6): 864-872

442. Yeatman T.J. (2004). Cell adhesion at adherens junctions and focal adhesions. *Nature Rev. Cancer*; 4: 470-480

443. Yeung T., Georges P.C., Flanagan L.A., Marg B., Ortiz M., Funaki M., Zahir N., Ming W., Weaver V., Janmey P.A. (2005). Effects of substrate stiffness on cell morphology, cytoskeletal structure, and adhesion. *Cell Mot. Cytoskel.*; 60: 24-34

444. Yin T. and Li L. (2006). The stem cell niches in bone. *J. Clin. Invest*.; 116: 1195-1201

445. Yoshida M., Westlin W.F., Wang N., Ingber D.E., Rosenweig A., Resnick N., Gimbrone M.A. Jr. (1996). Leukocyte adhesion to vascular endothelium induces e-selectin association with the actin cytoskeleton. *J. Cell Biol*.; 133: 445-455

446. Zandstra P.W., Lauffenburger D.A., Eaves C.J. (2000). A ligandreceptor signaling threshold model of stem cell differentiation control: a biologically conserved mechanism applicable to hematopoiesis. *Blood*; 96: 1215-1222

447. Zhang J., Niu C., Ye L., Huang H., He X., Tong W-G., Ross J., Haug J., Johnson T., Feng J.Q., Harris S., Wiedemann L.M., Mishina Y., Linheng L. (2003). Identification of the haematopoietic stem cell niche and control of the niche size. *Nature*; 425: 836-841

448. Zhang X.R. and Xu X. (2004). Development of a biosensor based on laser-fabricated polymer microcantilevers. *Appl. Phys. Lett*.; 85(12): 2423-2425

449. Zhang W.J., Park C., Arentson E., Choi K. (2005). Modulation of hematopoietic and endothelial cell differentiation from mouse embryonic stem cells by different culture conditions. *Blood*; 105: 111-114

450. Zhang H. and Liu K.K. (2008). Optical tweezers for single cells. *J. R. Soc. Interface.*; 5: 671–690

451. Zheng J., Lamoureux P., Santiago V., Dennerll T., Buxbaum R.E., Heidemann S.R. (1991). Tensile regulation of axonal elongation and initiation. *J. Neurosci*.; 11: 1117–1125

452. Zheng W., Nowakowski R.S., Vaccarino F.M. (2004). Fibroblast growth factor 2 is required for maintaining the neural stem cell pool in the mouse brain subventricular zone. *Dev. Neurosci*.; 26: 181- 196

453. Zhou Q. and Melton D.A. (2008). Extreme makeover: Converting one cell into another. *Cell Stem Cell*; 382-388

454. Zhuang H., Wang W., Seldes R., Tahernia D., Fan H., Brighton C. (1997). Electrical stimulation induces level of TGF-B1 mRNA in osteoblastic cells by a mechanism involving calcium/calmodulin pathway. *Biochem. Biophys. Res. Commun.*; 237: 225-229

455. Ziegler C. (2004). Cantilever-based biosensors. *Anal. Bioanal. Chem.*; 379(7-8): 946-959

APPENDIX I

For cells in one dimension

In a one dimensional random walk the cell (particle) moves along the *x* axis only. The particle starts from its origin $x = 0$, and every τ seconds, the particle steps a distance δ along the axis. Thus the average speed of the particle is δ/τ. The direction of the particle is matter of chance.

To calculate the average, we track the random walk of *N* cells. Let $x_i\,(n)$ be the location on the *x* axis after the cell has taken *n* steps. Therefore from the previous assumption, we get the equation:

$$x_i\,(n) = x_i\,(n-1) \pm \delta \tag{5.1}$$

In other words, each step the cell moves either left or right by δ, on the axis.

The average position of the cells after *n* steps is calculated by

$$< x(n) > = \frac{x_1(n)+x_2(n)\ldots.+x_N(n)}{N} \tag{5.2}$$

$$= \frac{1}{N}\sum_{i=1}^{N} x_i(n) \tag{5.3}$$

Where $\sum$ means that the position of all the cells numbered $1 - N$ is added up, after *n* steps.

Therefore the equation can be expanded by replacing $x_i\,(n)$ with $x_i\,(n\text{-}1) \pm \delta$ which is:

$$< x(n) > = \frac{1}{N}\sum_{i=1}^{N}[x_i(n-1) \pm \delta] \tag{5.4}$$

$$= \frac{1}{N}\sum_{i=1}^{N} x_i(n-1) + \frac{1}{N}\sum_{i=1}^{N} \pm \delta \tag{5.5}$$

But since half the time δ is to the right and half the time it is to the left, the average of $\pm\,\delta$ should be 0. Therefore

$$< x(n) > = < x(n-1) > \tag{5.6}$$

It can be said that the average position of the cell after *n* steps is the same as the position after $n - 1$ steps. This means that on average, the cells starting at the origin remain at the origin. Since this suggests that the cells, on average, go nowhere, this does not imply that all particles remain at the origin. This only tells us that for every cell, that is at a position $x = +5$, on average there is a cell at position $x = -5$. Therefore, although there is considerable spread of cells, the average net movement is 0.

The distance of the cell from its origin can be calculated in a separate way. Taking the absolute values of the each cell's location after *n* steps and squaring the values would always

give a positive value. The squares of all the locations can be averaged; the average distance travelled by the cell from the origin can be calculated.

The number of steps *n* in terms of the location *n-1* steps could be expressed as

$$x_i^2(n) = [x_i(n-1) \pm \delta]^2 \tag{5.7}$$

$$= x_i^2(n-1) \pm 2\delta x_i(n-1) + \delta^2 \tag{5.8}$$

On averaging the value for *N* cells, we get

$$< x^2(n) > = \frac{1}{N}\sum_{i=1}^{N} [x_i^2(n-1) \pm 2\delta x_i(n-1) + \delta^2] \tag{5.9}$$

$$= \frac{1}{N}\sum_{i=1}^{N} x_i^2(n-1) + \frac{1}{N}\sum_{i=1}^{N} \pm 2\delta x_i(n-1) + \frac{1}{N}\sum_{i=1}^{N} \delta^2 \tag{5.10}$$

$$= \frac{1}{N}\sum_{i=1}^{N} x_i^2(n-1) + \frac{1}{N}\sum_{i=1}^{N} \delta^2 \tag{5.11}$$

$$=< x^2(n-1) > + \delta^2 \tag{5.12}$$

Note: the average value of $\pm \delta = 0$.

The result shows that the average/mean square of position after *n* steps is greater by δ^2 than the average square of position after *n-1* steps. It was assumed before that the mean square position after 0 steps is 0. After 2 steps, the average square position is $2\delta^2$. Thus:

$$< x^2(n) > = n\delta^2 \tag{5.13}$$

It also means that the square of the displacement from the starting point increases directly with the number of steps taken. Therefore by taking the square root of the equation:

$$\sqrt{< x^2(n) >} = x_{rms} = \sqrt{n}\delta \tag{5.14}$$

The value $\sqrt{< x^2(n) >}$ is called the *root mean square* or *rms* displacement. It is a measure of how far, on average, the cells have travelled from their origin after taking *n* steps. The *rms* displacement is also the standard deviation.

Regarding the random walk, the original assumption was that the cell takes a step every τ seconds, the number of steps taken being equal to t/τ, where t is the time since the particle started its walk. Inserting this expression for n in 6.13 gives:

$$< x^2(t) >= \frac{\delta^2}{\tau} t \qquad (5.15)$$

The mean squared distance travelled by the cell increases directly with time at a rate that is dependent on the ratio of δ^2 to τ (Denny, 1993).

$$\text{Diffusion coefficient } D = \frac{\delta^2}{\tau}$$

APPENDIX II

MATLAB calculation for cells in the centre of the aggregate

```
clear all
close all
%x1 y1 x2 y2 x3 y3 x4 y4 are theco-ordinates of different cells x1y1 and
%x2y2 being in aggregate A and x3y3 and x4y4 in aggregate B; scale is
%multiplied by 10 to represent the micrometer scale;
x6=[16.5,17.7,18,19,20,21.7,23,24,25.2,26.4,27,28.3,28,29,29.8,31,30,29.6,29
.9,30.4,29.4,28.7,29.1,28.1,28.3];
y6=[13.6,13.7,14.6,15,16,16.1,16,16.8,17,17.8,18.8,18.8,17.7,18,17.6,17.9,18
.8,18.7,18.4,18.9,19.4,19.8,20.5,20.6,20.1];
x6=x6*10;
y6=y6*10;
x7=[17,17.2,17.9,18.9,19.9,21.2,22.1,22.9,24.2,23.6,24.4,23.9,24,24.6,25.5,2
4.8,23.3,23.4,23.7,22.1,21.6,21.1,21,20.4,20.7];
y7=[17.1,16.4,16.7,17.1,17,17.6,17.9,19.1,20.2,20.3,21.5,21.2,22.9,24.2,23.6
,23.5,25,26.7,28.8,31,30,28.9,30.1,29,27.9];
x7=x7*10;
y7=y7*10;
x9=[31.1,32.1,32.8,33.5,33.5,34,34.1,33.4,33,33.7,33.4,33.7,32,32.2,31.9,31.
3,31,31.1,30.9,31,31.3,32.1,31.1,31.3,31.2,30.5,30,30.9,29.1,30.9];
y9=[19,19.8,18.9,19.9,21,21.9,23.1,22.7,23,23.6,24.4,24.9,26.8,27.2,27.6,27.
2,27.5,27.9,28,28.6,28.8,29.9,30.8,31.4,32,31.8,31.9,32.9,32.4,32];
x9=x9*10;
y9=y9*10;
x13=[36.1,35.5,36,36.8,36.5,34.9,36.1,36.9,37.1,37,37.6,37.6,37.9,37,37,36,3
6.2,35.9,36.6,36.5,35.7,36,35.2,35.3,34.9,33.5,33];
y13=[16.9,17,16,17,17.5,18,18.8,19,19.8,20.8,21,22,22.9,23.1,24.1,24.5,25.5,
26,26.2,27,27.5,28.1,28.9,30.9,31.5,31.2,30.5];
x13=x13*10;
y13=y13*10;
x15=[29.8,29.2,28.5,29.5,29.7,30,30.3,30.9,31.3,31.6,31.1,31.5,31.1,31,31.5,
31.1];
y15=[14,13.4,14,14.9,15.8,16.5,17.2,17.9,18.3,19,19.9,20.5,21.2,21.2,22.2,23
.3];
x15=x15*10;
y15=y15*10;
x17=[32.2,33.1,34.4,34.9,35.7,35,34.4,35,35,34,34.8,35.1,34.7,35.1,35.8,35.8
,36.2,35.1,36.5,36,37.2,38.2];
y17=[13,14,14.7,15.7,16.8,17.5,18.5,19.7,21.1,22,22.7,23.7,24.6,25.5,26.8,27
.9,28.8,29.7,30.5,31.1,30,31];
x17=x17*10;
y17=y17*10;
x18=[20.2,20.8,21.8,21.7,22,21.2,22,21.1,21.2,19.8,18.2,17.3,16.2,15.5,16,16
.2,16,15.2,14.8,15.2,14.5,13.8,14.2,13.5,14.7,15,16,17,18];
y18=[16.8,17.8,18,19,19.8,20,20.8,21.2,22.2,22.8,22.1,23,23.8,23.2,22.3,23,2
3.1,22.1,23.2,24.4,24.8,23.5,22.8,22,21.8,21,21.2,22,24];
x18=x18*10;
y18=y18*10;
x19=[14.1,14.4,13.8,14.5,14.2,15.5,16,15.4,16.1,15.6,14.5,13.5,13.2,14.1,15.
5,15.2,15.8,15,15.5,16.4,16,17.1,17];
y19=[10.7,11.9,12.1,13,13.5,13.9,12.5,12,14,14.5,14.7,14.2,15.1,15.5,16,16.9
,17.9,18.3,20,19.2,18.5,18.4,19.5];
x19=x19*10;
y19=y19*10;
x20=[13,12.1,12.1,13,12,12.1,11.5,12,11.6,12.5,12.9,13.4,12.5,14,14.1,13.5,1
4.5,14.9,12.5,14,14.2,13.2,15.5,16.2];
```

```
y20=[11,11.5,12.5,13,14,14.8,15,16,16.8,17,16,16.9,17.5,17.6,16.5,15.9,15.9,
17.1,18,18.9,19.8,19.4,18.9,20];
x20=x20*10;
y20=y20*10;
x21=[37.9,38.5,38,37.2,38.3,39.2,40.5,41.2,40.6,39.9,39.7,39.7,39,38.6,38,37
,36.4,37,37.3,38.1,37.7,38.8,40,41];
y21=[22,22.5,21.5,21.1,20.9,20.7,20,20.2,20.8,20.8,21.5,22.7,23.7,24.5,25.5,
26,27,28,29,30,30.7,31.2,31.5,32];
x21=x21*10;
y21=y21*10;
x22=[20.9,20,19.5,20.5,19.1,19.5,18,17.8,18.9,18,18.7,17.5,17,16,16.2,15,16.
3,17];
y22=[9.9,10,10.9,11,11.1,12.1,12,13.5,14.7,15,15.5,14.2,15,15.9,14.8,15.2,16
.7,13.9];
x22=x22*10;
y22=y22*10;
x23=[18,19,19,18,19,18,17.5,16.5,15.5,15,16,15.5,14,13,13.5,14.4,12.8,13.8,1
3.7,15];
y23=[10,9.5,10.7,11.1,12,12.8,12.5,11.9,11,12,12.5,13.4,13.7,13,13.7,13,13.5
,14,15,14.5];
x23=x23*10;
y23=y23*10;
x27=[16,16.7,17.7,18,18.5,18.6,18,19.7,19.5,20.1,21.4,22.4,22.4,23.2,24.4,25
.4,26.2,26.2,26.4,27,26.9,27.8,28,29,30,31.5,33,34.2];
y27=[18.5,19.5,19.5,19,19.5,20.1,21,22,21.5,22,22.4,23.2,24.5,24.9,24.5,25.2
,26.4,28,29,29.5,31,32,33,33.2,34,34,33.8,33];
x27=x27*10;
y27=y27*10;
% r,b are the colours of the lines; '.' are for the points on the line
% and 's'is to indicate the starting position of every cell ans numel is the
number of elements in the vector/matrix
plot(x6,y6,'r.-', x7,y7,'k.-', x9,y9, 'k*-', x13,y13, 'rx-', x15,y15,'b.-
',x17,y17,'c.-',x18,y18,'g.-',x19,y19,'m.-',x20,y20,'bx-',x21,y21,      'b*-
',x22,y22,'y.-',x23,y23,'k.-',x27,y27,'cx-',x6(1),y6(1),'o',
x7(1),y7(1),'o',      x9(1),y9(1),      'o',      x13(1),y13(1),      'o',
x15(1),y15(1),'o',x17(1),y17(1),'o',x18(1),y18(1),'o',x19(1),y19(1),'o',x20(
1),y20(1),'o',x21(1),                                                  y21(1),
'o',x22(1),y22(1),'o',x23(1),y23(1),'o',x27(1),y27(1),'o',x6(numel(x6)),y6(n
umel(y6)),'s',x7(numel(x7)),y7(numel(y7)),'s',x9(numel(x9)),y9(numel(y9)),'s
',x13(numel(x13)),y13(numel(y13)),'s',x15(numel(x15)),y15(numel(y15)),'s',x1
7(numel(x17)),y17(numel(y17)),'s',x18(numel(x18)),y18(numel(y18)),'s',x19(nu
mel(x19)),y19(numel(y19)),'s',x20(numel(x20)),y20(numel(y20)),'s',x21(numel(
x21)),y21(numel(y21)),'s',x22(numel(x22)),y22(numel(y22)),'s',x23(numel(x23)
),y23(numel(y23)),'s',x27(numel(x27)),y27(numel(y27)),'s')
xlabel('Distance in micrometers')
ylabel('Distance in micrometers')
% axis is to manipulate the area of the matrix
axis([0,550,0,350])
```

APPENDIX III

MATLAB calculation for cells in the periphery of the aggregate

```
clear all
close all
%x1 y1 x2 y2 x3 y3 x4 y4 are the co-ordinates of different cells x1y1 and
%x2y2 being in aggregate A and x3y3 and x4y4 in aggregate B; scale is
%multiplied by 10 to represent the micrometer scale;
x1=[10.5,11.3,10.5,9.5,9.3,8.2,9.1,8,9,11.2,12.2,16.1,19.4,21,22.6,25.2,27.6
,28.7,29.5];
y1=[22,21.5,23,21.6,20.4,21.9,22.2,24.5,25.6,27,29.2,30.4,30.1,28.8,28.2,28.
4,28.7,29.8,31];
x1=x1*10;
y1=y1*10;
x2=[22.5,20.8,22.8,24,25.2,25.4,26.8,27.7,29,30.4,30.3,29.9,32.1,32.3,34,36,
37.2,38.1,40.4];
y2=[24.8,23.2,23.7,24.5,25.8,27,27.8,27.3,28.5,29.2,28.8,28.4,30,28.7,30,30.
2,31.1,32.4,32.6];
x2=x2*10;
y2=y2*10;
x3=[24,25,26.2,25.1,26.8,27.6,27.8,28.7,29.3,30.1,29.4,28.9,30];
y3=[6.5,6.7,7.7,8.5,8.4,6.7,5.1,4.7,4,4,3.2,3.8,4.6];
x3=x3*10;
y3=y3*10;
x4=[38.3,39.9,41.2,42.6,44.3,44.8,45.2,44.8,44.6,44.9,45.4,46.3,47,47.1,47.6
,47.3,48.9,49.3,47.9];
y4=[9.2,9.8,9,8.5,8.3,7.2,6.9,6.5,6.8,7,5.9,5,4,3.4,3.6,4,4.7,5.6,5.4];
x4=x4*10;
y4=y4*10;
x5=[15.2,14.2,14.5,14,14,14.2,14,14.1,13.5,12.2,11,10.3,9.3,9.9,9,10,10.1,10
.9,11.8,12.2,13.2,13.4,12.8,12.6,11.8,12.2,13,12.2,11.5];
y5=[25,25,25.5,25.7,24.5,24,24.3,24.8,23.8,23.2,23.8,23.9,23.2,24.6,25.2,26,
27,27.2,28.2,28.5,29,28,27.7,26.9,26.5,25.8,26.1,25.4,26];
x5=x5*10;
y5=y5*10;
x8=[33,34,36,37,37.5,38.2,37.9,38.6,38,38.2,38.2,38.9,38.5,38,37.5,38,38.2,3
7.5,37.5,37.9,37.5,37.9,38.2,37.2,37,37.9,38.2,38,37.6,38.3];
y8=[11.5,12,12.5,13.5,15,15.9,17,17.3,18.2,19.2,20.3,21,21.3,21.2,21.7,22.2,
23,24.2,25.7,26.9,27.2,28.2,28.9,29.2,29.8,30.1,29.8,29.5,29.8,30.5];
x8=x8*10;
y8=y8*10;
x10=[15.9,16.3,16.8,17.2,16.4,16.5,15.4,16,17.3,17.8,19.1,20.2,21.3,22.9,23.
8,25.1,26.5,28,29,31,31.1,32.2,33.3];
y10=[28.2,28,28.2,29.5,30,29,29.2,30.2,30.2,31,31.2,31.3,30.5,30.8,31.9,31,3
1.8,32,31.7,31.9,31.7,32.2,33];
x10=x10*10;
y10=y10*10;
x11=[28.5,29.1,29,29.8,29.2,29.5,29,29.6,29.4,29.6,29,29.3,28.7,29,29.1,29.8
,29.4,30,29.2,29.8,29,29.5];
y11=[18.5,19.3,20,21,22,22.8,23.9,24,25,26,26.8,27,27.5,28,28.5,29,29.8,30,3
0.2,31,31.2,33];
x11=x11*10;
y11=y11*10;
x12=[32.2,33,33.5,34.4,34.3,34.5,34.2,34.9,34.5,34.9,34.4,35.2,35,35.2,35,35
.5,35.4,34.8,35.1,34.5,34.5,33.8,33.9,34.5,34.2,34.3,33.8,34.2,33.2,33.4];
y12=[11,10,9,9.5,10,11,12.2,13.5,15,16,16.8,17.9,19,20.1,21,22,23.1,24.1,25,
26,27.1,28,28.9,29,30,31,31.7,32.2,32.8,32];
```

```
x12=x12*10;
y12=y12*10;
x14=[36,37.1,38,36.9,36.2,38.2,39,40,40.9,41.9,41,41.5,40.2,42,42.8,43,43.2,
44.5,43.5,42.5,44,43.7,44.5,43.6];
y14=[10.9,10.2,9.2,7.5,9,10.2,9,8.6,9.6,10.1,11,12,12,11,10,11,12.1,11.5,11,
12.2,12.8,11.5,10.4,9.9];
x14=x14*10;
y14=y14*10;
x16=[22,22.9,22.2,23.2,24.2,25.4,26,26.2,27.2,27.2,28,27.9,28.8,29.1,28.5,28
.9,27.9,28,27,27.5,28.2,28.2];
y16=[10,9.9,11.3,12,13,13.7,14.8,15.5,16,17.1,18,19.9,21,22,23.2,24.8,25.5,2
7,27.4,28.7,29.5,30.5];
x16=x16*10;
y16=y16*10;
x17=[32.2,33.1,34.4,34.9,35.7,35,34.4,35,35,34,34.8,35.1,34.7,35.1,35.8,35.8
,36.2,35.1,36.5,36,37.2,38.2];
y17=[13,14,14.7,15.7,16.8,17.5,18.5,19.7,21.1,22,22.7,23.7,24.6,25.5,26.8,27
.9,28.8,29.7,30.5,31.1,30,31];
x17=x17*10;
y17=y17*10;
x21=[37.9,38.5,38,37.2,38.3,39.2,40.5,41.2,40.6,39.9,39.7,39.7,39,38.6,38,37
,36.4,37,37.3,38.1,37.7,38.8,40,41];
y21=[22,22.5,21.5,21.1,20.9,20.7,20,20.2,20.8,20.8,21.5,22.7,23.7,24.5,25.5,
26,27,28,29,30,30.7,31.2,31.5,32];
x21=x21*10;
y21=y21*10;
x24=[21.2,20.5,21.8,23.2,24.5,26.7,28,29.5,31,32,33,34.5,35.3,37,38];
y24=[24.8,24.2,25.8,26.2,27.7,28.2,28.4,30,30.9,30.9,32,32,33,33.2,33];
x24=x24*10;
y24=y24*10;
x29=[31.1,31.4,32.2,32.2,32.5,33,34,33.5,33.4,33.4,34.2,34,34.9,34.5,33,33,3
2,32.9,33.1,33.8,34.8,35.8];
y29=[7.8,8.7,8.9,10,11,12,13,14,15.7,17,18,19,20,21,22,23,24,25,24.8,25.5,26
,25.9];
x29=x29*10;
y29=y29*10;
x30=[30.5,30.5,31.2,32,33.5,33.5,33,32.5,33,32,31.5,32.3,32.7,32];
y30=[25.4,26.4,27,26,26.8,28,29.4,28.2,27.5,27,27.8,27.9,27,26.5];
x30=x30*10;
y30=y30*10;
% r,b are the colours of the lines; '.' are for the points on the line
% and 'o'is to indicate the starting position of every cell
plot(x1,y1,'b+-',x2,y2,'g.-',x3,y3,'gx-',x4,y4,'c*-',x5,y5,'m.-',x8,y8,'y.-
',x10,y10,'rx-',x11,y11,'cx-',x12,y12,'b.-',x14,y14,'k.-',x16,y16,'r*-
',x17,y17,'c.-',x21,y21,    'r.-',x24,y24,'bx-',x29,y29,'mx-',x30,y30,'kx-',
x1(1),y1(1),'o',x2(1),y2(1),'o',x3(1),y3(1),'o',x4(1),y4(1),'o',x5(1),y5(1),
'o',x8(1),y8(1),'o',x10(1),y10(1),'o',x11(1),y11(1),'o',x12(1),y12(1),'o',x1
4(1),y14(1),'o',x16(1),y16(1),'o',x1(19),y1(19),'s',x21(1),y21(1),'o',
x17(1),y17(1),'o',x24(1),y24(1),'o',x29(1),y29(1),'o',x30(1),y30(1),'o',x2(1
9),y2(19),'s',x3(13),y3(13),'s',x4(19),y4(19),'s',x5(29),y5(29),'s',x8(30),y
8(30),'s',x10(23),y10(23),'s',x11(22),y11(22),'s',x12(30),y12(30),'s',x14(24
),y14(24),'s',x16(22),y16(22),'s',x17(numel(x17)),y17(numel(y17)),'s',x21(nu
mel(x21)),y21(numel(y21)),'s',x24(numel(x24)),y24(numel(y24)),'s',x29(numel(
x29)),y29(numel(y29)),'s',x30(numel(x30)),y30(numel(y30)),'s')
xlabel('Distance in micrometers')
ylabel('Distance in micrometers')
% axis is to manipulate the area of the matrix
axis([0,550,0,350])
%legend is to indicate which line is what cell
```